New aspects of the Middle-Late Triassic terrestrial impact cratering record

^{40}Ar/^{39}Ar dating of the Rochechouart (France), Manicouagan (Canada), and Paasselkä (Finland) impact structures, paleoenvironmental considerations, and a critical look at the Late Triassic multiple impact theory

A thesis accepted by the Faculty of Aerospace Engineering and Geodesy of the Universität Stuttgart in partial fulfilment of the requirements for the degree of Doctor of Natural Sciences (Dr. rer. nat.)

by

Martin Schmieder

born in Schorndorf (Württemberg), Germany

main referee:	PD Dr. rer. nat. Elmar Buchner
co-referee:	Prof. Dr. rer. nat. Hartmut Seyfried
	Prof. Dr. sc. techn. Wolfgang Keller
date of defence:	16.04.2010

Institut für Planetologie

Universität Stuttgart

2010

Abstract

This thesis critically addresses the question whether Earth experienced a giant multiple cosmic strike in the Late Triassic ~214 million years (Ma) ago, as postulated by Spray et al. in 1998. According to this theory, the large ~100 km Manicouagan impact structure (Québec, Canada), the ~40 km Lake Saint Martin impact structure (Manitoba, Canada), the ~25 km Rochechouart impact structure (France), the ~20 km Obolon impact structure (Ukraine), and the ~9 km Red Wing Creek impact structure (North Dakota, USA) are potential members of a large-scaled, ~4,500 km long impact crater chain, compatible with coeval impact ages available in 1998. However, especially against the background that the formation of crater chains appears to be highly unlikely on Earth, no geologic evidence for the multiple Late Triassic impact scenario has been presented since that time. In this study, I present new ^{40}Ar/^{39}Ar data for the Rochechouart and Manicouagan impact structures, along with new constraints for the timing of the Obolon impact structure based on paleoenvironmental considerations. The new results are set in the context of recent chronological data available for the Lake Saint Martin impact structure, geochemical data, and the physical background of impact crater chain formation. Furthermore, paleoenvironmental implications are discussed.

^{40}Ar/^{39}Ar dating of sanidine and hydrothermally grown adularia separated from impact-metamorphosed gneiss from the Rochechouart impact structure (France) yielded a Latest Triassic (Rhaetian) combined age of 201 ± 2 Ma (2σ), indistinguishable within uncertainty from the age of the Triassic/Jurassic boundary. This new age value is within the range of earlier dating results but distinctly younger than the previously obtained 214 ± 8 Ma (Karnian-Norian) age for Rochechouart and, therefore, is in conflict with the Late Triassic multiple impact theory postulated by Spray et al. (1998). In agreement with the paleogeographic conditions in the western Tethys domain, the near-coastal to shallow marine Rochechouart impact is compatible with the formation of seismites and tsunami deposits in the latest Triassic of the British Islands and possible related deposits in other parts of Europe. Apparently shocked quartz reported from uppermost Triassic sediments of the Northern Apennines (Italy), as well as an enigmatic spherule layer recently detected in the upper Rhaetian Fatra Formation of the High Tatra Mountains (Slovakia) are discussed as possible distal Rochechouart ejecta. The comparatively small crater size of ≤50 km, however, suggests no direct link between the Rochechouart impact and the global mass extinction at the Triassic/Jurassic boundary.

[40]Ar/[39]Ar dating of a fine-grained crystalline impact melt rock from the Manicouagan impact structure (Québec, Canada) yielded a Late Triassic (Norian) age of 211 ± 2 Ma (2σ) close to the widely cited ages of ~215 Ma. However, a set of precise and well-established U/Pb ages have previously been reported for the Manicouagan impact, and this dating attempt could not notably improve the impact age estimates. The influence of the Manicouagan impact on the Late Triassic biosphere is still a matter of debate.

Recent (U-Th)/He ages obtained for the Lake Saint Martin impact structure (Manitoba, Canada) suggest a Middle to Late Triassic (Ladinian to Karnian) impact age of ~235-230 Ma. No isotopic ages are available for the Red Wing Creek impact structure (North Dakota, USA), stratigraphically dated at ~220-200 Ma. In addition, palaeogeographic studies have shown that the Obolon (Ukraine) impact age is notably younger than previously stated, roughly ~185-170 Ma, placing the impact in the Early-Middle Jurassic. The new dating results for Rochechouart and Manicouagan, together with the recent age estimations for the Lake Saint Martin and Obolon impacts, rule out a ~214 Ma Late Triassic multiple impact event on Earth, and it is suggested that the five impact structures discussed were formed by spatially and temporally individual impact events in Triassic to Jurassic time.

In addition, I present a first detailed petrographic and geochemical description of impact melt rocks from the Paasselkä impact structure, Finland. The degree of shock metamorphism suggests initial whole-rock melting at peak shock pressures of ≥35 GPa and post-shock temperatures of up to ~1,500 °C; the geochemical composition of the Paasselkä impact melt rocks is roughly consistent with the compositions of melt rocks from a number of impact structures located within the crystalline basement of the Baltic Shield. [40]Ar/[39]Ar dating of recrystallized feldspar glass particles separated from the impact melt rocks yielded a Middle to Late Triassic (Ladinian-Karnian) age of 229 ± 3 Ma (2σ). This new age makes Paasselkä the first known Triassic impact structure dated by isotopic methods on the Baltic Shield. Due to the small crater size, a link between the Paasselkä impact and a postulated Middle/Late Triassic extinction event is unlikely. The new Paasselkä impact age is, within uncertainty, coeval with isotopic ages recently obtained for the Lake Saint Martin impact structure in Canada, indicating a new Middle to Late Triassic impact crater population on Earth.

Zusammenfassung

Diese Arbeit geht der Frage nach, ob die Erde in der späten Trias vor etwa 214 Millionen Jahren (Ma) Zeuge eines gigantischen kosmischen Mehrfachtreffers wurde, wie dies 1998 von Spray et al. postuliert wurde. Dieser Theorie zufolge gehören die ~100 km große Impaktstruktur von Manicouagan (Québec, Kanada), die ~40 km große Impaktstruktur von Lake Saint Martin (Manitoba, Kanada), die ~25 km große Impaktstruktur von Rochechouart (Frankreich), die ~20 km große Impaktstruktur von Obolon (Ukraine) und die ~9 km große Impaktstruktur von Red Wing Creek (North Dakota, USA) einer etwa 4500 km langen Kraterkette an; die im Jahre 1998 gültigen zeitlich übereinstimmenden Altersdaten für die jeweiligen Impaktstrukturen stützten diese Theorie. Bisher konnte allerdings noch kein geologischer Beweis für das spättriassische Mehrfachtreffer-Szenario erbracht werden. Darüber hinaus gilt die Bildung von Kraterketten auf der Erde als sehr unwahrscheinlich. In der vorliegenden Arbeit präsentiere ich neue $^{40}Ar/^{39}Ar$-Altersdaten für die Impaktstrukturen von Rochechouart und Manicouagan und diskutiere das Alter des Obolon-Einschlags mittels paläogeographischer Studien. Die neuen Datierungsergebnisse werden vor dem Hintergrund neuer Altersdaten für die Impaktstruktur von Lake Saint Martin, sowie geochemischer Daten und den himmelsmechanisch-physikalischen Grundlagen der Kraterkettenbildung diskutiert. Darüber hinaus stelle ich Betrachtungen über mögliche Auswirkungen der Impaktereignisse auf die Paläoumwelt an.

Die $^{40}Ar/^{39}Ar$-Datierung von Sanidin und hydrothermal gewachsenem Adular aus einem stark impaktmetamorph überprägten Gneis der Impaktstruktur von Rochechouart (Frankreich) ergaben ein kombiniertes spättriassisches Alter von 201 ± 2 Ma (2σ) (Rhät), das im Rahmen der Ungenauigkeit mit dem Alter der Trias/Jura-Grenze übereinstimmt. Der neue Alterswert liegt im Rahmen früherer Datierungsergebnisse, ist aber deutlich jünger als das zuletzt vermutete Alter von etwa 214 ± 8 Ma (Karn-Nor) und widerspricht damit der Mehrfachtreffertheorie von Spray et al. (1998). Im paläogeographischen Zusammenhang könnte der Rochechouart-Einschlag die Bildung großflächiger Seismit- und Tsunami-Ablagerungen auf den Britischen Inseln und in anderen Teilen der westlichen Tethys zur Zeit der ausgehenden Trias erklären. Mutmaßlich geschockte Quarze in Ablagerungen der obersten Trias des nördlichen Apennins (Italien) und eine rätselhafte Sphärulenlage in Trias/Jura-Grenzschichten der Hohen Tatra (Slowakische Republik) werden als mögliche distale Auswurfmassen des Rochechouart-Impakts diskutiert. Der vergleichsweise kleine Kraterdurchmesser von ≤50 km legt jedoch nahe, dass der

Rochechouart-Einschlag zumindest nicht direkt mit dem Massenaussterbe-Ereignis an der Trias/Jura-Grenze im Zusammenhang steht.

Die [40]Ar/[39]Ar-Datierung eines feinkörnigen Impaktschmelzgesteins von der Impaktstruktur von Manicouagan (Québec, Kanada) ergab ein spättriassisches (norisches) Alter von 211 ± 2 Ma (2σ), das nahe an den bisher zitierten Datierungsergebnissen um 215 Ma liegt. Angesichts präziser U/Pb-Daten für das Manicouagan-Ereignis konnte diese Datierung nicht nennenswert zur genaueren Eingrenzung des Manicouagan-Alters beitragen. Der Einfluss des Manicouagan-Einschlags auf die Lebewelt der späten Trias ist noch Gegenstand der Diskussion.

Neue (U-Th)/He-Altersdaten für die Impaktstruktur von Lake Saint Martin (Manitoba, Kanada) ergaben ein mittel- bis spättriassisches Impakt-Alter um 235-230 Ma. Für die Impaktstruktur von Red Wing Creek (North Dakota, USA) liegen keine isotopischen Altersdaten vor, das Einschlags-Alter kann aber stratigraphisch auf ca. 220-200 Ma eingegrenzt werden. Weiterhin haben paläogeographische Studien gezeigt, dass der Obolon-Einschlag (Ukraine) wesentlich später als bisher vermutet, nämlich im frühen bis mittleren Jura vor etwa 185-170 Ma, stattfand. Die neuen Datierungsergebnisse widersprechen einem kosmischen Mehrfachtreffer in der späten Trias vor rund 214 Millionen Jahren; vielmehr zeigen die Ergebnisse an, dass jede der fünf diskutierten Impaktstrukturen sowohl örtlich als auch zeitlich unabhängig voneinander in der Trias und im Jura entstanden sind.

Des Weiteren gebe ich eine erste petrographisch-geochemische Beschreibung von Impaktschmelzgesteinen der Impaktstruktur von Paasselkä in Finnland. Die schockmetamorphen Bildungsbedingungen entsprechen denen der initialen Gesamtgsteinsaufschmelzung bei Druckspitzen von über 35 GPa und post-Schock-Temperaturen von bis zu ca. 1500°C. Die geochemische Zusammensetzung der Impaktschmelzgesteine ähnelt weitgehend der von Schmelzgesteinen anderer Impaktstrukturen im Kristallin des Baltischen Schildes. Die [40]Ar/[39]Ar-Datierung rekristallisierter Feldspatgläser in den Schmelzgesteinen ergaben ein mittel- bis spättriassisches Alter (Ladin-Karn) von 229 ± 3 Ma (2σ). Damit ist der Paasselkä-Krater die erste bekannte nachweislich triassische Impaktstruktur auf dem Baltischen Schild. Auf Grund des kleinen Kraterdurchmessers kann jedoch ein Zusammenhang zwischen dem Paasselkä-Einschlag und einem vermuteten Aussterbeereignis an der Ladin/Karn-Grenze weitgehend ausgeschlossen werden. Im Rahmen der Datierungsungenauigkeit sind die Impaktstrukturen von Paasselkä und Lake St. Martin etwa gleichzeitig entstanden, womit eine bisher unbekannte mittel- bis spättriassische Impaktkrater-„Population" auf der Erde nachgewiesen werden kann.

Acknowledgements

I am greatly indebted to several persons who made this work possible. These include: my advisor and first referee PD Dr. Elmar Buchner (Institut für Planetologie, Universität Stuttgart), who stimulated fruitful discussion about almost everything related to impact - it was always a pleasure to get out in the field with you! My co-referees Prof. Dr. Hartmut Seyfried (Institut für Planetologie, Universität Stuttgart), as well as Prof. Dr. Wolfgang Keller (Geodätisches Institut, Universität Stuttgart). Importantly, PD Dr. Mario Trieloff and Dr. Winfried Schwarz (Institut für Geowissenschaften, Universität Heidelberg) who carried out the technical part of $^{40}Ar/^{39}Ar$ dating and helped me to get somewhat more experienced with $^{40}Ar/^{39}Ar$ geochronology. Dr. Philippe Lambert (Sciences and Applications, Bordeaux Merignac, France) and Dr. Fred Jourdan (Western Australian Argon Isotope Facility, Curtin University of Technology, Perth, Australia) for helpful discussions about the Rochechouart crater, isotopic dating, and beyond. Odile Dupuy, Dr. Claude Marchat (Association Pièrre de Lune, Rochechouart, France), and the Espace Météorite Paul Pellas museum, who were greatly hospitable field guides at Rochechouart. Natalie Marsan and Bob Burke, who made possible to see the magnificent Manicouagan melt sheet. Jarmo Moilanen (Oulu, Finland), who kindly provided impactites from the Paasselkä impact structure for study. Dr. Ruth Bezys (formerly Manitoba Geological Survey, Saskatchewan, Canada) and Lynne Bobier (Manitoba Science, Technology, and Mines) for providing impact melt rocks from Lake Saint Martin. My Oulu colleague Teemu Öhman (Department Geology, University of Oulu, Finland) who was always open for discussion about the Finnish impact craters. Dr. Jo-Anne Wartho and Dr. Matthijs van Soest (Arizona State University, Tempe, Arizona, USA) who collaborated with (U-Th)/He dating of the Lake Saint Martin impact structure. Prof. Dr. Dieter Stöffler and Prof. Dr. Uwe Reimold (Museum für Naturkunde, Leibniz-Institut für Evolutions- und Biodiversitätsforschung, Humboldt-Universität zu Berlin) for inviting me to talk about the Rochechouart impactites some time ago. Steven Goderis (Vrije Universiteit Brussel, Belgium) for preliminary impactor ID studies. Dr. Jörg Kröchert (Institut für Planetologie, Universität Stuttgart) for interesting coffee breaks and discussions about the world and everything. Christoph Wimmer-Pfeil and Moritz Schmelz (Universität Stuttgart) for thorough thin section preparation. Dr. Thomas Theye (Institut für Mineralogie und Kristallchemie, Universität Stuttgart) for microprobe and X-ray diffraction measurements. Dr. Jens Hopp (Institut für Geowissenschaften, Universität Heidelberg) for supporting sample preparation.

This work was partially funded by the Landesgraduiertenförderung (LGFG) by the Land Baden-Württemberg (2005-2008), which is kindly acknowledged.

I dedicate this thesis to my father Günter Schmieder who enabled me to attend University (and who, by the way, sometimes served as scale in some of the Ries suevite outcrops).

Table of contents

1. Introduction

1.1. Impact cratering on Earth through geologic time– a brief summary

Large meteorite impacts have been affecting and changing Earth since its birth and still do today. After the Earth's formation about 4.56 billion years (Ga) ago, the Moon is believed to have formed as a product of the 'Giant Impact' of a roughly Mars-sized body onto the Proto-Earth (e.g., Cameron and Ward 1976; Boss 1986; Canup and Righter 2000; Canup and Asphaug 2001). Even hundreds of millions of years (Ma) later, during post-accretionary bombardment and the 'Late Heavy Bombardment' (the latter peaking about 3.9 Ga ago) and still later on, our planet was severely struck by numerous large impacts within the Earth-Moon system (e.g., Hartmann et al. 2000; Ryder et al. 2000; Glikson 2001; Morbidelli et al. 2001; Kring and Cohen 2002; Koeberl 2006a,b; Grieve et al. 2006; Stöffler et al. 2006). The most likely source for the large cosmic projectiles (at cosmic velocities of ~11-72 km/s) is the asteroid belt between Mars and Jupiter; however, comets thought to originate from the Kuiper Belt and the Oort cloud on the outskirts of the Solar System have been discussed as potential impactors on Earth (e.g., Oort 1950; Shoemaker 1983; Stern 2003). By the recognition of Archean spherule (distal impact ejecta) layers, the terrestrial sedimentary record today provides invaluable insights into large impacts on the early Earth during the Archean (4.0-2.5 Ga; e.g., Koeberl 2006a;b). Two outstanding examples are the spherule layers in the Barberton Greenstone Belt (~3.2 Ga; South Africa; e.g., Lowe et al. 2003; see also Hofmann et al. 2006 for discussion) or the Hamersley Basin (~2.6 Ga; Western Australia; Simonson 2003; Simonson and Glass 2004; Rasmussen et al. 2005). However, impact craters as a potential source for these Archean impact ejecta are not preserved due to terrestrial magmatic/tectonic recycling and erosion. The ~300 km in diameter and 2.023 Ga Paleoproterozoic Vredefort impact structure (South Africa), which is today deeply eroded, is the oldest and largest impact structure currently known on Earth (Kamo et al. 1996; Gibson et al. 1997; Reimold and Gibson 2005). Of similar size, the ~250 km diameter and 1.85 Ga Sudbury impact structure (Ontario, Canada) is the second largest and second oldest terrestrial impact structure (Krogh et al. 1984; Ames et al. 1998;

Davis 2008), also associated with a Paleoproterozoic distal impact ejecta layer (Addison et al. 2005; Pufahl et al. 2007). Along with the progressive organization of the asteroid belt, the frequency of large impacts in the Earth-Moon system has strongly decreased since the Archean and the Proterozoic (2.5 Ga-~542 Ma; e.g., Neukum et al. 2001; Stöffler and Ryder 2001; Langenhorst 2002).

Large meteorite impacts that affected terrestrial life at the global scale were, however, comparatively rare. Statistically, as inferred from the current state of knowledge on the terrestrial impact cratering record, a bolide that creates a ~50-100 km-sized crater hits the Earth once in about 30 million years (e.g., French 1998). The best-studied large impact event in the Phanerozoic (~542 Ma-today) is certainly the one that produced the ~190 km Chicxulub crater on the Yucatán peninsula (Mexico) at the Cretaceous/Paleogene (K/P; formerly Cretaceous/Tertiary; K/T) boundary ~65 Ma ago, which has promoted the idea that large impacts may cause the global distribution of impact ejecta and chemical anomalies in the sedimentary record (e.g., the commonly cited iridium anomaly), severe worldwide biological crises and mass extinctions (e.g., among the dinosaurs), large impact-induced tsunamis when the impactor strikes the sea, as well as atmospheric and climatic perturbations (Alvarez L. et al. 1980; Alvarez W. et al. 1995; O'Keefe and Ahrens 1982; Bohor et al. 1987; Hildebrand et al. 1991; Hildebrand 1993; Swisher et al. 1992; Kring et al. 1996; Smit 1999; Claeys et al. 2002; Koeberl 2007; Weiss and Wünnemann 2007; see also, e.g., Keller et al. 2004 for the 'Chicxulub debate'). The mass extinction at the K/P boundary is one of the 'big five' extinction events in the history of life (e.g., Benton 1995). Apart from the K/P boundary mass extinction, an even more dramatic extinction event occurred at the Permian/Triassic boundary ~250 Ma ago, in addition to the major extinctions associated with the Ordovician/Silurian boundary at ~445 Ma, the Frasnian/Famennian boundary at ~376 Ma (Late Devonian), and the Triassic/Jurassic boundary at ~200 Ma (e.g., Raup 1992; Rampino and Haggerty 1996; Hallam and Wignall 1997; Becker et al. 2004; Reimold 2007a; see also Koeberl and MacLeod 2002 and contributions therein). Although evidence for impact at these time boundaries is not always convincing, all of the latter extinction events are discussed as being (at least in parts) associated with catastrophic impact events (sometimes the term 'New Catastrophism' is used in this

context; Ager 1995; Reimold 2007a). The largest European impact structure, the ~85 km Siljan impact structure (Sweden), has yielded an age roughly consistent with the Frasnian/Famennian boundary (Henkel and Aaro 2005; Reimold et al. 2005a), and is possibly linked with a spherule layer recognized in Uppermost Devonian sections in Belgium (Claeys et al. 1992; 1996). Likewise, the large ~70 km Morokweng impact structure (South Africa) dated at ~145 Ma well corresponds with the age of the Jurassic/Cretaceous boundary (Koeberl et al. 1997a). The temporal coincidence between major impacts, the formation of large igneous provinces on Earth (such as the ~250 Ma Siberian and Emeishan trap basalts, the ~200 Ma Central Atlantic Magmatic Province, or the ~65 Ma Dekkan basalts), and biotic effects is still a matter of speculation (e.g., Alvarez 2003; Kelley 2007). Multiple impacts in the Triassic (Spray et al. 1998) have been discussed as possible trigger mechanisms for environmental change during the Mesozoic (~250-65 Ma), for example, the ~100 km in diameter and ~215 Ma Manicouagan impact structure (Québec, Canada) potentially associated with a minor extinction event at the Karnian/Norian or Norian/Rhaetian boundary within the Late Triassic (Benton 1986; 1991; Hodych and Dunning 1992; Sephton et al. 2002). Impacts that occurred during the Triassic, especially in Middle to Late Triassic time, will be the main focus of this thesis.

In the aftermath of the Chicxulub impact, the Cenozoic Era (~65 Ma-today) is characterized by an impact cluster around ~35-37 Ma, represented by the two large ~100 km Popigai (Siberia, Russia) and ~90 km Chesapeake Bay (Virginia, USA) impact structures that were struck during a Late Eocene asteroid shower (Glass et al. 1986; Bottomley et al. 1997; Stöffler and Claeys 1998; Tagle and Claeys 2005). Distal impact ejecta (clinopyroxene-bearing spherules) at Eocene/Oligocene boundary sections worldwide, with the global stratotype at Massignano (Italy), have been shown to be related with the Popigai impact structure (Montanari and Koeberl 2000; Whitehead et al. 2000; Koeberl 2009), whereas the North American tektites (bediasites and georgiaites) have been linked with the slightly younger Chesapeake Bay impact (e.g., Glass 2002; Deutsch and Koeberl 2006; Koeberl 2009). The Wanapitei (Ontario, Canada), Mistastin (Labrador, Canada), and Haughton (Devon Island, arctic Canada) impact structures are also members of this Late Eocene impact cluster (Mak et al. 1976;

Bottomley et al. 1979; Sherlock et al. 2005; see also Grieve 2006). About 14.4 Ma ago, in the Miocene, Central Europe was hit by the impact of a binary asteroid, which produced the ~24 km Ries crater and the ~3.8 km Steinheim Basin in Southern Germany, as well as the Central European tektite strewn field ('Ries tektites'; also known as moldavites) that extends over parts of Germany, Austria, and the Czech Republic (Koeberl 1986; von Engelhardt et al. 1987; Schwarz and Lippolt 2002; Trnka and Houzar 2002; Stöffler et al. 2002). Larger impacts in later Cenozoic times formed the ~52 km Kara-Kul impact structure in the Pamir Mountains (Tajikistan) ~5 Ma ago (Gurov et al. 1993) and the El'Gygytgyn crater (Chukotka, Siberia) ~3.5 Ma ago (Gurov et al. 1978; 2007; Layer 2000); the latter is currently subject to deep drilling and detailed impact geological and climatologic investigations (Koeberl et al. 2009). About 1.07 Ma ago — the genus *Homo* already existed — a notable impact produced the ~10.5 km Bosumtwi crater (Ghana) in tropical West Africa and the Ivory Coast tektites (Koeberl 1994; Koeberl et al. 1997b; 1998; Artemieva 2002; Ferrière et al. 2008). The ~14 km Zhamanshin crater (Kazakhstan), associated with tektite-like impact glasses (zhamanshinites and irghizites), was created only ~800 thousand years (ka) ago (Florensky et al. 1977; Matsubara et al. 1991). Of similar age, an assumedly large impact event that produced the ~780 ka Australasian tektites (Koeberl 1986; Izett and Obradovich 1992; Lee and Wei 2000) is still enigmatic, and no source crater has been identified to date (Schnetzler 1992; Hartung and Koeberl 1994). The probably most famous impact crater on Earth is the impressive ~1.2 km Meteor (Barringer) crater in the desert of Arizona (USA), which was struck by the impact of the Canyon Diablo iron meteorite ~49 ka ago (Barringer 1905; Spencer 1933; Sutton 1985; Kring 2007).

In prehistoric and historical times, only comparatively small impacts occurred, such those that produced the Kaali impact crater field (Saarema Island, Estonia) ~1690 B.C. (Kraus and Meyer 1928; Reinwaldt 1928; Veski et al. 2004; 2007; Raukas et al. 2005), the Wabar iron meteorite impact (Saudi Arabia) ~300 years ago (Chao et al. 1961; Wynn and Shoemaker 1998; Prescott et al. 2004; Basurah 2003), or the still enigmatic Tunguska event in the Siberian taiga on June 30, 1908 (Kulik 1927; Shuvalov and Artemieva 2002; Boslough and Crawford 2008; Longo 2007; Steel 2008). The geologically youngest impact structure (in the sense of a crater at least several meters in

diameter) is the ~13 m Carancas crater in the Peruvian Highlands that was formed very recently, on September 15, 2007 (Kenkmann et al. 2008a,b; 2009; Le Pichon et al. 2008).

1.2. Not only single craters?

Since the first comprehensive studies of shock metamorphic effects and the confirmation of an impact origin of the Ries crater by Shoemaker and Chao (1961), the Ries is generally accepted as the 'cradle of impact geology', and the 'Ries-Steinheim event' is of particular interest to (not only European) impact research, still posing new questions with regard to the exact age of both craters and the nature of both impactors (Reiff 1988; Schmidt and Pernicka 1994; Stöffler et al. 2002; Schmieder and Buchner 2009; Buchner et al. 2009b). In addition to the Ries-Steinheim doublet craters, the two Carboniferous-Permian (~290 Ma?) impact structures of Clearwater West and East (Québec, Canada), the Eocene ~49 Ma Gusev and Kamensk craters (Russia), and the Proterozoic (>700 Ma?) Suvasvesi impact structures (Finland) most likely represent doublet impact craters struck by binary asteroids (Beals and Halliday 1967; Bottomley et al. 1990; Melosh and Stansberry 1991; Bottke and Melosh 1996a;b; Masaitis 1999; Werner et al. 2001; 2002; Buchner et al. 2009c), as known on the Moon, Venus, or Mars (Melosh and Stansberry 1991; Melosh et al. 1996; Cook et al. 2003). Similarly, impact crater chains composed of more than two impact craters in a row occur on the Moon and other planetary bodies (Melosh and Schenk 1993; Melosh and Whitaker 1994; Wichman and Wood 1995; Schenk et al. 1996). However, although at least three suspected terrestrial impact crater chains have been proposed (Ocampo and Pope 1996; Rampino and Volk 1996; Spray et al. 1998; Walkden et al. 2002), no impact crater chain is finally proven on Earth. A key point in double and multiple impact studies was the collision of at least 21 fragments of comet Shoemaker-Levy 9 with the atmosphere of Jupiter generating a chain of giant impact plumes, which was observed by the Hubble Space Telescope and from space observatories in July 1994 (Orton et al. 1995; Levy 1998), and it was soon speculated whether this type of impact could also happen on Earth (Miller and Tennyson 1995). At the smaller scale, fields of comparatively closely spaced (sometimes overlapping) small craters usually not lager than ~150-200 m in diameter

are thought to form by impacts of meteorites that experienced atmospheric breakup; examples for such crater fields are those at Morasko (Poland; 7 craters), Kaali (Estonia; 9 craters), Henbury (Australia; 16 craters), Odessa (Texas, USA; 5 craters), Wabar (Saudi Arabia; 4 craters), or Macha (Russia; 5 craters; Passey and Melosh 1980; Gurov and Gurova 1998), all of which are geologically young (Quaternary) in age.

1.3. Current research on terrestrial impact structures

The above sections illustrate that – after about 50 years of impact research – impact events through geologic time have always been a 'usual' and significant process for more than 4 billion years and that large impacts may have notable influence on the surface shape, life, and climate on Earth (Shoemaker 1977; Grieve 1997; Melosh 1996; French 1998; Montanari and Koeberl 2000; Reimold 2007a; Pati and Reimold 2007; Ivanov 2008; Reimold and Koeberl 2008). 176 impact structures are currently (September 2009) known on Earth (Fig. 1.1). Among these, some particular geological structures have been interpreted as endogenic (volcanic or sedimentary) features for decades but finally turned out to be of impact origin by the detection of unequivocal evidence of 'shock metamorphism' in the rocks (e.g., Amor et al 2008; Buchner and Kenkmann 2008; Salameh et al. 2008). A large number of impact structures could be added to the terrestrial impact crater database (e.g., the *Earth Impact Database*) during the last years, and further new impact structures have recently been confirmed (e.g., the Jebel Waqf as Suwwan impact structure, Jordan; Salameh et al. 2008; the Santa Fe impact structure, New Mexico, USA; Fackelman et al. 2008; the Whitecourt crater, Alberta, Canada; Herd et al. 2008; the remnants of a large impact structure in northwestern Scotland; Amor et al. 2008; the Dhala impact structure, India; Pati et al. 2008; or the Matt Wilson impact structure, Australia; Kenkmann and Poelchau 2009) and will be recognized in the future. In particular, no impact structures have so far been detected in large countries such as China, the Democratic Republic of Congo, Sudan, Angola, or Mozambique, either due to political restrictions, instability, or civil war that precluded impact geologic field work (e.g., Schmieder and Buchner 2007). Nevertheless, the use of satellite imagery and remote sensing techniques has greatly improved the search for possible impact

structures on Earth (and other planetary bodies) and is also a useful tool in the study of proven impact structures (e.g., Crósta 1987; Grieve et al. 1988; Abels et al. 2000; Koeberl 2004; Schmieder and Buchner 2007; Buchner and Schmieder 2007; Schmieder et al. 2009b). Despite the destructive nature of large impacts and the continuing threat of being hit by Near-Earth Asteroids (NEAs; e.g., Chapman and Morrison 1994; Chapman 2004), about one third of the terrestrial impact structures is exploited for world-class economic resources, such as gold (at Vredefort), copper, nickel, platinum group elements (at Sudbury), lead-zinc (e.g., at Siljan), uranium (e.g., at Carswell, Saskatchewan, Canada), or Petroleum and gas (e.g., Viewfield, Saskatchewan, Canada; Red Wing Creek, North Dakota, USA; or Ames, Oklahoma, USA); a review of the economic potential of terrestrial impact structures is given by Grieve and Masaitis (1994), Grieve (2005), and Reimold et al. (2005b). Last but not least, in contrast to the important role of large impacts in the New Catastrophism, recent investigations have been made to clarify whether life could be transported by meteorites and whether microbial life might be able to survive impacts (e.g., Stöffler et al. 2007; Horneck et al. 2008). Related to this is the comparative study of impact-induced hydrothermal systems and alteration within/beneath impact structures on Earth and Martian analogs that provides estimations of the habitability of the early Earth and Mars (e.g., Newsom 1980; Osinski et al. 2001; Abramov and Kring 2004; 2005, Zürcher and Kring 2004).
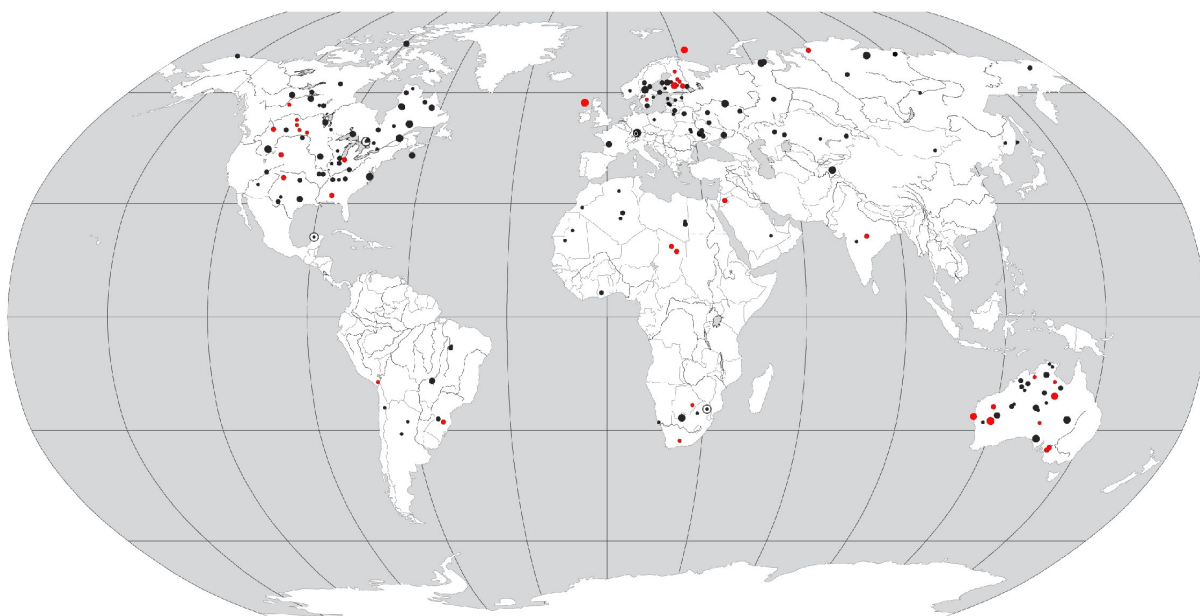
Fig. 1.1: World map showing distribution of terrestrial impact structures. Black dots: impact structures as of 1998; red dots: impact structures discovered since 1998 (map modified after French 1998).

1.4. A closer look at the terrestrial impact cratering record

The scientific study and characterization of terrestrial impact structures comprises variable geoscientific disciplines, just to mention the classical field geological investigation together with structural (e.g., Kenkmann et al. 2005), petrographic-geochemical-petrological (e.g., in the following chapters), geophysical (e.g., Pesonen et al. 1999a), geochronological (e.g., Schwarz and Lippolt 2002; Jourdan et al. 2008; this work), sedimentologic (e.g., Dypvik and Jansa 2003; Buchner and Schmieder 2009a), biologic (e.g., Cockell and Lee 2002), and remote sensing studies (e.g., Abels et al. 2000; Schmieder et al. 2009b), as well as drilling (e.g., Gohn et al. 2008) and numerical modeling of impacts (e.g., Collins and Wünnemann 2005). Among these approaches the geochemical identification of impactor traces in impact lithologies (e.g., Palme 1980; Palme et al. 1981; Koeberl 1998; Tagle and Claeys 2005; Tagle and Hecht 2006; Alwmark and Schmitz 2007; Goderis et al. 2009; Schmieder and Buchner 2009) and constraints of the timing of the impact event using variable (stratigraphic, isotopic, and paleomagnetic) dating techniques (e.g., Bottomley et al. 1990; Deutsch and Schärer 1994; Schmieder and Buchner 2008; Jourdan et al. 2009b; Schmieder et al. 2009c) are

major aspects and crucial for the understanding of the terrestrial impact rate (e.g., Bland 2005; Stöffler et al. 2006). In the ideal case, these parameters can answer the questions (1) what type of asteroid targeted Earth and (2) when (exactly) the impact occurred. Among the isotopic dating techniques, the $^{40}Ar/^{39}Ar$ and U/Pb systems have turned out to produce the most reliable data (e.g., Deutsch and Schärer 1994). However, from a geochronological point of view, the majority (>80%) of the 176 impact structures currently confirmed on Earth is still insufficiently dated (e.g. Reimold 2007b; Renne et al. 2007; Schmieder and Buchner 2008; Jourdan et al. 2009b). In many cases, the age of the target rock provides the only (maximum) age constraint for crater formation, for example at the < 170 Ma Upheaval Dome impact structure (Utah, USA; e.g., Buchner and Kenkmann 2008). Apart from some exceptionally good ages, e.g. the ~14.4 Ma age for the Ries crater, Germany (Buchner et al. 2003; 2009b); the 682 ± 4 Ma age for the Jänisjärvi impact structure (Russia; Jourdan et al. 2008), or the 2,023 ± 4 Ma age for the Vredefort impact structure (South Africa; Kamo et al. 1996), isotopic age data obtained from impactites (impact melt rocks and glasses) are commonly of high apparent precision but of equivocal accuracy due to the use of poorly reliable chronometers (e.g. K/Ar or Rb/Sr) or overinterpretation of inaccurate or scattered dating results caused by poor melt homogenization, rock alteration, or post-impact thermal overprint (Jourdan et al. 2007b; 2008; Renne et al. 2007; Jourdan et al. 2009b). At impact structures that lack lithologies suitable for isotopic dating, tentative stratigraphic dating commonly accounts for significant age uncertainties of up to 100 % (e.g. the 250 ± 80 Ma Kursk impact structure, Russia, or the 200 ± 100 Ma Wells Creek impact structure, Tennessee, USA). At higher levels of precision, biostratigraphic dating may yield apparently precise age data (e.g. the 167 ± 3 Ma age for the large Puchezh-Katunki impact structure, Russia; Masaitis and Pevzner 1999) but these techniques still lack satisfactory international calibration (e.g. Pálfy 2004). A recent critical appraisal of the published ages of terrestrial impact structures is presented by Jourdan et al. (2009b). The geochronology of impact cratering on Earth is the main focus of this study.

2. Impact cratering – process and effects

2.1. The cratering process

Since the discovery of the Lunar craters on the pockmarked Moon by Galilei in 1609, impact cratering as the result of the collision of two bodies (impactor and target) has been discussed mainly in the astronomical context (see Melosh 1996; French 1998; and Koeberl 1999 for a historical summary of impact cratering). However, it was only some ~350 years later that impact cratering was recognized as a fundamental 'geologic' process on Earth (e.g., Shoemaker and Chao 1961; French and Short 1968; Melosh 1996; Grieve 1997; French 1998; Pati and Reimold 2007; Reimold and Koeberl 2008). The term 'hypervelocity impact' was issued for the impact of cosmic objects (defined as meteorites on the Earth's surface) that are large enough (some ~50 m and ~20 m in diameter for stony and iron meteorites, respectively) to strike the Earth at largely undecelerated cosmic velocity (~12-72 km/s). This is in contrast to comparatively slow (some hundreds of meters per second) ballistic impacts of small bodies that are strongly decelerated along with disintegration and ablation within the Earth's atmosphere. The highly dynamical hypervelocity impact cratering process can be subclassified into three stages:

Firstly, the contact and compression stage (parts of a second; Fig. 2.1 top) during which the impactor - also commonly denominated as 'projectile' - meets a planetary surface at cosmic speed, generating a shock wave that penetrates both the target and the projectile. The target rock at the impact point is instantaneously subjected to shock pressures of up to ~100 GPa (1 GPa = 10 kbar = 10,000 atmospheric pressures), by far exceeding the highest pressures reached by endogenic terrestrial processes (e.g., compare ultrahigh pressure metamorphism at collision and subduction zones with maximum lithostatic pressures of ~5 GPa) and causing effects of 'shock metamorphism' in the rocks. The uppermost parts of the target rock are strongly accelerated and ejected upon the (most commonly oblique) projectile-target contact (e.g., Melosh 1996, Artemieva 2002). The shock wave that travels through the projectile itself is reflected at its farside as a tensional rarefaction (release) wave, causing immediate pressure

unloading and vaporization of the projectile within the target rock (e.g., French 1998; Reimold and Koeberl 2008).

Secondly, the excavation stage (some seconds; Fig. 2.1 middle) is the actual crater-forming time interval. As the projectile penetrates the target rock (down to 1-2 projectile diameters) and finally vaporizes, a roughly hemispherical shock wave rapidly propagates the target rock radially away from the impact point. Due to energy loss within the shock-compressed target, the shock wave is attenuated with increasing travel width. In the near-surface zone, the shock waves are reflected as rarefaction waves within the target, and much of the shock wave energy is converted to kinetic energy by complex wave interference and interaction with the ground surface, causing an outward excavation flow that finally opens a hemispherical transient crater cavity (at a typical depth-to-diameter ratio of 1:3 to 1:4). At this stage, target rock material is partially molten and excavated from the transient cavity laterally and upward as an impact ejecta plume and displaced downward into the subcrater target (e.g., Melosh 1996; French 1998).

Thirdly, the modification stage (usually some seconds to minutes) – in contrast to the excavation stage dominated by plastic deformation and flow caused by shock compression and decompression – comprises gravity-driven rearrangement of the transient crater in dependence of the physical properties of the target rock. Whereas small craters (up to ~2-4 km in diameter on Earth) keep a simple, bowl-shaped morphology and an uplifted crater rim, larger craters (≥~2-4 km on Earth) tend to form rim terraces and central uplifts as a result of impact crater collapse accompanied by inward (and in larger craters upward) material flow in order to attain stable crater geometry (Fig. 2.1 bottom). The modification stage is generally associated with intense tectonic faulting, brecciation, and melting within the target. For further details and references on the physical and dynamical characteristics of the impact cratering process I refer to the benchmark papers and books by French and Short (1968), Melosh (1980; 1996), French (1998), and Melosh and Ivanov (1999).
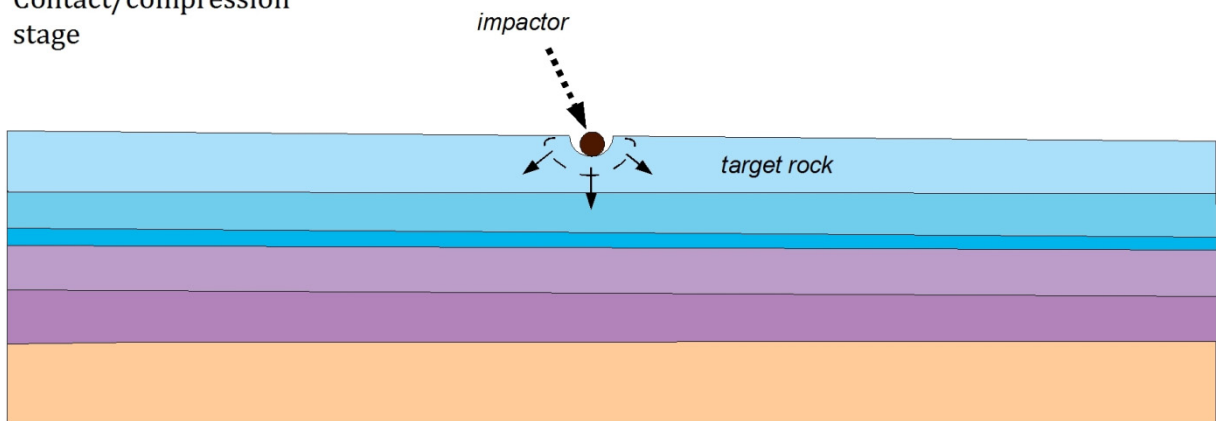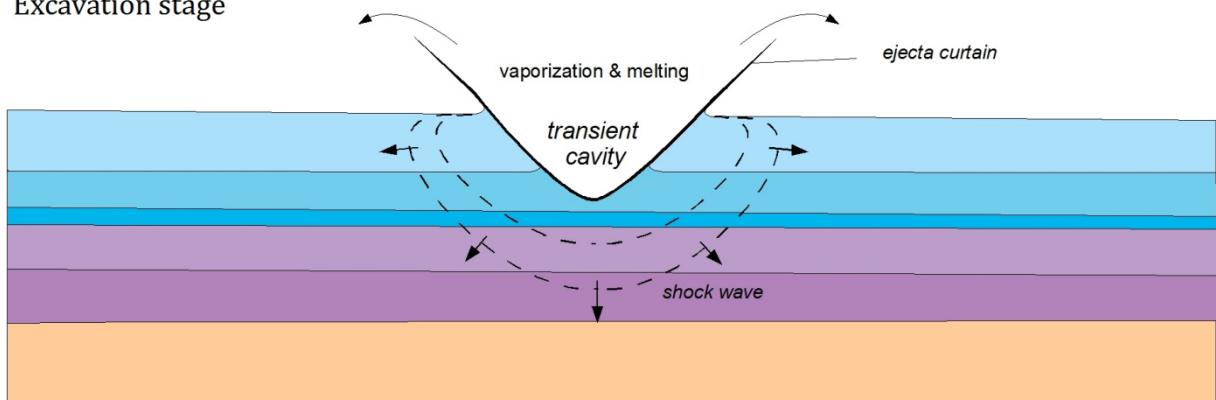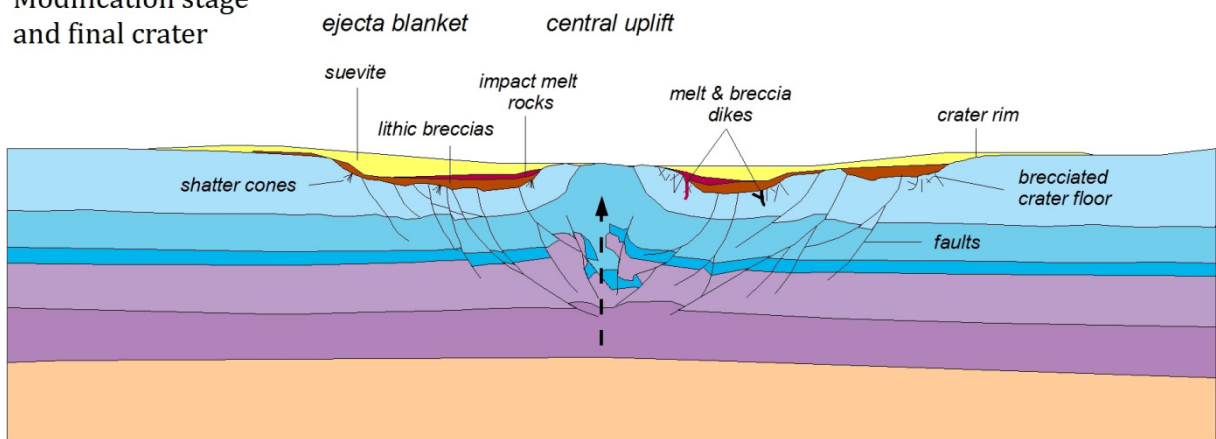
Fig. 2.1.: Schematic sequence of the impact cratering process with contact/compression stage (top), excavation stage (center), as well as the final (complex) impact crater modified by inward and upward readjustment (modified after Mattmüller 1984; Melosh 1996; French 1998).

2.2. Crater morphologies

On solid planetary bodies such as Earth, Moon, or Mars, impact craters show different morphologies depending on a combination of several major physical factors: firstly, the gravity of the host planetary body; secondly, the size, density, velocity, and impact angle of the cosmic projectile; thirdly, the type of target rock, in the way that massive crystalline rocks and porous sedimentary rocks may notably influence the final crater shape and target rock melting/vaporization processes. On Earth, impact craters with diameters of up to ~2-4 km typically occur as simple, bowl-shaped craters with a depth-to-diameter ratio of ~1:5 (French 1998). The most popular example of a simple impact crater on Earth is certainly the ~1.2 km Meteor (Barringer) Crater (Arizona, USA; e.g., Kring 2007), but also the ~0.9 km Wolfe Creek (Australia; e.g., Haines 2005), the ~1.1 km Tswaing (South Africa; Reimold et al. 1999; Fig. 2.2), or the ~1.8 km Lonar (India; e.g., Fredriksson et al. 1973) impact craters. At larger diameters exceeding about 2-4 km on Earth, impact craters tend to build up a central uplift by the elastic rebound of the target rock during the modification stage of the impact cratering process. Such types of impact craters are defined as complex craters. The threshold crater size that determines the simple-complex transition is strongly influenced by the mechanical strength of the target rock: whereas the largest terrestrial simple impact crater (Brent crater, Ontario, Canada, located in crystalline rocks of the Canadian Shield; e.g., Grieve 1978; 2006) has a diameter of ~3.8 km, the smallest complex impact structure on Earth (the BP impact structure in the Nubian Sandstone of southeastern Libya) has a distinctly smaller diameter of ~2 km (Koeberl et al. 2005). On smaller planetary bodies with lower gravity, the simple-complex transition occurs at larger crater diameters, such as at ~8-12 km on Mars and ~15-20 km on the Moon (Pike 1980a,b). Complex impact craters are generally shallower than simple craters, with a depth-to-diameter ratio of usually about 1:10 or even less. Small terrestrial complex impact craters, such as the BP structure, the ~3.8 km Steinheimer Becken (Steinheim Basin; Germany; e.g., Heizmann and Reiff 2002; Fig. 2.3), the ~5.5 km Jebel Waqf as Suwwan impact structure (Jordan; Salameh et al. 2008), or the ~10.5 km Bosumtwi impact structure (Ghana; e.g., Ferrière et al. 2008) exhibit prominent central uplifts in the form of central peaks. A special candidate is the ~5 km Goat Paddock impact structure (Australia) that appears to represent a

transitional type between simple and complex impact structures (Milton and Macdonald 2005). At larger impact crater diameters, central peaks become unstable and collapse, forming ring-shaped morphological features. The resulting impact structures are by convention referred to as central-peak-basin structures, as in the case of the ~28 km Mistastin impact structure (Labrador, Canada; e.g., Grieve 1975; 2006), and peak-ring-basin structures, such as the ~24 km Nördlinger Ries crater (Germany; e.g., Hüttner and Schmidt-Kaler 1999, Stöffler et al. 2002; Fig. 2.4), the ~36 km Clearwater West (Québec, Canada; e.g., Grieve 2006; Fig. 2.5), or the ~80 km Puchezh-Katunki impact structure (Russia; e.g., Masaitis and Pevzner 1999). The largest impact structures are multiring basins, generally shallow structures characterized by multiple concentric rings and ridges (Spudis 1993). On Earth, this type of impact structure may be represented by the largest terrestrial impact structures with diameters in excess of ~100 km, such as the Chicxulub (Mexico), Sudbury (Canada), and Vredefort (South Africa; Fig. 2.6) impact structures (e.g., French 1998; Grieve and Therriault 2000). A systematic review of the terminology and definitions related to the study of impact craters and the internal structural features is given by Turtle et al. (2005). Especially in the Russian and French literature, eroded impact structures that lost their primary crater shape are commonly referred to as 'astroblemes' (e.g., Masaitis et al. 1980; Rondot 1993).

Fig. 2.2: The ~1.1 km Tswaing crater (South Africa), a simple, bowl-shaped impact crater. Blocks in the foreground are shocked Nebo granite in the uplifted crater rim. Photograph taken on the *Large Meteorite Impacts and Planetary Evolution IV* 2008 field trip.

Fig. 2.3: The ~3.8 km Steinheimer Becken (Steinheim Basin, Germany), a small complex impact crater with central uplift. Aerial view towards the North; note the annular basin and the distinct central uplift ('Klosterberg' and 'Steinhirt'; center) with the village of Steinheim at its northern flank. Image from Google Earth.

Fig. 2.4: View across the ~24 km Ries crater (Germany), a complex impact crater with peak ring. Photograph taken at the southwestern crater rim, looking towards the center of the Ries crater. The church St. Georg at Nördlingen (with the famous 'Daniel' church tower; right of center) made of suevite rests on the inner ring of the crater; northeastern crater rim in the background. The Ries is filled with post-impact crater lake sediments.
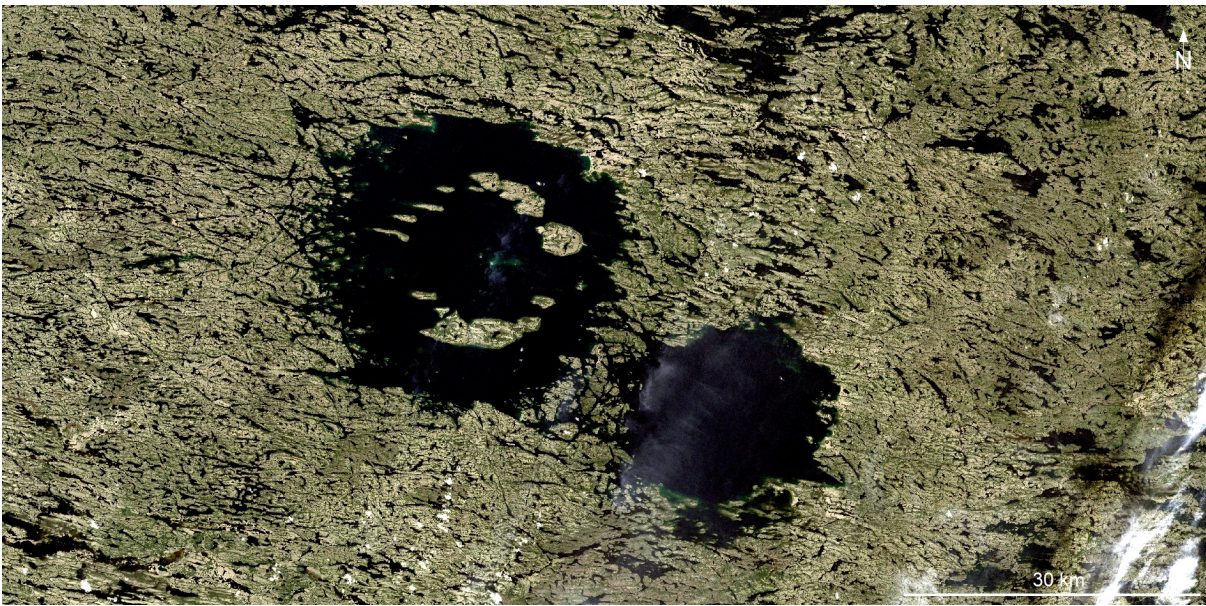
Fig. 2.5: Landsat-7 satellite image scene of the ~36 km Clearwater West (left) and ~26 km Clearwater East (right) impact structures (Québec, Canada), two complex impact structures. The islands in the Clearwater West impact structure represent the inner ring of the structure, where massive impact melt rocks occur.
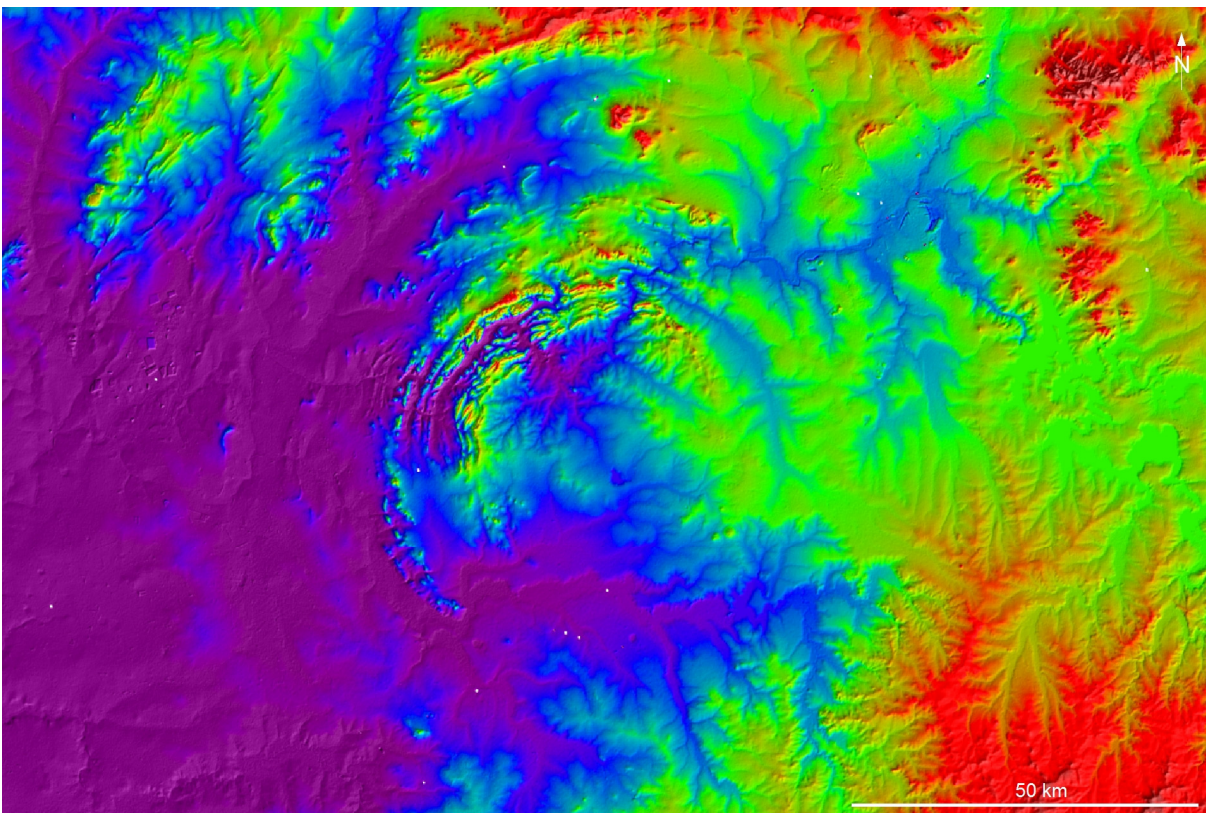
Fig. 2.6: Shuttle Radar Topographic Mission scene (color-coded terrain) of the Vredefort Dome (South Africa), the central part (diameter ~60-70 km) of the largest impact structure on Earth, most likely a multiring basin ~300 km in original diameter.

2.3. Shock metamorphic effects

When a large meteorite strikes Earth at cosmic velocity, the target rock experiences pressures and temperatures far beyond the conditions reached by usual endogenic terrestrial processes (such as ultrahigh pressure metamorphism) – within parts of seconds. For this spontaneous type of metamorphism, the term 'shock metamorphism' was created. Under shock metamorphic conditions caused by a large impact, rocks initially undergo peak shock pressures of up to ~300-400 GPa and post-shock temperatures of up to ~10,000°C near the impact point during the contact/compression stage (O'Keefe and Ahrens 1975; 1977; Melosh 1996) and up to ~60-80 GPa and ~2,000-3,000°C in larger parts of the surrounding target rocks (French 1998). A number of specific and impact-diagnostic macro- and microstructural shock metamorphic effects have been recognized to reflect the imprint of shock for specific pressure and temperature ranges in terrestrial rocks (in contrast to microdeformation features maybe related to tectonic activity; e.g., Gratz et al. 1996). Rocks affected and altered by impacts and associated shock effects are summarized as 'impactites' (at this place, I also like to mention the collection of impactites from ~60 terrestrial impact structures compiled by the author and currently stored for scientific study at the Institut für Planetologie, Universität Stuttgart). The progressive shock metamorphic conditions are subdivided into five stages (I-V) of variable shock pressure and post shock temperature ranges (Stöffler 1971; 1984; French 1998).

Initial brecciation of the rocks and the generation of breccia dikes may occur at pressures as low as <1 GPa (e.g., Okubo and Schultz 2007). At comparatively low shock pressures in the range of ~2-20 GPa (and probably higher), 'shatter cones', characteristic conical fractures in the rock are generated upon the penetration by the shock wave (Dietz 1947; 1960; French 1998; Baratoux and Melosh 2003; Sagy et al. 2004; Fig. 2.7A). Shatter cones are the only macroscopic features unequivocally diagnostic for impact in the field and are restricted to impact structures; they form in all kinds of rocks but are most conspicuous in homogenous, fine-grained lithologies. The smallest shatter cones may be at the scale of some millimeters to centimeters but the largest shatter cones known on Earth may reach several meters in size (e.g., those at the Charlevoix impact structure, Québec, Canada; or at the Slate Islands impact structure,

Ontario, Canada; Dressler et al. 1999). Some terrestrial impact structures are 'confirmed' based on the presence of shatter cones alone (whereas other diagnostic shock effects are missing), for example, the Île Rouleau impact structure, Québec, Canada (e.g., Grieve 2006) or the recently detected Santa Fe impact structure, New Mexico, USA (Fackelman et al. 2008). Due to the fine-grained nature of the host limestones, the shatter cones at the Steinheim Basin, Germany (already described by Branco and Fraas in 1905; see also Heizmann and Reiff 2002) count among the most typically developed shatter cones worldwide (Fig. 2.7A).

As the most widespread minerals in upper crustal rocks, quartz (SiO_2) and feldspar (orthoclase: $KAlSi_3O_8$; albite: $NaAlSi_3O_8$; anorthite: $CaAl_2Si_2O_8$) represent the most representative crystalline phases that can record shock effects in terrestrial impactites. At shock pressures in the range of ~5-10 GPa (shock stage I after Stöffler 1971; 1984), planar fractures (PFs), open fractures mainly parallel to the (0001) basal (pinacoid) plane and the {10-11} rombohedron crystal plane, as well as Brazil twins along (0001) are developed in quartz (e.g., French 1998). Another low-pressure shock feature in quartz are 'feather textures', which consist of thinly spaced planar lamellae that branch off from a main planar fracture; these features also indicate shock pressures of ~5-10 GPa (Poelchau and Kenkmann 2009; Fig. 2.7B). At pressures above ~10 GPa, quartz is characterized by the presence of planar deformation features (PDFs), closely spaced (typically ~2-10 μm) and narrow (usually <3 μm) planar lamellae parallel to the {10-13} rombohedron plane, usually filled with an amorphous silica glass phase and minute inclusions of high pressure silica polymorphs (e.g., Alexopoulos et al. 1988; Goltrant et al. 1991; French et al. 1998). At pressures of >20 GPa, additional sets of PDFs occur in quartz, mainly along the rombohedron (e.g., {10-12}, {10-11}), prism (e.g., {10-10}), trapezohedron (e.g., {51-61}), and dipyramid (e.g., {11-22}) crystal planes (e.g., Stöffler and Langenhorst 1994; Langenhorst 2002), and a total of up to 18 individual sets of PDFs have been recognized in a strongly shocked single quartz crystal (Montanari and Koeberl 2000). Planar deformation features in quartz may appear as either faint, sharp lamellae ('undecorated' PDFs) or lamellae traced by small fluid inclusions ('decorated' PDFs; Fig. 2.7C). Planar fractures, planar deformation features, and feather textures can be summarized as planar microstructures in quartz. Specific features of shocked quartz

grains that exhibit multiple sets of PDFs are mosaicism (internal disturbances in the quartz lattice) and the 'toasting effect' caused by numerous tiny vesicle and fluid inclusions incorporated during post-shock annealing (Ferrière et al. 2009b; cf. Whitehead et al. 2002). Planar deformation features and mechanical twinning are also known in feldspar (Fig. 2.7D). At shock pressures of >12-15 GPa, stishovite, a dense silica polymorph is formed from quartz. Likewise, coesite is formed from quartz at pressures above ~30 GPa (e.g., Stöffler and Langenhorst 1994; French 1998; Stähle et al. 2008); this is in strong contrast to endogenic crustal deformation where coesite crystallization starts at lithostatic pressures exceeding ~2 GPa, which underlines the particular time-pressure-temperature conditions of shock metamorphism. As a well-known exemplary case, the detection of coesite in impactites led Chao et al. (1960) and Shoemaker and Chao (1961) to propose that the Ries crater (Germany) represents an impact structure. At pressures exceeding ~35 GPa (shock stage II after Stöffler 1971; 1984), quartz and feldspars undergo a (from ~25 GPa onward successive) solid-state transition to amorphous diaplectic glass (e.g., von Engelhardt 1972; Stöffler and Hornemann 1972; Stöffler 1972; 1974; 1984; Stöffler and Langenhorst 1994; Grieve et al. 1996) of lowered density; diaplectic feldspar (plagioclase) glass is also referred to as maskelynite commonly found in meteorites but also in terrestrial impact structures (such as the Ries, Germany; or Manicouagan, Québec, Canada, where the central uplift of the structure is today represented by the Mont Babel and 'Maskelynite Peak' mountains; e.g., Bunch et al. 1967). As no silica (and whole-rock) melting is achieved at these pressures and post-shock temperatures below ~900°C, the original (sometimes even idiomorphic) crystal shape and internal microstructures are commonly preserved in diaplectic glasses (Fig. 2.7E). At shock pressures above ~45 GPa (shock stage III after Stöffler 1971; 1984) and concomitant post-shock temperatures of >900°C, feldspars melt, transform to normal glasses, and commonly recrystallize to spherulitic aggregates (Bischoff and Stöffler 1984). Above shock pressures of ~60 GPa (shock stage IV after Stöffler 1971; 1984), partial to complete melting of silica and rocks is achieved at post-shock temperatures exceeding ~1,500°C; lechatelierite, fluidal silica glass (Fig. 2.7F) commonly rich in vesicles and traces of unmolten crystal domains and inclusions ('schlieren') is formed. A microstructural feature indirectly suggestive of shock metamorphism is 'ballen silica' (Fig. 2.7F) that may occur as 'fish-scale'-textured

α-cristobalite or α-quartz and which forms at high post-shock temperatures exceeding ~1,000-1,200°C (in response to stage III-IV shock). Whereas ballen-textured cristobalite was also observed in siliceous volcanic rocks (Schmieder et al. 2009a), ballen quartz (with variable optical properties) appears to be restricted to impactites. The formation of ballen quartz is commonly explained by the transformation of α-quartz to β-cristobalite at temperatures >1,000°C (1,470°C in the pure silica system) and backward transformation to α-quartz via α-cristobalite (along with volume shrinkage and ballen formation) upon cooling (e.g., Carstens 1975). A recent summary of ballen silica is given by Ferrière et al. (2009a). At the highest shock pressures (>100 GPa) and post-shock temperatures (>2,500°C) the target rock is vaporized (shock stage V after Stöffler 1971; 1984) and may be subsequently condensed to impact glasses, such as tektites and microtektites (e.g., French 1998; Dressler and Reimold 2001; Artemieva 2002). The decreasing stage of shock metamorphism with increasing distance from the impact point allows shock zoning studies in (eroded) terrestrial impact structures (e.g., Lambert 1977; Dressler 1990).

The above shock pressure and post-shock temperature calibrations are mainly suitable for crystalline crustal rocks. In contrast to crystalline rocks, sedimentary rocks – exemplified by sandstones and carbonates – show a specific shock behavior. Due to their porosity responsible for shock wave attenuation and pronounced heat generation, sandstones strongly tend to melt at significantly lower post-shock temperatures than do crystalline rocks, with lechatelierite being formed from quartz at peak shock pressures as low as ~13-30 GPa and post-shock temperatures of ≥~950 GPa (Kieffer 1971; Stöffler 1972, 1984; Grieve et al. 1996; French 1998; Stöffler and Grieve 2007). Carbonates undergo melting at shock pressures of >~10 GPa and post-shock temperatures of >~1,700°C, causing the formation of 'feathery textures' in calcite after quenching of the carbonate melt (e.g., Jones et al. 2000; Osinski and Spray 2001; Salge 2007; Fig. 2.7G). A widespread accessory mineral in crustal crystalline and sedimentary rocks, zircon ($ZrSiO_4$), also exhibits a set of distinctive shock features, for example, the formation of planar microstructures (Fig. 2.7H) and the high pressure polymorph reidite at shock pressures in excess of ~20 GPa, the decomposition to SiO_2 and ZrO_2 polymorphs (baddeleyite) at post-shock temperatures exceeding ~1,700°C, and the development of

granular textures (e.g., El Goresy 1965; Bohor et al. 1993; Corfu et al. 1993; Leroux et al. 1999; Glass et al. 2002; Wittmann et al. 2006). As impact structures in (ultra-)basic crystalline target rocks are scarce on Earth, the shock metamorphism of olivine $((Fe,Mg)_2SiO_4)$, pyroxenes (augite: $(Ca,Mg,Fe)SiO_3$), and others have been largely studied in stony meteorites (e.g., Stöffler et al. 1991). However, the presence of some impact structures in basaltic (e.g., Lonar, India; Logancha, Russia; or Vargeão, Brazil) and anorthositic (e.g., Manicouagan, Québec, Canada) target rocks also provide some additional information on the shock metamorphism of silica-poor rocks on Earth (e.g., Fredriksson et al. 1973; Kieffer et al. 1976; Vishnevsky 1986; Crósta et al. 2005, Osae et al. 2005). Graphite in the target rocks can be converted to impact diamonds upon shock (e.g., at the large Popigai impact structure, Siberia, Russia; Koeberl et al. 1997c; Montanari and Koeberl 2000). Thorough reviews of shock metamorphic effects in terrestrial impactites and minerals are given by French and Short (1968), von Engelhardt et al. (1969), Stöffler and Langenhorst (1994), Grieve et al. (1996), French (1998), Montanari and Koeberl (2000), and Langenhorst (2002).

2.4. Other impact signatures

In addition to macro- and microstructural shock features in rocks and minerals, terrestrial impact structures are commonly associated with geophysical anomalies, such as incoherent seismic reflections and low-velocity signatures attributed to subsurface brecciation and faulting, as well as local gravity and magnetic anomalies (predominantly lows) that truncate the regional fabric; detailed reviews and case studies on the geophysical signature of impact structures are given by, e.g., Pilkington and Grieve (1992), Grieve and Pilkington (1996), Plado et al. (1996; 1999), Brittan et al. (1999), Tsikalas et al. (1999), Werner et al. (2002), and Grieve (2006). The admixture of projectile matter to impact melt rocks and breccias sometimes causes more or less distinctive geochemical anomalies, such as enrichment in nickel, cobalt, chromium, and/or platinum group elements in the rocks (e.g., Schmidt et al. 1997; Koeberl 1998; Tagle and Hecht 2006). For example, the impact melt lithologies of the Rochechouart impact structure (France) are characterized by a strong enrichment in nickel with

respect to the surrounding target rocks (e.g., Lambert 1975; 2009), whereas the resurge deposits of the Lockne impact structure (Sweden) contain comparatively high amounts of extraterrestrial chromite (Alwmark and Schmitz 2007). Likewise, the Chicxulub impact (Mexico) at the Cretaceous/Paleogene boundary is linked with the widely known globally distributed iridium anomaly (e.g., Smit and Hertogen 1980; Bohor et al. 1984; Montanari and Koeberl 2000).

Fig. 2.7 (next page): Macroscopic and microscopic shock features in rocks and minerals at terrestrial impact structures. **A**: Well-developed shatter cone in limestone (Steinheim Basin, Germany); **B**: planar fractures (PFs) and 'feather textures' in quartz in a lithic impact breccia (Rochechouart, France; cross-polarized light); **C**: shocked quartz with two distinct sets of (decorated) planar deformation features (PDFs) in an impact melt rock (Suvasvesi South, Finland; plane-polarized light); **D**: shocked feldspar with PDFs in suevite (Manicouagan, Québec, Canada; cross-polarized light); **E**: diaplectic quartz glass that retained the original shape of a mountain crystal in suevite (Logoisk, Byelorussia; cross-polarized light; partially tilted polarizers); **F**: fluidal silica (former lechatelierite) recrystallized to 'ballen quartz' in suevite glass (Dellen, Sweden; plane-polarized light); **G**: carbonate melt droplets in impact melt rock (Tenoumer, Mauritania; cross-polarized light); **H**: shocked zircon with planar microfeatures in impact melt rock (Manicouagan, Québec, Canada; cross-polarized light).
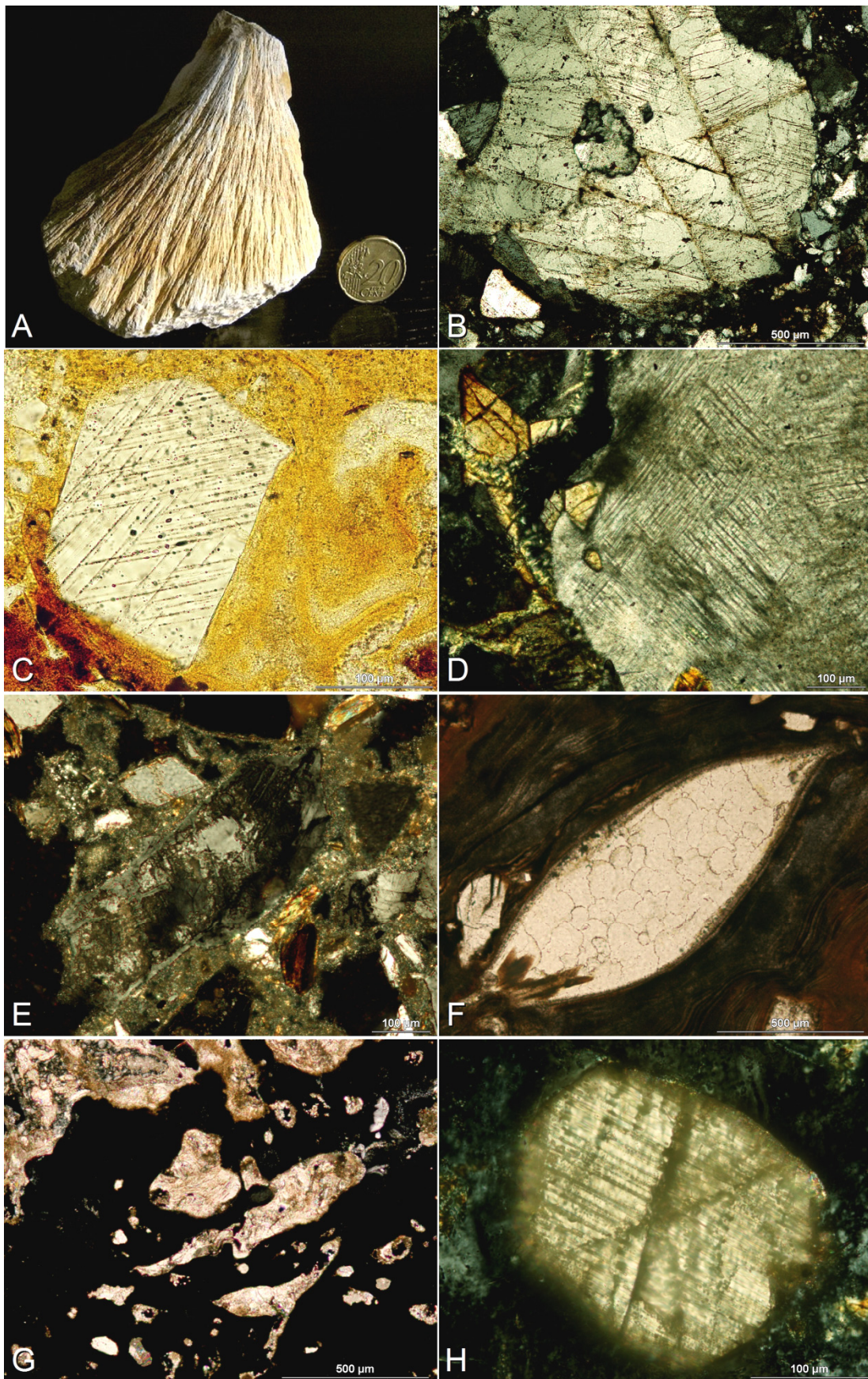
2.5. Impactite classification

Two main groups of impactites can be distinguished: proximal and distal impact ejecta. Proximal ejecta occur within ejecta blankets in and outside the actual impact structures within a distance of five crater radii (e.g., the well-known impact crater deposits at the Ries crater, Germany) and are further subdivided into parautochthonous (to autochthonous) and allochthonous impactites, i.e., shocked rocks that largely remained in their original position and deposits replaced during the excavation and modification stage of the cratering process, respectively. Autochthonous and parautochthonous impactites usually occur within the crater basement or are structurally linked with the actual crater floor, such as massive shocked basement rocks or predominantly monomictic lithic impact breccias made up of target rock fragments. Allochthonous impactites comprise a set of lithologies: monomictic or polymictic (depending on the target rock composition) lithic impact breccias (Fig. 2.8A-B) are mainly composed of mineral and rock debris; they occur as mixed target rock material displaced from the original position during excavation or as breccia dikes in the crater basement (e.g., Abadian 1972; Lambert 1981a; Heizmann and Reiff 2002). Suevites, lithic impact breccias that contain aerodynamically shaped impact melt (glass) particles ('flädle'; see Hörz 1965; Hüttner and Schmidt-Kaler 1999; Fig. 2.8C-D), are air-fall deposits produced by the collapsing impact ejecta plume during the excavation stage; the type locality for this rock (suevite = 'the rock of Swabia'; Sauer 1901; Fraas 1919) is the old Altebürg quarry at the Ries crater (Germany; see also Buchner and Schmieder 2009b for a recent brief compilation of suevites from a number of impact structures worldwide). Clast-free, clast-poor, or clast-rich impact melt rocks (e.g., Dressler and Reimold 2001), with a glassy to crystalline melt groundmass, predominantly occur as sheets or lenses within the crater-filling breccia lens or as dikes injected into the crater floor (Fig. 2.8E-I). A special type of melt rocks, generated by friction melting mainly during the modification stage of the cratering process (but probably also during the compression stage) are pseudotachylitic breccias in the shocked crater basement (e.g., Dressler and Sharpton 1997; Kelley and Spray 1997; Melosh 2005; Reimold and Gibson 2005; 2006; Lieger et al. 2009; see also Shand 1916 for original description of this rock type; Fig. 2.8K-L). Distal impact ejecta generally form more or less thin layers of shocked and unshocked

rock debris, minerals, and impact melt particles at distances of >5 crater radii away from the source crater (tektites and spherule layers; e.g., Simonson and Glass 2004); they are of outstanding importance in impact stratigraphy, because impact layers can pinpoint the corresponding impact event in the stratigraphic column, such as the spherule layer in the Upper Triassic of Britain (Walkden et al. 2002; Thackrey et al. 2009), microtektites and microkrystites in the Cretaceous/Paleogene boundary ejecta layer (e.g., Glass and Burns 1988; Smit 1999; Claeys et al. 2002), distal impact ejecta in the Upper Eocene (e.g., Montanari and Koeberl 2000), the Ries tektites in Miocene sediments of Central Europe (Lange 1996; Stöffler et al. 2002; Fig. 2.8M), or the Pleistocene Ivory Coast tektites (Koeberl et al. 1997b), just to mention some.
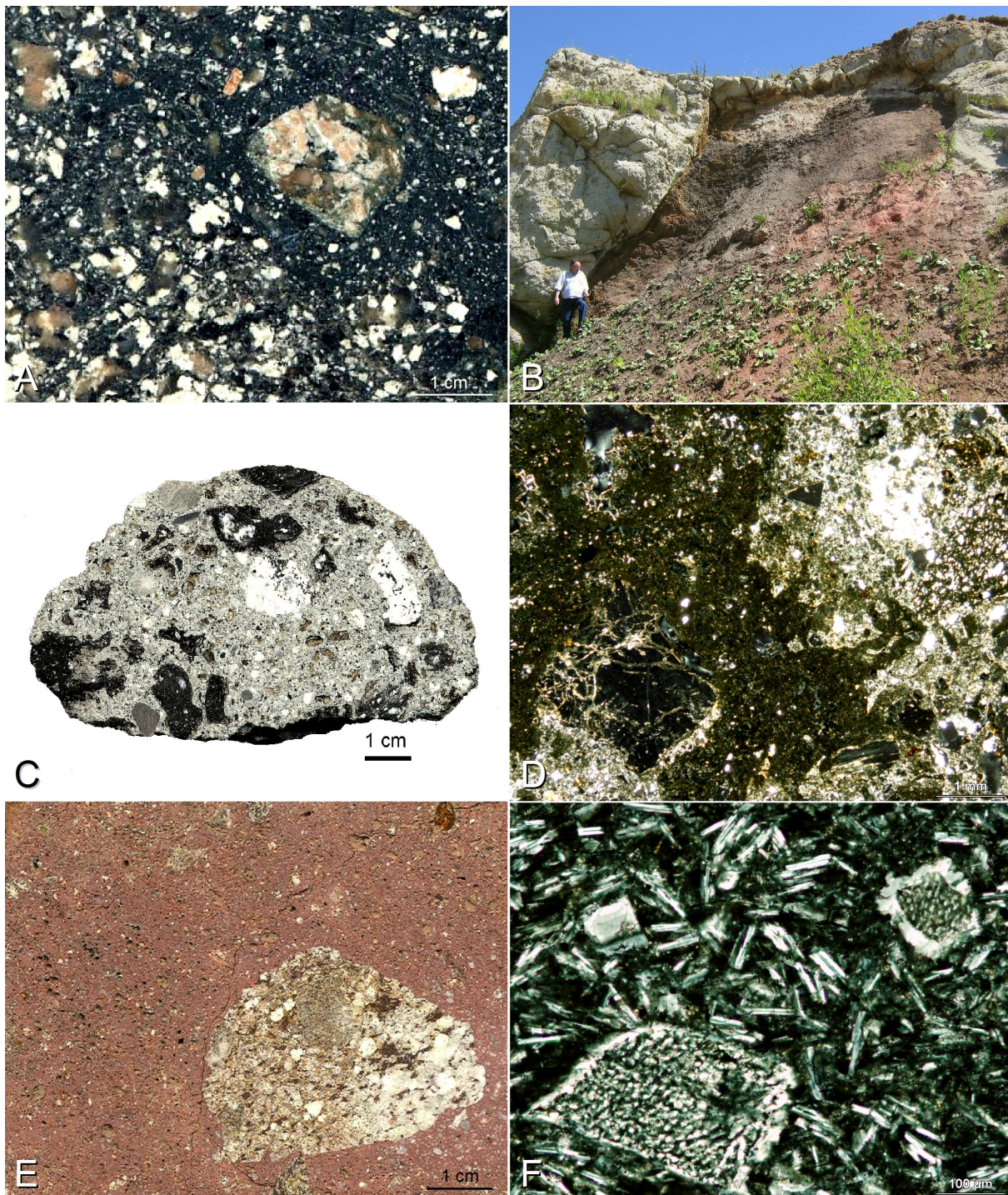
Fig. 2.8: Impactites. **A**: Lithic impact breccia mainly composed of crystalline rock and mineral fragments (Söderfjärden, Finland; polished section); **B**: lithic impact breccia ('Bunte Breccia'; dark) overlain by suevite (bright; Ries crater Germany); **C**: suevite with dark impact glass particles ('flädle') and bright crystalline rock clasts within a fine-grained lithic groundmass (Logoisk, Byelorussia drill core sample); **D**: thin section photomicrograph of suevite with dark (isotropic) impact glass and lithic groundmass (Bosumtwi, Ghana; cross-polarized light); **E**: impact melt rock with granite clast (Ries crater, Germany; polished section); **F**: thin section photomicrograph of impact melt rock with an aphanitic crystalline matrix and larger feldspar crystals (Mistastin, Labrador, Canada; cross-polarized light).
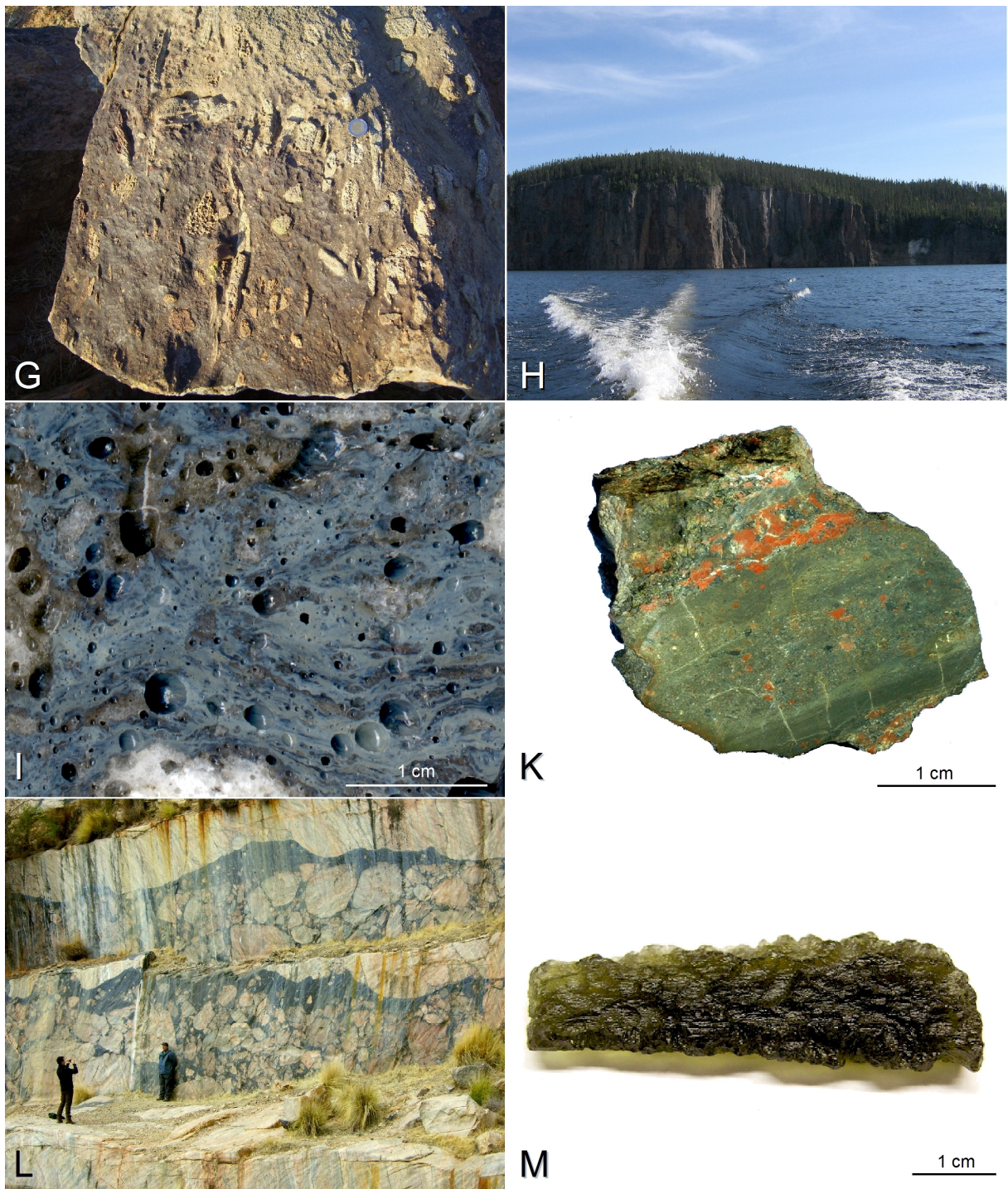
Fig. 2.8 (continued): **G**: impact melt rock emplaced as a dike in the crater floor (Vredefort, South Africa; 'Vredefort Granophyre'; coin for scale); **H**: impact melt rocks of a thick melt sheet with lithic limestone megaclast (bright; Manicouagan, Québec, Canada); **I**: fluidal impact glass with numerous vesicles (Wabar, Saudi Arabia); **K**: pseudotachylitic breccia (Keurusselkä impact structure; Finland; polished section); **L**: large-scaled pseudotachylitic breccia at the Leeukop quarry (Vredefort, South Africa); **M**: moldavite from the Central European (Ries) tektite strewn field.

The general succession of proximal impactites at terrestrial impact structures is basal autochthonous to parautochthonous lithic breccias overlain by a sheet or lenses of coherent impact melt rocks and, finally, suevite (fallback/crater suevite within the actual impact crater and fallout suevite outside the crater within the proximal ejecta blanket; e.g. French 1998; Stöffler and Grieve 2007), sometimes topped by fine-grained air-fall deposits (e.g., Lambert 1977; 2009). Whereas the basal lithic impact breccias are commonly affected by rather weak shock (shock stage I or lower), suevites and impact melt rocks show features that correspond to higher stages of shock metamorphism (shock stages I-IV). One of the best preserved larger terrestrial impact structures, the ~24 km Ries crater (Germany) displays a complete suite of proximal and distal impact ejecta, with basal lithic impact breccias ('Bunte Brekzie' and 'Kristallinbrekzie') overlain by local impact melt rocks and suevite in its ejecta blanket, as well as tektites at distances of up to ~450 km (Central European tektites; 'moldavites') away from the Ries crater (e.g., Hüttner and Schmidt-Kaler 1999; Stöffler et al. 2002). However, even eroded impact structures may preserve the original suite of impactites, such as the ~25 km Rochechouart impact structure (France), where basal lithic breccias, impact melt rocks, and suevites are still accessible in the field (Lambert 1977; 2009). A systematic classification scheme for terrestrial impactites is given by Stöffler and Grieve (2007). Further thoughts on impactite nomenclature (and recent problems and debates) are provided by Reimold et al. (2008), Osinski et al. (2008a,b), and Osinski and Grieve (2009).

3. Theoretical and technical background

3.1. Background theory – the Late Triassic multiple impact scenario

The background hypothesis on which this thesis is based on was postulated more than ten years ago when Spray et al. (1998) suggested that a large, roughly 4,500 km-long impact crater chain was produced by the multiple impact of a fragmented asteroid in the Late Triassic, about 214 Ma ago, similar to the spectacular impact of the fragmented comet Shoemaker-Levy 9 on Jupiter as revealed by the Hubble Space Telescope in summer 1994 (Orton et al. 1995; Levy 1998; Fig. 3.1). The postulated Triassic impact crater chain comprises the ~100 km Manicouagan impact structure (Québec, Canada), the ~40 km Lake Saint Martin impact structure (Manitoba, Canada), the ~25 km Rochechouart impact structure (France), the ~20 km Obolon impact structure (Ukraine), and the ~9 km Red Wing Creek impact structure (North Dakota, USA); the ~12 km Wells Creek (Tennessee, USA; e.g., Stearns et al. 1968), and the ~3 km Newporte (North Dakota, USA; Koeberl and Reimold 1995b) impact structures were considered possible additional candidates. Plotted on Late Triassic paleogeographic maps, the three largest of these impact structures, Manicouagan, Lake Saint Martin, and Rochechouart, were co-latitudinal at 22.8° N, within a paleolongitude span of ~43.5°. In addition, the Rochechouart and Obolon, as well as the Lake Saint Martin and Red Wing Creek structures, respectively, lie on great circles with a declination of 37.2° (Fig. 3.2). This particular arrangement, supported by statistical probability tests (Monte Carlo simulations), led Spray et al. (1998) to propose that the members of this hypothetical impact crater chain were struck at the same time – probably within hours – which was in accord with stratigraphic and isotopic ages available for these impact structures in 1998 (Manicouagan 214 ± 1 Ma, Hodych and Dunning 1992; Rochechouart 214 ± 8 Ma, Kelley and Spray 1997; Lake Saint Martin 219 ± 32 Ma; Reimold et al. 1990; Obolon 215 ± 25 Ma, Masaitis et al. 1980; and Red Wing Creek ~200 ± 25 Ma; Gerhard et al. 1982). The multiple impact theory was subsequently followed by Walkden et al. (2002).

Like the postulated Late Triassic multiple impact system proposed by Spray et al. (1998), two other possible impact crater chains had previously been postulated on Earth, such as a chain composed of eight Paleozoic structures (two of which, Crooked

Creek and Decaturville, Missouri, USA, are proven impact structures) in the eastern USA (Rampino and Volk 1996; see also Evans et al. 2008) and another suspected crater chain linked with the Paleozoic Aorounga impact structure in Chad, Africa (Ocampo and Pope 1996). However, both crater chains are doubtful because of the lack of unequivocal signs of shock in the rocks at the candidate structures (e.g., Melosh 1998).
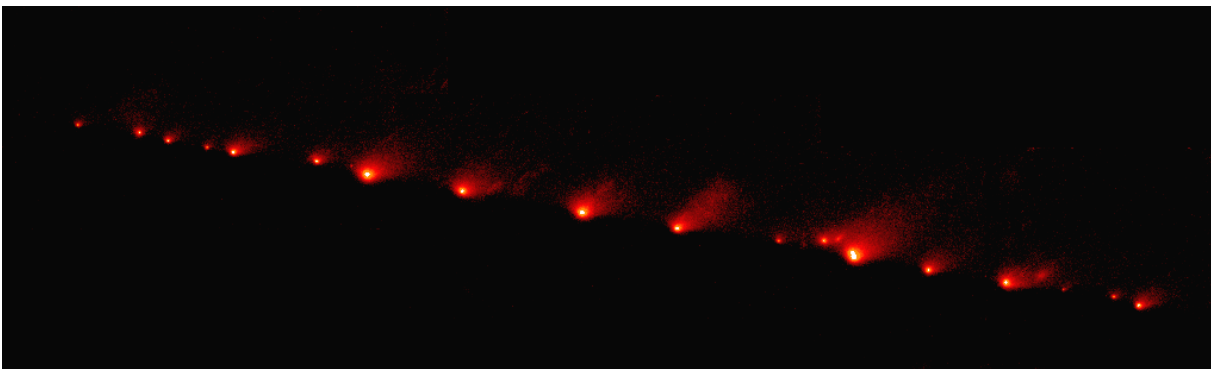
Fig. 3.1: Chain of at least 23 impact plumes caused by the impact of comet Shoemaker-Levy 9 on Jupiter as observed in summer 1994. Image: Hubble Space Telescope.
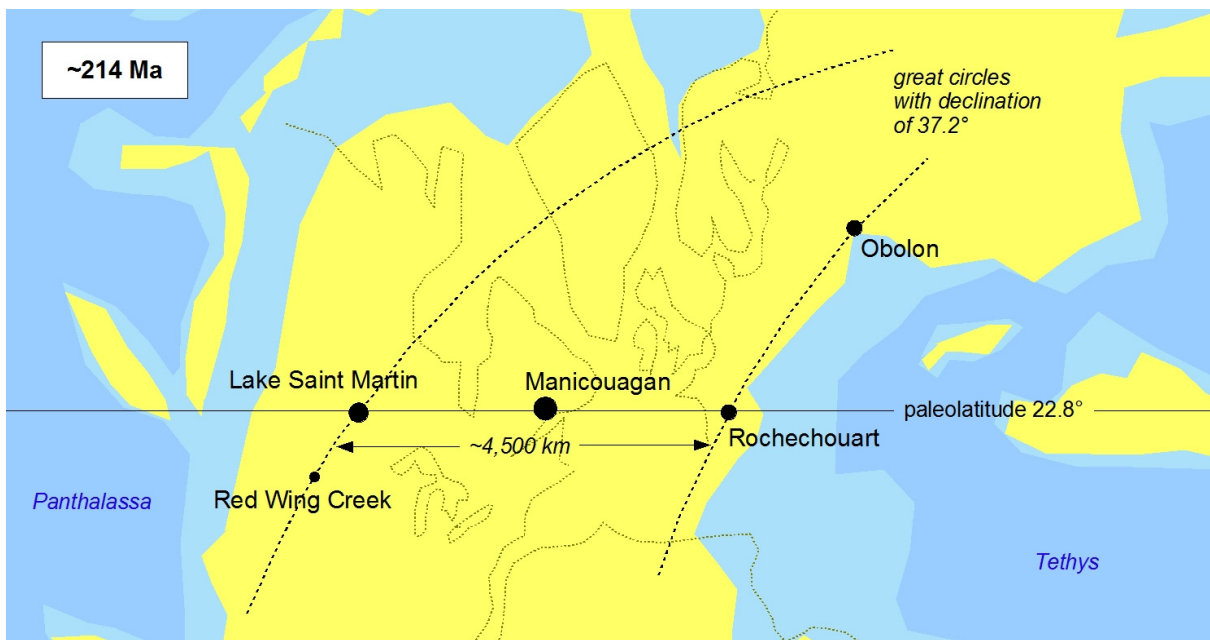
Fig. 3.2: Postulated Late Triassic multiple impact scenario as proposed by Spray et al. (1998; modified).

3.2. Aims and scopes of this study

In order to properly discuss the theory postulated by Spray et al. (1998) and as impact craters as members of a single crater chain must have identical ages (e.g., Bottke et al. 1997), the precise determination of impact ages is critical to the interpretation of possible multiple impact systems. This thesis focuses on the dating of the Rochechouart and Manicouagan impact structures by isotopic methods, as well as a discussion of the impact ages with respect to the paleogeographic and paleoenvironmental conditions at the impact sites. $^{40}Ar/^{39}Ar$ ages for Rochechouart and Manicouagan are set in the context of the Late Triassic multiple impact theory in order to provide unequivocal proof or disproof of the crater chain hypothesis on the basis of robust geochronological data. The age of the Lake Saint Martin impact structure is discussed against the background of recent (U-Th)/He age data; in the case of the Obolon impact structure, the impact age is discussed within an approach of 'paleogeographic dating'. As a secondary focus, the novel description of impact melt rocks and a new $^{40}Ar/^{39}Ar$ age are reported for the Paasselkä impact structure (Finland) and discussed in the context of the Triassic impact cratering record on Earth.

3.3. Dating of terrestrial impact structures – technical background

A number of techniques have been used to determine the formation ages of impact structures on Earth. The easiest way to date impact craters is (bio-)stratigraphic dating, by which a certain time difference between the formation of the youngest pre-impact rocks (the actual target rocks in the strict sense) and the oldest syn- to post-impact rocks (e.g., rock clasts and fossils in the impact breccias and crater lake sediments) is noted and calibrated against international stratigraphic time scales (Ogg et al. 2008). A number of terrestrial impact structures are dated by stratigraphic techniques, and many of them are associated with large errors, for example, the Kursk impact structure (Russia; stratigraphically dated at 250 ± 80 Ma; Masaitis 1999) or the Wells Creek impact structure (Tennessee, USA; stratigraphically dated at 200 ± 100 Ma; Grieve 1991). In some cases, mainly at eroded impact structures that lack the primary crater infill and post-impact sediments, only the age of the target rock is known, which

provides a maximum impact age; this was the case at the Paasselkä impact structure, Finland, which formed in Paleoproterozoic rocks of the Baltic Shield that constrained an impact age of $<\sim$1.88 Ga (e.g., Pesonen et al. 1999b). Other impact structures are associated with stratigraphic ages of apparent high precision, such as the Puchezh-Katunki impact structure, Russia, which was dated at 167 ± 3 Ma based on palynostratigraphic methods (Masaitis 1999; Masaitis and Pevzner 1999; Schmieder and Buchner 2008). However, stratigraphic ages of high precision should be used with care, at least because of the poor international intercalibration of the biostratigraphic timescale.

In contrast to 'relative' stratigraphic dating, isotopic dating techniques provide 'absolute' ages of variable accuracy (geologic truth of the age obtained) and precision (degree of reproducibility). The dating techniques applied on terrestrial impactites mainly comprise the following methods: potassium-argon (K/Ar; e.g., French et al. 1970; Wolfe 1971; 1972; Alexandre et al. 2009) and argon-argon (^{40}Ar/^{39}Ar; e.g., McDougall and Harrison 1999; see below), rubidium-strontium (Rb/Sr; e.g., Reimold and Oskierski 1987), uranium-lead (U/Pb, e.g., Hodych and Dunning 1992; Kamo et al. 1996; Kalleson et al. 2009), apatite and glass fission track dating (e.g., Wagner and Storzer 1975), thermoluminescence dating (e.g., Prescott et al. 2004), cosmogenic nuclides (e.g., Phillips et al. 1991), paleomagnetic dating (e.g., Pesonen et al. 1999b; Werner et al. 2002; Carporzen and Gilder 2006), and, rather recently, uranium-thorium-helium (U-Th)/He dating (van Soest et al. 2009; Wartho et al. 2009; see also Farley 2002; Farley and Stockli 2002; Ehlers and Farley 2003; Min et al. 2003; Reiners et al. 2004; Reiners 2005). From long-time experience with isotopic dating of terrestrial impact structures through the past decades, K/Ar, Rb/Sr, fission track, and paleomagnetic dating are widely considered as poor geochronometers, and ages obtained using these methods are largely not robust and sometimes even geologically meaningless (sometimes the exception proves the rule); this particularly holds true for rocks that were not completely homogenized during impact melting or impactites altered subsequent to the impact event (Deutsch and Schärer 1990).

^{40}Ar/^{39}Ar dating (based on the K/Ar isotopic system) has commonly yielded high-precision (and accurate) ages compatible with results obtained by other methods and

biostratigraphy. Given that most crustal rocks on Earth contain more or less high amounts of potassium, this technique is best suitable when impact-generated silicatic melts are dated, preferably impact melt rocks and glasses. Also, U/Pb dating of uranium-bearing minerals newly grown (or overgrown along rims) in impact melt rocks, such as zircon or titanite, has yielded precise ages (e.g., Hodych and Dunning 1992; Kamo et al. 1996; Corfu et al. 2003; Ramezani et al. 2005; Davis 2008). A complete detailed description of the dating techniques listed above would go far beyond the scope of this thesis; I refer to the benchmark papers by Bottomley et al. (1990), Deutsch and Schärer (1990), and Jourdan et al. (2009b) on the dating of terrestrial impact structures, which provide details on the specific isotopic systems and dating techniques, potential problems encountered during dating, as well as on approaches and solutions towards the reasonable interpretation of the dating results.

3.4. $^{40}Ar/^{39}Ar$ dating

All impactite samples dated in this study were analyzed using the $^{40}Ar/^{39}Ar$ stepwise heating method, which is addressed in some more detail in the following lines. The $^{40}Ar/^{39}Ar$ method is directly derived from the K/Ar method (e.g., Faure 1986). Potassium naturally occurs in three isotopes, stable ^{39}K (~93.3%), unstable (radioactive) ^{40}K (~0.01%), and stable ^{41}K (~6.73%); ^{40}K decays to ^{40}Ca (~89.5%) and ^{40}Ar (~10.5%) within a half time of 1.25 billion years (e.g., Steiger and Jäger 1977). The main stable isotopes of argon on Earth are ^{40}Ar (~99.6%), ^{36}Ar (~0.34%), and ^{38}Ar (~0.06%). ^{39}Ar and ^{37}Ar are unstable isotopes with a half life of ~269 years and ~35 days, respectively; except for ^{39}Ar in rocks exposed to cosmic rays (e.g., meteorites), ^{39}Ar does not naturally occur in terrestrial rocks. Radiogenic ^{40}Ar ($^{40}Ar*$) produced from ^{40}K is trapped in natural minerals, rocks, and glasses of variable argon retentivity, depending on their specific closure temperature, below which no significant amounts of argon are lost from the crystal lattice (or amorphous glass structure) over geologic time. The isotopic system (i.e., the internal 'clock') may, however, be reset (or at least disturbed) by thermal events, such as metamorphism or impact, causing the complete (or partial) release of ^{40}Ar from the host phase (e.g., McDougall and Harrison 1999).

In the ^{40}Ar/^{39}Ar method, a portion of ^{39}K in the dating material is converted to radioactive ^{39}Ar by neutron irradiation in a nuclear reactor, as introduced by Merrihue and Turner (1966). The measurement of ^{39}Ar in an argon mass spectrometer, therefore, reflects the original content of potassium in the rock or mineral, and the ratio of the radiogenic daughter product ^{40}Ar* to ^{39}Ar (together with ^{37}Ar, ^{38}Ar, and ^{40}Ar) can be measured in the same sample. This constitutes a practical technical advantage over conventional K/Ar dating, where the ^{40}K and ^{40}Ar must be measured separately, and gives improved accuracy and precision. A standard (monitor) of known and intercalibrated age, e.g., the 328.5 ± 1.1 Ma (1σ) BMus/2 'Bärhalde muscovite' standard (Black Forest, Germany; Schwarz and Trieloff 2007), irradiated together with the impactite sample determines the J value as a parameter representative of the neutron fluence during irradiation. Similar to the age calculation in the conventional K/Ar dating technique, the resulting ^{40}Ar*/^{39}Ar ratio is proportional to the age t of the dating sample:

$$t_{sample} = 1/\lambda \bullet \ln \left[1 + (^{40}Ar*/^{39}Ar) \bullet J\right]$$

where λ = 5.543 • 10^{-10} a^{-1} (K decay constant recommended by Steiger and Jäger 1977)

$$and\ J = (e^{\lambda t_{standard}} - 1)/(^{40}Ar*/^{39}Ar)_{standard}$$

^{40}Ar/^{39}Ar Dating is carried out by the stepwise heating of the purified (e.g., acid-leached) impactite sample in a high-vacuum furnace (typically up to ~1,500°C), by which portions of the argon trapped in the rock are consecutively released. The ^{40}Ar/^{39}Ar age is calculated using the K decay constants by Steiger and Jäger (1977, see above equations and following chapters for discussion) and corrected for mass discrimination, argon decay, isotopic interferences (e.g., interferences on various argon isotopes due to neutron irradiation of Ca, K, Ar, and Cl in the sample; see McDougall and Harrison 1999), and extraction line blanks (details on these parameters are given in the respective chapters and 'samples and analytical techniques' subsections and in the argon isotopic tables). The cumulative stepwise release of ^{39}Ar is usually displayed in a ^{40}Ar/^{39}Ar age spectrum, which, in the ideal case, yields a 'plateau' of a number of consecutive 'step ages' identical within error (see chapters 5, 6, and 8); in agreement with the criteria for defining plateaux in ^{40}Ar/^{39}Ar geochronology, at least 50% (70%) of the total ^{39}Ar released must yield concordant (overlapping) ages at the 2σ (95% confidence) level

within at least five consecutive steps. In some cases, post-shock loss of radiogenic ^{40}Ar by recrystallization or alteration (causing too young apparent ages and commonly hump- to bell-shaped age spectra), the presence of extraneous (inherited and excess) radiogenic ^{40}Ar in incompletely homogenized and degassed rocks (where the initial ^{40}Ar/^{36}Ar ratio is larger than the atmospheric value of >295.5, causing too old apparent ages and saddle-shaped age spectra; e.g., Kelley 2002a), and argon recoil redistribution during neutron irradiation (especially in fine-grained rock samples that yield hump-shaped age spectra) may account for problems in ^{40}Ar/^{39}Ar age interpretation (e.g., Bogard et al. 1988; McDougall and Harrison 1999; Jourdan et al. 2009b). In addition to the age spectrum, the Ca/K spectrum (calculated from the ^{37}Ar/^{39}Ar ratio) and three isotope isochron plots may reveal mineral-specific argon degassing, the presence of an excess argon component, or alteration (e.g., Lanphere and Dalrymple 1976; Kelley and Spray 1997; Kelley 2002a; Kuiper 2002). The statistical robustness of an age plateau is characterized by the MSWD (mean squared weighted deviate) as a measure of statistical best-fit. The MSWD value is used in conjunction with the probability (P) value calculated using chi square tables, which determines the 'probability of occurrence' for an ^{40}Ar/^{39}Ar age obtained; more information of the statistical treatment of argon isotopic data and tests for systematic errors is given by, for example, York (1969), DeVor (1992), Min et al. (2000), and Baksi (2003; 2005). Valuable reviews and case studies of ^{40}Ar/^{39}Ar dating as guidelines for the interpretation of ^{40}Ar/^{39}Ar age spectra are provided by Bottomley et al. (1990), Deutsch and Schärer (1990), Müller et al. (1990), Trieloff et al. (1998), Bottomley et al. (1997), McDougall and Harrison (1999), Kelley (2002a;b; 2007), Schwarz and Lippolt (2002), and Jourdan et al. (2007b; 2008; 2009b).

4. Current status of the Triassic terrestrial impact cratering record

4.1. Impact structures of proven Triassic age

The Triassic period, bordered by two of the five most severe mass extinction events in the history of life at the Permian/Triassic and Triassic/Jurassic boundaries, respectively (e.g., Benton 1995; Hallam and Wignall 1997), is of particular interest with respect to the possible influence of large meteorite impacts on Earth. Among the 176 terrestrial impact structures, only five yielded reliable Triassic stratigraphic and/or isotopic ages, namely Manicouagan (Québec, Canada), Lake Saint Martin (Manitoba, Canada), Rochechouart (France), Araguainha (Brazil), and Red Wing Creek (North Dakota, USA). More detailed reviews of these impact structures, together with the Obolon impact structure (Ukraine), are presented in the following lines and chapters. A summary of impact structures that yielded proven and possible Triassic ages is given in Fig. 4.1 and Table 4.1.

Fig. 4.1.: Distribution of terrestrial impact structures of proven and possible Triassic age (modified after Buchner and Schmieder 2009c).

The ~40 km in diameter Araguainha impact structure (Brazil; centered at 16°47' S, 52°59' W; Figs. 4.1. and 4.2; Table 4.1) is the largest impact structure so far recognized in South America, hosted by flat-lying Devonian to Permian sediments and the underlying Ordovician crystalline basement of the northern Paraná Basin. The Araguainha Dome was originally discussed as a probable astrobleme by Dietz and French (1973) and subsequently confirmed as of impact origin (Theilen-Willige 1982; Crósta 1983; von Engelhardt et al. 1985). Impact lithologies at Araguainha comprise the fractured bedrock (granite in the central uplift) with shock veins and shatter cones, overlain by lithic impact breccias and impact melt rocks (Fig. 4.3A); reviews of the geologic setting of the Araguainha impact structure and the associated impactites are given by Crósta (1987), von Engelhardt et al. (1992), Hippertt and Lana (1998), Lana et al. (2007; 2008), Machado et al. (2009), and Lana and Marangoni (2009). $^{40}Ar/^{39}Ar$ dating of impact melt rocks by Hammerschmidt and von Engelhardt (1995) yielded earliest Triassic impact ages of 245.5 ± 3.5 Ma and 243.3 ± 3.0 Ma, in compatibility with earlier Rb/Sr ages (Buhl et al. 1990; Martinez et al. 1991; Deutsch et al. 1992). Based on the re-interpretation of the $^{40}Ar/^{39}Ar$ data obtained by Hammerschmidt and von Engelhardt (1995), Jourdan et al. (2009b) recently recommended an age of ~246 Ma. Together with the occurrence of distal Araguainha impact ejecta at the Permian/Triassic (P/T) boundary in Brazil, this age has revitalized the debate about the possible influence of (the Araguainha) impact on the mass extinction at the P/T boundary ~250 Ma ago (Miura et al. 1998; Théry et al. 2003; Jourdan et al. 2009b; Lana and Marangoni 2009), the most severe of the 'big five' mass extinctions in Earth history (e.g., Erwin 1990; Hallam and Wignall 1997). However, global evidence for a major impact event at the P/T boundary remains equivocal (Koeberl et al. 2004; Renne et al. 2004; Langenhorst et al. 2005). For further reading and references, I refer to the review by Buchner and Schmieder (2009c) for a discussion of possible impacts and impact structures at the P/T boundary, for example, the role of the postulated large Wilkes Land (Antarctica) and Bedout (offshore Australia) features of suspected and unproven impact origin (Weihaupt 1979; Becker et al. 2004; von Frese et al. 2009).
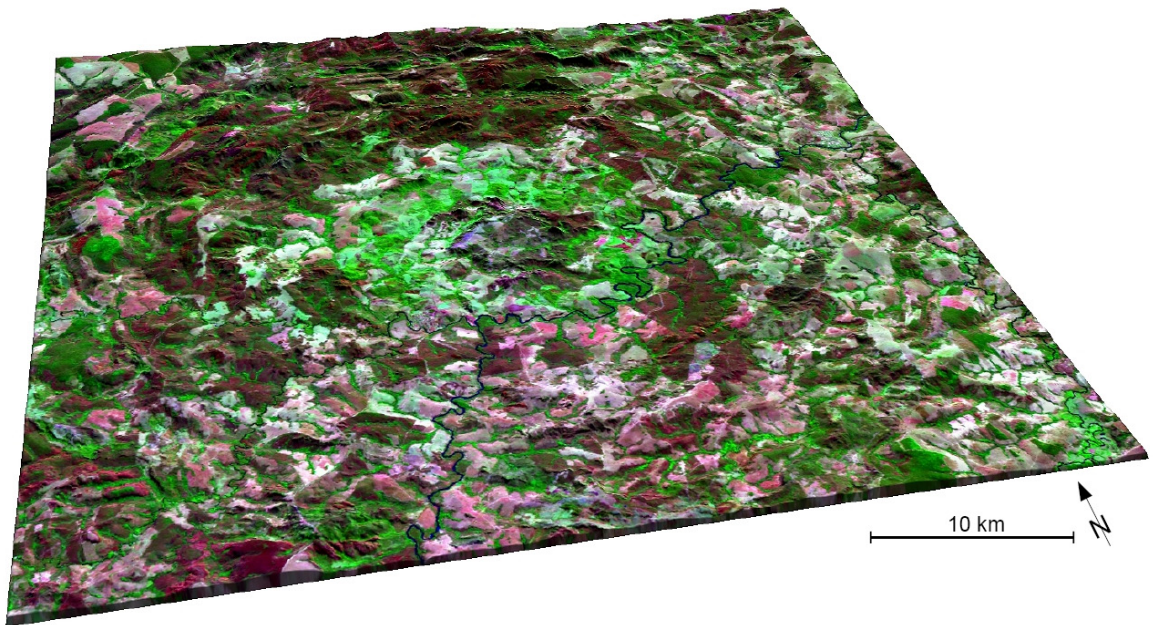
Fig. 4.2.: The Araguainha impact structure, Brazil, a medium-sized complex impact structure. Landsat-7 ETM+ satellite image (bands 5-4-2 merged with band 8) draped over Shuttle Radar Topographic Mission (SRTM) terrain data; 2-fold vertical exaggeration.
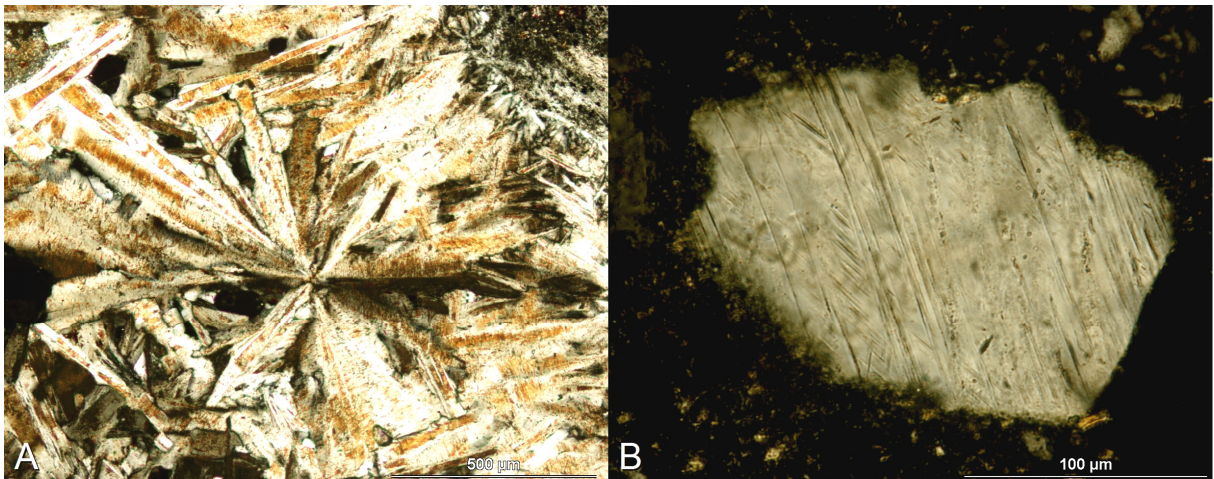
Fig. 4.3.: Thin section photomicrographs of impactites from impact structures mentioned in this chapter. **A**: Spinifex-textured feldspar crystals in impact melt rock from the Araguainha impact structure (Brazil; cross-polarized light); **B**: shocked quartz with three sets of planar deformation features (PDFs) in suevite from the Puchezh-Katunki impact structure (Russia; cross-polarized light).

Table 4.1: Summary of terrestrial impact structures of proven and possible Triassic age (modified after Buchner and Schmieder 2009c).

| Impact structure	Country	Lat	Long	Diameter (km)	Age (Ma)
proven Triassic age					
Manicouagan	Québec, Canada	51°23' N	68°42' W	100	214 ± 1*
Araguainha	Brazil	16°47' S	52°59' W	40	~246**
Lake Saint Martin	Manitoba, Canada	51°47' N	98°32' W	40	235 ± 6
Rochechouart	France	45°50' N	0°56' E	~25 (40-50?)	214 ± 8*
Red Wing Creek	North Dakota, USA	47°36' N	103°33' W	9	~200-220
possible Triassic age					
Puchezh-Katunki	Russia	56°58' N	43°43' E	80	~203-168**
Obolon	Ukraine	49°35' N	32°55' E	20	215 ± 25? 169 ± 7*?
Wells Creek	Tennessee, USA	36°23' N	87°40' W	12	200 ± 100*
Cloud Creek	Wyoming, USA	43°07' N	106°45' W	7	~190 ± 20*
Kursk	Russia	51°42' N	36°00' E	6	250 ± 80*
Riachão	Brazil	7°43' S	46°39' W	4.5	≤200*
Gow	Saskatchewan, Canada	56°27' N	104°29' W	4	≤~250
Viewfield	Saskatchewan, Canada	49°35' N	103°04' W	2.5	190 ± 20*
Liverpool	Australia	12°24' S	134°03' E	1.6	150 ± 70*
Karikkoselkä	Finland	62°13' N	25°15' E	1.5	~230*

*age listed in the Earth Impact Database (2009); **age recommended by Jourdan et al. (2009b)

4.2. Impact structures of probable/possible Triassic age

The ~80 km Puchezh-Katunki impact structure (Russia; centered at 56°58' N, 43°43' E; Fig. 4.1; Table 4.1) counts among the ten largest impact structures known on Earth and even among the five largest that were formed during Phanerozoic time. The whole structure lies within Archean crystalline and uppermost Proterozoic to Lower Triassic sedimentary rocks of the Russian Platform and is overlain by Middle–Upper Jurassic and younger post-impact sediments. Impactite lithologies comprise lithic impact breccias, suevites (Fig. 4.3B), and subordinate impact melt rocks (Masaitis and Mashchak 1990; Masaitis et al. 1996; Masaitis 1999; Pálfy 2004). Although extensively studied and deeply drilled in the central uplift area (the Vorotilovo deep scientific well drilled 1989–1992 reached a depth of 5,374 m), the Puchezh-Katunki impact structure still has not

yielded reliable age data. Masaitis and Mashchak (1990) and Ivanov (1994) proposed a Late Triassic age of 220 ± 10 Ma by stratigraphic methods. In contrast, K/Ar dating of impactites by Masaitis and Pevzner (1999) resulted in ages of 200 ±3 Ma and 183 ± 5 Ma, which suggest impact ages respectively at the Triassic–Jurassic transition or in the Lower Jurassic (the latter would also correlate with the first stratigraphic age estimations of ~180–200 Ma for Puchezh-Katunki given by Firsov, 1973). Masaitis (1999) and Masaitis and Pevzner (1999) reported a Middle Jurassic age of 167 ± 3 Ma for Puchezh-Katunki obtained by palynostratigraphic studies of the oldest crater lake deposits. A discussion of the impact age of the large Puchezh-Katunki structure and its possible relation to Mesozoic extinction events is given by Pálfy (2004), who concluded that 'the possibility cannot be ruled out that the Puchezh-Katunki impact is coeval with either the end-Triassic or the Early Jurassic (Pliensbachian–Toarcian) extinction'. In summary, the available isotopic and stratigraphic ages for the Puchezh-Katunki impact structure are highly incoherent and associated with an age uncertainty of up to 66 million years (Schmieder and Buchner 2008).
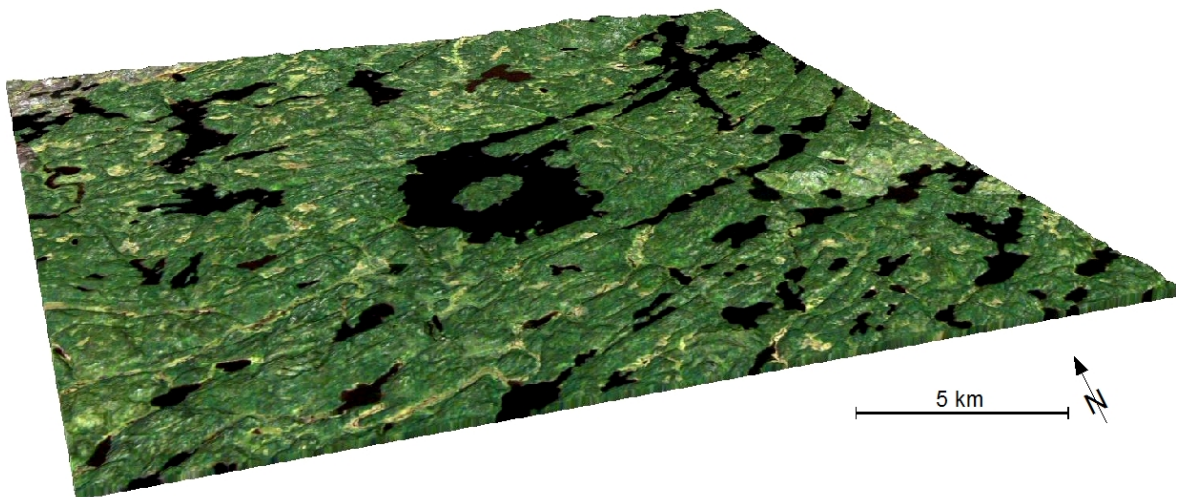
Fig. 4.4.: The Gow impact structure (Saskatchewan, Canada), a small, complex impact structure. The central island (Calder Island) represents the eroded remnants of the central uplift. Landsat-7 satellite image (bands 3-2-1 merged with SPOT 4/5 Canadian Orthoimage 2005-2010) and draped over Canadian Digital Elevation Data (CDED); 2-fold vertical exaggeration.

In addition to the two large impact structures of Araguainha and Puchezh-Katunki, a set of smaller impact structures <20 km in diameter might be Triassic in age, such as the ~12 km Wells Creek (Tennessee, USA; e.g., Stearns et al. 1968), the ~7 km Cloud Creek (Wyoming, USA; Stone and Therriault 2003), the ~4 km Gow (Saskatchewan, Canada; e.g., Thomas et al. 1977; Grieve 2006; Fig. 4.4), and the ~2.5 km Viewfield (Saskatchewan, Canada; e.g., Sawatzky 1975; Grieve 2006) impact structures in North America; the ~6 km Kursk (Russia) and ~1.5 Karikkoselkä (Finland) impact structures in Europe; as well as the ~4.5 km Riachão impact structure (Brazil) in South America; and the ~1.6 km Liverpool impact structure in Australia (e.g., Haines 2005). The impact structures listed above are summarized in Fig. 4.1 and Table 4.1. Apart from impact melt lithologies from the Gow impact structure (impact melt rocks on Calder Island; Fig. 4.4) that yielded a ^{40}Ar/^{39}Ar 'maximum age' of ~250 Ma (Bottomley et al. 1990), no melt lithologies have been reported from these impact structures. The Karikkoselkä impact structure was dated at ~230-260 Ma by paleomagnetic methods (Pesonen et al. 1999a) but this age appears poorly constrained regarding notably older (Proterozoic to Ordovician) stratigraphic age estimates (e.g., Grieve 1997; Abels et al. 2002).

5. The Rochechouart impact structure (France)

5.1. Geologic setting and previous work

The ~20-25 km in diameter, complex Rochechouart impact structure (France, départements Haute-Vienne and Charente; centered at 45°50' N, 0°56' E; Fig. 5.1) is hosted by Precambrian to Paleozoic (Variscan) crystalline rocks of the northwestern French Massif Central, predominantly gneisses, leptynites, and granites, as well as some granitic to dioritic dikes (e.g., Chèvremont et al. 1996; Lambert 2009; Fig. 5.2). As the Rochechouart impact structure is deeply eroded down to the crater floor, no primary crater morphology is preserved, and estimates for the pre-erosional original diameter of the impact structure are ~40-50 km (Lambert 1977; 2009). The shocked crater basement is characterized by the occurrence of shatter cones (Fig. 5.3A), as well as lithic and pseudotachylitic breccia dikes. Crater-filling impact lithologies comprise a ~60 m pile of basal lithic impact breccias (~30 m in thickness; Fig. 5.3B) overlain by lenses of impact melt rocks (up to ~10 m; Fig. 5.3C-F) and suevite (~20 m; Fig. 5.3G-H), finally topped by a fine-grained, ash-like impactoclastic layer. A geologic summary of the Rochechouart impact structure and associated impactites is given by Lambert (1977), Reimold and Oskierski (1987), Kelley and Spray (1997), and Lambert (2008; 2009). Geophysical measurements yielded a gravity minimum of down to -10 mgal at the center of the impact structure (Pohl et al. 1978). Most recently, geochemical analyses of impact melt rocks suggested an iron meteorite as the Rochechouart impactor (Tagle et al. 2009), in compatibility with earlier suggestions (Janssens et al. 1977; Horn and El Goresy 1979; Tagle et al. 2003) and a strong enrichment of nickel in the Rochechouart impact melt lithologies with respect to the unshocked target rock (Lambert 1975; 2009). Although Rochechouart was early confirmed as of impact origin by Kraut (1969) and studied through decades, the Rochechouart impact age has been a matter of debate for a long time. Previous investigations, including K/Ar (Kraut and French 1971; Lambert 1974), Rb/Sr (Reimold and Oskierski 1987), apatite and glass fission track (Wagner and Storzer 1975), as well as paleomagnetic dating (Pohl and Soffel 1971; Carporzen and Gilder 2006), resulted in a broad (Middle Triassic to Late Jurassic) time window for the

Rochechouart impact. $^{40}Ar/^{39}Ar$ laser spot dating of pseudotachylites from the Champagnac quarry in the northeastern part of the impact structure (see Fig. 5.2) yielded a Karnian to Norian age of 214 ± 8 Ma (Kelley and Spray 1997; see also Fig. 5.4 for summary). Precise and accurate dating is essential regarding paleoenvironmental considerations for the Rochechouart impact scenario (i.e., proximity and possible influence of the nearby Triassic to Jurassic shoreline and/or sediments upon crater formation and vice versa). This chapter presents new $^{40}Ar/^{39}Ar$ age data for the Rochechouart impact structure that are discussed with respect to high-energy paleoenvironmental events (earthquakes and tsunamis), possible impact ejecta in the latest Triassic sedimentary record of Europe, and the Late Triassic multiple impact theory (Spray et al. 1998).
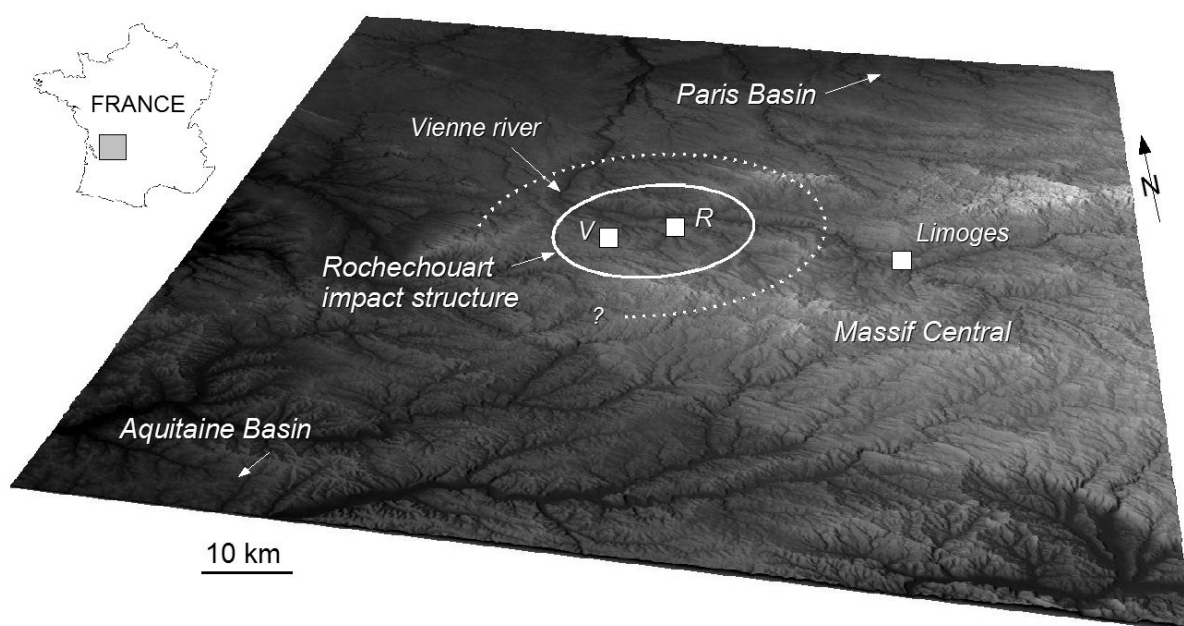
Fig. 5.1: Position of the Rochechouart impact structure at the northwestern margin of the French Massif Central and surrounding sedimentary basins (see map inset for position of the scene). Solid circle: present diameter of the eroded impact structure (23 km); dotted circle: possible pre-erosional diameter (~40 km). Abbreviations: R: city of Rochechouart; V: village of Videix. Scene computed from Shuttle Radar Topographic Mission (SRTM) data.
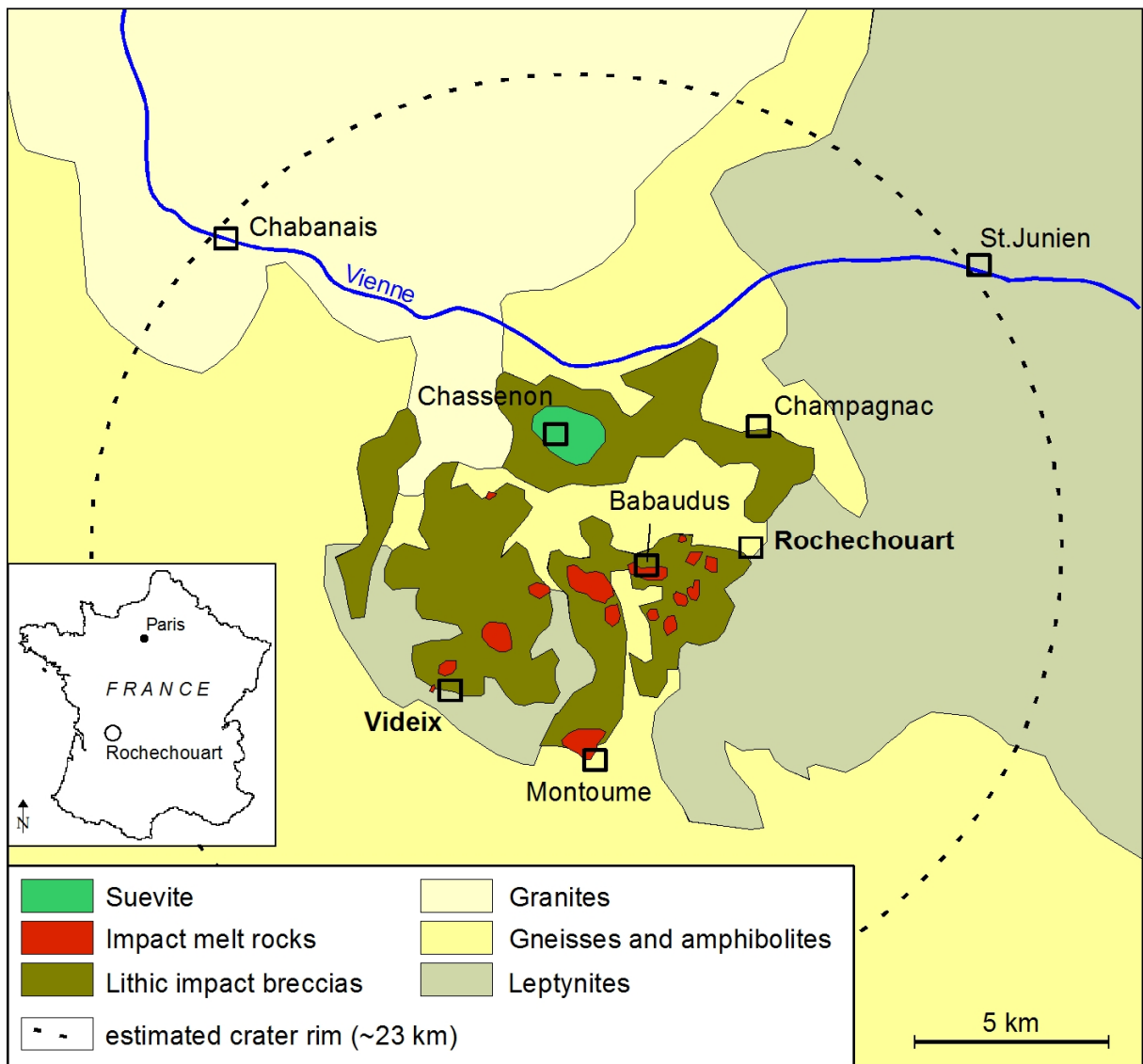
Fig. 5.2: Simplified geological map of the Rochechouart impact structure, France (modified after Chèvremont et al. 1996; Kelley and Spray 1997).
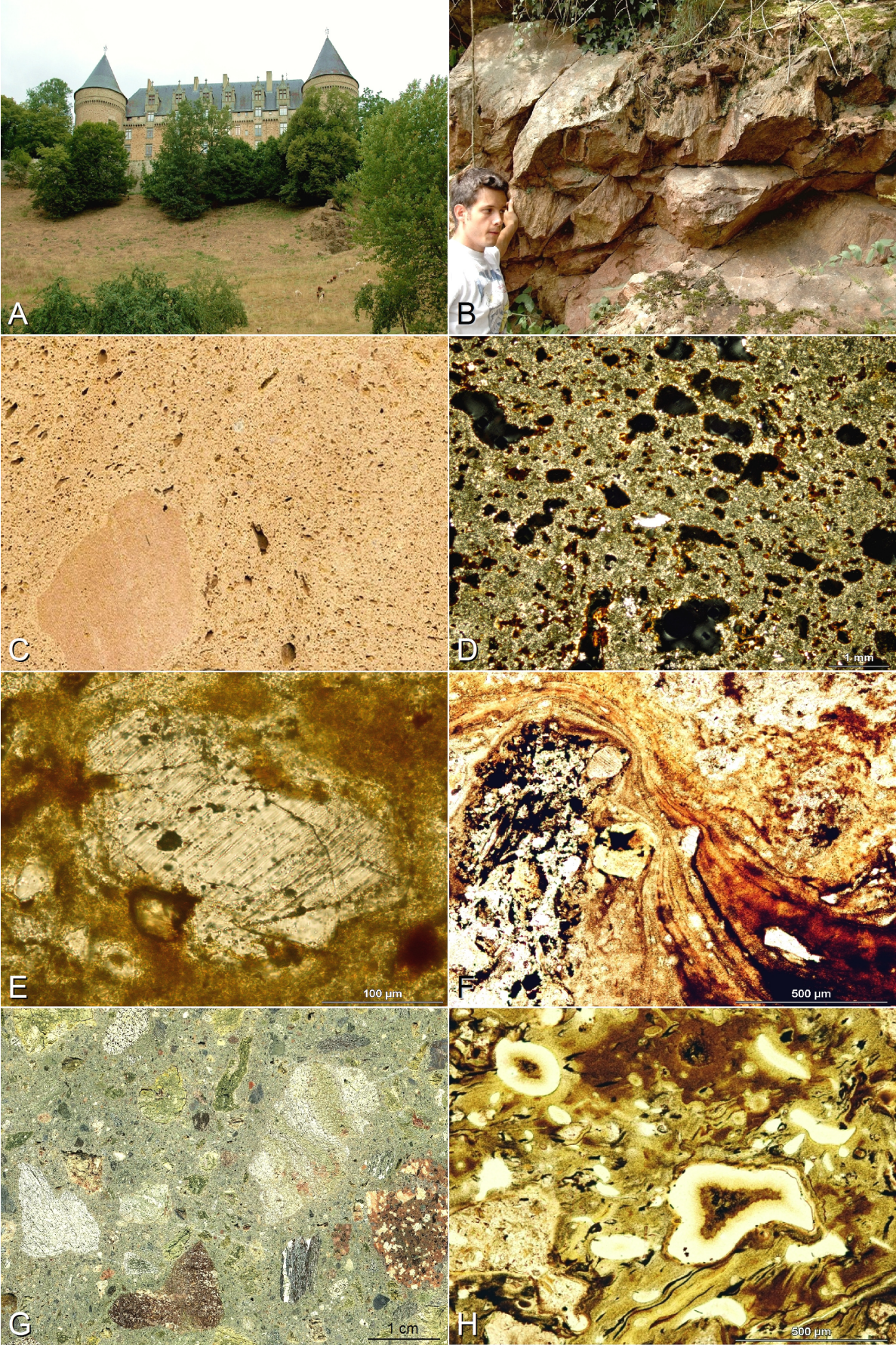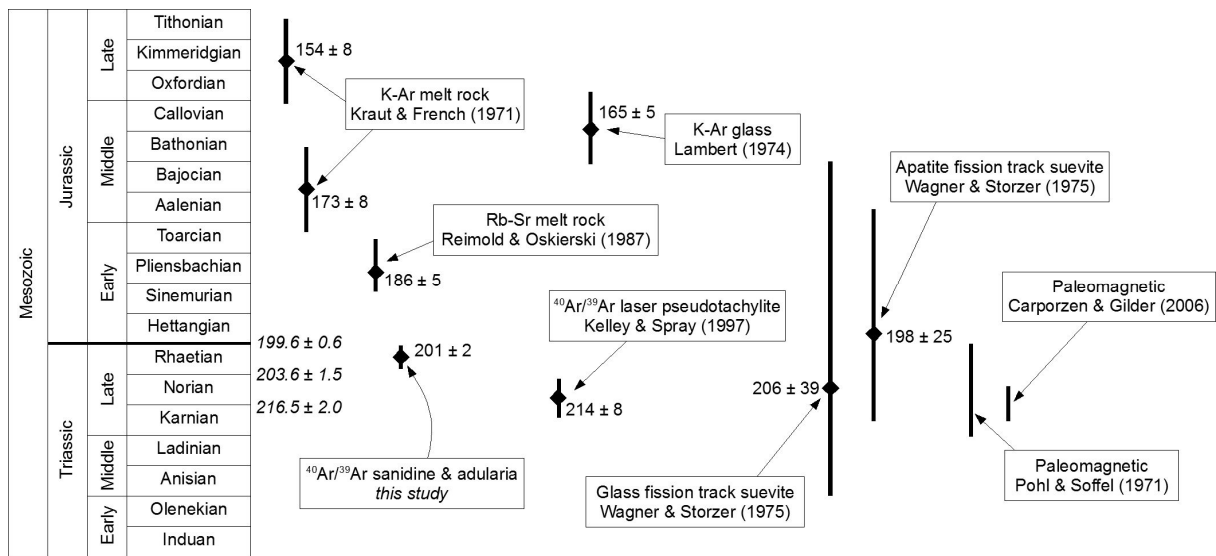
Fig. 5.4: Ages so far reported for the Rochechouart impact structure. Stage boundary ages after Ogg et al. (2008).

< Fig. 5.3 (previous page): Impactites at the Rochechouart impact structure, France. **A**: The Rochechouart castle (13th century) is built of impactites, mainly lithic impact breccias; the castle rests on the basal lithic impact breccias that overlie the structural crater floor (roughly indicated by the group of goats); **B**: *in situ* shatter cones in shocked autochthonous basement rocks at the small abandoned Champonger quarry south of Chassenon; **C**: vesicular yellow impact melt rock from the central part of the Rochechouart impact structure (village of Babaudus); note the largely digested lithic clast (polished slab); **D**: thin section photomicrograph of the melt rock shown in C; the rock is notably altered, and vesicles are lined by iron hydroxides (cross-polarized light); **E**: shocked quartz in massive clast-poor impact melt rock (Babaudus; plane-polarized light); **F**: fluidal microtexture of clast-rich reddish-brown impact melt rock from the central part of the impact structure (Valette; plane-polarized light); **G**: green suevite from Chassenon in the northern part of the impact structure; the rock contains numerous lithic clasts of crystalline rocks of the French Massif Central, as well as green altered impact glasses (polished section); **H**: fluidal and partially altered domain of impact glass in the Chassenon suevite (plane-polarized light).

5.2. Samples and analytical techniques

Optically fresh aggregates of sanidine and adularia separated from impact-metamorphosed gneiss found near the village of Videix in the western central part of the Rochechouart impact structure (see Fig. 5.1 for location) were chosen as material for dating. Sampling was carried out during a field trip in summer 2005 (together with Dr. Elmar Buchner). The modal and geochemical composition of the rock was determined by optical microscopy, energy dispersive X-ray (EDX) measurements (CamScan™ SC44 scanning electron microscope-EDAX™ PV 9723/10 system, Institut für Planetologie, Universität Stuttgart), and X-ray diffractometry (XRD; Bruker-AXS D8 affiliation, Institut für Mineralogie and Kristallchemie, Universität Stuttgart).

5.3. Petrography and geochemistry

The reddish shocked gneiss shows a partially fluidal texture that overprints a relict foliation fabric (Fig. 5.5A-B) and is mainly composed of potassium feldspar (Fig. 5.5C-D), silica (Fig. 5.5E-F), and some accessory minerals. Potassium feldspar occurs as both spherulitic to blocky intergrown crystals of sanidine (Figs. 5.5C-D; 5.6) and idiomorphic adularia grown in cavities (Fig. 5.5D; Fig. 5.6, Fig. 5.7). Silica forms commonly vesicular microcrystalline masses of α-quartz that largely retained the original clast shape and display relict shock metamorphic features (Figs. 5.5E; 5.6) and domains of toasted appearance that locally consist of ballen quartz (Fig. 5.5F). Besides hematite crystallites (partially distributed within sanidine), accessories predominantly comprise zircon and Fe-Ti oxides. EDX measurements yielded a siliceous-potassic whole-rock composition of the Videix gneiss (~66 wt% SiO_2; ~11 wt% K_2O; ~0.2 wt% Na_2O; ~0.2 wt% CaO), similar to that of impact melt rocks found in the central part of the Rochechouart impact structure (e.g., Oskierski and Bischoff 1983; Lambert 2009; Table 5.1). Feldspars represent essentially pure potassium end members, whereas silica contains up to ~1.5 wt% Al_2O_3. XRD analyses suggest that sanidine occurs as the high sanidine modification indicated by comparatively high 2θ values of up to 61.8° (e.g., Kroll et al. 1986).
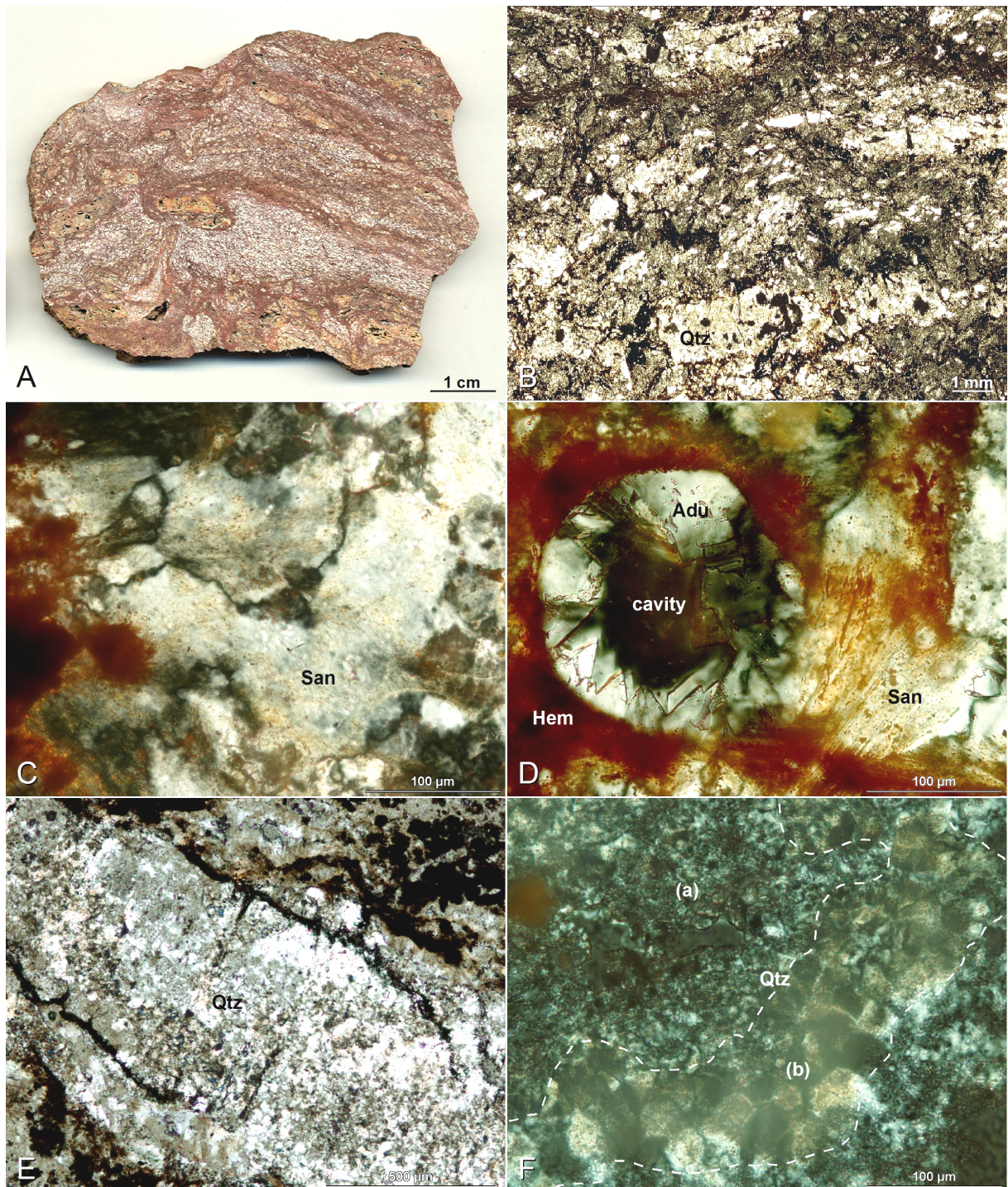
Fig. 5.5: Impact-metamorphosed gneiss from Videix; **A**: Polished slice of the rock with larger domains of recrystallized silica (center left); **B**: overall thin section image showing a partially fluidal relict gneiss fabric and larger domains of recrystallized K-feldspar and silica (bright; plane-polarized light); **C**: intergrown crystals of essentially pure sanidine (San; cross-polarized light); **D**: sheaf-like aggregate of sanidine (San), microcrystalline hematite (Hem), and secondary idiomorphic crystals of adularia (Adu) grown in a cavity (cross-polarized light); **E**: clast of recrystallized microcrystalline quartz (Qtz) with relict shock features (planar fractures; cross-polarized light); **F**: vesicular aggregate of silica with domains of microcrystalline quartz (a) and ballen quartz in locally toasted domains (b) (cross-polarized light).
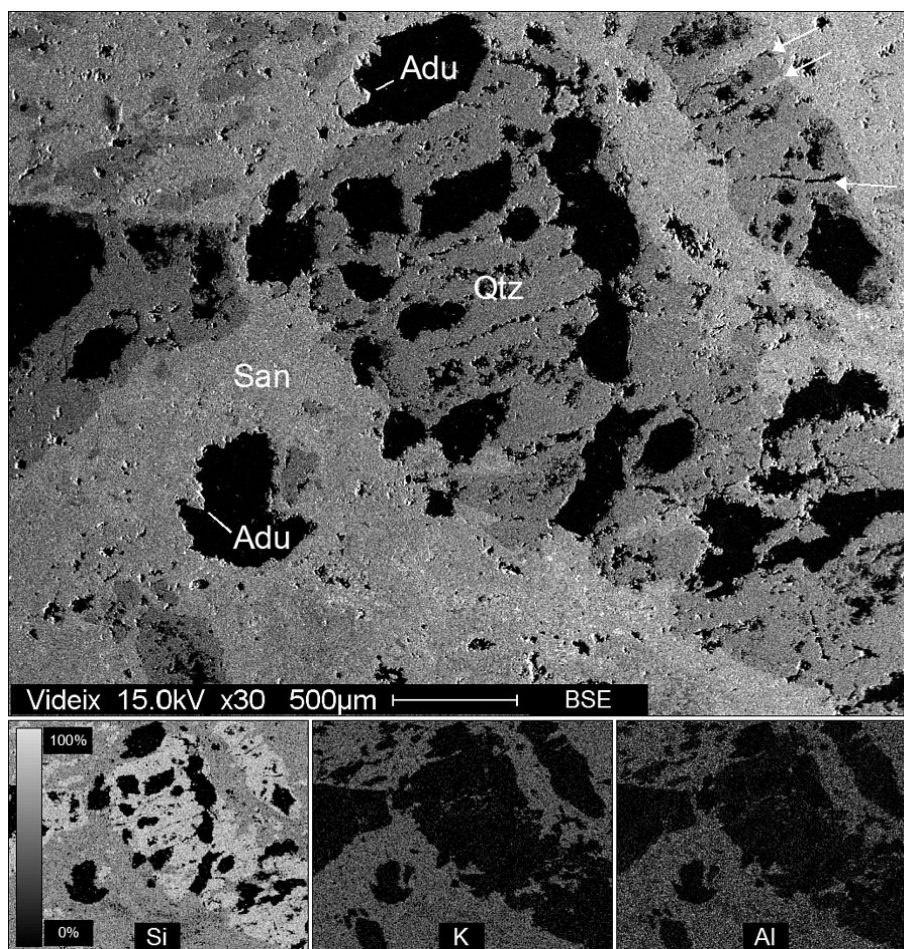
Fig. 5.6: Backscattered electron image of the Videix gneiss with recrystallized microcrystalline quartz (Qtz) with relict shock features (white arrows), sanidine (San), and cavity-filling adularia (Adu); bottom: element distribution maps for Si, K, and Al.

Table 5.1: Average whole-rock composition of Rochechouart impact melt rocks, target gneiss (data from Lambert 1977; 2009), and the Videix gneiss.

	Impact melt rocks	Target gneiss	Videix gneiss*
SiO_2	66.6	66.2	66.1
TiO_2	0.8	0.8	0.8
Al_2O_3	16.2	16.2	16.9
$Fe_2O_3 + FeO$	4.2	5.8	4.1
MgO	1.3	2.8	0.5
CaO	0.3	1.8	0.2
Na_2O	0.3	2.9	0.2
K_2O	10.2	3.3	11.0
Total	99.9	99.8	99.8

*average of 10 EDX measurements

5.4. Interpretation of shock metamorphic conditions and petrologic considerations

The paragenesis of the impact-metamorphosed Videix gneiss (sanidine – α-quartz – hematite – adularia; Fig. 5.5A-B) suggests that sanidine (Figs. 5.5C-D; 5.6) formed as an early recrystallization product of normal K-feldspar glass, most likely at high post-shock temperatures of ~850-1,000°C (Bischoff and Stöffler 1984). The partially spherulitic character of sanidine might be related to early post-shock devitrification processes at fast cooling rates (e.g., Lofgren 1971). Microcrystalline quartz aggregates that have commonly retained the original angular shape and display relict shock features (Figs. 5.5E-F; 5.6) probably represent domains of strongly recrystallized diaplectic quartz glass or maybe quartz clasts partially molten but not assimilated by the surrounding (feldspar) melt, suggesting peak shock pressures of >35 GPa and post-shock temperatures of up to ~1,500°C (Stöffler and Langenhorst 1994; French 1998; Lambert 2009). The presence of ballen α-quartz (Ferrière et al. 2009a; Fig. 5.5F) in relict toasted silica domains is compatible with post-shock temperatures exceeding 1,000°C and indicates the transition of protolith quartz to β-cristobalite during post-shock heating and back to quartz (via α-cristobalite) upon cooling; this is also in agreement with the incorporation of higher amounts of Al_2O_3 (>1 wt%) into silica at high temperatures (e.g., Osinski 2004). Due to pervasive post-shock annealing and recrystallization, no primary shock features (such as optically sharp planar deformation features) are preserved in the microcrystalline silica domains. The vesicular microfabric of recrystallized quartz clasts and the distinct toasting effect, furthermore, underline the influence of a strong post-shock thermal overprint (Ferrière et al. 2009b; cf. Whitehead et al. 2002). Very similar thermal effects in silica have also been observed in melt rocks (and, particularly, in lithic clasts within the melt rocks) from the Rochechouart impact structure (e.g., at Montoume or Babaudus; Lambert 2009). The crystallization of hematite may be related to the breakdown of precursor protolith biotite (e.g., Schneider 1974). Adularia crystallization, as an expression of potassic metasomatic-hydrothermal overprint, has been described from some impact structures on Earth, e.g., Chicxulub (Mexico; Tuchscherer et al. 2006) and Kärdla (Estonia; Versh et al. 2005); like in the Videix gneiss, adularia was also observed in vesicles of melt rocks from the central part of the

Rochechouart impact structure (Babaudus, Valette, and La Chauffie), as well as in the Chassenon suevite.

Hydrothermal systems associated with larger terrestrial impact structures, responsible for penetrative post-shock alteration of impact breccias and melt rocks, are known from a long list of impact structures (see summary by Naumov 2005). Potassium metasomatism in impactites, indicated by a notable enrichment in K with respect to the unshocked target rocks, is also known from a number of terrestrial impact structures, such as Ilyinets (Ukraine; Gurov et al. 1998), the Ries crater (Germany; Osinski 2005), or Siljan (Sweden; Reimold et al. 2005a). A review of the selective melting of K-feldspar and superimposed K-metasomatism (together with the relative depletion of Na and Ca) in the Rochechouart impactites is given by Lambert (1981b; 2009) and Reimold et al. (1984). In particular, specific potassium enrichment in the Videix gneiss, together with high K_2O/Na_2O (~50) and K_2O/CaO (~100) ratios compared to the unshocked target rock gneisses (K_2O/Na_2O ~1.2; K_2O/CaO ~1.8; see Table 5.1), appears to be in analogy to shocked and selectively K-enriched lithic target rock clasts in the Rochechouart impact melt rocks (Lambert 2009; his Table 2); the same phenomenon was also observed at other terrestrial impact structures (e.g., strongly K-enriched gneiss clasts in impact melt rocks from the Brent crater, Canada; Grieve 1978). Cavity-filling adularia in the Videix gneiss most likely crystallized at moderate to low temperatures in a typical range of ~350-100°C (e.g., Naumov 2005; Versh et al. 2005). Thus, at least at the hand specimen scale, sanidine and adularia reflect the local cooling history of the rock from high post-shock temperatures of up to ~1,500°C down to ~200°C or lower. This suggests that the Videix gneiss was subjected to the pervasive K-metasomatism and hydrothermal overprint caused by (and typical for) the Rochechouart impact, possibly in close contact to the (overlying) impact melt sheet.
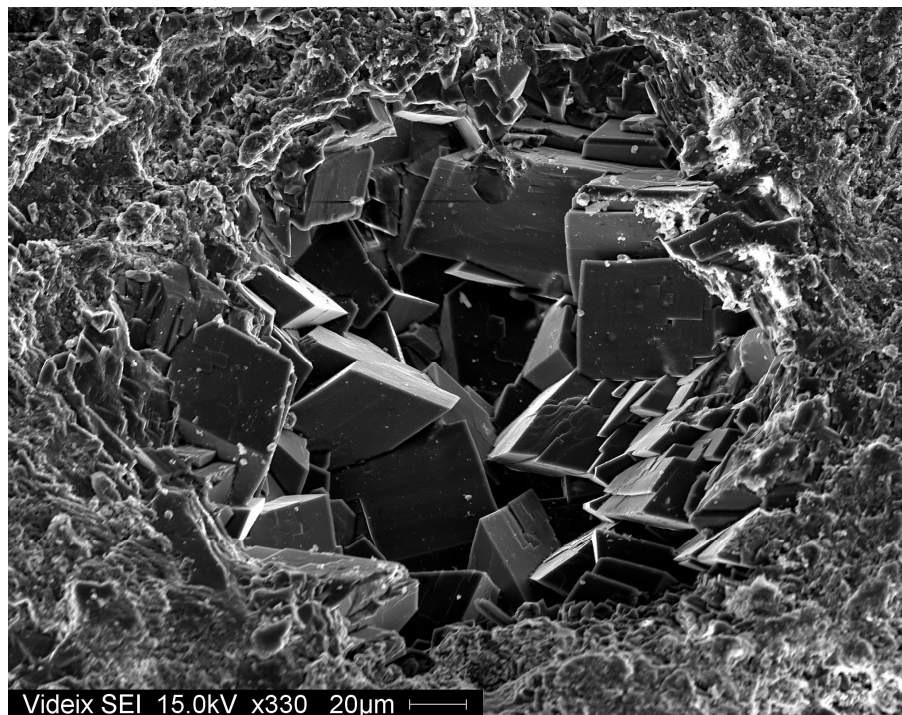
Fig. 5.7: Scanning electron microscope (secondary electron) image of a cavity filled with idiomorphic adularia; rim is mainly sanidine and microcrystalline quartz.

5.5. $^{40}Ar/^{39}Ar$ dating – sample choice and methods

Sanidine and adularia aggregates (up to ~0.5 mm in size, with K contents of ~2 wt% and ~7 wt%, respectively) were handpicked from the crushed rock on the basis of their fresh optical appearance and rinsed with ethanol and deionized water in an ultrasonic cleaner. $^{40}Ar/^{39}Ar$ dating was done at the Institut für Geowissenschaften, University of Heidelberg (Dr. W. H. Schwarz and Dr. M. Trieloff; see Trieloff et al. 2005; Schwarz and Trieloff 2007a for technical details), using the decay constants determined by Steiger and Jäger (1977); due to miscalibration of the K decay constants compared to the U-decay series constants, the $^{40}Ar/^{39}Ar$ ages have to be c. 1% higher in the age range of the Mesozoic with respect to those calculated with the constants recommended by Steiger and Jäger (1977; see also Villeneuve et al. 2000; Ramezani et al. 2005; Mundil et al. 2006; Schwarz and Trieloff 2007b; Jourdan et al. 2009a). The samples were wrapped in Al-foil, packed in quartz ampoules (12x55 mm), Cd-shielded (to avoid isotopic interferences), and irradiated for 5 days at the GKSS Geesthacht, Germany. After

irradiation, the samples were heated in an inductively heated Mo-furnace up to ~1,500°C in several temperature steps. The gas was cleaned with Zr-, Ti-, Cu/CuO-, and Al-Getters. Argon was measured using a MAT GD150 mass spectrometer. The argon results were corrected for mass discrimination, argon decay, isotopic interferences (all information listed in Tables 5.2 and 5.3), and blanks from the extraction line (glass and furnace). The argon isotopic composition of blanks was always atmospheric within uncertainty. Ages were calculated against the BMus/2 (Bärhalde muscovite, Black Forest, Germany) standard with an age of 328.5 ± 1.1 Ma, which was calibrated against 5 further international $^{40}Ar/^{39}Ar$ dating standards; for further information about the analytical procedure see Schwarz and Trieloff (2007a).

5.6. Dating results and interpretation

$^{40}Ar/^{39}Ar$ step-heating analyses yielded two plateau ages of 201.4 ± 2.4 Ma (2σ; ± 2.8 Ma including standard error; MSWD=1.07, P=0.38) for sanidine (~19-99% of ^{39}Ar released; steps 4-11 of 12 extractions shown in Table 5.2) and 200.5 ± 2.2 Ma (2σ; ± 2.6 Ma including standard error; MSWD=0.21, P=0.99) for adularia (~14-100% of ^{39}Ar; steps 4-13 of 14 extractions shown in Table 5.3), respectively (Fig. 5.8), giving a combined age of 201 ± 2 Ma (2σ). Except for some younger apparent ages in the low-temperature extractions, both plateaux show concordant step ages that overlap at the 95% confidence level. Ages calculated from the total gas release, including apparent younger ages obtained during the low-temperature heating steps from sample sites of lower argon retentivity, are just slightly (~2 Ma) younger than the plateau ages. A summary of isotopic data for sanidine and adularia is given in Tables 5.2 and 5.3. Inverse isochron plots show a $^{36}Ar/^{40}Ar$ intercept at ~0.0034 for sanidine and adularia (Fig. 5.9). This ratio is indistinguishable from atmospheric argon composition and suggests that the samples are not disturbed by inherited ^{40}Ar or secondary ^{40}Ar loss (e.g., McDougall and Harrison 1999; Jourdan et al. 2008). Given the largely Ca-free nature of the essentially pure K-feldspar phases, the K/Ca ($^{39}Ar/^{37}Ar$) ratio is variable (partially not defined, as Ca-derived ^{37}Ar was below detection) over the age plateaux. A relatively high amount of ^{40}Ar degassed during the highest-temperature extractions (1,350-1,450°C) and a

comparatively low K content in handpicked aggregates suggest that sanidine was intergrown with some microcrystalline quartz that contained additional atmospheric argon released at high extraction temperatures. Our new sanidine and adularia age is in contradiction with earlier dating results, yet within the general range of previously determined isotopic and paleomagnetic ages (compare summary by Kelley and Spray 1997; Fig. 5.4) and suggest a Rhaetian Rochechouart impact age (see international stratigraphic chart by Ogg et al. 2008). The new age is, within error, indistinguishable from the isotopic age for the Triassic/Jurassic boundary and the slightly earlier phase of Central Atlantic Magmatic Province (CAMP) volcanism (e.g., Marzoli et al. 2008), recently dated at 201.7 ± 0.6 Ma (Pálfy et al. 2008) and 201.58 ± 0.17 Ma (Schaltegger et al. 2008) using the $^{206}Pb/^{238}U$ technique (keeping in mind the miscalibration between U and K decay series), as well as 201.7 ± 2.4 Ma to 197.8 ± 0.7 (Verati et al. 2007) and 201.0 ± 1.4 Ma to 198.1 ± 1.1 Ma (Jourdan et al. 2009a) by the $^{40}Ar/^{39}Ar$ method, respectively. The new age is also coeval with a K/Ar age obtained for the ~80 km Puchezh-Katunki impact structure, Russia (200 ± 3 Ma; Masaitis and Pevzner 1999; see also Pálfy 2004; Schmieder and Buchner 2008 for discussion of the Puchezh-Katunki impact age).
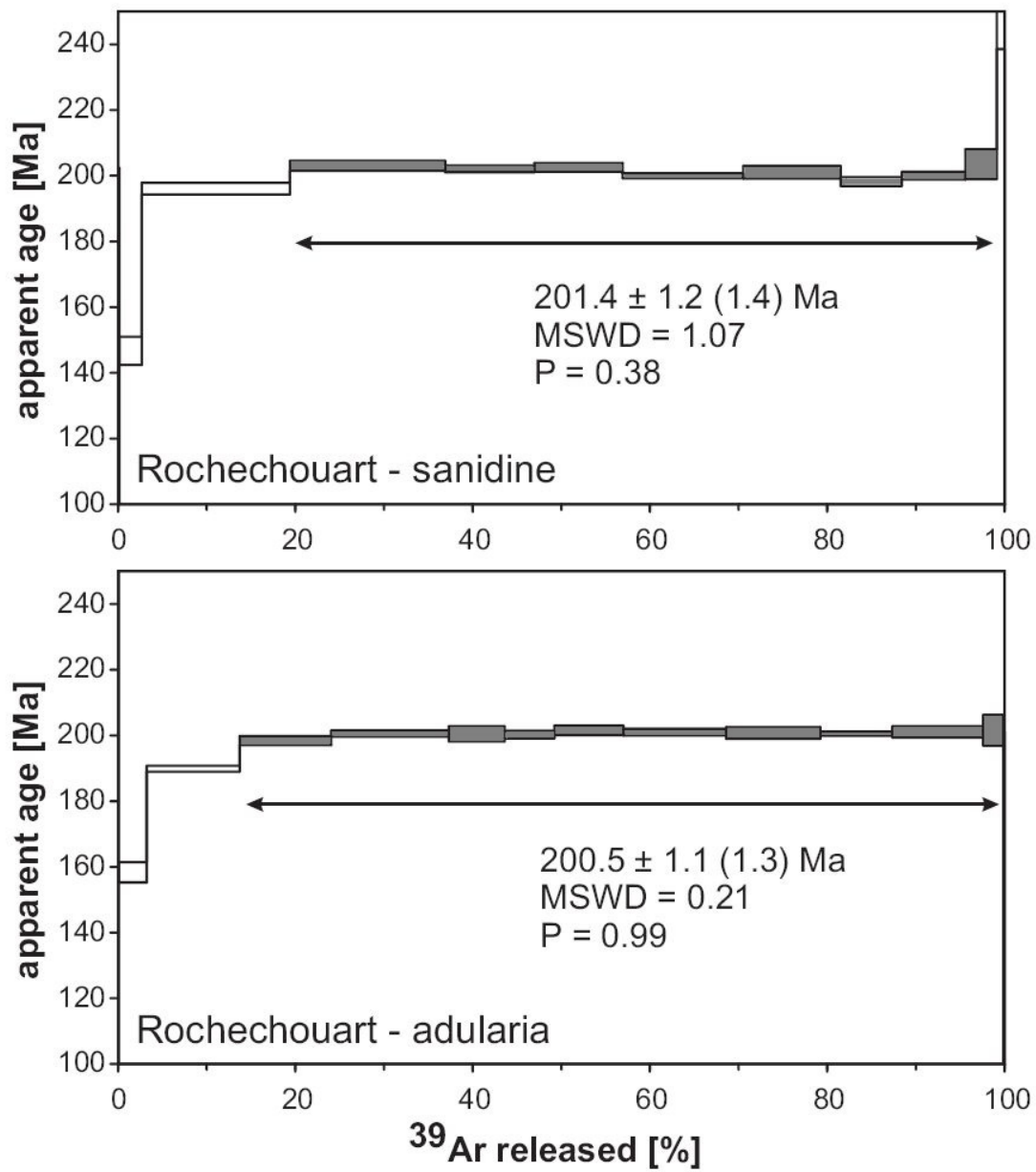
Fig. 5.8: ^{40}Ar/^{39}Ar age spectra for sanidine (top) and adularia (bottom) separated from the impact-metamorphosed Videix gneiss; uncertainties are at the 1σ level; errors in parentheses include standard errors (compare isotopic data given in Tables 5.2 and 5.3).
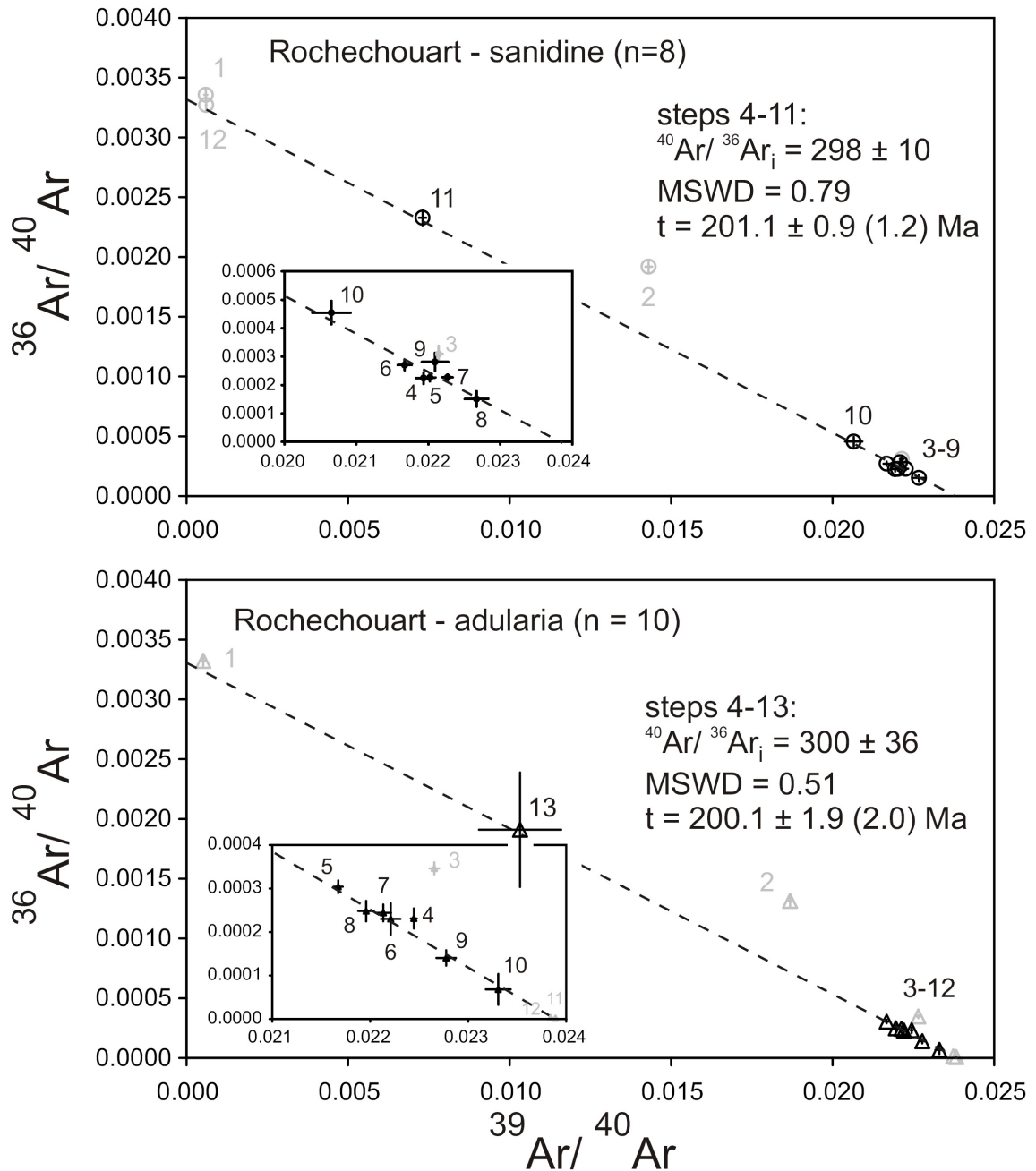
Fig. 5.9: Inverse isochron plots for sanidine (circles; top) and adularia (triangles; bottom). Gray symbols represent argon extraction steps outside the plateau fraction not included in isochron calculation; small numbers denote individual extraction steps – see inset boxes for steps 3-9 for sanidine and 3-12 for adularia; cross symbols mark uncertainties at the 1σ level; errors in parentheses include standard errors (compare isotopic data given in Tables 5.2 and 5.3).

Table 5.2: Isotopic argon dataset and ages for sanidine separated from impact-metamorphosed gneiss, Videix, Rochechouart impact structure; errors in parentheses include monitor error; bold notations indicate data included in the plateau calculation.

Step #	Temp [°C]	^{36}Ar [fA] ± 1σ	^{37}Ar$_{Ca}$ [fA] ± 1σ	^{38}Ar [fA] ± 1σ	^{39}Ar$_K$ [fA] ± 1σ	^{40}Ar [fA] ± 1σ	^{40}Ar* [fA]	± 1σ	^{36}Ar/^{40}Ar ± 1σ [•10^{-6}]	^{39}Ar/^{40}Ar ± 1σ [•10^{-5}]	^{39}Ar [%]	Age [Ma]	± 1σ
1	500	7.76 0.13	0 0	1.51 0.06	1.38 0.11	2312.2 1.5	18.7	38.2	3357 56	59.6 4.9	0.15	67	135 (135)
2	600	3.12 0.07	25.87 0.52	1.11 0.04	23.30 0.17	1628.3 3.6	705.3	21.0	1918 44	1431 11	2.52	146.7	4.3 (4.3)
3	690	2.15 0.20	10.09 0.21	3.24 0.22	154.14 0.36	6960.9 8.0	6324.8	59.3	309 29	2214 6	16.70	196.1	1.8 (1.9)
4	**740**	1.66 0.15	11.53 0.23	3.15 0.15	161.80 0.52	7376.6 26.2	6886.9	51.1	225 20	2193 10	17.53	**203.0**	**1.6 (1.7)**
5	**760**	0.96 0.06	15.62 0.31	1.93 0.17	93.06 0.04	4225.8 14.4	3942.8	21.2	227 14	2202 8	10.08	**202.1**	**1.0 (1.3)**
6	**800**	1.14 0.08	0 0	1.85 0.08	91.79 0.25	4235.8 14.8	3897.6	25.3	270 18	2167 10	9.95	**202.5**	**1.3 (1.5)**
7	**860**	1.28 0.06	0 0	2.83 0.26	125.38 0.20	5630.9 15.4	5252.9	18.2	227 10	2227 7	13.59	**200.0**	**0.7 (1.0)**
8	**930**	0.68 0.12	0 0	1.71 0.11	101.51 0.32	4477.4 28.9	4277.7	41.2	151 27	2267 16	11.00	**201.1**	**1.9 (2.1)**
9	**1000**	0.81 0.09	0 0	1.45 0.15	63.73 0.12	2884.7 23.5	2645.0	18.2	281 31	2209 18	6.91	**198.2**	**1.3 (1.5)**
10	**1100**	1.45 0.13	18.72 0.39	1.50 0.15	66.03 0.21	3197.0 40.0	2767.5	14.9	455 41	2065 27	7.15	**200.0**	**1.2 (1.4)**
11	**1200**	10.48 0.25	0 0	2.45 0.14	32.87 0.15	4498.9 67.5	1403.0	32.5	2329 65	731 11	3.56	**203.5**	**4.6 (4.6)**
12	1350	42.37 0.52	9.63 0.22	8.14 0.15	7.89 0.09	12953 155	432.4	33.4	3271 56	60.9 1.0	0.86	257	19 (19)
Weighted plateau: 201.4 ± 1.2 (1.4) Ma (1σ), n = 8 steps, MSWD = 1.07, P = 0.38						J = 0.0028005 ± 0.0000011			Std: BMus/2; t = 328.5 ± 1.1 Ma		100.00	199.4	1.2 (1.4)

Table 5.3: Isotopic argon dataset and ages for adularia separated from shocked gneiss, Videix, Rochechouart impact structure; ; errors in parentheses include monitor error; bold notations indicate data included in the plateau calculation.

Step #	Temp [°C]	^{36}Ar [fA] ± 1σ	^{37}Ar$_{Ca}$ [fA] ± 1σ	^{38}Ar [fA] ± 1σ	^{39}Ar$_K$ [fA] ± 1σ	^{40}Ar [fA] ± 1σ	^{40}Ar*[fA]	± 1σ	^{36}Ar/^{40}Ar ± 1σ [•10^{-6}]	^{39}Ar/^{40}Ar ± 1σ [•10^{-5}]	^{39}Ar [%]	Age [Ma]	± 1σ
1	500	8.17 0.10	12.42 0.25	1.83 0.24	1.28 0.19	2459.3 3.0	44.9	29.4	3322 40	51.8 7.9	0.08	170	109 (109)
2	600	3.51 0.11	4.30 0.09	1.64 0.23	49.92 0.05	2672.1 6.3	1634.9	33.0	1314 42	1868 5	3.15	158.3	3.1 (3.1)
3	665	2.54 0.10	10.08 0.21	3.38 0.18	166.33 0.29	7342.1 8.3	6591.1	29.8	346 13	2265 5	10.49	189.9	0.9 (1.1)
4	**690**	1.69 0.17	16.06 0.36	3.13 0.26	163.76 0.13	7296.0 7.8	6797.6	49.4	231 23	2244 3	10.33	**198.4**	**1.4 (1.5)**
5	**700**	2.95 0.14	13.65 0.27	4.47 0.07	210.24 0.26	9700.1 16.6	8828.4	43.8	304 15	2167 5	13.26	**200.6**	**1.0 (1.2)**
6	**715**	1.03 0.16	20.77 0.46	2.24 0.40	99.70 0.27	4489.3 16.0	4184.2	49.5	230 36	2221 10	6.29	**200.5**	**2.3 (2.4)**
7	**740**	0.98 0.08	16.56 0.33	2.00 0.14	89.33 0.16	4036.1 12.4	3745.0	22.1	244 19	2213 9	5.63	**200.3**	**1.2 (1.4)**
8	**800**	1.39 0.13	0.25 0.07	2.70 0.31	123.32 0.21	5616.2 18.1	5204.4	38.0	248 24	2196 8	7.78	**201.5**	**1.4 (1.6)**
9	**880**	1.13 0.14	3.60 0.09	3.48 0.16	183.56 0.39	8059.7 30.8	7725.3	39.5	140 18	2277 10	11.58	**201.0**	**1.1 (1.3)**
10	**950**	0.49 0.26	5.42 0.14	3.06 0.19	168.47 0.24	7228.4 37.9	7082.9	65.6	68 35	2331 13	10.63	**200.8**	**1.8 (1.9)**
11	**1030**	0 0.22	4.67 0.16	2.11 0.17	128.66 0.21	5401.5 14.8	5401.5	14.8	--	2382 29	8.12	**200.5**	**0.6 (0.9)**
12	**1170**	0 0.56	5.67 0.25	2.75 0.38	162.31 0.28	6834.2 60.0	6834.2	60.0	--	2375 60	10.24	**201.1**	**1.7 (1.8)**
13	**1330**	6.69 1.46	4.15 0.11	1.93 0.29	36.16 0.24	3503 431	1526.5	36.0	1909 479	1032 127	2.28	**201.6**	**4.7 (4.7)**
14	1450	0 3.15	12.04 0.25	-0.87 0.62	2.29 0.07	70.8 25.4	70.8	25.4	--	3234 1160	0.14	149	52 (52)
Weighted plateau: 200.5 ± 1.1 (1.3) Ma (1σ), n = 10 steps, MSWD = 0.21, P = 0.99						J = 0.0027979 ± 0.0000015			Std: BMus/2; t = 328.5 ± 1.1 Ma		100.00	198.0	1.0 (1.2)

5.7. Discussion of $^{40}Ar/^{39}Ar$ data

Since the establishment of the $^{40}Ar/^{39}Ar$ dating method (see original paper by Merrihue and Turner 1966), this technique has been applied to impact melt rocks and glasses from a number of impact structures on Earth (e.g., Bottomley et al. 1990; Müller et al. 1990; Swisher et al. 1992; Deutsch and Schärer 1994; Trieloff et al. 1994; 1998; Schwarz and Lippolt 2002; Buchner et al. 2003; Reimold et al. 2005a; Jourdan et al. 2008; Schmieder et al. 2009c). Sanidine, the high-temperature form of K-feldspar, is considered to be preferentially suitable for $^{40}Ar/^{39}Ar$ dating and also used as standard in $^{40}Ar/^{39}Ar$ geochronology (e.g., McIntosh et al. 1990; McDougall and Harrison 1999; Jourdan and Renne 2007). In impact geochronological studies, sanidine has been used as dating material for the 142.5 ± 0.8 Ma Gosses Bluff impact structure (Australia; Milton and Sutter 1987) and the 74.1 ± 0.1 Ma Manson impact structure (Iowa, USA; Izett et al. 1998), both associated with fairly robust ages. The use of adularia as geochronological proxy is largely restricted to thermochronologic studies of hydrothermal ore deposits; however, similar to sanidine, adularia has yielded high-precision $^{40}Ar/^{39}Ar$ ages in many cases (e.g., Mertz et al. 1991; Lang et al. 1994; Ward et al. 2005; Arancibia et al. 2006).

The characteristics of the $^{40}Ar/^{39}Ar$ age plateaux for sanidine and adularia (Fig. 5.8), the consistency of ages between the high- and low-temperature phases of K-feldspar, as well as robust dataset statistics (e.g., a representative number of heating steps with concordant step ages and a high probability of 99% for the adularia age; Fig. 5.8; Tables 4.1 and 4.2), provide a valuable internal geochronological age countercheck. The virtually fresh state of the impact-metamorphosed gneiss (i.e., there is no indication of intense rock alteration in thin section), comparatively large domains and crystals of sanidine and adularia, and the lack of visible fluid inclusions suggest that the internal K/Ar isotopic system is not notably disturbed by argon loss, recoil effects, or excess argon (e.g., McDougall and Harrison 1999; Kelley 2002a; Jourdan et al. 2007a,b); this is underlined by a good fit of data in inverse isochron plots (Fig. 5.9). Particular ^{39}Ar recoil features - occasionally disturbing age spectra of fine grained impact melt rocks (e.g., Bottomley et al. 1990; Müller et al. 1990; Trieloff et al. 1994; 1998) - seem to be absent, similar to age spectra of tektites (Schwarz and Lippolt 2002).

The stable position of the Rochechouart impact structure at the northwestern margin of the French Massif Central suggests that, apart from possible Permotriassic burial diagenesis, no thermometamorphism occurred subsequent to the Paleozoic Variscan orogeny. The youngest pre-impact rocks in the region, formed during the late stage of the Variscan orogeny, are ~300 Ma granitic to granodioritic and dioritic dikes that transect the gneisses, leptynites, and granites of the bedrock (Chèvremont et al. 1996; Lambert 2009). Apart from an apparently young Rb/Sr age of ~265 Ma for a pegmatitic dike (Champagnac; Reimold et al. 1987; see also Alexandrov et al. 2000 and Lambert 2009 for discussion), no post-Variscan magmatic activity is known to have occurred in the French Massif Central during the whole of the Mesozoic. Thus, we can exclude an endogenic thermal event at ~200 Ma that could have disturbed the isotopic system in the Rochechouart impactites. For the Videix gneiss, this provides evidence that thermal metamorphism was caused by the Rochechouart impact event.

Previous dating of impact melt rocks and glasses from the Rochechouart impact structure was hampered by either poor geochronometers (e.g., the Rb/Sr or K/Ar method associated with large dating errors) or poorly suitable dating material. For example, the fine-grained aphanitic impact melt rocks from the Babaudus area are notably rich in alteration phases, predominantly clay minerals and iron hydroxides. These rock properties may be responsible for the loss of radiogenic argon upon alteration and/or argon recoil redistribution within the sample during irradiation (e.g., McDougall and Harrison 1999; Jourdan et al. 2007a), causing inaccurate and imprecise (younger) apparent ages (e.g., results by Kraut and French 1971; Lambert 1974; Reimold and Oskierski 1987; Fig. 5.4). [40]Ar/[39]Ar dating of the Champagnac pseudotachylites by Kelley and Spray (1997) was carried out using laser spot dating on a thin rock tile and age determination by inverse isochron calculations. Ages of single spots yielded comparatively old ages between 231 Ma and ~1.67 Ga, indicative of a distinct excess argon component (Kelley and Spray 1997; McDougall and Harrison 1999; Kelley 2002a) in parts of the sample material that was probably not completely degassed upon friction melting. The MSWD value calculated in the inverse isochron plot given by Kelley and Spray (1997) was rather high (up to 4.0), defining a less robust 214 ± 8 Ma 'preferred' age for the Rochechouart impact. The concordant plateau ages for

sanidine and adularia demonstrate that, in addition to impact melt rocks and glasses, hydrothermal phases crystallized during the post-shock cooling process are suitable for isotopic dating of impact events (see also Ames et al. 1998).

6. The Manicouagan impact structure (Québec, Canada)

6.1. Geologic setting and previous work

The Manicouagan impact structure (Québec, Canada; centered at 51°23' N, 68°42' E; Figs. 6.1; 6.2; 6.3A), with an estimated diameter of ~100 km, counts among the four largest impact structures on Earth. The target rocks at Manicouagan mainly comprise ~1 Ga old gneisses, anorthosites, gabbroids, as well as an overlying thin layer of Ordovician limestones of the Grenville Province of the Canadian Shield. A comprehensive geological review of the Manicouagan impact structure is given by Murtaugh (1976) and Grieve (2006). Whilst the Manicouagan structure was considered as a volcanic feature by some authors until the 1970s (e.g., Currie 1972), shock metamorphic effects in the Manicouagan impactites were described by, for example, Bunch et al. (1967), Dworak (1969), Wolfe (1971), Murtaugh (1972; 1976), and Dressler (1990), confirming an impact origin. The central uplift, represented by the Mont Babel (957 m) and Maskelynite Peak (945 m) mountains, also forms the topographically highest point within the central part of the impact structure (Fig. 6.2-6.3A-B). The uplifted inner zone is surrounded by an annular depression roughly 65 km in diameter, occupied by the Manicouagan water reservoir (Figs. 6.1-6.3A). On the central René Levasseur Island, massive impact melt rocks overlie lithic impact breccias and the crystalline basement (Fig. 6.3C-G). Recent drilling revealed a maximum thickness of the Manicouagan impact melt sheet of locally up to ~1,100 m, predominantly in tectonic depressions (Spray 2008). Detailed petrographic and geochemical studies of the Manicouagan impact melt rocks, fine-grained and clast-rich near the footwall and progressively coarse-grained and clast-poor towards the top (Figs. 6.3C-L), are provided by Floran et al. (1978), Grieve and Floran (1978), Simonds et al. (1978), and comprehensively summarized by Grieve (2006). The Manicouagan impact structure became moderately eroded and impactites reworked and transported during the last glaciation (Buchner and Schmieder 2009a). Suevites can be found as rounded allochthonous pebbles and boulders on the Levasseur Island (Fig. 6.3M-N). Ordovician limestones occur as outliers in the tectonic ring depression along the shoreline of

Levasseur Island and as clasts within the melt rocks (Fig. 6.3O-P). As for now, no impactor traces could be unequivocally detected in the impact melt rocks (Palme et al. 1981; Grieve and Pesonen 1992; Grieve 2006), which might suggest that the Manicouagan crater was struck by a differentiated achondritic projectile. The mode of impact melt formation at Manicouagan with high volumes of melt within a differentiated melt sheet derived from partially anorthositic rocks, furthermore, provides insights into possible analogous impact melt generation, emplacement, and differentiation in Lunar impact basins (e.g., Floran 1976; Floran et al. 1976; Simonds et al. 1976; Orphal and Schulz 1978; Spray 2008; Spray et al. 2009). A distal impact ejecta layer that contains reworked glauconitic spherules, shocked quartz, and kinked mica discovered in southwestern Britain (Walkden et al. 2002; Kirkham 2003) was recently linked with the Manicouagan impact based on the provenance analysis of the heavy mineral association (Thackrey et al. 2008; 2009). Dating of the Manicouagan impact structure by various methods during the last decades yielded generally compatible ages: fission track dating of impact melt rocks by Fleischer et al. (1969) yielded an age of 208 ± 25 Ma; K/Ar dating by Wanless et al. (1965) and Wolfe (1971) resulted in ages of 225 ± 30 Ma and 214 ± 8 Ma, respectively, in agreement with a Rb/Sr (mineral isochron) age of 214 ± 5 Ma (Jahn et al. 1978). These ages are also in compatibility with high-precision U/Pb ages of 214 ± 1 Ma (Hodych and Dunning 1992) and 215.56 ± 0.05 Ma (Ramezani et al. 2005) obtained from melt-grown zircons. Previous ^{40}Ar/^{39}Ar dating yielded ages around ~212 Ma (Trieloff and Jessberger 1992) and, more recently, a more precise age of ~215.5 Ma (Ramezani et al. 2005). (U-Th)/He dating of zircon crystals recovered from impact melt rocks yielded an age of 213.6 ± 4.6 Ma (van Soest et al. 2009). Also, authigenic potassium feldspar in the British distal Manicouagan impact ejecta layer yielded a ^{40}Ar/^{39}Ar age of 214 ± 2.5 Ma (Walkden et al. 2002). In summary, the Manicouagan impact structure appears to be 'outdated', and its age can be considered well-constrained by different dating methods and samples.
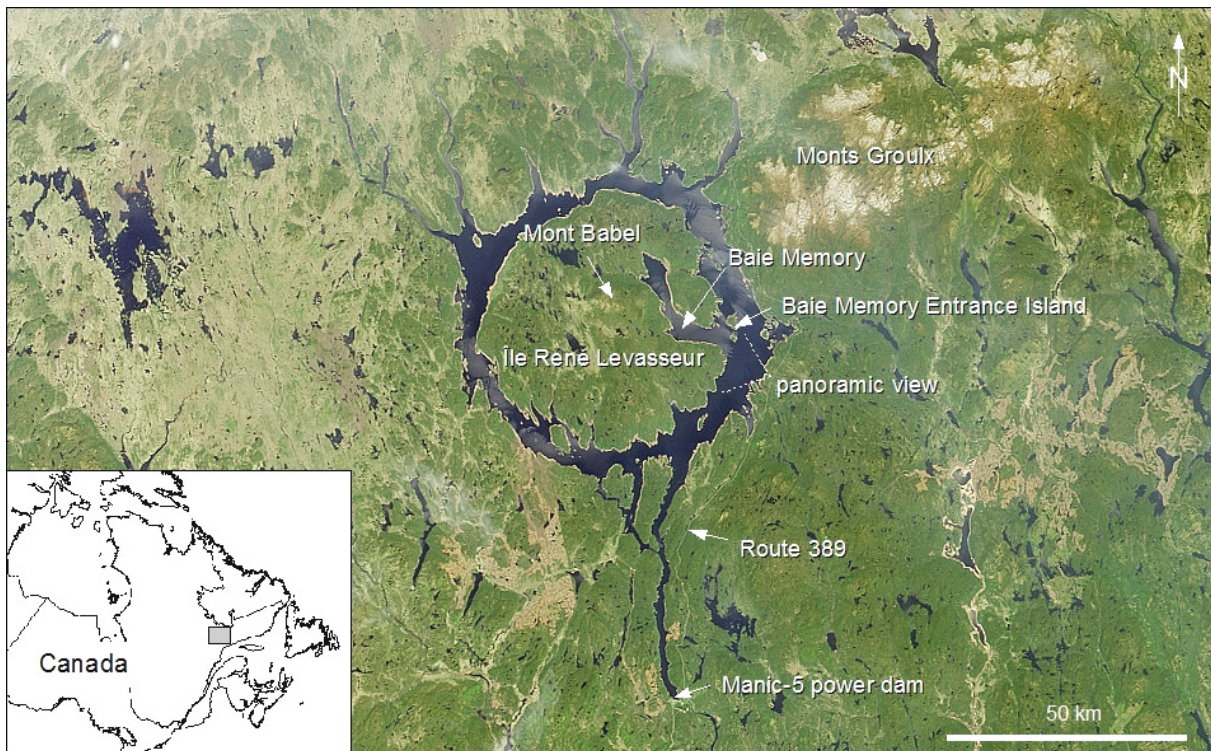
Fig 6.1: Satellite image scene of the Manicouagan impact structure occupied by a water reservoir. The fjord-like feature in the eastern part of the central Levasseur Island is Baie Memory; see gray box in inset map for location in Canada. Image: NASA Visible Earth.
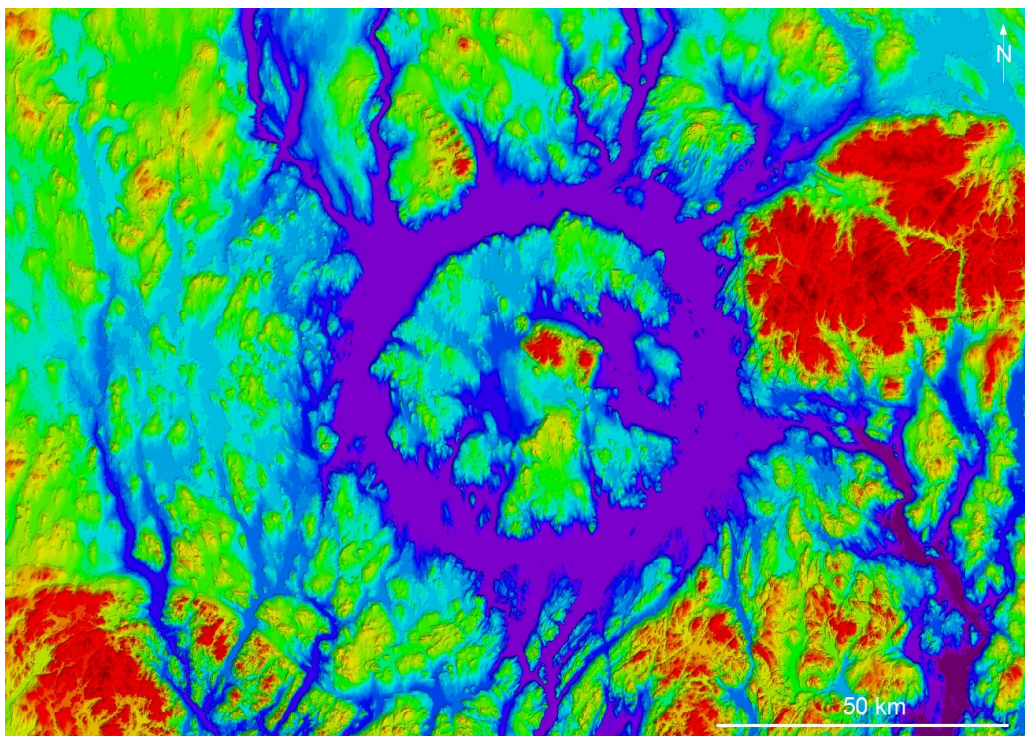
Fig 6.2: Color-coded Canadian Digital Elevation Data (CDED) terrain model of the Manicouagan impact structure. Color scale is from ~400 m (dark blue) to ~1100 m (red) above sea level. Note the topographic expression of the Mont Babel in the central uplift and the Monts Groulx northeast of the impact structure.
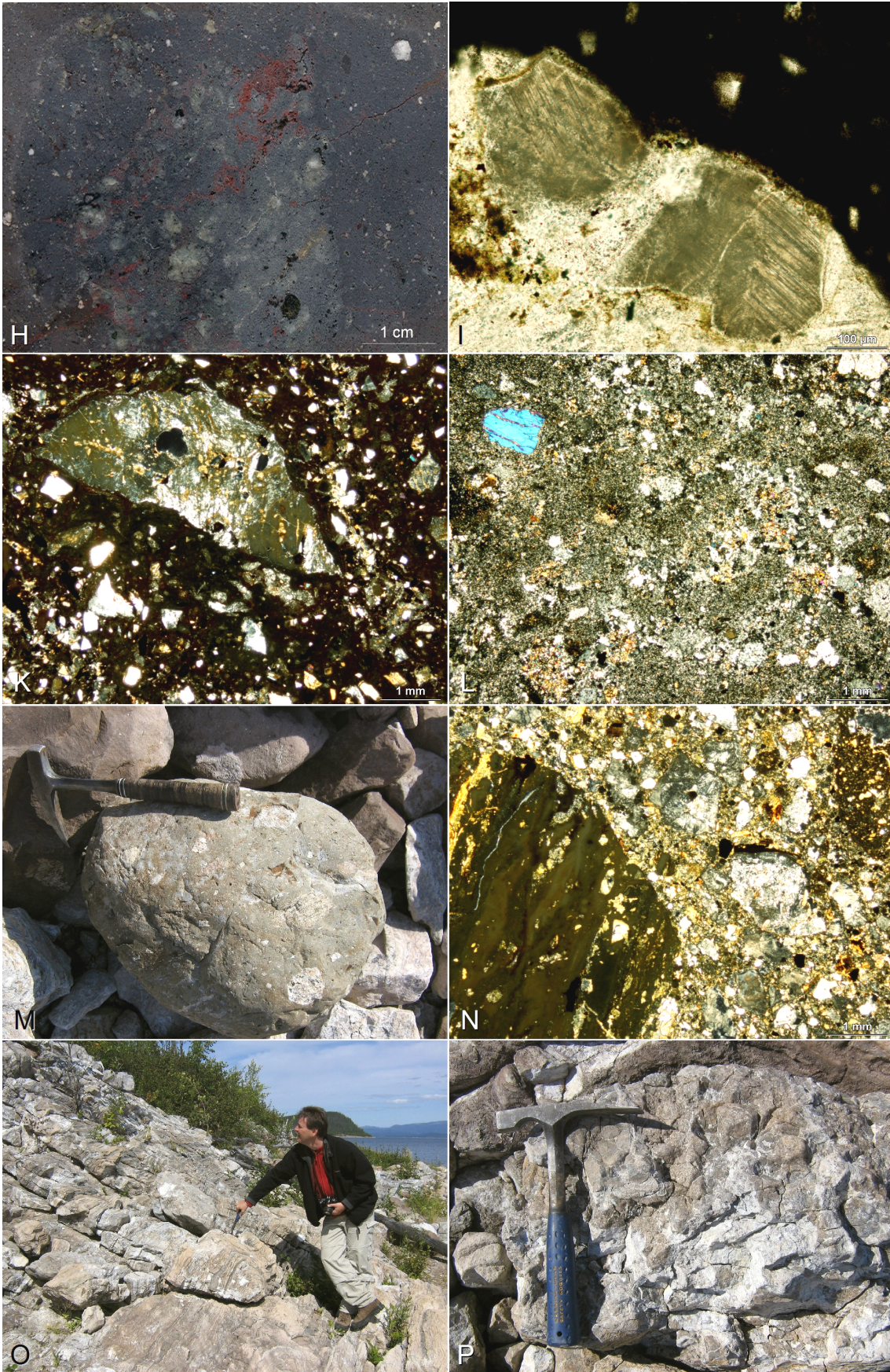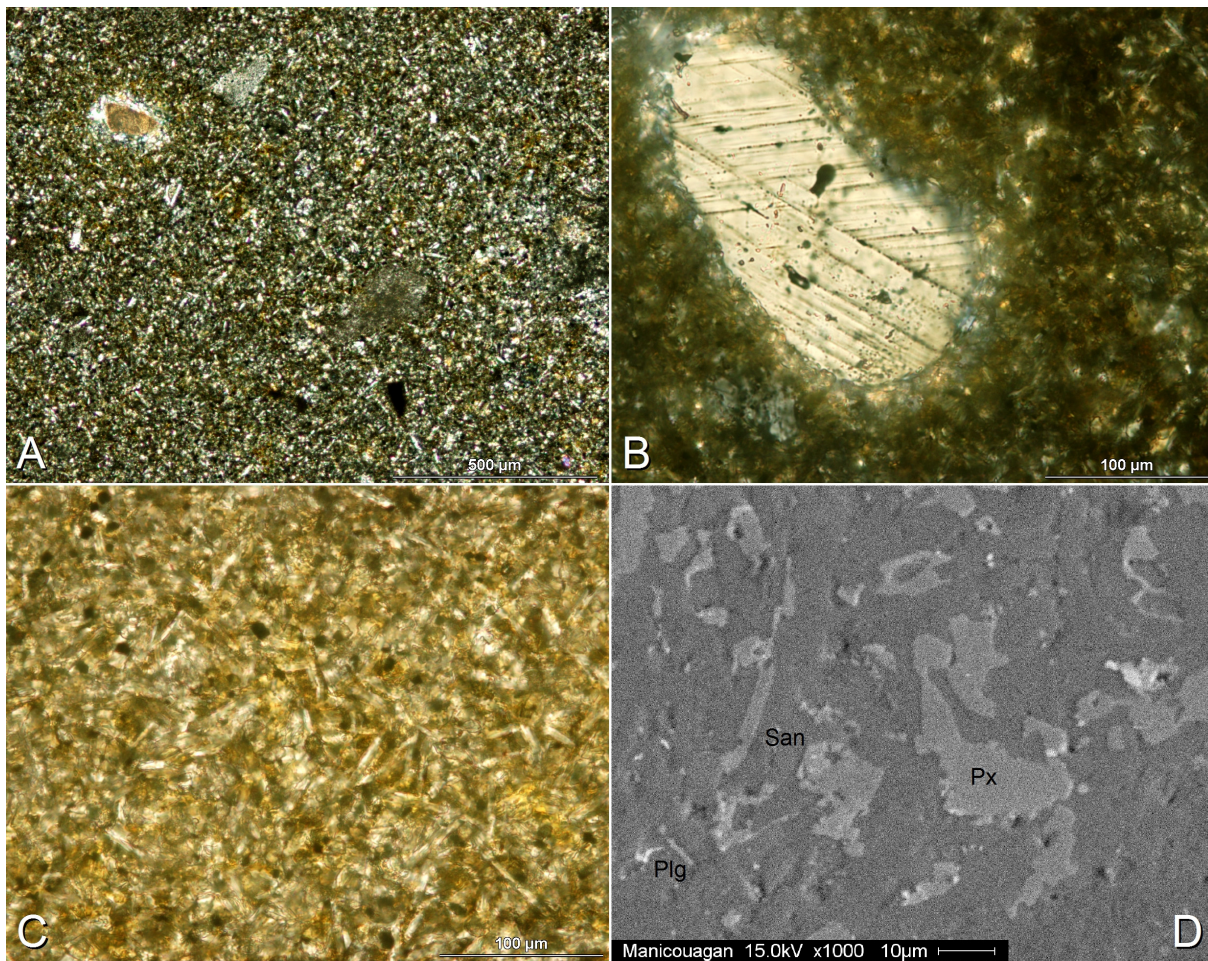
Fig 6.4: Thin section and scanning electron microscope photomicrographs of the Manicouagan impact melt rock used for dating; **A**: fine-grained aphanitic character of the melt rock; browinsh shocked and toasted quartz in upper left corner (cross-polarized light); **B**: shocked quartz surrounded by a pyroxene corona (bright) and fine-grained crystalline melt matrix (cross-polarized light); **C**: detailed view of the fine-grained crystalline melt matrix with lath-shaped crystallites of pyroxene and feldspar (plane-polarized light); **D**: backscattered electron image of the crystalline melt matrix with micron-scaled intergrowths of pyroxene (Px; light grey) and feldspar (San: sanidine; Plg: plagioclase; dark grey).

<< Fig 6.3 (previous pages): Field photographs and impactites of the Manicouagan impact structure. **A**: Panoramic view of the Manicouagan impact structure and water reservoir as seen from the eastern shore; cental uplift with Mont Babel in the background (see Fig. 6.1 for panoramic point); **B**: entrance of the Baie Memory with Mont Babel (built up by anorthositic rocks) in the background (see Fig. 6.1 for location); **C**: anorthositic lithic impact breccia, eastern shore of Levasseur Island; **D**: ~120 m high cliffs of the Manicouagan impact melt sheet showing columnar jointing; Baie Memory Entrance Island (see Fig. 6.1 for location); **E**: detailed view of columnar jointing in clast-poor impact melt rocks; Baie Memory Entrance Island; **F**: clast-rich impact melt rocks at the eastern shore of Levasseur Island; **G**: impact melt rocks with megaclast (bright); Baie Memory Entrance Island; **H**: polished section of dark, clast-rich impact melt rock from Baie Memory Entrance Island; **I**: thin section photomicrograph of strongly toasted shocked quartz grains surrounded by dark melt matrix (melt rock shown in H; plane-polarized light); **K**: thin section photomicrograph of clast-rich reddish impact melt rock from Levasseur Island (cross-polarized light); **L**: thin section photomicrograph of medium-grained dark impact melt rock from Baie Memory Entrance Island (cross-polarized light); **M**: rounded boulder of suevite at the eastern shore of Levasseur Island; **N**: thin section photomicrograph of suevite with large fluidal impact melt particles (left and upper right) in a lithic groundmass; **O**: outlier of shocked Ordovician limestones preserved in the structural annular graben, eastern shore of Levasseur Island (E. Buchner for scale); **P**: close-up view of brecciated Ordovician limestones as shown in O.

6.2. Samples and analytical techniques

A virtually fresh, fine-grained aphanitic and clast-poor dark impact melt dike rock (Fig. 6.4; Table 6.1) collected at the eastern shore of the Levasseur Island (south of Baie Memory) was chosen as material for optical study and dating. Sampling was carried out during a field trip in summer 2006 (together with Dr. Elmar Buchner and Bob Burke). The modal and geochemical composition of the rock was determined by optical microscopy and supporting energy dispersive X-ray (EDX) measurements (CamScan™ SC44 scanning electron microscope-EDAX™ PV 9723/10 system, Institut für Planetologie, Universität Stuttgart).

6.3. Petrography, geochemistry, and shock metamorphic conditions

In analogy to the descriptions by Floran et al. (1978) and Simonds et al. (1979), the mineralogy of the Manicouagan impact melt dike rock consists mainly of pyroxene, plagioclase, sanidine, quartz, and accessories (see also Grieve 2006; Fig. 6.4A-D). Quartz is commonly fractured and exhibits multiple sets of planar deformation features (PDFs) and toasting effects (Fig. 6.4A), and is often surrounded by a pyroxene corona (intra-melt reaction rim; Fig. 6.4B). Feldspars often exhibit checkerboard textures or have been transformed to recrystallized glasses (e.g., Bischoff and Stöffler 1984; Grieve 2006). The microcrystalline melt matrix is largely composed of intergrown pyroxene and feldspar crystals usually some tens of microns in size (Fig. 6.4C-D) making up a pseudoporphyritic texture of the rock in analogy to the petrographic description of melt rocks of the lowermost Manicouagan melt sheet unit by Floran et al. (1978; see also their Fig. 4a). The geochemical composition of the melt rock is similar to that of Manicouagan melt rocks reported in the literature (Currie 1972; Floran et al. 1978; Grieve 2006), with slightly higher contents in K, Ca, and Fe, and somewhat lower Na and Mg values (Table 6.1). The melt rock paragenesis suggests stage IV shock metamorphic conditions (Stöffler 1971; 1984) and whole-rock melting at peak shock pressures in excess of ~60 GPa and post-shock temperatures above ~1,200°C (e.g., Grieve and Floran 1978; French 1998).

Table 6.1: Average composition of impact melt rocks at Manicouagan as reported in the literature and measured for the dating sample (compare Fig. 6.4)

	Currie (1972)	Floran et al. (1978)	Dating sample*
SiO_2	57.7	57.8	58.9
TiO_2	0.7	0.8	1.3
Al_2O_3	18.7	16.5	15.7
Fe_2O_3 + FeO**	5.9	6.3	8.3
MnO	0.1	0.1	0.5
MgO	3.5	3.5	1.8
CaO	5.8	5.9	7.5
Na_2O	4.0	3.8	1.3
K_2O	3.1	3.0	4.3
Total	99.5	97.7	99.8

*average of 7 EDX measurements

** given as separate values by Currie (1972) and Floran et al. (1978)

6.4. $^{40}Ar/^{39}Ar$ dating – sample choice and methods

Virtually homogenous whole-rock chips of the melt rock up to ~5 mm in size (with K_2O contents of ~4 wt%; Table 6.1) were handpicked from the crushed rock on the basis of their fresh optical appearance and rinsed with ethanol and deionized water in an ultrasonic cleaner. $^{40}Ar/^{39}Ar$ dating was done at the Institut für Geowissenschaften, University of Heidelberg (Dr. W. H. Schwarz and Dr. M. Trieloff; see Trieloff et al. 2005; Schwarz and Trieloff 2007a for technical details), using the decay constants determined by Steiger and Jäger (1977); due to miscalibration of the K decay constants compared to the U-decay series constants, the $^{40}Ar/^{39}Ar$ ages have to be c. 1% higher in the age range of the Mesozoic with respect to those calculated with the constants recommended in Steiger and Jäger (1977; see also Villeneuve et al. 2000; Ramezani et al. 2005; Mundil et al. 2006; Schwarz and Trieloff 2007b; Jourdan et al. 2009a). The samples were wrapped in Al-foil, packed in quartz ampoules (12x55 mm), Cd-shielded (to avoid isotopic interferences), and irradiated for 5 days at the GKSS Geesthacht, Germany. After irradiation, the samples were heated in an inductively heated Mo-furnace up to ~1,500°C in several temperature steps. The gas was cleaned with Zr-, Ti-, Cu/CuO-, and Al-Getters. Argon was measured using a MAT GD150 mass spectrometer. The argon

results were corrected for mass discrimination, argon decay, isotopic interferences (all information listed in Table 6.2), and blanks from the extraction line (glass and furnace). The argon isotopic composition of blanks was always atmospheric within uncertainty. Ages were calculated against the BMus/2 (Bärhalde muscovite, Black Forest, Germany) standard with an age of 328.5 ± 1.1 Ma, which was calibrated against 5 further international $^{40}Ar/^{39}Ar$ dating standards; for further information about the analytical procedure see Schwarz and Trieloff (2007a).

6.5. Dating results and interpretation

$^{40}Ar/^{39}Ar$ step-heating analysis yielded a Late Triassic (Norian according to Ogg et al. 2008) weighted plateau age of 211 ± 2 Ma (including monitor error; 2σ; MSWD=0.18; P=0.99) for ~24-83% of the ^{39}Ar released during steps 5-10 of 12 extraction steps, with ages of individual extractions that overlap within the 2σ error limit (Fig. 6.5). The age spectrum exhibits slightly older apparent ages in the low-temperature extraction steps 2-3 (~0-24% of ^{39}Ar released) and in the highest-temperature step 12 (~97-100% of ^{39}Ar), forming a somewhat saddle-shaped age spectrum (e.g., Bottomley et al. 1990) with concordant intermediate step ages. The inverse isochron plot (Fig. 6.6) reveals that the lowest- and highest-temperature extractions are characterized by an atmospheric $^{40}Ar/^{36}Ar$ ratio (297.6 ± 1.3 and 310 ± 47, respectively, undistinguishable within error from the atmospheric value of 295.5 ± 0.5; Steiger and Jäger 1977) but that the mid-temperature fraction (steps 5-10 with ~59% of the total ^{39}Ar released) contains a detectable excess argon component (e.g., Kelley and Spray 1997; McDougall and Harrison 1999; Kelley 2002a) suggested by an initial $^{40}Ar/^{36}Ar$ ratio of 361 ± 17 and an apparently old total fusion age of ~219 Ma (Table 6.2). The partial isochron through steps 5-10 yields an apparent isochron age of 210 ± 5 Ma (2σ), in accord with the weighted plateau (Fig. 6.5) in the age spectrum corrected for excess argon (see Table 6.2). The Ca/K spectrum (Fig. 6.7) is saddle-shaped, with a high Ca/K ratio in step 1 (>8), lower ratios in steps 2-10 (~1-3) and high ratio in the high-temperature steps 11-12 (~6-7); this indicates that Ca is preferentially released from a Ca-rich crystalline phase (pyroxene) at high temperatures of >1,200°C. The high Ca/K ratios in steps 1 and 11-12

are probably caused by argon recoil redistribution (presumably degassing of a phase of low argon retentivity that acquired ^{37}Ar from pyroxene and donated ^{39}Ar to the pyroxene upon neutron irradiation; e.g., Turner and Cadogan 1974; Jourdan et al. 2007a; Trieloff 2009, pers. comm.), as suggested by the fine-grained aphanitic nature of the melt rock and micron-scaled intergrowths of feldspar and pyroxene crystals in the crystalline melt matrix (Fig. 6.4). ^{39}Ar and ^{37}Ar recoil redistribution obviously did not notably disturb the feldspathic crystalline impact melt, as indicated by low and rather homogenous Ca/K ratios and largely concordant step ages in steps 5-10. The argon isotopic data are summarized in Table 6.2. Considering the current miscalibration of the K/Ar decay system against the U/Pb decay series and slightly (~2%) older 'real' ^{40}Ar/^{39}Ar age values for the Mesozoic, both the 211 ± 2 (2σ) weighted plateau age (Fig. 6.5) and the 210 ± 5 Ma (2σ) isochron age (Fig. 6.5) are widely consistent with (or at least close to) the earlier dating results of 214 ± 1 Ma (U/Pb; Hodych and Dunning 1992) and 215.56 ± 0.05 Ma (U/Pb; Ramezani et al. 2005). Expectedly, this dating attempt could not improve the Manicouagan impact age but represents an exemplary case of ^{40}Ar/^{39}Ar dating of fine-grained impact melt rocks and associated problems (excess argon; argon recoil redistribution) to identify and overcome. I, therefore, refer to the well-defined previous isotopic ages for Manicouagan as the currently recommended ages (see also Jourdan et al. 2009b).
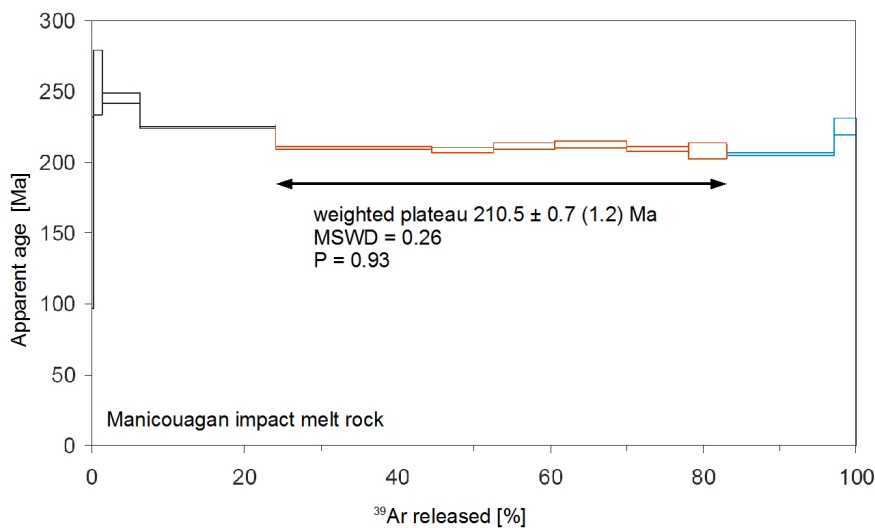
Fig. 6.5: ^{40}Ar/^{39}Ar age spectrum for fine-grained impact melt rock (whole-rock sample) from the Manicouagan impact structure. Steps 5-10 (red) corrected for initial ^{40}Ar/^{36}Ar ratio of 361 ± 17 (see inverse isochron plot shown in Fig. 6.6), steps 1-4 and 11-12 with ratio ^{40}Ar/^{36}Ar ratio of 295.5 ± 0.5 (Steiger and Jäger 1977); errors are at the 1σ level, error in parentheses includes standard error.
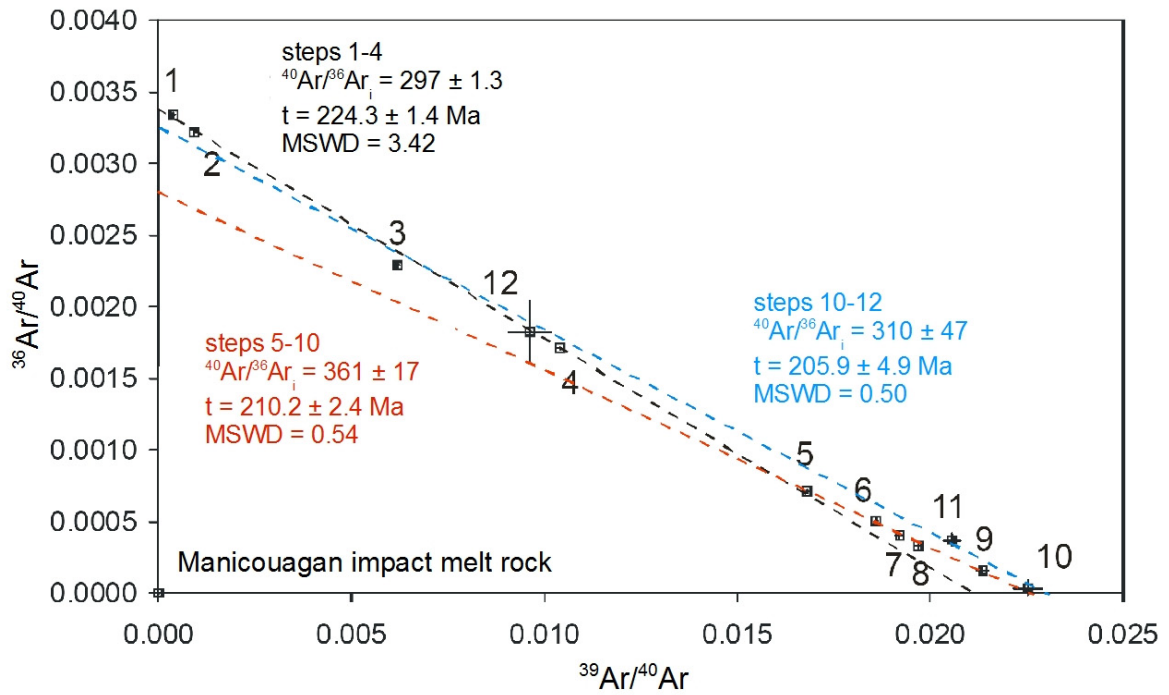
Fig. 6.6: Inverse isochron plot for impact melt rock (whole-rock sample) from the Manicouagan impact structure. Steps 1-4 (black) and 10-12 (blue) define specific isochrons with initial $^{40}Ar/^{36}Ar$ ratios that are atmospheric within error (Steiger and Jäger 1977); steps 5-10 (red) define an isochron that reveals excess argon with an initial $^{40}Ar/^{36}Ar$ ratio >295.5. Errors are at the 1σ level.
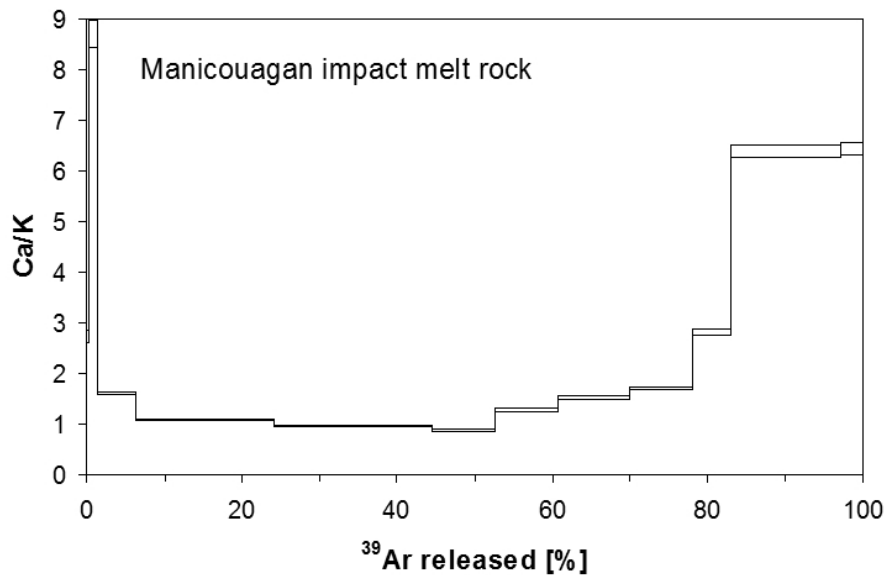
Fig. 6.6: Ca/K spectrum for impact melt rock (whole-rock sample) from the Manicouagan impact structure.

Table 6.2: Isotopic argon dataset and ages for fine-grained impact melt rock (whole-rock) sample from the Manicouagan impact structure; errors in parentheses include monitor error; bold characters denote extraction steps included in the partial plateau calculation.

Step #	Temp [°C]	^{36}Ar [fA]	± 1σ	$^{37}Ar_{Ca}$ [fA]	± 1σ	^{38}Ar [fA]	± 1σ	$^{39}Ar_K$ [fA]	± 1σ	^{40}Ar [fA]	± 1σ	$^{40}Ar^*$ [fA]	± 1σ	$^{36}Ar/^{40}Ar$ [•10⁻⁶]	± 1σ	$^{39}Ar/^{40}Ar$ [•10⁻⁶]	± 1σ	^{39}Ar [%]	Age [Ma]	± 1σ	Age [Ma][1]	± 1σ[1]
1	600	19.89	0.11	3.31	0.1	3.88	0.11	2.32	0.09	5957	10	79	34	3339	19	390	15	0.2	165	68 (68)	165.0	68 (68)
2	690	46.08	0.18	60.7	1.2	8.96	0.15	13.31	0.32	14347	39	731	68	3212	15	928	22	1.3	257	23 (23)	257.0	23 (23)
3	760	18.77	0.13	42.7	0.8	4.28	0.18	50.86	0.17	8204	15	2658	40	2288	16	6200	24	4.8	245.5	3.6 (3.7)	245.5	3.6 (3.7)
4	820	31.04	0.09	107.1	2.1	9.52	0.10	188.65	0.25	18154	16	8983	29	1709.6	5.0	10392	16	17.8	225.0	0.9 (1.2)	225.0	0.9 (1.2)
5	**840**	9.18	0.12	108.3	2.1	5.74	0.29	217.19	0.62	12934	26	10222	42	709.6	9.6	16792	59	20.5	222.6	1.2 (1.4)	**210.5**	**1.3 (1.5)**
6	**850**	2.31	0.08	39.4	0.8	2.19	0.19	85.43	0.14	4596	11	3913	22	503	19	18588	56	8.1	216.9	1.3 (1.5)	**209.3**	**1.9 (2.1)**
7	**870**	1.78	0.08	56.6	1.1	2.00	0.16	85.00	0.29	4426	13	3900	22	402	19	19205	88	8.0	217.3	1.4 (1.6)	**211.4**	**2.0 (2.2)**
8	**910**	1.66	0.14	79.9	1.6	2.45	0.15	99.47	0.22	5056	18	4564	41	329	28	19675	84	9.4	217.3	1.9 (2.1)	**212.7**	**2.7 (2.8)**
9	**980**	0.64	0.08	75.6	1.5	2.56	0.03	85.09	0.11	3983	25	3796	17	160	21	21361	139	8.0	211.6	1.0 (1.3)	**209.7**	**2.2 (2.3)**
10	**1090**	0.09	0.14	80.0	1.6	1.30	0.12	54.10	0.17	2400	39	2374	20	36	59	22546	370	5.1	208.4	1.8 (2.0)	**208.1**	**5.6 (5.7)**
11	1230	2.69	0.28	499.2	9.9	4.48	0.34	148.94	0.30	7250	77	6454	33	372	38	20545	221	14.0	205.9	1.1 (1.4)	205.9	1.1 (1.4)
12	1400	5.74	0.61	102.0	2.0	2.03	0.16	30.28	0.05	3145	177	1448	40	1826	220	9628	543	2.9	225.9	5.9 (6.0)	225.9	5.9 (6.0)
Weighted plateau: 210.5 ± 0.7 (1.2) Ma (1σ), n = 6 steps, MSWD = 0.18, P = 0.99										J = 0.0027896 ± 0.0000067				Std: BMus/2; t = 328.5 ± 1.1 Ma				100	219.2	1.4 (1.5)	--	--

[1] calculated steps 5-10 with initial $^{40}Ar/^{36}Ar$ ratio of 361 ± 17, steps 1-4 and 11-12 with Steiger and Jäger (1977) ratio of 295.5 ± 0.5

7. The Lake Saint Martin (Manitoba, Canada), Red Wing Creek (North Dakota, USA), and Obolon (Ukraine) impact structures

7.1. Lake Saint Martin (Manitoba, Canada)

The ~40 km Lake Saint Martin impact structure (Manitoba, Canada; centered at 51°47' N and 98°32' W), located in the southern Manitoban Interlake Region (Fig. 7.1), is hosted by Ordovician to Devonian sedimentary rocks (sandstones, shales, and carbonates) on the northeastern flank of the Williston Basin, which overlie Precambrian granites of the Superior Province of the Canadian Shield. Originally interpreted as a Permian to Triassic volcanic 'cryptoexplosion' feature (Currie 1970), the Lake Saint Martin structure was soon confirmed as an impact structure by the detection of shock metamorphic features in the rocks (Dence 1970). Impact lithologies (also locally termed the 'St. Martin Series'; e.g., McCabe and Bannatyne 1970) comprise carbonate, granitic, and suevitic breccias together with impact melt rocks (Fig. 7.2A-D) partially covered by post-impact Jurassic red beds and evaporites, as well as by Pleistocene glacial till. Outcrops of coherent impact melt rocks occur in the eastern central part of the impact structure. A detailed geologic overview of the Lake Saint Martin impact structure and associated impactites is given by McCabe and Bannatyne (1970), Simonds and McGee (1979), Bannatyne and McCabe (1984), and Grieve (2006). Geochemical studies revealed no detectable impactor signature in the melt rocks from the Lake Saint Martin impact structure (Göbel et al. 1980; Reimold et al. 1990; Goderis 2009; pers. comm.), suggesting an achondritic projectile (Palme 1980). In addition to the currently accepted whole-rock and mineral isochron Rb/Sr age of 219 ± 32 Ma (Reimold et al. 1990), previous age determinations yielded K/Ar whole rock ages for impact melt rocks of 200 ± 25 Ma and 250 ± 25 Ma, respectively (McCabe and Bannatyne 1970), as well as an apatite fission track age of 208 ± 14 Ma (Kohn et al. 1995; Grieve 2006). Recently, Wartho et al. (2009) have used the (U-Th)/He geochronological technique on individual zircon and apatite crystals (see also van Soest et al. 2009 for the application of this dating technique to a set of terrestrial impact structures). Individual euhedral zircon and apatite crystals separated from massive impact melt rocks collected ~7 km northeast of

the center of the Lake Saint Martin impact structure yielded Middle to Late Triassic (Anisian to Karnian; Ogg et al. 2008) mean (U-Th)/He ages of 235 ± 6 Ma for a set of four zircon grains and 232 ± 7 Ma for five apatite grains, respectively, in agreement with earlier dating results (Wartho et al. 2009).
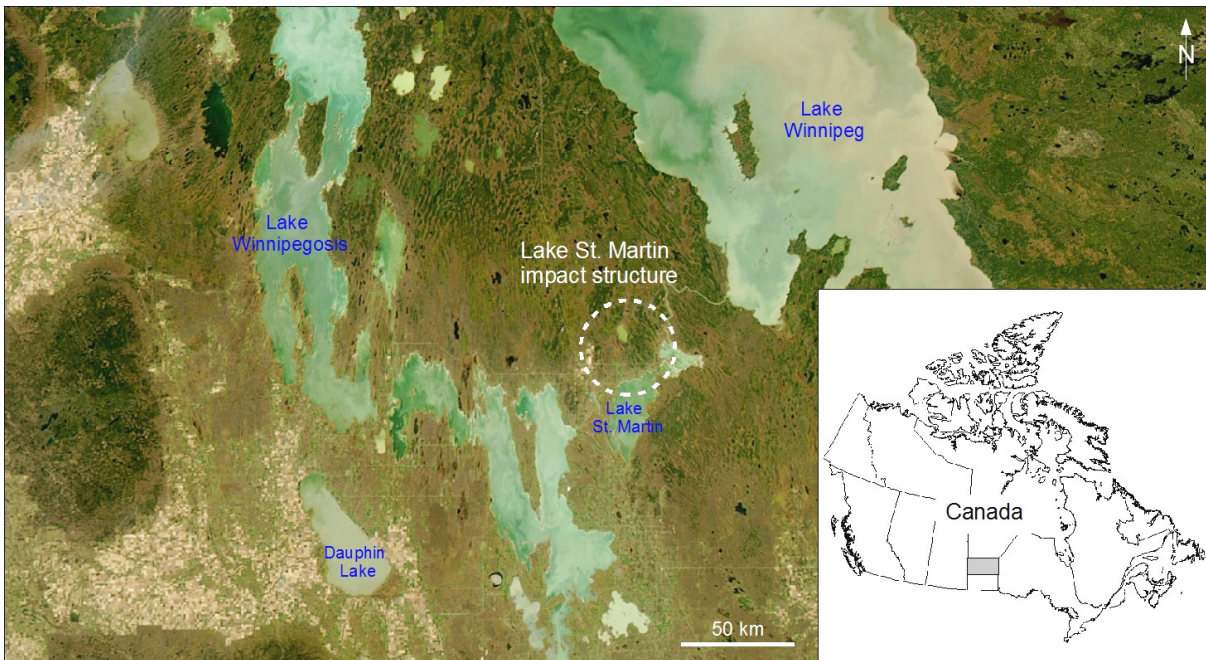
Fig. 7.1: The Lake Saint Martin impact structure in the Interlake Region of Manitoba, Canada; see gray box in inset map for position of the satellite image scene in Canada. Image source: NASA Visible Earth.
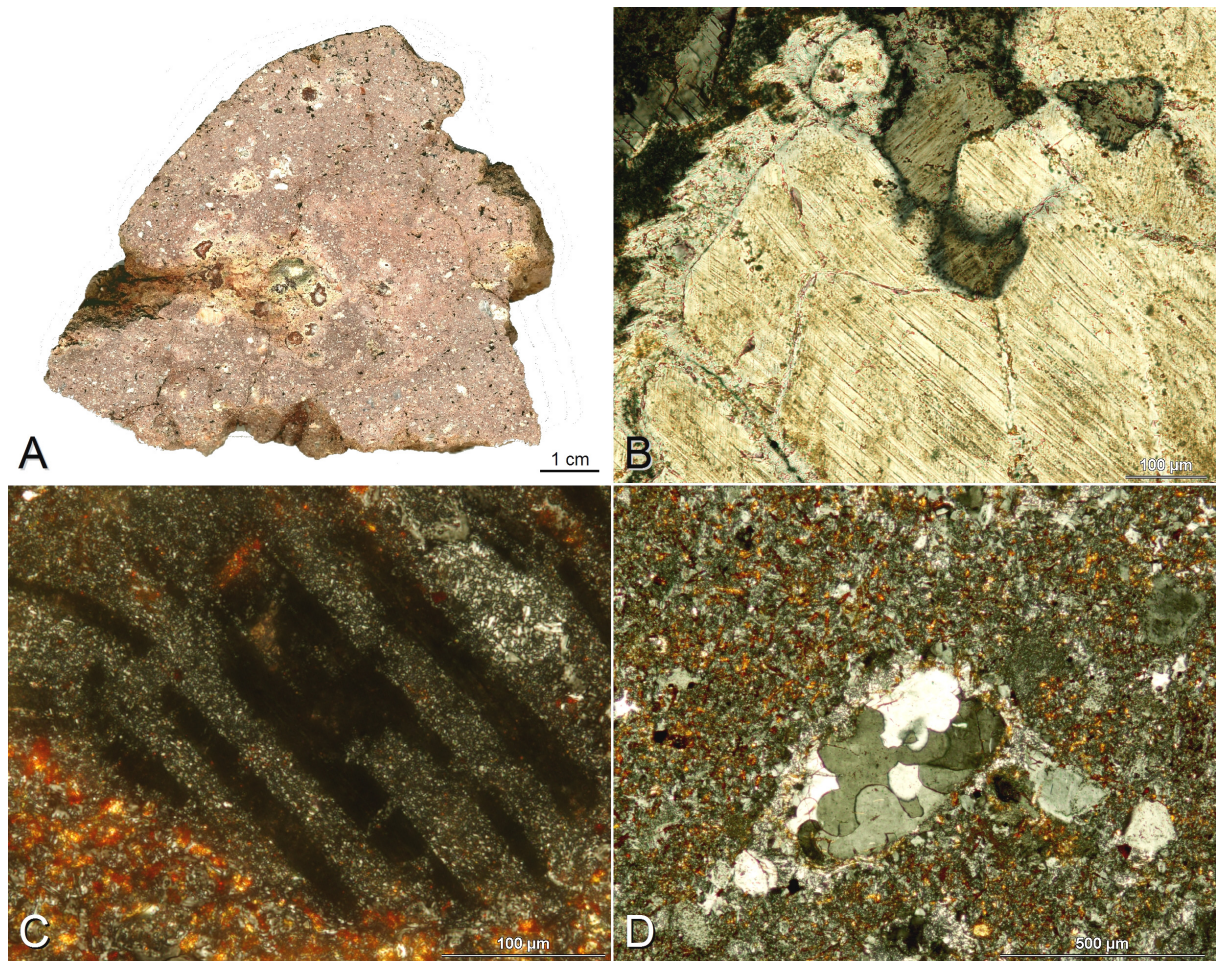
Fig. 7.2: Impact melt rocks from the Lake Saint Martin impact structure. **A**: Polished rock section; **B**: shocked quartz with planar deformation features (PDFs; cross-polarized light); **C**: isotropic diaplectic plagioclase glass (maskelynite; cross-polarized light); **D**: 'ballen quartz' in aphanitic melt matrix (cross-polarized light).

7.2. Red Wing Creek (North Dakota, USA)

The ~9 km Red Wing Creek impact structure (North Dakota, USA; centered at 47°36' N, 103°33' W) is buried beneath a ~2,000-2,500 m thick pile of Jurassic and younger sedimentary rocks of the North American intracratonic Williston Basin. On seismic datasets, the Red Wing structure is characterized by the occurrence of intensely deformed Devonian and Carboniferous rocks that overlie the largely undisturbed Ordovician, accompanied by a gravity high corresponding with the central uplift of the structure, where the sedimentary strata are uplifted by ~1 km. The central uplift is surrounded by a ~2 km wide annular depression, and an outer anticline (e.g., Brenan et al. 1975; Sawatzky 1975; Grieve et al. 1981). Stratigraphic relations constrain an impact

age of ~220-200 Ma (Koeberl et al. 1996a); Gerhard et al. (1982) and Grieve (1991) state stratigraphic ages of 200 ± 25 Ma and 200 ± 5 Ma, respectively, corresponding to Triassic-Jurassic. Deep drillings encountered lithic impact breccias that contain shatter cone fragments and shocked quartz with multiple sets of PDFs, and no larger impact melt particles were recovered (Koeberl and Reimold 1995a; Koeberl et al. 1996a). Accordingly, no unambiguous geochemical signature of the impactor is available (however, slight enrichment of siderophile elements in one drill cutting sample might suggest a chondritic projectile; Koeberl et al. 1996a). Detailed geologic reviews of the Red Wing Creek impact structure are given by Brenan et al. (1975) and Koeberl et al. (1996a). Like some other impact structures in the Williston Basin, e.g., the ~16 km Ames (Oklahoma, USA) and the ~2.5 km Viewfield (Saskatchewan, Canada) impact structures, the Red Wing impact structure as a structural trap is associated with outstanding hydrocarbon deposits (e.g., Sawatzky 1975; Donofrio 1981; 1998; Grieve 2005; Reimold et al. 2005b; Schmieder et al. 2009b).

7.3. Obolon (Ukraine)

The ~20 km marine Obolon impact structure (Ukraine; centered at 49°35' N, 32°55' E) is located within Carboniferous to Lower Triassic sedimentary rocks that overlie Early Proterozoic crystalline rocks of the northeastern Ukrainian Shield (Donets Graben region; e.g., Gurov and Gurova 1995; Masaitis 1999; Valter et al. 2000; Valter 2002; Fig. 7.3). The impact structure, with a deep central annular basin, a flat central uplift, local depressions, and gentle outer slopes, is covered by up to 500 m of Middle Jurassic to Cenozoic sedimentary rocks. Core drilling recovered lithic breccias and suevites in the annular trough of the structure (Masaitis 1999). The Obolon impactites are characterized by specific (mostly soft) rock deformation behavior and features related to submarine sedimentary processes involved in crater formation (such as deposition of 'resurge breccia'; see also Sturkell 1998; Ormö and Lindström 2000; King et al. 2002; Dypvik and Jansa 2003; Dypvik et al. 2004; Poag et al. 2004 for specific processes and features associated with marine impact structures). A recent review of the Obolon impact structure and its impact ejecta is given by Gurov et al. (2009). Small particles of

FeNi (taenite and kamacite) found in suevite were interpreted as remnants of the Obolon impactor (Valter and Ryabenko 1977), probably an iron meteorite (Grieve 1991; Grieve and Pesonen 1992). Enrichment in Cl and Br in impact glasses (Gurov and Gurova 1995), together with an 'inverted sombrero' structure and the presence of poorly graded 'resurge breccia' deposits in the central crater basin, indicate a shallow marine Obolon impact scenario (Valter 2002). Stratigraphic dating by Masaitis et al. (1980) suggested a most likely Late Triassic age of 215 ± 25 Ma for the Obolon impact structure (see also Grieve 1987, 1991; Spray et al. 1998). K/Ar ages of suevite glass samples, in contrast, yielded a Middle Jurassic age of 169 ±7 Ma (Masaitis 1999; Valter et al. 2000). So far, K/Ar ages are the only isotopic data available for the Obolon impact structure (Gurov 2009; pers. comm.), and ^{40}Ar/^{39}Ar dating of impact melt lithologies is still outstanding. Similar to the large age uncertainties associated with the Puchezh-Katunki impact (see chapter 4), stratigraphic and isotopic ages for the Obolon impact structure cover a time span of up to 78 million years (Schmieder and Buchner 2008). An alternative approach of 'paleogeographic dating' using paleogeographic data (Ziegler et al. 1983; Golonka 2000; 2007) in conjunction with the marine crater-specific (Valter et al. 2000; Gurov et al. 2009) and regional sedimentologic framework (marine ingression in the Obolon/Donets Graben region in the Early Toarcian at ~180-185 Ma; Krymholts 1972; Ziegler at al. 1983; Pálfy 2004) provided additional impact age constraints. Given that Obolon is a marine impact structure, this rules out a Triassic impact age (which would have occurred under continental conditions) and provides an Early Jurassic maximum age of ~185 Ma (Schmieder and Buchner 2008; Fig. 7.4), constraining the Obolon impact age to ~185-170 Ma.
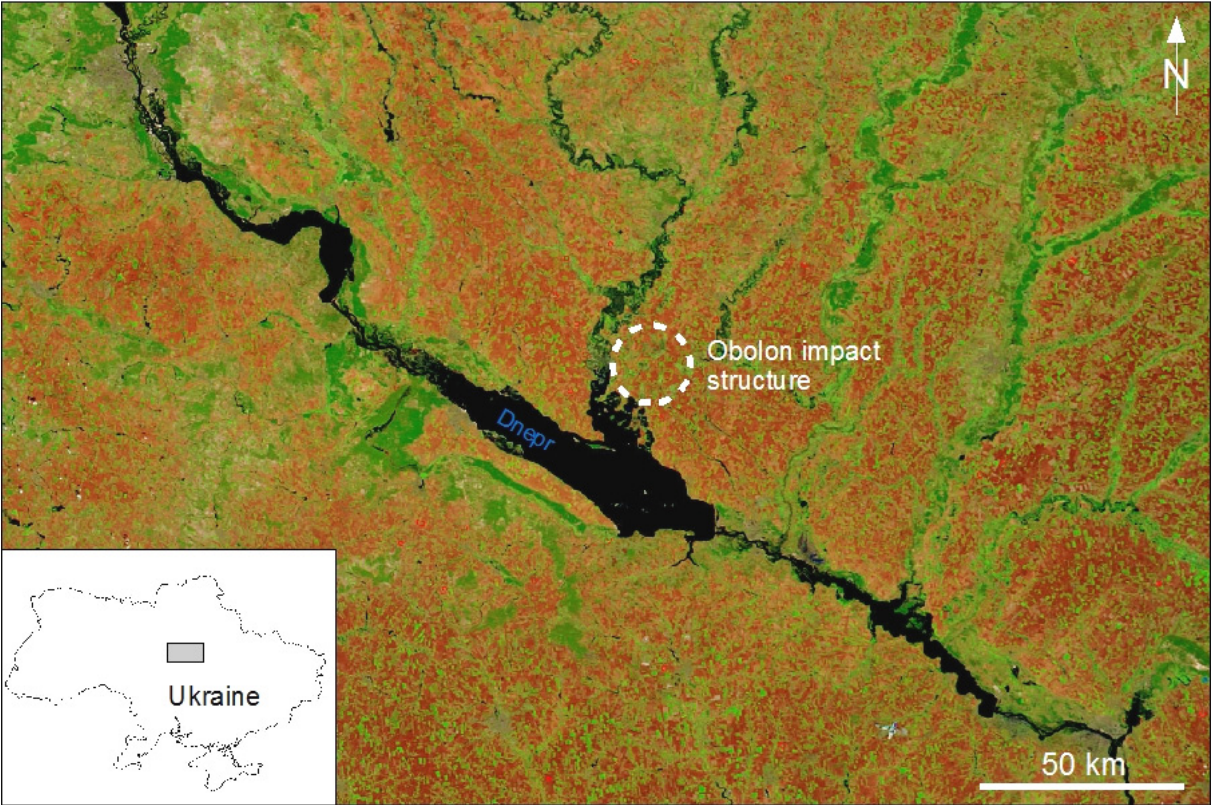
Fig. 7.3: Position of the obolon impact structure in Ukraine; see grey box in inset map for position of the satellite image scene in Ukraine. Image source: NASA Visible Earth (Terra MODIS false color).
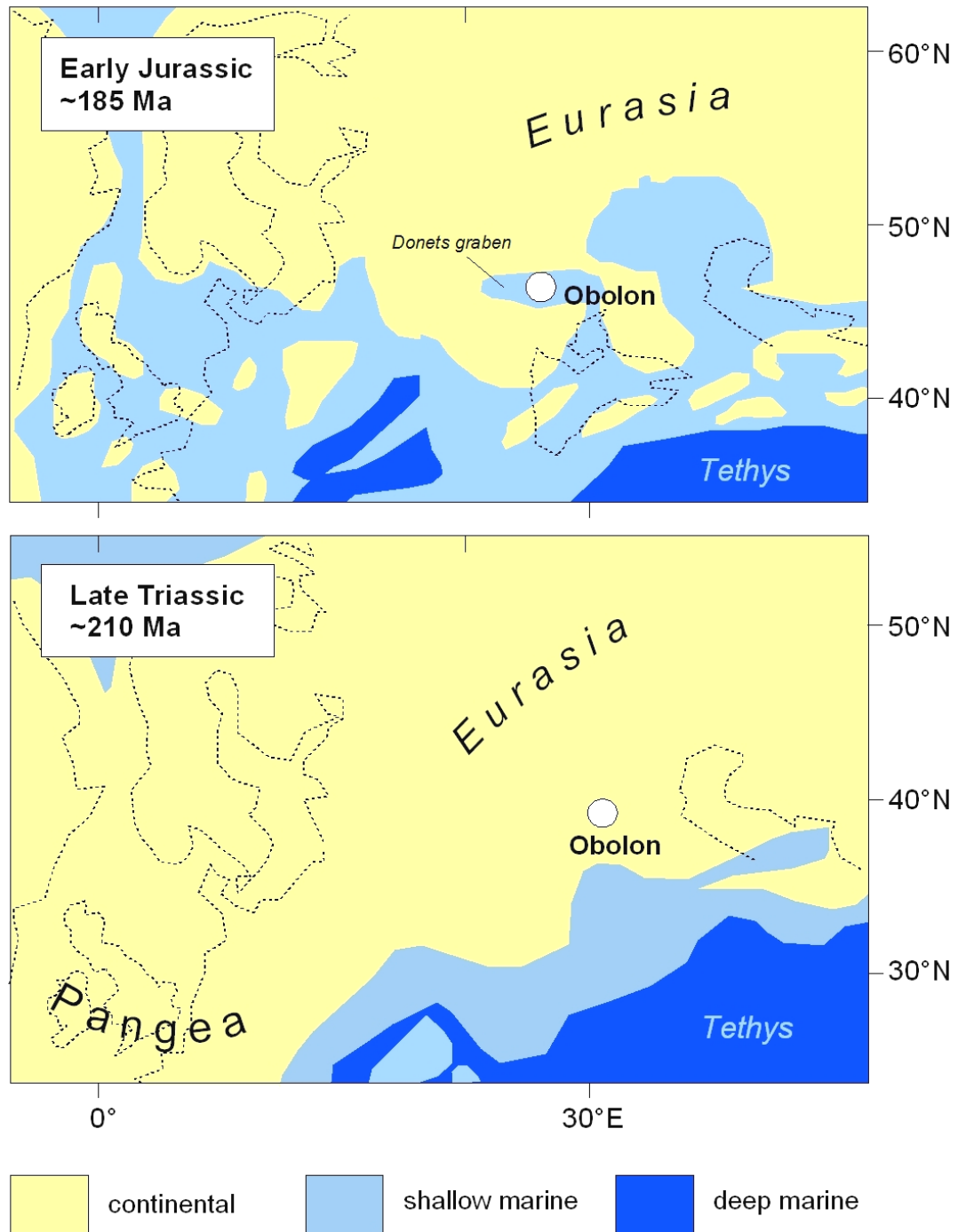
Fig. 7.4: Paleogeographic map of Eurasia in Late Triassic and Early Jurassic time and the position of the Obolon impact structure (Mollwide projection; modified from Ziegler et al. 1983; Golonka 2000; 2007; Schmieder and Buchner 2008).

8. The Paasselkä impact structure (Finland)

8.1. Geologic setting and previous work

Among the 11 impact structures confirmed to date in Finland (Pesonen et al. 2005; Dypvik et al. 2008; Fig. 8.1), Paasselkä, with a diameter of ~10 km (Pesonen et al. 1999b), is the third largest. The Paasselkä impact structure centered at 62°09′ N, 29°25′ E, is entirely occupied by the oval-shaped Lake Paasselkä (also called Paasivesi in older literature; Fig. 8.2). The whole structure has been deeply eroded since its formation, especially by Pleistocene glaciation (see Puura and Plado 2005; Buchner and Schmieder 2009a; Fig. 8.3). A negative gravimetric anomaly associated with Lake Paasselkä was first noted and discussed by Elo (1979) and Elo et al. (1984). A possible impact origin of the Paasselkä structure was earlier proposed by Henkel and Pesonen (1992) and finally confirmed by the detection of shock deformation in brecciated bedrock (Pesonen et al. 1999b; Kuivasaari et al. 2000). Target rocks at Paasselkä comprise ~1.9 Ga (Pesonen et al. 1999b) mica schists, together with subordinate mafic intrusions, granitic and pegmatitic dikes, as well as some pre-impact sedimentary rocks of the Karelian Supergroup of the Baltic (Fennoscandian) Shield (see Korsman et al. 1997; Pesonen et al. 1999b; Puura and Plado 2005). A general geological overview of the region is given by Nykänen (1975), Lavikainen (1986), and Korsman et al. (1997). A drilling program carried out by the Geological Survey of Finland in 1999 recovered a ~200 m core of brecciated target rock material from the center of the Paasselkä impact structure, overlain by some Quaternary deposits (Pesonen et al. 1999b). Impact-related geophysical anomalies (Abels et al. 2002) and possible impactor contamination in the form of Fe-Ni-Co sulfides in impactites from the Paasselkä impact structure were reported by Öhman et al. (2003) and Badjukov and Raitala (2006). Further analyses of potential impactor contamination in the melt rocks, so far, yielded no detectable meteoritic signature (platinum group elements below the detection limit, at a terrestrial Ni/Cr ratio; Goderis 2009; pers. comm.), and additional work will be necessary. Öhman et al. (2003) suggested the occurrence of heavily altered impactites (referred to as possible former impact melt breccias) that lack a primary breccia matrix. Accordingly,

no impact melt rocks have been reported from the Paasselkä impact structure so far (see also Puura and Plado 2005), and no isotopic dating of the Paasselkä impact structure has been done to date. Thus, only a maximum age for the Paasselkä impact event—the actual age of the Proterozoic ~1.9 Ga target rock—is mentioned in the literature and terrestrial impact crater listings (e.g., Pesonen et al. 1999b). Due to the presence of shock-molten sandstones (probably clasts of the Proterozoic 'Jotnian sandstone') in impact melt rocks, the Paasselkä impact age was recently revised to <1.4 Ga (Öhman et al. 2003; Buchner et al. 2009a). This chapter presents impact melt rocks from the Paasselkä impact structure (Fig. 8.4) collected in a till pit near Sikosärkät (62°06′17″ N, 29°31′05″ E), about 1 km southeast of the southeastern shore of Lake Paasselkä, along with a detailed petrographic and geochemical description of these melt rock samples. Northwest to southeast trending glacial striation on the bedrock around Lake Paasselkä (see Figs. 8.2 and 8.3) indicates that impactite boulders and pebbles in the till pit are most likely derived from the Paasselkä crater (Buchner and Schmieder 2009a). Apart from the isotopic ages available for the Lappajärvi (Mänttäri and Koivisto 2001), Sääksjärvi (Müller et al. 1990; Mänttäri et al. 2004), Keurusselkä (Schmieder et al. 2009c), and the Suvasvesi South (Buchner et al. 2009b) impact structures, the majority of impact structures in Finland is still insufficiently dated (see also Schmieder and Buchner 2008). The first ^{40}Ar/^{39}Ar age data for the Paasselkä impact structure are presented in this chapter.

Fig. 8.1: Satellite image scene of Fennoscandia and position of impact structures in Finland (Iso-Naakkima; Karikkoselkä, Keurusselkä, Lappajärvi, Lumparn, Paasselkä, Saarijärvi Sääksjärvi, Söderfjärden, Suvasvesi North, and Suvasvesi South), Estonia (Ilumetsä, Kaali, Kärdla, and Neugrund), and Russia (Jänisjärvi and Mishina Gora). Image source: Terra MODIS image, NASA Visible Earth.
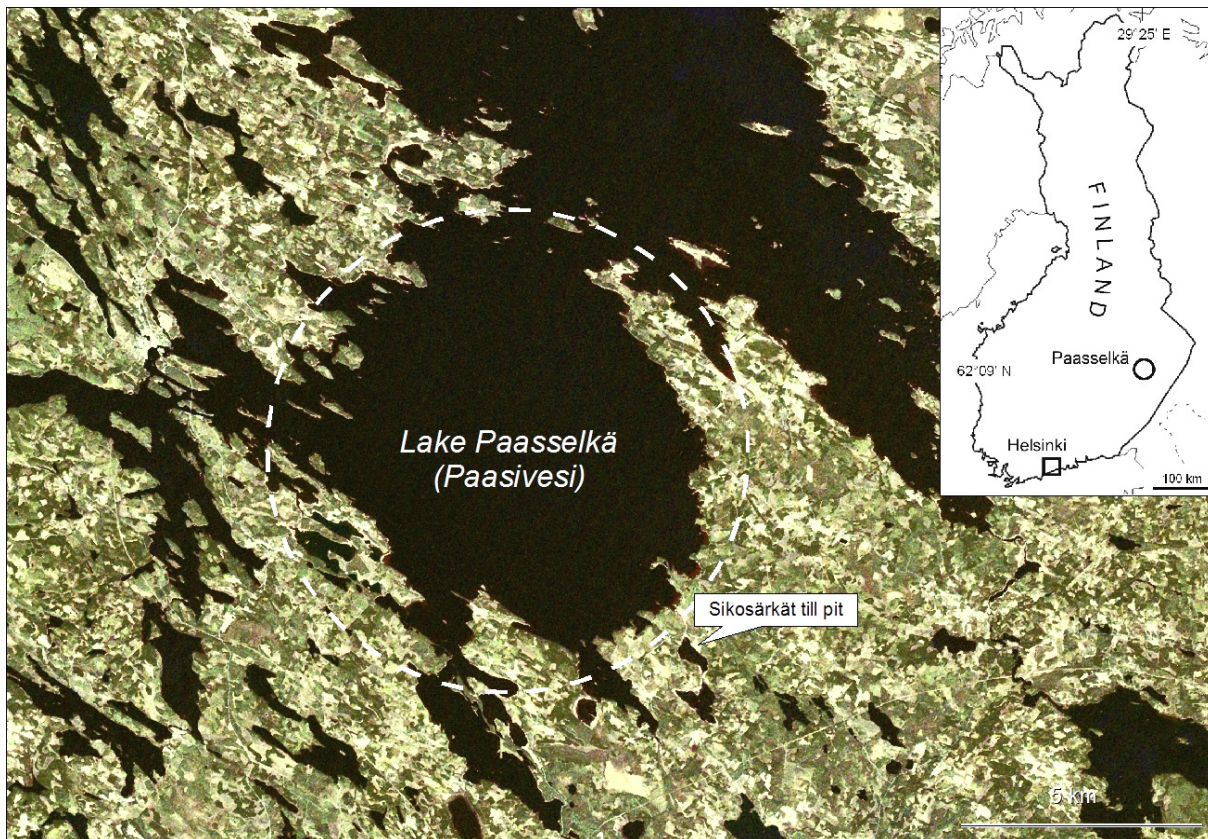
Fig. 8.2: Landsat-7 ETM+ visible light satellite image scene of the Paasselkä impact structure occupied by Lake Paasselkä (Paasivesi). Label indicates the position of the Sikosärkät till pit where the impact melt rocks were recovered; see inset map for position in Finland.
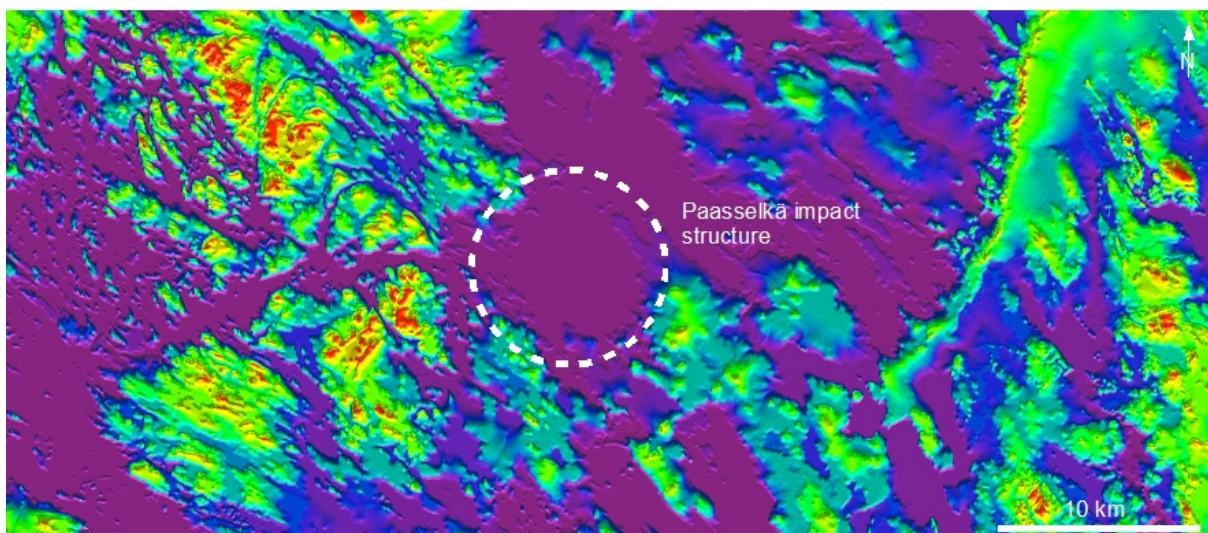
Fig. 8.3: Color-coded Shuttle Radar Topographic Mission (SRTM) scene of the Paasselkä impact structure; elevation ranges from ~40 m (dark blue) to ~200 m (red) above sea level. Note the weak topographic expression of the impact structure and the NW-SE-trending glacial striation.

Fig. 8.4: Polished slabs of Paasselkä impact melt rocks. A distinct overall flow structure and shocked target rock components (crystalline rocks and impact-metamorphosed sandstones) are visible in the hand specimen.

8.2. Samples and analytical techniques

Two samples of allochthonous impact melt rocks from the Sikosärkät till pit (collected in the field and kindly provided by Jarmo Moilanen, Oulu; Figs. 8.2 and 8.4) were investigated by optical microscopy of polished thin sections. Geochemical analysis was carried out using a CamScan™ SC44 scanning electron microscope (SEM)—EDAX™ PV 9723/10 energy dispersive X-Ray (EDX) system (Institut für Planetologie, Universität Stuttgart) and a CAMECA™ SX 100 electron microprobe equipped with five wavelength dispersive spectrometers (Institut für Mineralogie und Kristallchemie, Universität Stuttgart). Melt matrix composition was determined by in situ microprobe measurements on optically preselected areas of polished thin sections (the electron-beam diameter was 5 μm at a current of 8 nA and an acceleration voltage of 15 kV). Whole-rock composition was determined by analyzing polished thin sections (SEM-EDX measurements at low magnifications under defocused beam and an acceleration voltage

of 15 kV) and additional EDX analyses of homogenized rock powder tablets. Microspec™ olivine, apatite, and kryolite (analyzed by the Oxford Instruments™ Microanalysis Group) were used as compound standards for EDX analyses. The accuracy of the analyses was better than 5% (~2–5%) for the main elements (SiO_2, Al_2O_3, FeO, MgO, CaO, Na_2O, and K_2O). Volatile content (water and CO_2) of the melt rocks was measured using a LECO™ RC-412 Multiphase Carbon Determinator facility (Institut für Mineralogie und Kristallchemie, Universität Stuttgart).

8.3. Petrography and geochemistry

Uncut specimens of the Paasselkä impact melt rocks are surficially altered and have a coating of iron hydroxides; in fresh section, the melt rocks display a greenish-grey color. The rocks are rich in target rock inclusions and exhibit a distinct overall flow fabric, predominantly within domains rich in melt matrix, and reveal small vesicles as commonly observed in impact melt rocks (e.g., French 1998; Dressler and Reimold 2001; Stöffler and Grieve 2007; Figs. 8.4 and 8.5A). Target rock inclusions comprise lithic clasts (predominantly impact-metamorphosed clasts of mica schist, granite, and sandstone) and single mineral grains, most of which are quartz, feldspar, and decomposed mica flakes from the crystalline (and partially sedimentary) target rock. Various types of silica can be distinguished in the impact melt rocks: Firstly, shocked quartz with planar fractures together with single and multiple sets of decorated PDFs (up to 5 directions) as grains with original angular shapes. Shocked quartz grains are intensely toasted and exhibit a brownish hue due to a high content of minute fluid inclusions (see also Short and Gold 1993; Ferrière et al. 2009b; cf. Whitehead et al. 2002; Fig. 8.5B). Secondly, polycrystalline quartz aggregates do neither display PDFs nor fluidal texture and lack fluid inclusions. These aggregates commonly exhibit both angular and rounded grain shapes (Fig. 8.5C) and planar fracturing (see discussion section). Transitional types between shocked quartz and polycrystalline quartz aggregates also occur (Fig. 8.5D). Thirdly, in larger silica domains, recrystallized polycrystalline silica grains are surrounded by recrystallized fluidal silica glass rich in schlieren and fluid inclusions. Entrainment of recrystallized silica grains within fluidal

silica glass causes a distinctive 'snowball' fabric (Figs. 8.5E–F). In places, fluidal silica domains exhibit dendritic (skeletal) crystal morphologies (Fig. 8.5G). In some silica grains, spherulitic texture was observed (Fig. 8.5H). Some cavities are overgrown by idiomorphic quartz of yellow to brownish hue. Shocked feldspar grains with fractures and/or planar deformation features occasionally occur, whereas most of the protolith feldspar has been transformed into feldspar (plagioclase and K-feldspar) melt of both glassy and devitrified/recrystallized spherulitic appearance. Fluidal plagioclase glass was also observed. K-feldspar domains generally exhibit a fluidal texture and may reach several millimeters in size; domains of fluidally shaped K-feldspar glass are commonly recrystallized (spherulitic) and entrain grains of recrystallized silica grains (Fig. 8.5I-K). Veinlets of normal K-feldspar glass are present within larger silica domains. Feldspar glass of mixed feldspathic and plagioclase composition is abundant in the impact melt rocks and displays angular and roundish shapes. Plagioclase glass, in many cases, is partially recrystallized to minute andesine laths (Fig. 8.5L-N). Protolith-derived biotite flakes were completely decomposed into semi-opaque and opaque phases, iron oxides, and minute acicular Fe-Mg-Ti-crystallites (see also Schneider 1974; Feldman 2001), and are partly replaced by chlorite. Semi-translucent Fe-Mg-rich phases occur as devitrified materials with spherulitic texture (Fig. 8.5O). The glassy to cryptocrystalline melt matrix (Figs. 8.5 and 8.6) is semi-translucent in thin section and partially altered to goethite. Vesicles within the melt matrix are commonly lined by chlorite and goethite.

Scanning electron microscope-EDX and electron microprobe measurements of the Paasselkä impact melt rocks revealed that the melt rocks are remarkably siliceous in bulk composition (>60 wt% SiO_2; the local silica content, however, varies widely between ~62 and ~71 wt%; Table 8.1). This is in contrast to the melt matrix, which is relatively poorer in silica (~51–63 wt% SiO_2), but somewhat richer in Fe, Mg, and K. Different compositional varieties of glass components can be distinguished within the impact melt rocks: Firstly, Na-Ca-rich plagioclase glasses of andesine composition, predominantly occurring as partially recrystallized grains (samples G-01-G-17; Table 8.2); secondly, recrystallized K-feldspar glass that predominantly builds up larger fluidal domains (samples G-18-G-26; Table 8.2); thirdly, glasses of mixed feldspathic composition, which plot in the actual miscibility gap of feldspars (samples G-27-G-33;

Fig. 8.7; Table 8.2). Incipient recrystallization of glass was observed in plagioclase glasses, where small laths of andesine feldspar (within a compositional range of $Ab_{62-46}An_{31-40}Or_{4-17}$) have formed. Fourthly, some glass components turned out to be of 'mafic' (chloritic) composition, rich in Fe, Mg, Al, and volatiles (as inferred from electron microprobe analyses) but poor in silica (samples G-34-G-38; Table 8.3). In addition, precursor biotite grains have been decomposed to various types of iron oxides and hydroxides, together with some subordinate Fe-K-Mg-Al-rich glasses and Fe-Mg-Ti-rich crystallites, which are restricted to decomposed protolith mica flakes. Fluidal silica domains revealed an elevated content of Al ($Al_2O_3 > 1.2$ wt%) and other metals (CaO > 0.3 wt%; $Na_2O > 0.2$ wt%; FeO > 0.1 wt%) with respect to recrystallized polycrystalline silica. Additionally, dendritic silica crystals (Fig. 8.5G) are enriched in Al (Table 8.3). A summary of the various fresh to recrystallized glass types and their geochemical composition is given in Tables 8.2 and 8.3 and plotted in Fig. 8.7.
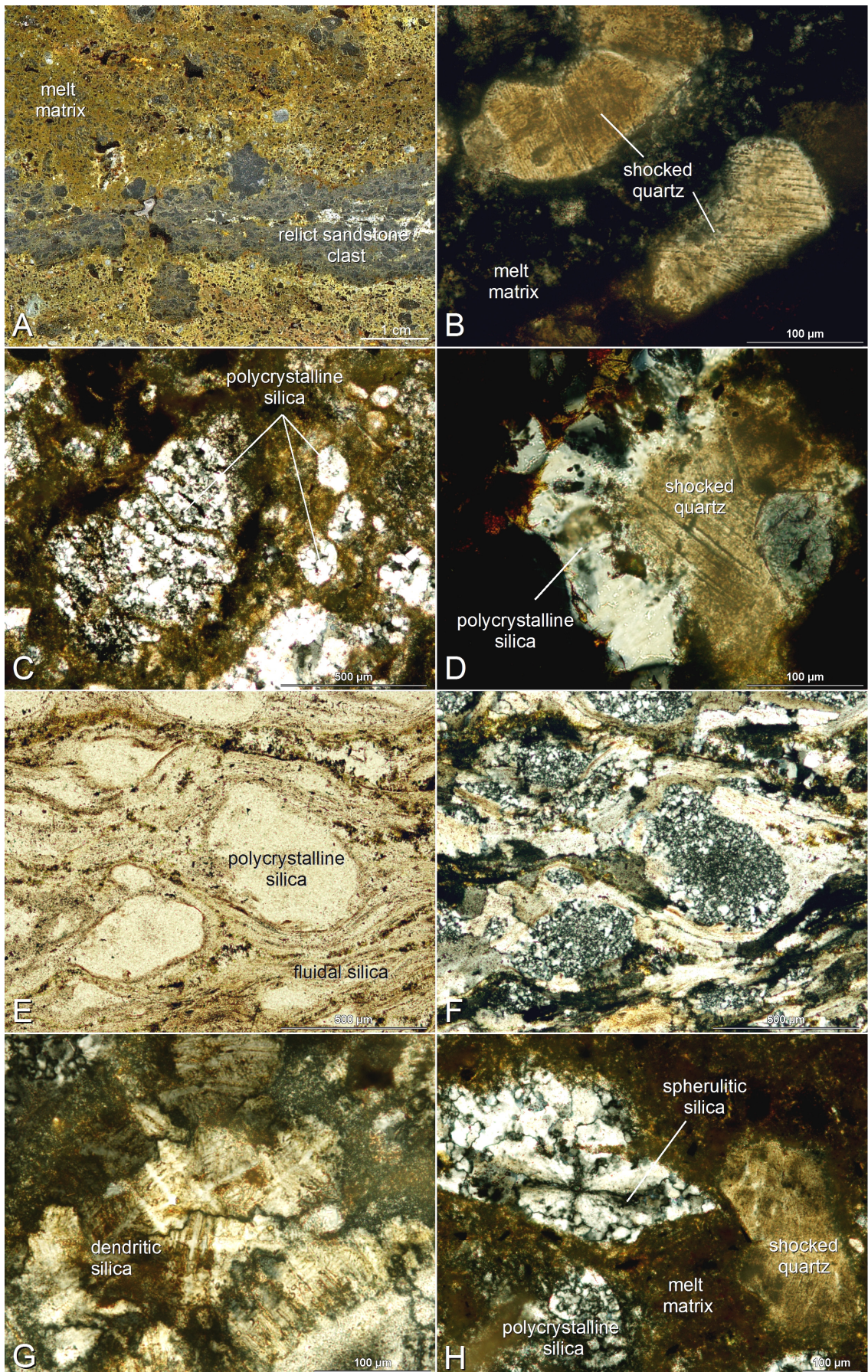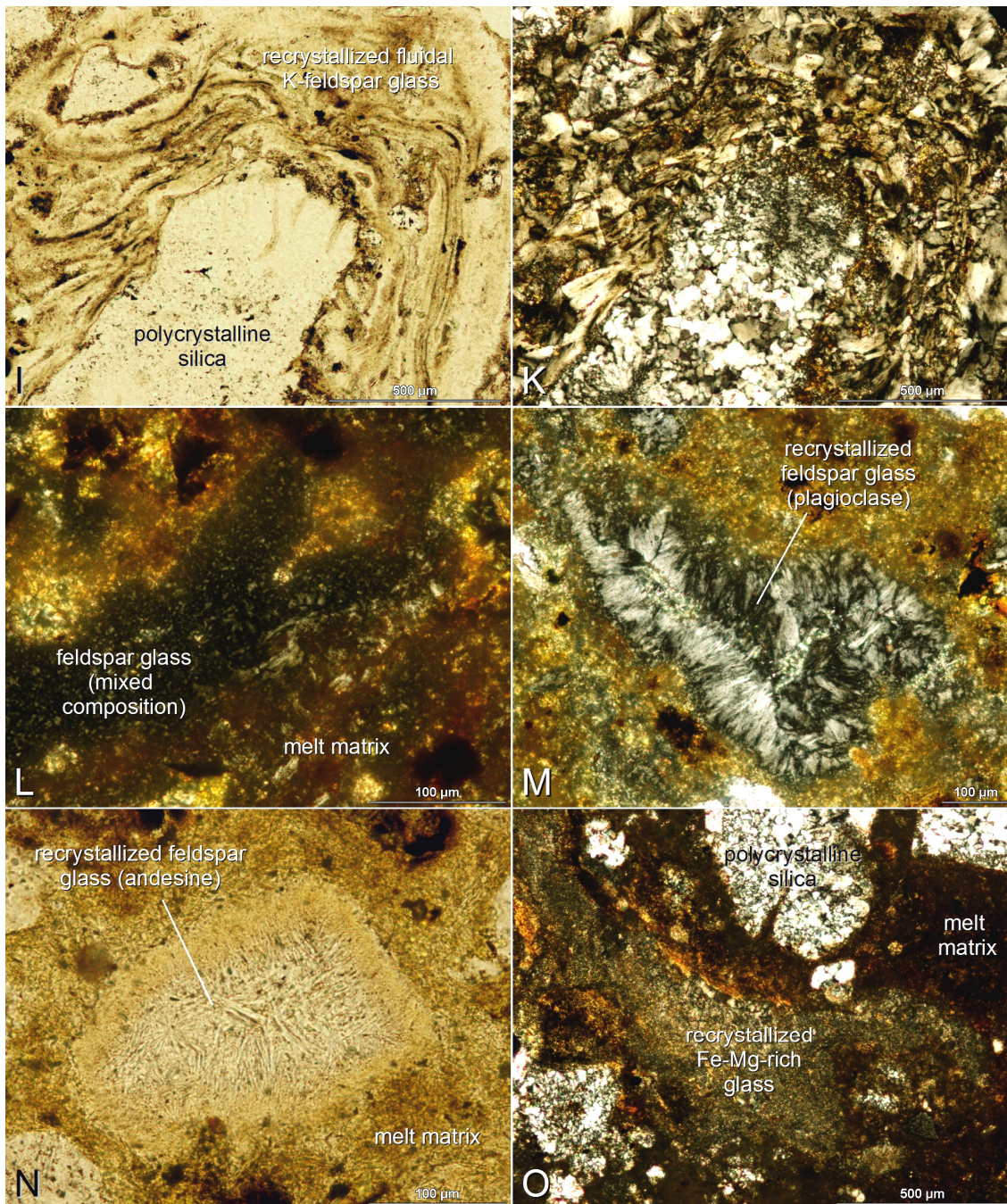
Fig. 8.5 (this and previous page): Thin section photomicrographs of Paasselkä impact melt rocks. **A**: Fluidal texture of the rock with domain of recrystallized fluidal silica (reflected light); **B**: shocked and toasted quartz grain with two sets of planar deformation features (cross-polarized light); **C**: polycrystalline silica with angular shape and relict planar fractures (cross-polarized light); **D**: shocked quartz partially transformed to polycrystalline silica (cross polarized light); **E**: delta clasts of polycrystalline and fluidal recrystallized silica (plane-polarized light); **F**: same scene as E (cross-polarized light); **G**: dendritic silica in fluidal silica domain (cross-polarized light); **H**: polycrystalline silica with spherulitic extinction (cross-polarized light); **I**: fluidal recrystallized K-feldspar glass entraining recrystallized polycrystalline silica with relict fractures (plane-polarized light); **K**: same scene as I (cross-polarized light); **L**: largely fresh feldspar glass of mixed composition (cross-polarized light); **M**: recrystallized feldspar glass of plagioclase composition (cross-polarized light); **N**: recrystallized feldspar glass of plagioclase composition with andesine crystallites (plane-polarized light); **O**: fluidal recrystallized Fe-Mg-rich glass (cross-polarized light).
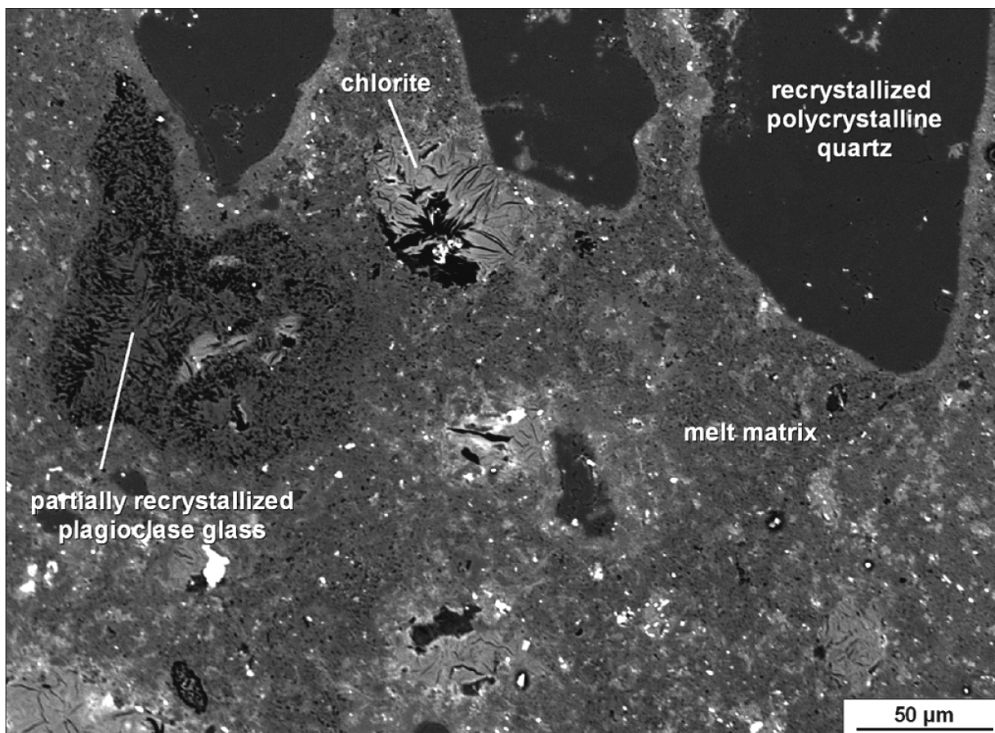
Fig. 8.6: Backscattered electron image of the glassy to cryptocrystalline melt matrix of the Paasselkä impact melt rocks. Note partially recrystallized feldspar glass (plagioclase), roundish grains of recrystallized polycrystalline quartz (dark grains), and melt vesicles filled by secondary chlorite.
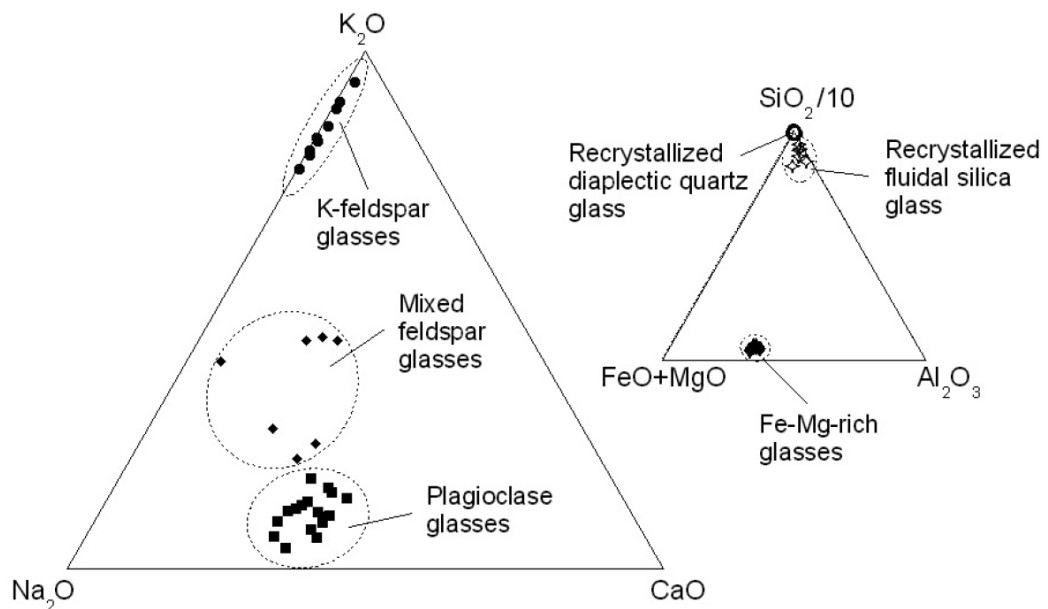
Fig. 8.7: Chemical composition of fresh and recrystallized glasses (Na-Ca-rich plagioclase glasses; K-feldspar glasses; mixed feldspathic glasses; Fe-Mg-rich mafic glasses; recrystallized diaplectic and fluidal silica glasses) in the Paasselkä impact melt rocks. Note the scaling factor of 1/10 for SiO_2 in the small diagram.

8.4. Interpretation of shock metamorphic conditions and petrologic considerations

From the petrographic observations, shock metamorphic conditions can be constrained for the Paasselkä impact melt rocks. Shocked quartz grains with multiple sets of PDFs (Fig. 8.5B,D;H) suggest shock pressures exceeding 20 GPa (e.g., Stöffler and Langenhorst 1994; French 1998). Polycrystalline silica grains commonly exhibit relict angular grain shapes, relics of planar fractures, and generally show no internal fluidal fabric (Fig. 8.5C); thus, I interpret these silica grains as recrystallized diaplectic quartz glass. Transitional types most likely represent shocked quartz grains partially transformed into diaplectic glass (Fig. 8.5D). The frequency of recrystallized former diaplectic quartz glass implies that much of the clast component of the impact melt rocks experienced minimum shock pressures in excess of ~35 GPa (von Engelhardt et al. 1967; von Engelhardt 1972; Stöffler and Langenhorst 1994; French 1998; Langenhorst 2002). By the presence of roundish grains of recrystallized diaplectic quartz glass it can be assumed that these grains also experienced marginal melting of silica (probably 'secondary' melting of diaplectic quartz glass; see Grieve et al. 1996) at shock pressures ≥35 GPa and temperatures up to ~1,500 °C (but obviously below the melting point of silica at 1,713 °C; compare to French 1998). This also agrees with the temperatures required for the formation of glasses of mixed feldspar composition and spherulitic aggregates from feldspar glass at temperatures exceeding ~850 °C (Bischoff and Stöffler 1984). The occurrence of sedimentary rock units in the Paasselkä area was reported by Puura and Plado (2005). Highly shocked and molten sandstone clasts were also described by Öhman et al. (2003). Domains of fluidal silica and recrystallized diaplectic quartz glass in the melt rock samples most likely derive from preferentially molten quartz sandstones of the target rock (i.e., initially porous target rock units). Accordingly, the arrangement of recrystallized diaplectic quartz glass grains together with fluidal silica might be interpreted as a relict sandstone fabric, and internal ductile deformation (due to flow in the viscous melt) may be inferred from the geometry of silica delta clasts (Fig. 8.5E-F). With respect to the shock behavior of dense crystalline rocks, more heat is generated in porous sedimentary rocks, and melting of sandstone may occur at comparatively low shock pressures (e.g., French 1998). Recrystallized fluidal, schlieren-rich silica glass domains enriched in Al are restricted to partially molten sandstone

clasts and suggest the formation of normal silica glass (lechatelierite) at shock pressures of ~13–30 GPa and post-shock temperatures of ≥~950 °C (Kieffer 1971; Stöffler 1972; 1984; Grieve et al. 1996; French 1998; Stöffler and Grieve 2007). Dendritic silica crystals within the fluidal silica domains indicate rapid crystal growth upon cooling of the local silica melt. The high degree of shock metamorphism of the Paasselkä impact melt rocks and incipient whole-rock melting at peak shock pressures of ≥35 GPa and post-shock temperatures of probably up to ~1,500 °C suggests the shock stages III–IV according to Stöffler (1971; 1984) and Stöffler and Grieve (2007). The presence of subordinate non-molten feldspar grains may be explained by the incorporation of cooler, less shocked target rock clasts and mineral grains upon melt movement during the excavation stage (see French 1998). Crystallization of post-impact secondary phases, such as vesicle-lining chlorite and idiomorphic goethite-bearing quartz, can be ascribed to post-shock processes at low temperatures. Due to the lack of a representative mineralogical data set of Paasselkä impactites, it remains unresolved whether these phases formed by impact-induced hydrothermal activity (e.g., Newsom 1980; Naumov 2005; Osinski 2005; Versh et al. 2005) or by regional hydrothermal overprint not related to the Paasselkä impact event.

Target rock clasts, mineral grains, and glasses of variable size and composition are irregularly distributed within the Paasselkä impact melt rocks and, therefore, are the cause of a rather inhomogeneous whole-rock composition (average values are given in Table 8.1). SiO_2 enrichment of the whole-rock with respect to the glassy to cryptocrystalline melt matrix (Fig. 8.11) corresponds to a large number of silica grains (shocked quartz, recrystallized diaplectic quartz glass, and recrystallized fluidal silica) embedded within the melt matrix; Fe- and Mg-rich phases (such as decomposed biotite flakes, opaque iron oxides, Fe-Mg-rich glasses, and secondary vesicle-lining chlorite and goethite) are responsible for locally occurring higher Fe values. The intermediate SiO_2 content of the melt matrix and higher Al, Na, and K values with respect to the whole-rock probably reflect the preferential and selective melting of hydrous mica, amphiboles, and feldspars of the target rock (compare Table 8.1). The rather inhomogeneous distribution of Fe, Mg, Ca, and alkali elements in the melt might point to incipient and/or irregular melt matrix alteration. Linings of secondary chlorite and goethite in melt matrix vesicles

indicate the mobilization of iron and magnesium during post-shock cooling and alteration processes; however, chlorite is largely restricted to vesicles (Fig. 8.6) and domains of decomposed biotite flakes. The compositional variance within the melt matrix (see Table 8.1) and fresh to recrystallized glasses (Tables 8.2 and 8.3) suggests that the Paasselkä impact melt — at least at the scale of the melt rock samples — was not affected by complete homogenization and that the different glass components of the impact melt rocks (i.e., discrete domains of different monomineralic and mixed-mineral melts) reflect the mixed composition of the crystalline target rock. Enrichment in Al (containing up to 1.28 wt% of Al_2O_3; see Fig. 8.7, Table 8.3) and other ions (Fe, Mg, and Ca; Table 8.3) in the fluidal silica domains of the Paasselkä impact melt rocks could be related to the crystallization of cristobalite or tridymite. Stevens et al. (1997) and Osinski (2004) stated that Al and other metals may be preferably incorporated into the open cristobalite structure. The formation of cristobalite from silica glass indicates temperatures of ≥1,100 °C (Rehfeldt-Oskierski et al. 1986; Shoval et al. 1997). Elevated Al contents are restricted to fluidally shaped silica domains and were not noted in recrystallized diaplectic quartz glass (see Table 8.3). Feldspars and mica of the target rock are unstable at the post-shock melt temperatures estimated (compare to Schneider 1974; Bischoff and Stöffler 1984; Table 8.1) and might be regarded as the source for Al. The geochemical observations are in good agreement with the mixed character of the target rock (mica schists, granitic and pegmatitic dikes, mafic intrusions, as well as sandstones). I refer to von Engelhardt et al. (1969), von Engelhardt and Graup (1984), and Osinski (2003), who distinguished different textural and compositional types of glasses in suevite of the Ries crater, Germany, corresponding to the mixed crystalline-sedimentary target rock sequence. Fe-Mg-rich volatile-rich glasses of chlorite composition (Fig. 8.5O) probably represent local melts from biotite schists. Lavikainen (1986), furthermore, noted amphibolites and mafic clinopyroxene-olivine-rich hornblendites west of Lake Paasselkä, which provide high concentrations of Fe and Mg, and which might represent protoliths for Fe-Mg-rich glasses, as well. The hydrous and semi-translucent nature of Fe-Mg-rich glasses suggests enhanced local glass devitrification and alteration. A geochemical comparison of the Paasselkä impact melt rocks with a representative data set for melt rocks from selected impact structures of the Baltic Shield (Lappajärvi, Finland; Sääksjärvi, Finland; Siljan, Sweden; Dellen,

Sweden; Mien, Sweden; Gardnos, Norway; Jänisjärvi, Russia) reveals that all these impact melt rocks are of generally similar composition (Fig. 8.8). SiO_2 contents slightly lower than those of the above-mentioned impact melt rocks might reflect the predominance of biotite-rich mica schists over granitic rocks (and the lack of quartz-rich gneisses) in the Paasselkä area. Alkali contents are widely consistent with the Fennoscandian impact melt rocks; there is no obvious indication of emphasized alkali metasomatism, such as notable K enrichment and stronger Na depletion (see Tables 8.1 and 8.2) as typical for post-shock hydrothermal alteration and weathering (e.g., Grieve 1978; Newsom 1980; Reimold and Oskierski 1987; Koeberl et al. 1996b; Gurov et al. 1998; Hecht et al. 2004; Naumov 2005; Osinski 2005; Versh et al. 2005).
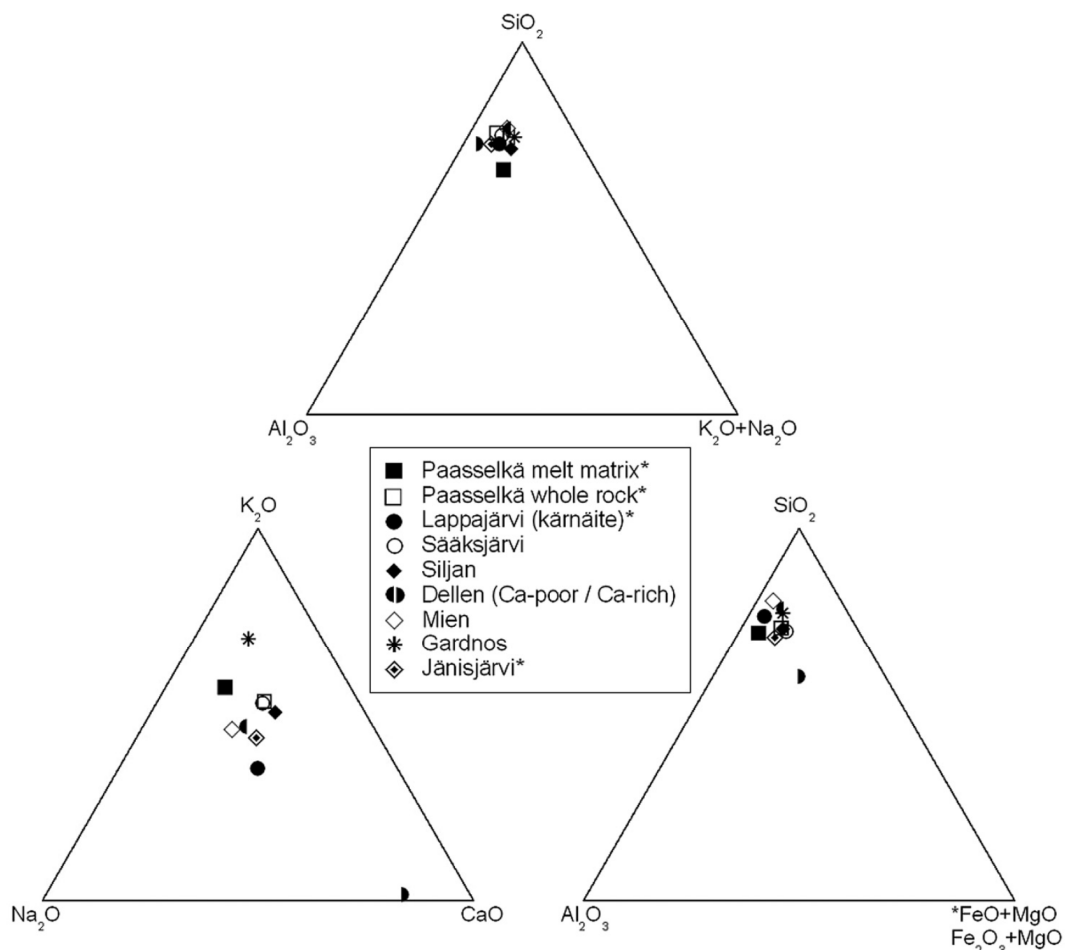
Fig. 8.8: Chemical composition of the Paasselkä impact melt rocks in comparison to impact melt rocks from some impact structures of the Baltic Shield. Plot based on geochemical data from Reimold (1980; Lappajärvi); Bischoff and Stöffler (1984; Lappajärvi); French et al. (1997; Gardnos); Schmidt et al. (1997; Dellen, Mien, Sääksjärvi); Badjukov and Raitala (1998; Jänisjärvi); Reimold et al. (2005a; Siljan); *iron oxide content measured as FeO in the case of Paasselkä, Lappajärvi, and Jänisjärvi; note that the chemical data were determined by different methods.

8.5. $^{40}Ar/^{39}Ar$ dating – sample choice and methods

Optically fresh particles of recrystallized feldspar glass separated from clast-rich impact melt rocks from the Sikosärkät till pit (Figs. 8.2 and 8.4) were chosen for $^{40}Ar/^{39}Ar$ dating. The melt rocks were crushed, particles sieved (<500 μm), rinsed with distilled water in an ultrasonic cleaner, and handpicked on the basis of their optical freshness. Geochemical analysis of recrystallized K-feldspar glasses (SiO$_2$ ~53-64 wt%; K$_2$O ~8-13 wt%; Na$_2$O ≤3 wt%; CaO ≤0.15 wt%; compare Table 8.2; Fig. 8.5I-K), plagioclase glasses of andesine composition (SiO$_2$ ~58-62 wt%; K$_2$O ≤2.5 wt%; Na$_2$O ~7-9 wt%; CaO ~4-6 wt%), and 'mixed' feldspathic glasses (SiO$_2$ ~59-62 wt%; K$_2$O ~3-6 wt%; Na$_2$O ~5-7 wt%; CaO ~1-4 wt%; Fig. 8.5L-M) was carried out using a CAMECA™ SX 100 electron microprobe (Institut für Mineralogie und Kristallchemie, Universität Stuttgart). $^{40}Ar/^{39}Ar$ step-heating analysis of ~130 mg of hand-picked recrystallized glass particles was done at the Institut für Geowissenschaften, University of Heidelberg (Dr. W. H. Schwarz and Dr. M. Trieloff; see Trieloff et al. 2005; Schwarz and Trieloff 2007a for technical details), using the decay constants determined by Steiger and Jäger (1977). It should be noted that insufficient cross calibration between decay constants of the $^{40}K/^{40}Ar$ and U/Pb decay systems result in systematic age differences of c. 1% in the age range of Mesozoic time – thus, the $^{40}Ar/^{39}Ar$ ages calculated with the constants recommended by Steiger and Jäger (1977) should be c. 1% higher (see also Villeneuve et al. 2000; Ramezani et al. 2005; Mundil et al. 2006; Schwarz and Trieloff 2007b). The samples were wrapped in Al-foil, packed in quartz ampoules (12x55 mm), Cd-shielded (to reduce isotopic interferences), and irradiated for 5 days at the GKSS Geesthacht, Germany. After irradiation, the samples were heated in an inductively heated Mo-furnace up to ~1,500°C in several temperature steps. The gas was cleaned with Zr-, Ti-, Cu/CuO-, and Al-Getters. Argon was measured using a MAT GD150 mass spectrometer. The argon results were corrected for mass discrimination, argon decay, isotopic interferences (all information listed in Table 8.4), and blanks from the extraction line (glass and furnace). The argon isotopic composition of blanks was always atmospheric within uncertainty. Ages were calculated against the BMus/2 (Bärhalde muscovite, Black Forest, Germany) standard with an age of 328.5 ± 1.1 Ma (1σ), which was calibrated against 5 further international $^{40}Ar/^{39}Ar$ dating standards; for further

information about the analytical procedure see Schwarz and Trieloff (2007a). Errors given in parentheses include standard errors.

8.6. *Dating results and interpretation*

$^{40}Ar/^{39}Ar$ step-heating analysis yielded a Middle-Late Triassic (Ladinian-Karnian according to Ogg et al. 2008) pseudo-plateau age of 229 ± 3 Ma (2σ; MSWD=1.01; P=0.42) for ~53-100% of the ^{39}Ar released during the 9 final temperature steps, with ages of individual extractions that overlap within the 2σ error limit (Fig. 8.9). The age spectrum exhibits younger apparent ages in the low-temperature extraction steps (~0-9% of ^{39}Ar released) probably due to ^{39}Ar redistribution during neutron irradiation (e.g., Turner and Cadogan 1974) and/or radiogenic ^{40}Ar ($^{40}Ar*$) loss via recrystallization or alteration. The intermediate steps (~9-53% of ^{39}Ar) show older apparent ages that form a hump-shaped spectrum suggestive of ^{39}Ar recoil redistribution and/or ^{40}Ar inherited from incompletely degassed K-rich phases of the Paleoproterozoic target rocks (e.g., Bottomley et al. 1990; McDougall and Harrison 1999; Jourdan et al. 2007a,b). In the inverse isochron diagram, data points of steps 9-16 are linearly correlated (Fig. 8.10), yielding an initial $^{40}Ar/^{36}Ar$ intercept ratio of 279 ± 60 (MSWD = 0.73). This value is indistinguishable from the atmospheric $^{40}Ar/^{36}Ar$ ratio of 295.5, suggesting no notable portion of excess argon in these steps (e.g., Kelley and Spray 1997; McDougall and Harrison 1999; Kelley 2002a). The inverse isochron age of ~229 ± 3 Ma (2σ) calculated from steps 9-16 is, furthermore, consistent with the pseudo-plateau age (Fig. 8.9). Excluding steps 1-3, a second individual isochron can be drawn from steps 4-8 (Fig. 8.10; comparable to Korochantseva et al. 2007). The initial $^{40}Ar/^{36}Ar$ ratio of this second isochron is 1121 ± 88, with an inverse isochron age of 228 ± 4 Ma (2σ), which is in agreement with the pseudo-plateau and isochron ages of steps 9-16. The high $^{40}Ar/^{36}Ar$ ratio of 1121 ± 88 indicates the presence of excess ^{40}Ar in these steps. Recalculating the ages using this initial $^{40}Ar/^{36}Ar$ ratio leads to individual step ages of 202 ± 8, 229 ± 4, 233 ± 4, 228 ± 2 and 222 ± 4 Ma (2σ) for steps 4 to 8, respectively, which are indistinguishable from the isochron age of steps 9-16. However, the MSWD value of 4.09 for this second isochron (steps 4-8) is high compared to the MSWD of 0.73

for steps 9-16. This indicates that the roughly linear array of steps 4-8 is an artifact of ^{39}Ar recoil redistribution during irradiation. The redistribution of ^{39}Ar likely took place from the K-rich recrystallized feldspar to the K-poor microcrystalline silica, andesine crystallites, and/or the cryptocrystalline groundmass of the impact melt rocks that surrounds recrystallized feldspars (Fig. 8.5I-N). Accordingly, the Ca/K spectrum shows an irregularly distributed but generally low (<0.2) Ca/K ratio, which suggests that ^{39}Ar was predominantly released (and recoiled) from a K-rich phase (K-feldspar), and no temperature-dependent systematic degassing of plagioclase and mixed feldspar particles can be noted; Fig. 8.11). If the degassing temperature of the K-poor phases is lower than for the feldspar, the release of recoiled ^{39}Ar leads to younger apparent ages at the beginning of the age spectrum and higher ages at intermediate release temperatures. Steps 9-16 released argon only from the recrystallized feldspar unaffected by ^{39}Ar recoil loss. Thus, steps 1-8 were overprinted by ^{39}Ar redistribution leading to both younger and older apparent ages than the total gas age of 236 ± 2 Ma (2σ). The mean age of steps 9-17 is 229 ± 3 Ma (2σ), which is slightly lower than the total apparent age, indicating c. 1-3% ^{39}Ar loss during irradiation (thereby increasing the total apparent age of a sample), which is not unusual for fine-grained, intergrown phases (e.g. Hess and Lippolt 1986). With regard to the criteria for defining a plateau in ^{40}Ar/^{39}Ar geochronology (see McDougall and Harrison 1999), the new pseudo-plateau age should be considered as a preliminary *preferred* Paasselkä impact age, and further refining of the age might be desirable. The argon isotopic data are summarized in Table 8.4.
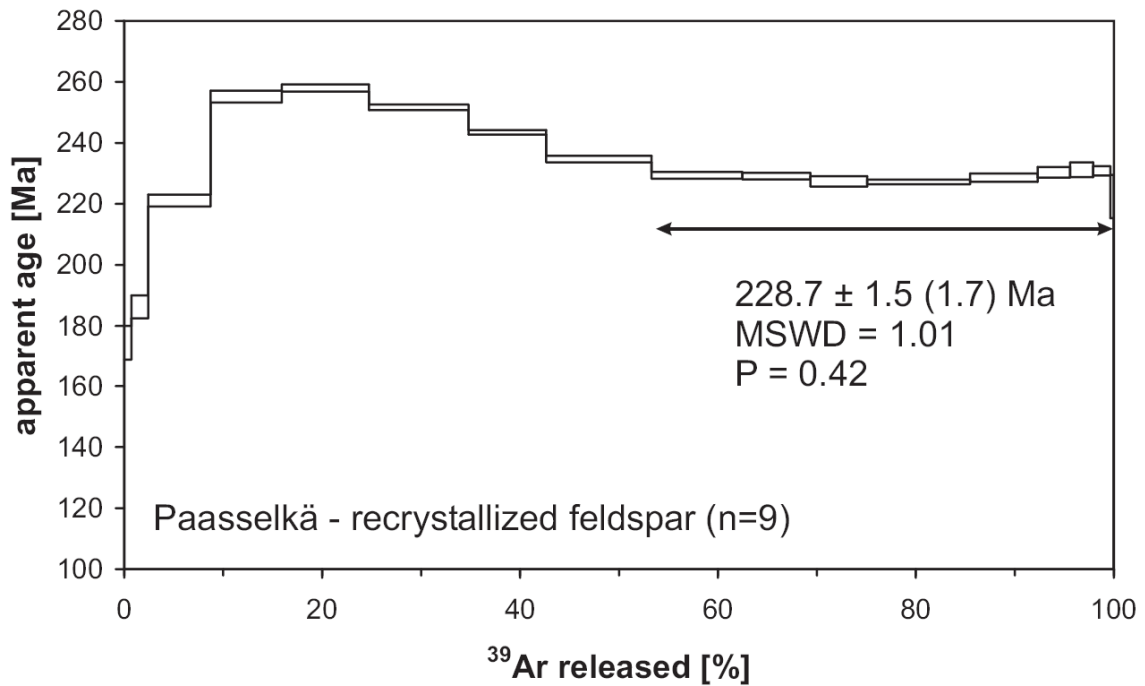
Fig. 8.9: $^{40}Ar/^{39}Ar$ age spectrum for recrystallized feldspar glass separate from Paasselkä impact melt rocks (Sikosärkät till pit); uncertainties and box sizes are at the 1σ level, the error in the parentheses includes the error on the age standard.
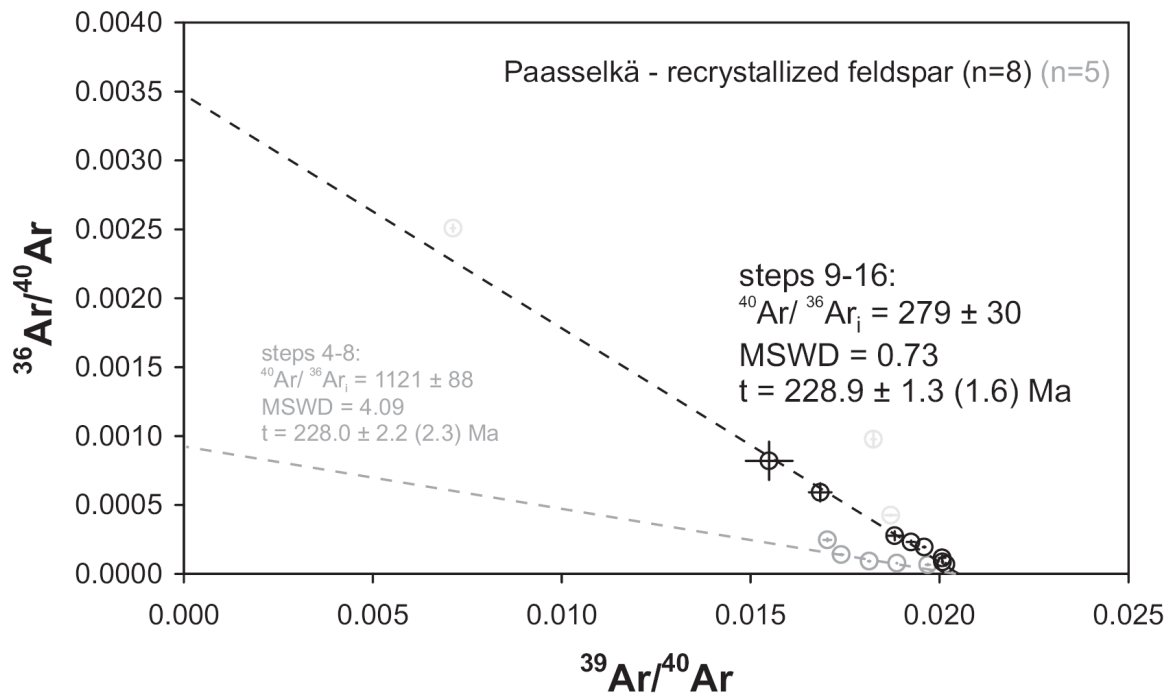
Fig. 8.10: Inverse isochron plot (black circles: steps included in the pseudo-plateau fraction; gray circles: steps outside the pseudo-plateau fraction; the errors are shown as crosses); uncertainties are at the 1σ level; the errors in the parentheses include the error on the age standard.
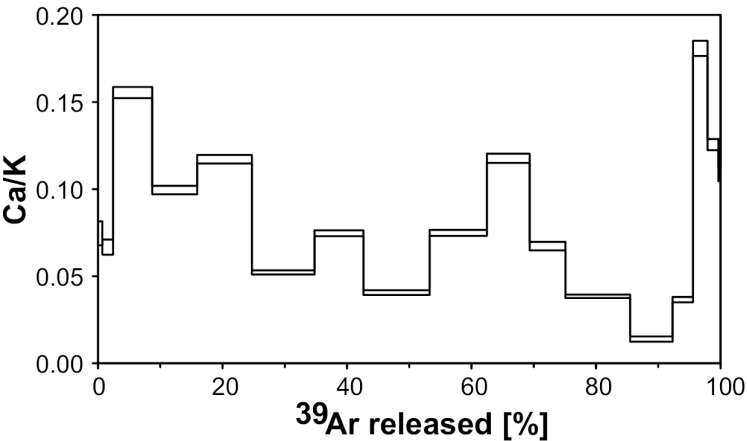
Fig. 8.11: Ca/K spectrum for recrystallized feldspar glass separate from the Paasselkä impact structure.

Table 8.1: Main oxide composition of melt matrix and whole rock composition of the Paasselkä impact melt rock (values in wt%; microprobe data)

	Melt matrix																Whole rock (EDX)*	Melt matrix (EDX)*
	#1	#2	#3	#4	#5	#6	#7	#8	#9	#10	#11	#12	#13	#14	Average		m=7	m=17
SiO$_2$	51.30	58.81	59.50	60.19	61.48	57.78	62.30	57.32	61.62	58.58	59.41	60.49	59.07	62.66	59.32	SiO$_2$	67.60	55.07
TiO$_2$	0.52	0.36	0.55	0.34	0.34	0.33	0.28	0.17	0.46	0.54	0.49	0.23	0.47	0.57	0.40	TiO$_2$	0.91	1.41
Al$_2$O$_3$	17.67	21.08	18.09	17.88	18.89	18.20	20.60	24.45	18.04	19.71	18.63	21.51	18.63	18.31	19.41	Al$_2$O$_3$	15.25	20.62
FeO	9.98	1.40	3.46	3.43	1.75	3.35	0.24	0.40	1.48	3.28	3.62	0.67	2.76	1.39	2.66	Fe$_2$O$_3$	6.88	10.25
MnO	0.00	0.02	0.02	0.02	0.00	0.01	0.00	0.01	0.00	0.05	0.00	0.00	0.03	0.00	0.01	MnO	0.34	0.40
MgO	6.42	0.65	0.25	1.58	0.36	1.97	0.02	0.02	0.59	0.81	1.17	0.05	1.09	0.46	1.10	MgO	1.82	3.07
CaO	0.58	3.12	1.34	0.20	0.79	0.80	2.76	6.92	0.44	1.79	1.18	3.80	1.39	0.65	1.84	CaO	1.65	1.67
Na$_2$O	1.95	5.19	3.60	1.70	2.91	2.95	5.29	6.92	2.13	3.60	3.52	6.52	4.30	3.93	3.89	Na$_2$O	1.50	1.51
K$_2$O	6.12	5.81	8.83	11.40	10.21	8.64	6.63	0.59	11.55	8.09	8.55	4.17	6.52	9.21	7.59	K$_2$O	4.05	6.01
Total	94.54	96.44	95.65	96.74	96.72	94.01	98.11	96.78	96.31	96.44	96.57	97.43	94.26	97.18	96.23	Total	100.00	100.00

*EDX measurements show average out of 7 area-integrated whole rock measurements and 17 area-integrated melt matrix measurements; note also the high Fe content due to contamination by opaque iron oxide phases. EDX values are normalized to 100%.

Table 8.2: Main oxide composition of fresh and recrystallized feldspar glasses in the Paasselkä impact melt rock (values in wt%; microprobe data)

	Plagioclase glasses																	
	G-01	G-02	G-03	G-04	G-05	G-06	G-07	G-08	G-09	G-10	G-11	G-12	G-13	G-14	G-15	G-16	G-17
SiO$_2$	60.10	61.20	59.38	59.22	58.78	59.32	60.19	59.81	59.68	59.68	60.10	60.23	58.63	58.96	61.92	61.92	61.03	59.97
TiO$_2$	0.12	0.00	0.00	0.03	0.05	0.00	0.00	0.00	0.00	0.00	0.01	0.00	0.02	0.21	0.00	0.00	0.00	0.00
Al$_2$O$_3$	21.98	22.14	23.46	23.01	23.31	22.87	22.68	23.14	23.82	23.38	22.90	22.24	21.39	24.42	22.98	22.56	23.15	21.68
FeO	1.15	0.11	0.21	0.33	0.52	0.35	0.50	0.42	0.17	0.29	0.36	0.07	0.47	2.20	0.08	0.12	0.16	0.29
MnO	0.00	0.00	0.00	0.02	0.00	0.00	0.00	0.00	0.00	0.00	0.01	0.02	0.00	0.00	0.00	0.00	0.05	0.00
MgO	0.02	0.02	0.05	0.02	0.06	0.11	0.10	0.13	0.00	0.07	0.15	0.02	0.14	0.92	0.01	0.03	0.05	0.00
CaO	4.26	4.38	5.36	5.35	5.54	5.63	4.70	5.49	6.05	5.65	5.23	4.88	4.16	4.94	4.96	4.74	5.72	4.61
Na$_2$O	8.37	7.97	7.01	7.17	7.61	7.38	7.37	7.57	7.00	8.03	7.52	7.69	8.13	7.34	8.81	8.12	7.93	7.59
K$_2$O	0.84	1.56	2.14	2.32	1.29	1.48	2.55	1.45	2.07	0.87	1.57	1.88	1.30	1.02	0.57	1.67	1.36	1.71
Total	96.83	97.36	97.61	97.47	97.15	97.14	98.08	98.00	98.79	97.97	97.85	97.02	94.24	100.00	99.32	99.16	99.45	95.85

Table 8.2 (continued)

	K-feldspar glasses									Mixed feldspar glasses						
	G-18	G-19	G-20	G-21	G-22	G-23	G-24	G-25	G-26	G-27	G-28	G-29	G-30	G-31	G-32	G-33
SiO_2	64.23	53.18	64.20	61.13	64.38	62.56	60.47	64.47	55.82	59.40	61.59	62.24	61.27	62.76	61.62	65.07
TiO_2	0.02	0.04	0.02	0.10	0.01	0.01	0.49	0.03	0.04	0.00	0.00	0.02	0.00	0.00	0.02	0.02
Al_2O_3	17.42	31.36	18.69	18.47	18.42	19.23	18.06	18.77	28.71	20.34	21.40	20.24	21.70	20.91	20.72	19.92
FeO	0.00	0.43	0.15	1.85	0.11	0.63	1.74	0.27	1.04	0.36	0.06	0.18	0.08	0.09	0.42	0.37
MnO	0.00	0.00	0.00	0.01	0.00	0.00	0.00	0.00	0.00	0.03	0.03	0.00	0.00	0.00	0.00	0.00
MgO	0.04	0.11	0.02	0.37	0.00	0.18	1.61	0.06	0.74	0.03	0.00	0.02	0.00	0.02	0.00	0.13
CaO	0.05	0.04	0.04	0.09	0.12	0.15	0.11	0.10	0.10	3.33	3.97	2.69	4.21	3.00	2.95	0.72
Na_2O	3.12	1.91	2.44	1.38	2.42	1.85	1.43	2.73	0.39	4.69	7.23	5.63	6.57	7.47	5.04	6.86
K_2O	10.73	8.22	12.23	13.35	11.96	11.75	12.34	11.27	7.74	6.32	3.01	6.45	3.43	3.90	6.46	5.07
Total	95.60	95.28	97.79	96.74	97.42	96.35	96.24	97.71	94.59	94.49	97.28	97.48	97.26	98.14	97.23	98.16

Table 8.3: Main oxide compositions of Fe-Mg-rich fresh to recrystallized mafic and silica glasses in the Paasselkä impact melt rock (values in wt%; microprobe data)

	Fe-Mg-rich 'chloritic' glasses**					Fluidal silica glass						Recrystallized diaplectic quartz glass		
	G-34	G-35	G-36	G-37	G-38	G-39	G-40	G-41	G-42	G-43	G-44	G-45	G-46	G-47
SiO_2	29.92	32.53	26.76	32.14	32.81	96.97	96.59	97.13	97.72	97.18	98.83	98.65	99.80	99.95
TiO_2	0.07	0.05	0.04	0.74	0.77	0.07	0.11	0.07	0.12	0.00	0.04	0.00	0.00	0.03
Al_2O_3	20.80	18.18	19.66	18.09	18.71	0.69	1.28	0.83	0.69	0.82	0.52	0.12	0.02	0.04
FeO	23.89	21.06	27.95	21.97	21.30	0.22	0.23	0.77	0.17	0.29	0.12	0.02	0.02	0.07
MnO	0.16	0.19	0.08	0.17	0.16	0.00	0.00	0.00	0.00	0.00	0.06	0.00	0.05	0.00
MgO	12.13	14.37	12.63	13.65	13.34	0.04	0.02	0.19	0.02	0.14	0.01	0.00	0.00	0.00
CaO	0.15	0.16	0.13	0.21	0.16	0.20	0.38	0.03	0.12	0.11	0.09	0.02	0.00	0.01
Na_2O	0.10	0.03	0.01	0.04	0.06	0.02	0.26	0.00	0.08	0.09	0.04	0.02	0.05	0.00
K_2O	0.72	0.48	0.06	1.16	1.21	0.02	0.03	0.07	0.02	0.04	0.03	0.01	0.01	0.00
Total	87.93	87.04	87.31	88.17	88.52	98.23	98.89	99.08	98.93	98.66	99.74	98.84	99.95	100.09

**Fe-Mg-rich glasses contain an average of ~12 wt% of volatiles

Table 8.4: Isotopic argon dataset and ages for recrystallized feldspar glass particles from the Paasselkä impact structure; errors in parentheses include error on the standard; bold characters denote extraction steps included in the pseudo-plateau calculation.

Step #	Temp [°C]	^{36}Ar [fA]	± 1σ	^{37}Ar$_{Ca}$ [fA]	± 1σ	^{38}Ar [fA]	± 1σ	^{39}Ar$_{K}$ [fA]	± 1σ	^{40}Ar [fA]	± 1σ	^{40}Ar*[fA]	± 1σ	^{36}Ar/^{40}Ar [•10^{-6}]	± 1σ	^{39}Ar/^{40}Ar [•10^{-5}]	± 1σ	^{39}Ar [%]	Age [Ma]	± 1σ
1	600	9.72	0.11	1.08	0.10	2.54	0.23	27.62	0.23	3877.6	7.2	1004	33	2508	28	712.2	6.2	0.72	174.3	5.7 (5.7)
2	650	3.53	0.18	2.31	0.15	2.12	0.24	66.01	0.22	3616.9	6.3	2573	53	976	49	1825.1	6.8	1.71	186.3	3.7 (3.8)
3	700	5.53	0.08	19.84	0.39	5.74	0.26	243.0	1.3	12990	75	11357	79	425.3	6.7	1871	15	6.29	221.1	1.9 (2.1)
4	720	4.03	0.18	14.53	0.35	5.65	0.17	278.3	1.3	16340	71	15150	90	246	11	1703	11	7.21	255.2	1.9 (2.1)
5	740	2.75	0.07	20.91	0.45	6.32	0.23	349.98	0.96	19545	39	18733	44	140.7	3.5	1739.5	6.0	8.80	258.0	1.1 (1.4)
6	760	1.96	0.11	10.63	0.23	6.87	0.12	388.48	0.46	21418	32	20837	45	91.7	5.2	1813.8	3.5	10.06	251.64	0.9 (1.3)
7	780	1.25	0.04	11.92	0.26	5.54	0.12	303.68	0.15	16093.4	8.4	15724	13	77.6	2.7	1887.0	1.4	7.86	243.48	0.7 (1.1)
8	820	1.40	0.13	8.77	0.29	7.48	0.05	410.97	0.89	20875	51	20462	63	66.9	6.1	1968.7	6.4	10.65	234.7	1.1 (1.4)
9	**860**	1.21	0.20	13.92	0.30	6.37	0.08	354.53	0.70	17581	26	17223	63	69	11	2016.6	5.0	9.18	**229.4**	**1.1 (1.4)**
10	**905**	1.15	0.17	16.38	0.38	5.03	0.33	265.17	0.22	13208	13	12868	48	87	13	2007.7	2.6	6.87	**229.1**	**1.1 (1.4)**
11	**970**	1.28	0.22	7.86	0.29	4.27	0.04	222.64	0.69	11096	39	10718	72	115	20	2006.5	9.3	5.76	**227.4**	**1.7 (1.9)**
12	**1070**	3.99	0.13	8.11	0.21	7.82	0.14	401.18	0.46	20476	36	19297	24	194.8	6.3	1959.2	4.1	10.39	**227.23**	**0.8 (1.1)**
13	**1120**	3.16	0.17	1.92	0.20	5.43	0.08	263.2	1.0	13675	66	12741	55	231	12	1924	12	6.81	**228.6**	**1.4 (1.6)**
14	**1170**	1.87	0.23	2.43	0.10	2.57	0.14	126.81	0.58	6742	60	6190	35	277	34	1881	19	3.28	**230.4**	**1.7 (1.9)**
15	**1250**	3.15	0.36	8.53	0.20	2.44	0.49	89.87	0.23	5336	96	4403	46	591	68	1684	30	2.33	**231.2**	**2.4 (2.5)**
16	**1350**	3.56	0.59	4.44	0.12	2.56	0.17	67.29	0.14	4344	175	3291	20	820	140	1549	62	1.74	**230.8**	**1.5 (1.7)**
17	**1450**	0	0.54	0.76	0.03	0.31	0.11	13.27	0.12	624	159	624	20	-	-	2127	804	0.34	**222.5**	**7.1 (7.1)**
Pseudo- plateau: 228.7 ± 1.5 (1.7) Ma (1σ), n = 9 steps, MSWD=1.01, P=0.42										J = 0.0027905 ± 0.0000085				Std: BMus/2; t = 328.5 ± 1.1 Ma				100.00	235.7	1.2 (1.4)

9. Discussion

9.1. The new $^{40}Ar/^{39}Ar$ impact ages: Paleoenvironmental implications

9.1.1. Rochechouart

Although no structural, lithological, or sedimentological criteria for a (shallow) marine impact scenario have been found to date, paleoenvironmental considerations suggest that the Rochechouart impact occurred very close to (or even beyond) the latest Triassic shoreline of the continental Massif Central, with the marine Aquitaine Basin and Biscay Rift (westernmost Tethys) to the West (e.g., Curnelle 1982; Ziegler 1990; Smith et al. 1994). This is in accord with earlier suggestions that the Rochechouart impact occurred within a shallow marine continental basin and the detection of elevated amounts of sulphur, phosphorous, and chlorine in the glassy mesostasis of the Champagnac pseudotachylites (Kelley and Spray 1997), which might indicate the influence of seawater.

Recently, Simms (2003; 2007) described a still puzzling ~2-4 m thick 'seismite' of large extent (>250,000 km²) partially overlain by 'tsunamite' in the uppermost Triassic of the British Isles (Cotham Member of the Lilstock Formation, Penarth Group, upper Rhaetian) a few meters below the biostratigraphic Triassic/Jurassic boundary. These peculiar deposits indicative of extensive soft-rock deformation were suggested to be incompatible with endogenic terrestrial mechanisms but consistent with a hitherto unknown high-energy end-Triassic impact event: 'The seismite certainly suggests an event that is unique in the Phanerozoic history of Britain and Ireland, and that is consistent with bolide impact', and 'impact of a km-scale asteroid here potentially could produce the observed sedimentological effects across the UK' (Simms 2007; see also Hesselbo et al. 2007 for discussion). Similarly, Mader (1992: his p. 306) noted potential tsunami deposits in the Lodève Basin of Southern France (Pégairolles de l'Escalette section, Languedoc-Roussillon; see Courtinat et al. 2003 for stratigraphic column), where an intercalation of 'exceptional and quasi-instantaneous character' in the Upper

Member of the Rhaetian contains 'allochthonous material' and 'could be attributed to a tsunami having been triggered by seismic instability in the basin' (Mader 1992). In the Northern Apennines of Italy, Rhaetoliassic sediments of the Grotta Arpaia section (basal Grotta Arpaia beds, Portovenere Limestone Member of the La Spezia Formation) interpreted as basin deposits distal to a carbonate ramp, contain slump deposits with storm layers, the composition of which 'implies that they were not due to tectonic activity at the platform margin, but that they originated inside the basin and affected the middle and outer part of the ramp' (Ciarapica 2007). Upper Rhaetian exotic high-energy deposits were also reported from the High Tatra Mountains of the Slovak Western Carpathians ('slumped beds' of the upper Fatra Formation; Michalík et al. 2007).

In agreement with the new latest Triassic 201 ± 1 Ma (2σ) ^{40}Ar/^{39}Ar age (see chapter 5) and paleogeographic studies, the near-coastal to shallow marine impact of the Rochechouart meteorite (see Fig. 9.1 for impact site at ~200 Ma) can be regarded as a potential trigger mechanism for a large tsunamigenic earthquake and the formation of end-Triassic tsunami deposits in the westernmost Tethys domain. The Aquitaine Basin, Biscay Rift, Western Approaches Trough, Bristol Channel, and Burgundy Gate (compare paleogeographic maps by Ziegler and Kent 1982; Ziegler et al. 1983; Fig. 9.1) represented channel-like sea passages that linked the Rochechouart impact site and the British Isles at the time of impact, maintaining high wave energy. The western Tethyan rift basins represented domains of pronounced subsidence during the Late Triassic (Ziegler and Kent 1982), suggesting a steep relief of the basins and deeper marine conditions. The distance between the impact site and the area of tsunami deposition was about 700-1300 km for the British Isles and notably shorter, about 300 km, for southern France (Lodève Basin). Just as well, the Northern Apennine and Western Carpathian domains were at paleodistances of ≤2000 km in the direction of the Neotethys Sea. Tsunamis, large sea waves caused by tectonic activity (earthquakes and faulting), submarine landslides, and volcanic eruptions, are known to produce distinct sedimentary features of high-energetic and complex erosion and deposition in the coastal run-up areas, commonly characterized by erosive fining-upward sequences (e.g., Bondevik et al. 1997; Dawson and Shi 2000; van den Bergh et al. 2003; Cantalamessa and Di Celma 2005); however, the destructive properties and specific sedimentological

features produced by tsunamis strongly depend on the location of the tsunami source, the regional geologic and topographic conditions, as well as on water depth and sea floor geometry (e.g., Dypvik and Jansa 2003; Satake 2007), and are still not fully understood (e.g., Bondevik et al. 1997; Gersonde et al. 2002). During the last decades, tsunami deposits formed by impact-triggered tsunamis have been recognized, e.g., those caused by the Chicxulub impact at the Cretaceous/Paleogene boundary (e.g., tsunamites in Texas and Mexico; Bourgeois et al. 1988; Smit et al. 1996), or in the Archean Hamersley Basin of Western Australia (Hassler et al. 2000). Just as well, tsunamites are associated with the Devonian Alamo impact (Nevada and Utah, USA; e.g., Warme and Kuehner 1998), the Devonian Kaluga impact (Russia; Dypvik et al. 2004), and the Cretaceous Tookoonooka impact (Australia; Bron 2009). Numerical modeling suggested that the Latest Jurassic marine impact that created the ~40 km Mjølnir impact structure in the Barents Sea off Norway also triggered a large tsunami (Glimsdal et al. 2007). A summary of impact-generated tsunamis is given by Ward and Asphaug (1999), Dypvik and Jansa (2003), Dypvik et al. (2004), and Goto (2008).

The Rochechouart impact energy exceeded the energy of the largest man-witnessed terrestrial earthquake (Valdivia, Chile, May 22, 1960; Richter scale magnitude 9.5 and a released energy of ~1.12×10^{19} Joules), capable of producing major seismic waves in the Earth's crust and tsunami waves in the sea. An impact energy of ~1.3×10^{21} Joules (equivalent to an earthquake of Richter scale magnitude 10.8-10.9) would have been associated with the impact of an iron meteorite ~1 km in diameter into largely crystalline rocks, at a typical impact velocity of 25 km/s and an impact angle of 45° (Marcus et al. 2004; Collins et al. 2005); these values are conservative estimates for the current (minimum) 20-25 km diameter of the eroded Rochechouart impact structure. Assuming a larger, ~2 km iron projectile and an original diameter of the Rochechouart impact structure of ~40-50 km (Lambert 2009), given the same impact angle and velocity, an impact energy of ~1.05×10^{22} Joules (corresponding to an earthquake of Richter scale magnitude 11.4-11.5) would have been released. In both cases, an impact-induced tsunamigenic earthquake could have caused the collapse of the local continental margin of the westernmost Massif Central and submarine landslides in the Aquitaine Basin and Biscay Rift as possible supporting mechanisms, maybe similar to the Eocene

marine Montagnais impact scenario on the Scotian shelf of Eastern Canada (Jansa 1993). Comparable to tsunamis caused by endogenic earthquakes, an impact tsunami wave is thought to contain kinetic and gravitational energy in the range of about 7-9% of the total impact energy (Ahrens and O'Keefe 1983; Dypvik and Jansa 2003). According to Jansa (1993), a marine impact producing a ~50 km crater would result in a 200 m high wave within a radius of 300 km and still a 40 m wave within a 3000 km radius. The height of the tsunami wave is greatly amplified when reaching the shallow sea and coastal areas, especially when the coastal geometry (for example, V-shaped bays, channels, or fjords etc.) supports effects of tsunami wave focusing and resonance (Satake 2007), as might have been the case on the Rhaetian British Isles.
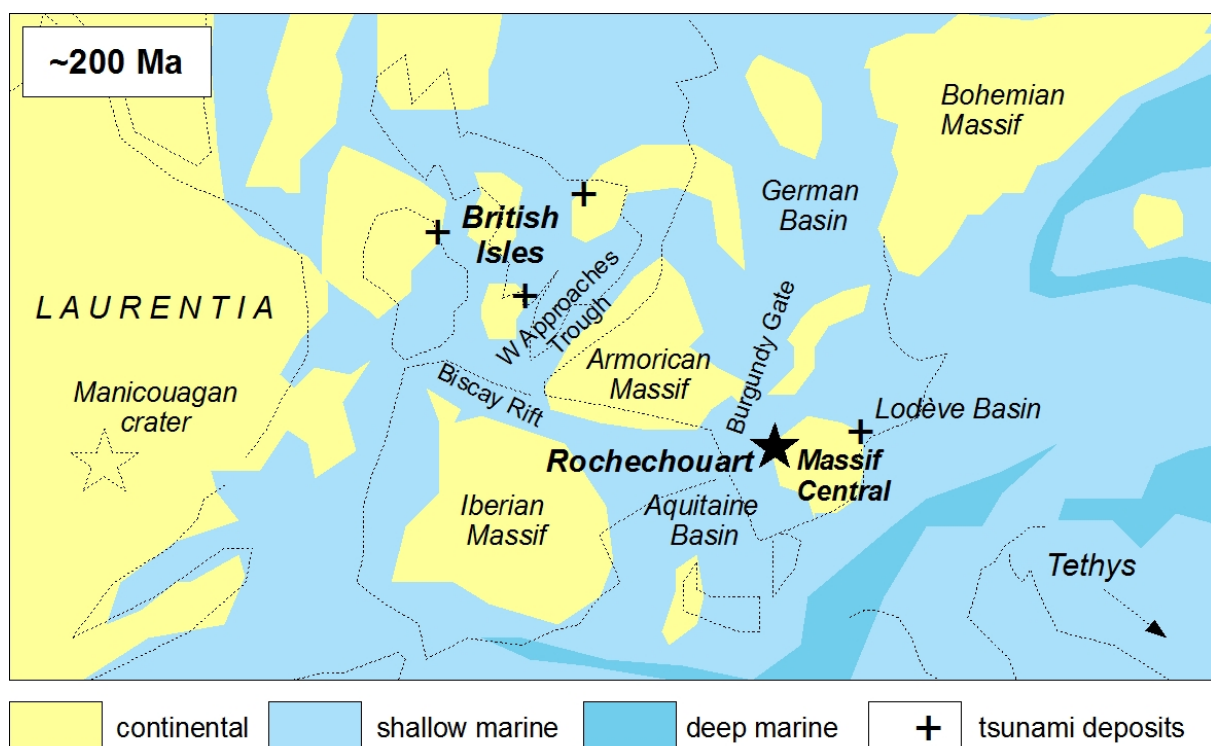
Fig. 9.1: Paleogeographic map of the western Tethys domain in the latest Triassic. Rochechouart impact site is indicated by black star (after Ziegler et al. 1983; Blakey 2006).

In contrast to the ~215 Ma and ~100 km in diameter Manicouagan impact structure (Hodych and Dunning 1992; Ramezani et al. 2005) associated with seismites in the Upper Triassic of the Fundy Basin in eastern Canada and a distal ejecta layer in Britain (Tanner 2002; Walkden et al. 2002; Kirkham 2003; Thackrey et al. 2008; 2009), no distal impact ejecta have so far been recognized to originate from the smaller Rochechouart impact. According to Walkden et al. (2002), a possible Rochechouart ejecta layer on the British Isles would have a primary thickness of about 1-1.6 mm, assuming a diameter of the Rochechouart impact structure of ~20-25 km; one could expect that ejecta might have been deposited on top of the seismites and prior to the formation of the tsunamites described by Simms (2003; 2007), which would warrant further investigations. In the more distal areas, Lintnerová et al. (2004) and Michalík et al. (2007) reported layers of enigmatic spherules in the Upper Rhaetian Fatra Formation of the High Tatra Mountains of Slovakia, some meters below the biostratigraphic Triassic/Jurassic boundary. A non-impact (volcanic or sedimentary) origin is discussed for the spherules, however, Michalík et al. (2007) resume that the spherules 'bear resemblance to small vitreous particles found in Cretaceous–Paleogene beds of the Caribbean region' and might have been formed by 'calcitization of glass droplets originating from a bolide impact, such as that postulated to occur immediately before the Rhaetian–Hettangian boundary'. Allegedly shocked quartz grains were reported in the Upper Rhaetian of the Northern Apennines, Italy (Bice et al. 1992) and the Northern Calcareous Alps, Austria (Badjukov et al. 1987) but unequivocal signs of shock could not be confirmed (Hallam 1990; 2002; Mossman et al. 1998; Simms 2007). It also remains speculative whether the iridium anomaly at the Triassic/Jurassic boundary in Eastern North America (Newark and Fundy basins; Olsen et al. 2002; Tanner and Kyte 2005) could be related to the impact of the Rochechouart iron meteorite (Tagle et al. 2009). The comparatively small crater size of ≤50 km (Lambert, 2009), however, suggests no direct relationship between the Rochechouart impact and the global end-Triassic mass extinction, one of the 'big five' extinction events in the history of life (e.g., Raup and Sepkoski 1982; Olsen et al. 1987; 2002; Hallam 1990; 2002; Benton 1991; 1995; Hallam and Wignall 1997; Pálfy et al. 2001; Ward et al. 2001; Hesselbo et al. 2002; Tanner et al. 2004). Possible distal impact ejecta produced by the Rochechouart impact in the European sedimentary record will require further study (see also Lambert 2009).

9.1.2. Manicouagan

The large crater size of the ~100 km Manicouagan impact structure makes this major impact a potential candidate for being linked with an impact-induced extinction event (see also 'impact-kill curve' relations by Raup 1992; Rampino 1999 and further thoughts by Walkden and Parker 2008). It was earlier suggested that the ~215 Ma Manicouagan impact (see chapter 6) might have been temporally related to the mass extinction that occurred at the Triassic/Jurassic boundary (e.g., Hodych and Dunning 1992; Olsen et al. 2002); however, the Triassic/Jurassic boundary was later shown to be distinctly younger, around ~200 Ma (e.g., Verati et al. 2007; Pálfy et al. 2008; Schaltegger et al. 2008; Jourdan et al. 2009a). Some researchers alternatively postulated one or more extinction events within the course of the Late Triassic, such as in the Karnian, at the Karnian/Norian stage boundary, and in the Norian (Benton 1986; 1991; 1995; Olsen et al. 1987; Sephton et al. 2002), as well as a severe climatic change suggested for the Norian/Rhaetian boundary (Cirilli 1995). A thorough discussion of Late Triassic extinction events is given by Tanner et al. (2004). However, at present, it can be stated that there is no unambiguous chemical or physical evidence for a link between the Manicouagan impact and a Late Triassic extinction event (e.g., Grieve 2006) but the occurrence of seismites in eastern North America and distal impact ejecta in Britain underline the at least semi-global scale of the Manicouagan impact (Tanner 2002; Walkden et al. 2002; Kirkham 2003; Thackrey et al. 2008; 2009).

9.1.3. Paasselkä

According to the international stratigraphic chart by Ogg et al. (2008), the new 229 ± 3 Ma (2σ) pseudo-plateau age for the Paasselkä impact structure (see chapter 8) falls within the age range for the Ladinian to Karnian, which within uncertainties is coeval to the ~228.7 ± 1.5 Ma Middle/Late Triassic (Ladinian/Karnian) boundary. Amongst a number of Mesozoic extinction events (e.g., Hallam and Wignall 1997), the

Ladinian/Karnian boundary is thought to be associated with a minor extinction that mainly affected marine vertebrates (Bardet 1994). However, the comparatively small size of the Paasselkä impact structure, probably about 10-20 km diameter in its pre-erosional state, suggests no direct relationship between the Paasselkä impact and a postulated Ladinian/Karnian biological crisis. The new Paasselkä age is, within uncertainty, coeval with the recently reported 235 ± 6 Ma zircon and 232 ± 7 Ma apatite (U-Th)/He ages for the Lake St. Martin impact structure (Manitoba, Canada; van Soest et al. 2009; Wartho et al. 2009; see chapter 6). In addition to impact structures that formed during the Late Triassic, e.g., the ~215 Ma Manicouagan impact structure (Québec, Canada; Hodych and Dunning 1992; Ramezani et al. 2005) and the 201 ± 2 Ma Rochechouart impact structure (France; chapter 5), this points towards a distinct new Middle to Late Triassic impact crater population on Earth. The Baltic Shield was characterized by cratonic continental conditions, erosion, and deep weathering during the Mesozoic (e.g., Ziegler 1988; Lidmar-Bergström 1991; Larsson and Tullborg 1993), and thus – with the exception of continental clastics and shallow marine sediments deposited along the southern, western, and northern margin of the Baltic craton at a paleodistance of ~1000 km from the Paasselkä impact site – no coherent suites of Triassic sediments are preserved in Finland and on the Baltic Shield (see also Korsman et al. 1997). Therefore, impact stratigraphic studies and a focused search for possible distal impact ejecta produced by the Paasselkä impact cannot be envisaged.

9.2. Implications for the Late Triassic multiple impact theory

9.2.1. Physical constraints

Primary impact crater chains (catenae) have been observed on other planetary bodies, such as the Moon (the comparatively young 47 km long Davy chain composed of 23 impact craters ~1-3 km in size; Fig. 9.2; as well as the ≥3.8 Ga old and ~200-260 km long Albufeda chain with 24 craters 5-13 km in size; Melosh and Whitaker 1994; Wichman and Wood 1995; Richardson et al. 1998), Jupiter's moons Callisto (e.g., the ~320 km long Gomul chain composed of 25 craters ~10-20 km in diameter; or the ~630 km long Gipul

catena with 18 craters 19-37 km in size; Fig. 9.3) and Ganymede (e.g., the ~160 km long Enki Catena composed of 13 craters 15-20 km in size; Fig. 9.4; Melosh and Schenk 1993; Schenk et al. 1996), or on Jupiter, where the linear string of fragments of the comet Shoemaker-Levy 9 disrupted upon close pass to Jupiter in July 1992 (~1.3 Jupiter radii; Sekanina et al. 1994) and created a chain of 23 large impact plumes visible to the Hubble Telescope in summer 1994 (Orton et al. 1995; Levy 1998; Fig. 3.2). By definition, crater chains are regularly spaced rows of three or more impact craters of similar sizes and identical apparent age hat line up like a 'string of pearls' (Bottke et al. 1997) with usually almost no deviation (≤1 crater radius) from the best-fit curve through the craters (Schenk et al. 1996; e.g., Figs. 9.2 and 9.3). The theory of primary crater chain formation near the inner planets of the Solar System is based on the assumption that most Near Earth Asteroids (NEAs) represent fragile 'rubble pile' aggregates of asteroid fragments rather than real solid bodies, generated by the forces of tidal disruption and kept together by self-gravity (Bottke et al. 1997; 1998; Richardson et al. 1998). This is supported by the presence of large impact craters on these asteroids (e.g., on asteroid 243 Mathilde; Yeomans et al. 1997) that imply major shock waves that travelled through and 'brecciated' the asteroid as a whole to piles of boulders (e.g., Chapman 1978; Asphaug et al. 1996), elongate and irregular (dynamic) forms of asteroids with comparatively low rotation velocities (e.g., Bottke et al. 1998), and a notably low density of these asteroids (e.g., ~1.3 g/cm^3 for 243 Mathilde). It has been suggested that the Lunar crater chains were formed via tidal disruption of the Shoemaker-Levy 9-type (S-type; compare Richardson et al. 1998; their Fig. 2), hitting the moon after being disrupted to a string of pearls by the Earth's tidal forces. As the craters that build up the Lunar crater chains are closely spaced, this also suggests that the multiple Lunar impacts occurred soon after the encounter of the rubble pile asteroid with Earth, too soon to be stretched so far that a recognizable crater chain could be produced (Melosh and Whitaker 1994; Wichman and Wood 1995; Richardson et al. 1998). The impact of binary asteroids, rubble pile asteroids separated during close encounter with a large planetary body, is also thought to generate doublet impact craters (e.g., Bottke and Melosh 1996a,b; Stöffler et al. 2002; Cook et al. 2003). Primary crater chains are distinguished from secondary crater chains, which are struck by the impact of larger blocks of impact ejecta in radial direction from the source impact crater and are often

characterized by a distinct 'herringbone' pattern (e.g., Melosh 1996; Schenk et al. 1996). Fields of closely spaced impact craters may be formed by the atmospheric breakup of smaller asteroids (Passey and Melosh 1980).

In analogy to the formation of Lunar crater chains, the generation of primary impact crater chains on Earth via tidal disruption of rubble pile asteroids — such as the large chain postulated by Spray et al. (1998) ~4,500 km long and composed of individual impact structures mostly larger than 20 km in diameter — most reasonably would require S-type disruption of the asteroids by the Moon (or another planetary body in the inner Solar System) prior to impact. However, considering the impact rate in the Earth-Moon system since the Late Heavy Bombardment, statistical modeling by Bottke et al. (1997) suggests that the Lunar crater chain production rate is ~10 times that of the Earth and that the number of expected primary impact crater chain on the Moon is about 1 over the last 3.8 Ga (in accordance with the observation of one old and one young crater chain on the Moon). The production rate of crater chains on Earth is notably lower, accounting for the formation of 0.1 crater chain during the last 3.8 Ga, which corresponds to a number of <<0.001 crater chains on Earth for the last 214 million years (Bottke et al. 1997). In turn, the presence of one ~214 Ma crater chain on Earth would suggest the presence of at least twenty comparatively fresh and distinct impact crater chains on the Moon, which is not the case. Given the geological activity of the Earth responsible for crustal recycling, the large areas covered by seawater, and the short list of ~176 or so known impact structures on Earth as a strongly biased database (e.g., Earth Impact Database 2009), this renders the occurrence of a Mesozoic primary impact crater chain on Earth highly unlikely (Bottke et al. 1997). In addition to the conventional model of S-type disruption of rubble pile asteroids, Richardson et al (1998) presented some alternative models to explain the tidal disruption of Earth-crossing asteroids other than by the Moon's gravity field, for example, disruption of very slow asteroids by three-body interaction with the Sun and Earth; the influence of the Moon that could lower the apogee of an Earth-captured rubble-pile asteroid; the impact of fragment chains on Earth generated during the flyby of another inner planet or the Sun; or aerobreaking of an asteroid or comet by ram pressure and tides as it penetrates the Earth's atmosphere very close to our planet. However, no such chains have been

observed on Mercury, Venus, or Mars (Schenk et al. 1996), and the aerobreaking event would cause highly oblique and closely spaced impact structures on the Earth's surface. Richardson et al. (1998) have shown that these alternative models are associated with very low probabilities of occurrence and also disagree with the formation of impact crater chains as the one suggested by Spray et al. (1998) in various aspects.

Fig. 9.2: The Davy crater chain (23 impact craters) on the Moon (NASA Apollo 16 image, AS16-1973)
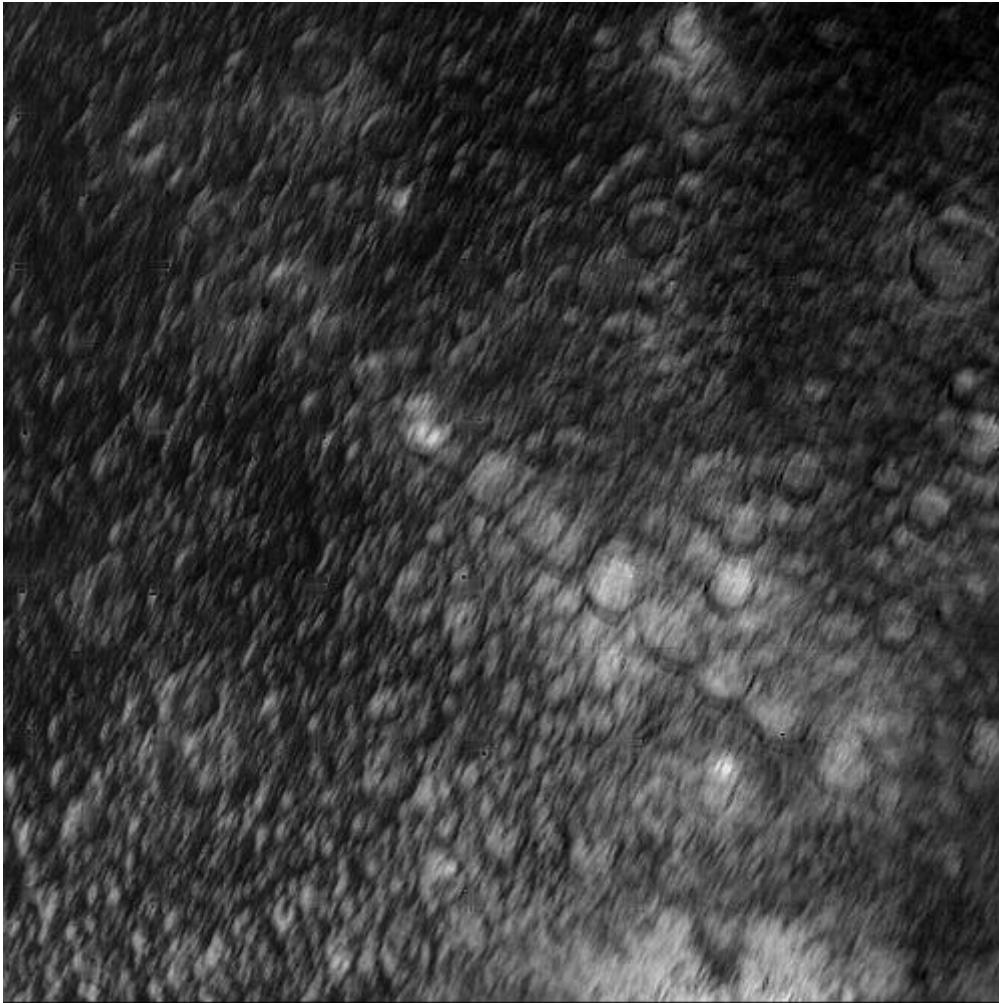
Fig. 9.3: Gipul catena (18 impact craters) on Jupiter's moon Callisto (NASA Voyager 1 Image, March 1979).

Fig. 9.4: Enki Catena (13 impact craters) on Jupiter's moon Ganymede (Galileo Probe image, 1994).

9.2.2. Geochemical considerations – the 'impactor ID problem'

Considering the tidal disruption of a rubble pile asteroid as the impacting projectile to generate a large-scaled impact crater chain on Earth, one can assume that the composition of each rubble pile fragment (i.e., the brecciated parts of the asteroid) should more or less reflect the composition of the primary asteroid. Larger asteroids may be differentiated into crust, mantle, and core (e.g., the ~530 km in size asteroid 4 Vesta, which is the second most massive asteroid in the asteroid belt and probably the parent body of the differentiated achondritic HED meteorites; McCord et al. 1970; Ghosh and McSween 1998; McSween et al. 2003; Thomas et al. 2005; see also the review on the evolution of the asteroid belt by Bottke et al. 2002), and differentiation is estimated to occur within bodies down to ~20-100 km in diameter (e.g., Middlefehldt et al. 1998; Binzel et al. 2003). If the crater chain postulated by Spray et al. (1998) was struck by the fragments of one common parent body none of which missed the Earth, the progenitor asteroid would have had an original size of roughly ~10 km in diameter, assuming crater sizes of 100 km for the Manicouagan, 40 km for Lake Saint Martin and Rochechouart, 20 km for Obolon, ~10 km for the Red Wing Creek impact structure, and terrestrial cater size versus impactor size scaling (with a constant factor of ~20; e.g., Holsapple 1993; Melosh 1996; French 1998). This value suggests that the impacting asteroid might have been rather homogenous in composition, i.e., non-differentiated, and all impact craters struck by that projectile should reveal similar projectile signatures in that case. However, impactor identification studies on impact melt rocks revealed no distinct meteoritic component for Manicouagan and Lake Saint Martin ascribed to the impact of an achondritic body (Göbel et al. 1980; Palme et al. 1981; Goderis 2009, pers. comm.) but suggested an iron meteorite for Rochechouart (Janssens et al. 1977; Horn and El Goresy 1979; Tagle et al. 2003; 2009), a probable iron meteorite for Obolon (Valter and Ryabenko 1977), as well as an uncertain chondritic component in impact breccias of the Red Wing Creek impact structure (Koeberl et al. 1996a). The inhomogeneous (although still poorly understood) distribution of impactor traces within the impact structures are, therefore, in conflict with the multiple impact of a fragmented small to medium-sized asteroid in the Late Triassic.

9.2.3. Geochronological constraints – the striking argument

A must criterion in identifying impact crater chains on Earth (and other planetary bodies) is geological evidence for the simultaneous formation of all members of the chain. Spray et al. (1998) largely based their multiple Late Triassic impact theory on the 1998 terrestrial impact age dataset in order to assess the credibility of the postulated scenario; ages were constrained at 214 ± 1 Ma for Manicouagan (Hodych and Dunning), 219 ± 32 Ma for Lake Saint Martin (Reimold et al. 1990), 214 ± 8 Ma for Rochechouart (Kelley and Spray 1997), 200 ± 25 Ma for Red Wing Creek (Gerhard et al. 1982), and 215 ± 25 Ma for Obolon (Masaitis et al. 1980), which were all compatible with a multiple impact event at ∼214 Ma. More recent dating results, however, suggest different and/or refined impact ages for at least three of these impact structures: as shown in the previous chapters, the Rochechouart impact structure was newly dated at 201 ± 2 Ma corresponding to the latest Triassic, within uncertainty coeval with the Triassic/Jurassic boundary, in conflict with the Late Triassic multiple impact theory. Based on paleomagnetic data, the coeval formation of the Manicouagan and Rochechouart impact structures was already questioned by Kent (1998) and other impact researchers (see Monastersky 1998). Recent (U-Th)/He ages for the Lake Saint Martin impact structure also favor an impact age around ∼235-230 Ma (van Soest et al. 2009; Wartho et al. 2009). Finally, the Obolon impact structure was shown to be significantly younger than Late Triassic, dated at ∼185-170 Ma corresponding to Early to Middle Jurassic (Schmieder and Buchner 2008). From these results, only the Manicouagan impact structure, with a well-established impact age of ∼215 Ma (Hodych and Dunning 1992; Ramezani et al. 2005) and the Red Wing Creek impact structure associated with a distinct stratigraphic age uncertainty could make up a 'binary set' of impact structures in compatibility with the ∼214 Ma impact age (Fig. 9.5).

For the above reasons – firstly, celestial conditions that render the formation of (primary) impact crater chains on Earth highly unlikely; secondly, inhomogeneous or missing impactor signatures in impactites; and thirdly, different impact ages – I conclude that there is no evidence for a Late Triassic multiple impact event on Earth and suggest that most of the impact structures discussed were rather formed by spatially and

temporally individual events. The new 229 ± 3 Ma age for the Paasselkä impact structure in Finland, however, adds one further impact structure to the list of Middle-Late Triassic impact structures on Earth (Fig. 9.5).
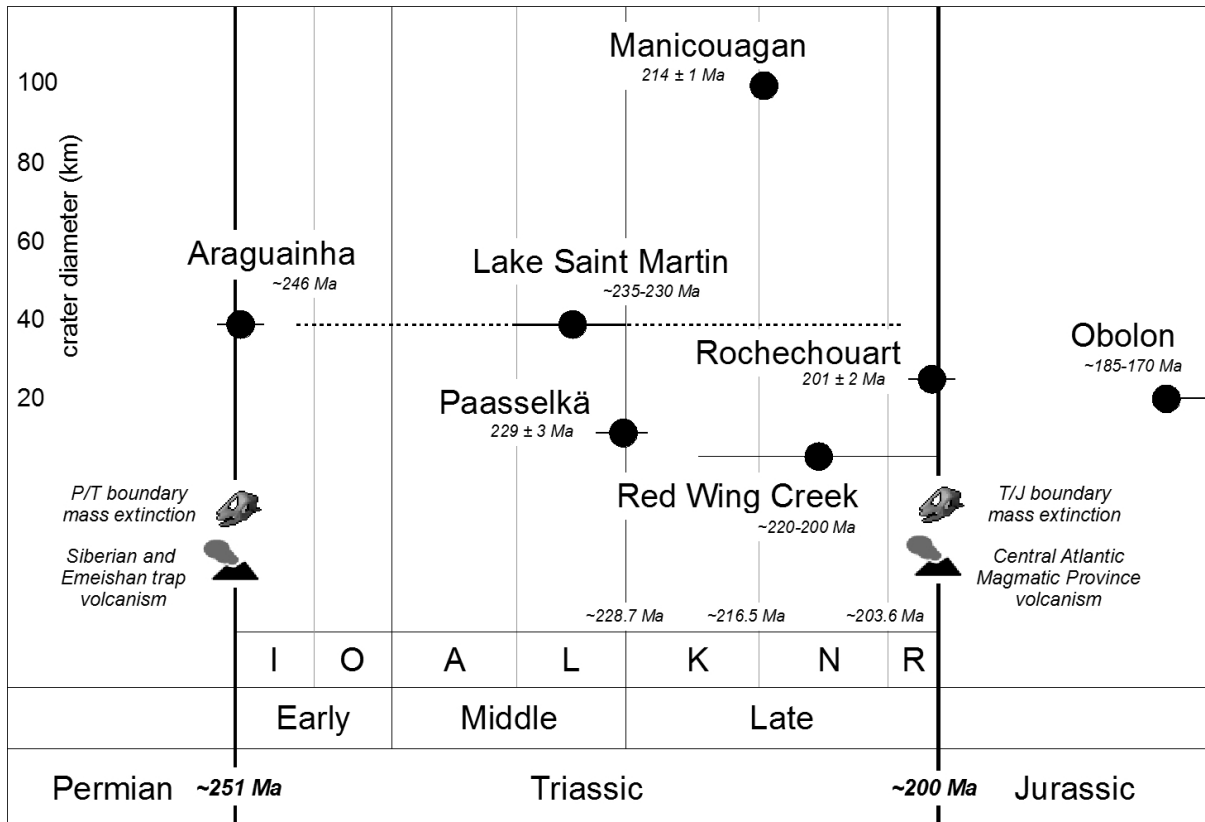
Fig. 9.5: Crater diameter versus impact age distribution for Triassic (to Jurassic) impact structures discussed in the text; abbreviations: I: Induan; O: Olenekian; A: Anisian; L: Ladinian; K: Karnian; N: Norian; R: Rhaetian; stage boundary ages after Ogg et al. (2008).

10. Conclusions

This study was performed in order to critically pursue the question whether the Late Triassic Earth at ~214 Ma experienced a semi global-scaled multiple impact event thought to have produced a large impact crater chain composed of the ~100 km Manicouagan (Québec, Canada), the ~40 Lake Saint Martin (Manitoba, Canada), the ~25 km Rochechouart (France), the ~20 km Obolon (Ukraine), and the ~9 km Red Wing Creek (North Dakota, USA) impact structures, respectively, as postulated by Spray et al. in 1998. As this theory was largely based on geochronologic data (i.e., impact ages available at that time), new ^{40}Ar/^{39}Ar dating of impact melt lithologies from Rochechouart and Manicouagan was carried out. The new data are set in the context of recent age determinations for Lake Saint Martin and Obolon and stratigraphic age estimates for Red Wing Creek. From this investigation, I conclude the following:

Rochechouart: ^{40}Ar/^{39}Ar dating of sanidine recrystallized from monomineralic potassium feldspar glass (plateau age of 201.4 ± 2.4 Ma; 2σ) and hydrothermally grown (potassium-metasomatic) adularia (plateau age of 200.5 ± 2.2 Ma; 2σ) separated from impact-metamorphosed gneiss found near Videix in the western central part of the Rochechouart impact structure yielded a Rhaetian combined age of 201 ± 2 Ma (2σ), coeval within uncertainty with the Triassic/Jurassic boundary. The new age is substantiated by robust internal statistics (concordant well-defined plateau ages for the high- and low-temperature K-feldspar phase; inverse isochron plots that indicate that there is no notable excess argon component) and is in the general range of previous dating results. However, the new age is by some million years younger than the 214 ± 8 Ma (Norian) age obtained by Kelley & Spray (1997; ^{40}Ar/^{39}Ar laser spot dating of pseudotachylites) and, therefore, contradicts the Late Triassic multiple impact theory postulated by Spray et al. (1998). In turn, a Rhaetian impact age is compatible with a near-coastal (or shallow marine) impact scenario making the Rochechouart impact event a potential trigger mechanism for the formation of seismites and tsunami deposits in the upper Rhaetian of the British Islands recently described by Simms (2003; 2007). Furthermore, upper Rhaetian tsunami and storm deposits in southern France and

northern Italy, as well as assumedly shocked quartz in upper Rhaetian sediments of the Northern Apennines (Italy) and an enigmatic spherule layer overlain by slump deposits in the Tatra Mountains of northern Slovakia, might be related to the Rochechouart event; the final confirmation of an impact origin of these deposits is, however, still outstanding. Given the comparatively small crater size, the Rochechouart impact was probably not the direct cause of the global Triassic/Jurassic boundary mass extinction (e.g., Benton 1995; Hallam and Wignall 197; Tanner et al. 2004).

Manicouagan: $^{40}Ar/^{39}Ar$ dating of a fine-grained impact melt dike rock from the Manicouagan impact structure yielded a weighted plateau age of 211 ± 2 Ma (2σ) very close to previous U/Pb dating results (considering the miscalibration of the K/Ar and U/Pb decay series; e.g., Schwarz and Trieloff 2007b). Expectedly, as the Manicouagan impact age is well established by high-precision U/Pb data (214 ± 1 Ma; Hodych and Dunning; 215.5 ± 0.05 Ma; Ramezani et al. 2005), this dating attempt could not significantly improve the isotopic dataset for Manicouagan but provides an exemplary case study of the degassing behavior of fine-grained crystalline impact melt rocks. The link between the Manicouagan and possible effects on the Late Triassic biosphere is still a matter of debate (e.g., Hodych and Dunning 1992; Grieve 2006).

Lake Saint Martin, Red Wing Creek, and Obolon: Isotopic ages available for the Lake Saint Martin impact structure are still associated with comparatively large errors (219 ± 32 Ma, Rb/Sr; Reimold et al. 1990). Recent (U-Th)/He dating of zircon and apatite grains recovered from impact melt rocks, however, have suggested an age of ~235-230 Ma for the Lake Saint Martin impact. Stratigraphic and K/Ar ages available for the Obolon impact structure were associated with large age uncertainties, ranging from Triassic to Jurassic (215 ± 25 Ma to 169 ± 7 Ma). In addition to isotopic and stratigraphic dating, paleogeographic studies can be an appropriate method to check and further constrain possible formation ages of terrestrial impact structures. Paleogeographic reconstructions, according to Late Triassic to Middle Jurassic paleogeographic maps by Ziegler at al. (1983) and Golonka (2000; 2007), have shown that the marine Obolon impact structure is younger than 185 Ma, suggesting an impact age of ~185-170 Ma. The

Red Wing Creek impact age can only be constrained by stratigraphic methods, and an impact age of roughly ~220-200 Ma (Koeberl et al. 1996) can be deduced.

Paasselkä: Finally, this thesis presents a first detailed petrographic and geochemical description of impact melt rocks from the ~10 km Paasselkä impact structure (Finland). The clast-rich impact melt rocks exhibit a distinct overall flow fabric and mainly consist of intensely shocked and toasted quartz grains, recrystallized and peripherally molten diaplectic silica glass grains, recrystallized fluidal silica glass opaque and semi-opaque iron oxide phases, and some secondary minerals within a glassy to cryptocrystalline melt matrix. Glasses may be divided into Na-Ca-rich and K-rich feldspathic, mixed feldspathic, Fe-Mg rich mafic, and essentially pure siliceous varieties and correspond to local melts formed from the mixed crystalline target rock of the Fennoscandian basement. The shock metamorphic observations on the impact melt rocks correspond to shock stage III–IV (according to Stöffler 1971, 1984) with initial whole-rock melting at peak shock pressures of ≥35 GPa and post-shock temperatures of up to ~1,500 °C. The Paasselkä impact melt rocks reflect the general geochemical character of melt rocks from impact structures of the Baltic Shield. $^{40}Ar/^{39}Ar$ dating of recrystallized feldspar glass particles separated from the impact melt rocks yielded a Middle to Late Triassic (Ladinian-Karnian) pseudo-plateau age of 229 ± 3 Ma (2σ). This makes Paasselkä the first Triassic impact structure dated by isotopic methods in Finland and on the Baltic Shield. The comparatively small cater size, however, suggests no direct relationship between the Paasselkä impact and a possible extinction event at the Middle/Late Triassic (Ladinian/Karnian) boundary (Bardet 1994).

The different impact ages for the Manicouagan (~215 Ma), Lake Saint Martin (~235-230 Ma), Rochechouart (~201 Ma), and Obolon (~185-170 Ma) impact structures, in conjunction with a low probability for the formation of impact crater chains on Earth in general (e.g., Richardson et al. 1998) and inhomogeneous or missing impactor signatures in impactites associated with these structures, breaks the impact crater chain postulated by Spray et al. (1998). From the geochronological results reported in this study, I suggest that there is no evidence for a Late Triassic terrestrial multiple impact event and that the impact structures discussed were most likely formed by temporally

and spatially individual impact events. The Paasselkä impact is, within uncertainty, coeval with the Lake Saint Martin impact in Canada and, thus, might suggest a new Middle to Late Triassic impact crater population on Earth.

11. References

Abadian M. 1972. Petrographie, Stoßwellenmetamorphose und Entstehung polymikter kristalliner Breccien im Nördlinger Ries. Contributions to Mineralogy and Petrology 35:245-262.

Abels A., Zumsprekel H. and Bischoff L. 2000. Basic remote sensing signatures of large, deeply eroded impact structures. In Koeberl C. and Gilmour I. (eds.) Impacts and the Early Earth, Springer, Heidelberg, p. 309-326.

Abels A., Plado J., Pesonen L. J. and Lehtinen M. 2002. The impact cratering record of Fennoscandia - a close look at the database. In Plado J. and Pesonen L. J. (eds.) Impacts in Precambrian Shields, Springer, Berlin, Heidelberg, p. 1-58.

Abramov O. and Kring D. A. 2004. Numerical modeling of an impact-induced hydrothermal system at the Sudbury crater. Journal of Geophysical Research 109:E10007, 16 p.

Abramov O. and Kring D. A. 2005. Impact-induced hydrothermal activity on early Mars. Journal of Geophysical Research 110:E12S09, 19 p.

Addison W. D., Brumpton G. R., Vallini D. A., Davis D. W., Kissin S. A., Fralick P. W., McNaughton N. J. and Hammond A. L. 2005. Discovery of distal ejecta from the 1850 Ma Sudbury impact event. Geology 33:193-196.

Ager D. 1995. The new catastrophism: the importance of the rare event in geological history. Cambridge University Press, UK, 231 p.

Ahrens T. J. and O'Keefe J. D. 1983. Impact of an asteroid or comet in the ocean and the extinction of terrestrial life. Journal of Geophysical Research 88:A799–A806.

Alexandre P., Cuney M. and Duhamel I. 2009. New K-Ar dating on impact-generated melt from the Carswell astrobleme, evidence for a Mesoproterozoic impact event. 72nd Annual Meeting of the Meteoritical Society, Meteoritics and Planetary Science Supplement, p. 5003.

Alexandrov P., Cheilletz A., Deloule E. and Cuney M. 2000. 319 ± 7 Ma crystallization age for the Blond granite (northwest Limousin, French Massif Central) obtained by U/Pb ion-probe dating of zircons. Âge de cristallisation à 319 ± 7 Ma du granite de Blond (NW Limousin, Massif central français) obtenu par datation U/Pb à la microsonde ionique sur zircons. Comptes Rendus de l'Académie des Sciences - Series IIA - Earth and Planetary Science 330:617-622.

Alexopoulos J. S., Grieve R. A. F. and Robertson P. B. 1988. Microscopic lamellar deformation features in quartz: Discriminative characteristics of shock-generated varieties. Geology 16:796-799.

Alvarez L. W., Alvarez W., Asaro F. and Michel H. V. 1980. Extraterrestrial cause for the Cretaceous-Tertiary extinction. Science 208:1095-1108.

Alvarez W. 2003. Comparing the evidence relevant to impact and flood basalt at times of major mass extinctions. Astrobiology 3:153-161.

Alvarez W., Claeys P. and Kieffer S. W. 1995. Emplacement of Cretaceous-Tertiary boundary shocked quartz from Chicxulub crater. Science 269:930-935.

Alwmark C. and Schmitz B. 2007. Extraterrestrial chromite in the resurge deposits of the early Late Ordovician Lockne crater, central Sweden. Earth and Planetary Science Letters 253:291-303.

Ames D. E., Watkinson D. H. and Parrish R. R. 1998. Dating of a regional hydrothermal system induced by the 1850 Ma Sudbury impact event. Geology 26:447-450.

Amor K., Hesselbo S. P., Porcelli D., Thackrey S. and Parnell J. 2008. A Precambrian proximal ejecta blanket from Scotland. Geology 36:303-306.

Arancibia G., Matthews S. J., Cornejo P., Pérez de Acre C., Zuluaga J. I. and Kasaneva S. 2006. $^{40}Ar/^{39}Ar$ and K–Ar geochronology of magmatic and hydrothermal events in a classic low-suphidation epithermal bonanza deposit: El Peñon, northern Chile. Mineralium Deposita 41:505-516.

Artemieva N. 2002. Tektite origin in oblique impacts: Numerical modeling of the initial stage. In Plado J. and Pesonen L. J. (eds.) Impacts in Precambrian Shields. Springer, Berlin, Heidelberg, p. 257-276.

Asphaug E., Moore J. M., Morrison D., Benz W., Nolan M. C. and Sullivan R. J. 1996. Mechanical and geological effects of impact cratering on Ida. Icarus 120:158-184.

Badjukov D. D. and Raitala J. 1998. The impact melt of the Jänisjärvi crater. 29th Lunar and Planetary Science Conference, abstract no. 1609.

Badjukov D. D. and Raitala J. 2006. Ni in impactite sulphides in the Lappajärvi, Sääksjärvi, Suvasvesi S, and Paasselkä impact craters in Finland. 37th Lunar and Planetary Science Conference, abstract no. 1676.

Badjukov D. D., Lobitzer H. and Nazarov M. A. 1987. Quartz grains with planar features in the Triassic-Jurassic boundary sediments from Northern Limestone Alps, Austria. Lunar and Planetary Science Conference 18:38-39.

Baksi A. 2003. Critical evaluation of $^{40}Ar/^{39}Ar$ ages from the Central Atlantic Magmatic Province: Timing, duration and possible migration of magmatic centers. American Geophysical Union Monograph 136:77-90.

Baksi A. 2005. Evaluation of radiometric ages pertaining to rocks hypothesized to have been derived by hotspot activity, in and around the Atlantic, Indian, and Pacific Oceans. Geological Society of America Special Paper 388:55-70.

Bannatyne B. B. and McCabe H. R. 1984. Manitoba crater revealed. GEOS 13:10-13.

Baratoux D. and Melosh H. J. 2003. The formation of shatter cones by shock wave interference during impacting. Earth and Planetary Science Letters 216:43-54.

Bardet N. 1994. Extinction events among Mesozoic marine reptiles. Historical Biology 7:313-324.

Barringer D. M. 1905. Coon Mountain and its crater. Proceedings of the Academy of Natural Sciences of Philadelphia 57:861-886.

Basurah H. M. 2003. Estimating a new date for the Wabar meteorite impact. Meteoritics and Planetary Science 39:A155-A156.

Beals C. S. and Halliday I. 1967. Impact craters of the Earth and Moon. Journal of the Royal Astronomical Society of Canada 61:295-313.

Becker L., Poreda R. J., Basu A. R., Pope K. O., Harrison T. M., Nicholson C. and Iasky R. 2004. Bedout: A possible end-Permian impact crater offshore of northwestern Australia. Science 304:1469-1476.

Benton M. J. 1986. More than one event in the late Triassic mass extinction. Nature 321:857-861.

Benton M. J. 1991. What really happened in the Late Triassic? Historical Biology 5: 263-278.

Benton M. J. 1995. Diversification and extinction in the history of life. Science 268:52-58.

Bice D. M., Newton C. R., McCauley S., Reiners P. W. and McRoberts C. A. 1992. Shocked quartz at the Triassic-Jurassic boundary in Italy. Science 255:443-446.

Binzel R. P., A'Hearn M., Asphaug E., Barucci M. A., Belton M., Benz W., Cellino A., Festou M. C., Fulchignoni M., Harris A. W., Rossi A. and Zuber M. T. 2003. Interiors of small bodies: foundations and perspectives. Planetary and Space Science 51:443-454.

Bischoff A. and Stöffler D. 1984. Chemical and structural changes induced by thermal annealing of shocked feldspar inclusions in impact melt rocks from Lappajärvi crater, Finland. Journal of Geophysical Research 89:B645-B656.

Blakey R. 2006. Global paleogeographic maps, available online at http://jan.ucc.nau.edu/~rcb7/ (accessed October 2009).

Bland P. A. 2005. The impact rate on Earth. Philosophical Transaction of the Royal Society (A) 363:2793-2810.

Bogard D. D., Hörz F. and Stöffler D. 1988. Loss of radiogenic argon from shocked granitic clasts in suevite deposits from the Ries Crater. Geochimica et Cosmochimica Acta 52:2639-2649.

Bohor B. F., Foord E. E., Modreski P. J. and Triplehorn D. M. 1984. Mineralogic evidence for an impact event at the Cretaceous-Tertiary boundary. Science 224:867-869.

Bohor B. F., Modreski P. J. and Foord E. E. 1987. Shocked quartz in the Cretaceous-Tertiary boundary clays: Evidence for a global distribution. Science 236:705-709.

Bohor B. F., Betterton W. J. and Krogh T. E. 1993. Impact-shocked zircons: discovery of shock-induced textures reflecting increasing degrees of shock metamorphism. Earth and Planetary Science Letters 119:419-424.

Bondevik S., Svendsen J. I. and Mangerud J. 1997. Tsunami sedimentary facies deposited by the Storegga tsunami in shallow marine basins and coastal lakes, western Norway. Sedimentology 44:1115-1131.

Boslough M. B. E. and Crawford D. A. 2008. Low-altitude airbursts and the impact threat. International Journal of Impact Engineering 35:1441–1448.

Boss A. P. 1986. The origin of the Moon. Science 231:341-345.

Bottke W. F. Jr. and Melosh H. J. 1996a. Formation of asteroid satellites and doublet craters by planetary tidal forces. Nature 381:51-53.

Bottke W. F. Jr. and Melosh H. J. 1996b. Binary asteroids and the formation of doublet craters. Icarus 124:372-391.

Bottke W. F Jr., Richardson D. C. and Love S. G. 1997. Can tidal disruption of asteroids make crater chains on the Earth and Moon? Icarus 126:470-474.

Bottke W. F Jr., Richardson D. C. and Love S. G. 1998. Production of Tunguska-sized bodies by Earth's tidal forces. Planetary and Space Science 46:311-322.

Bottke W. F. Jr., Cellino A., Paolicchi P. and Binzel P. R. 2002. An Overview of the Asteroids: The Asteroids III Perspective. In Bottke W. F. Jr., Paolicchi P., Binzel R. P. and Cellini A. (eds.) Asteroids III, University of Arizona Press, Tucson, Arizona, USA, p. 3-15.

Bottomley R. J., York D. and Grieve R. A. F. 1979. Possible source craters for the North American tektites – a geochronological investigation. EOS 60:309.

Bottomley R. J., York D. and Grieve R. A. F. 1990. ^{40}Argon-^{39}Argon dating of impact craters. Proceedings of the Lunar and Planetary Science Conference 20:421-431.

Bottomley R. J., Grieve R. A. F., York D. and Masaitis V. 1997. The age of the Popigai impact event and its relation to events at the Eocene/Oligocene boundary. Nature 388:365-368.

Bourgeois J., Hansen T. A., Wiberg P. A. and Kauffman E. G. 1988. A tsunami deposit at the Cretaceous-Tertiary boundary in Texas. Science 241:567-570.

Branco W. and Fraas E. 1905. Das kryptovulcanische Becken von Steinheim: Abhandlungen der königlich preussischen Akademie der Wissenschaft, physikalische Abhandlungen 1:1-64, Berlin, Germany (in German).

Brenan R. L., Peterson B.L. and Smith H. J. 1975. The origin of Red Wing Creek structure: McKenzie County, North Dakota. Wyoming Geological Association Earth Science Bulletin 8, 41 p.

Brittan J., Morgan J., Warner M. and Marin L. 1999. Near-surface seismic expression of the Chicxulub impact crater. Geological Society of America Special Paper 339:269-279.

Bron K. 2009. The Tookoonooka tsunami sequence: Evidence for marine impact in Australia's Lower Cretaceous. 40th Lunar and Planetary Science Conference, abstract no. 2560.

Buchner E. and Kenkmann T. 2008. Upheaval Dome, Utah, USA: Impact origin confirmed. Geology 36:227-230.

Buchner E. and Schmieder M. 2007. Mousso structure: A deeply eroded, medium-sized, complex impact crater in northern Chad? Journal of African Earth Sciences 49:71-78.

Buchner E. and Schmieder M. 2009a. Multiple fluvial reworking of impact ejecta - A case study from the Ries crater (Germany). Meteoritics and Planetary Science 44:1051-1060.

Buchner E. and Schmieder M. 2009b. Suevit - Entstehung und Auftreten in Meteoritenkratern der Erde. In Rosendahl W. and Schieber M. (eds.) Der Stein der Schwaben. Natur- und Kulturgeschichte des Suevits. Staatsanzeiger-Verlag, Stuttgart, Germany, p. 19-23 (in German).

Buchner E. and Schmieder M. 2009c. Die Erde unter dem Einfluss großer Impaktereignisse zur Zeit der Trias. In Hauschke N. and Wilde V. (eds.) Trias. Aspekte des frühen Erdmittelalters in Europa. Pfeil, Munich, Germany (in German; in press).

Buchner E., Seyfried H. and van den Bogaard P. 2003. ^{40}Ar/^{39}Ar laser probe age determination confirms the Ries impact crater as the source of glass particles in Graupensand sediments (Grimmelfingen Formation, North Alpine Foreland Basin). International Journal of Earth Sciences 92:1-6.

Buchner E., Moilanen J., Öhman T. and Schmieder M. 2009a. Shock-molten sandstone clasts in impact melt rocks: Age constraints for the Paasselkä impact structure (SE Finland). 40th Lunar and Planetary Science Conference, abstract no. 2169.

Buchner E., Schmieder M., Schwarz W. H., Trieloff M., Jourdan F., Wartho J.-A., van Soest M. C., Hodges K. V. and Pösges G. 2009b. A new look at the Ries-Steinheim event – A first report of different melt lithologies from the Steinheim Basin and a new ~14.4 Ma Ries impact age. Abstract presented at the first Arab Impact Cratering and Astrogeology Conference (AICAC), 9-11 November 2009, Amman, Jordan.

Buchner E., Schmieder M., Schwarz W. H., Trieloff M., Moilanen J., Öhman T. and Stehlik H. 2009c. A Proterozoic ^{40}Ar/^{39}Ar age for the Suvasvesi South structure (Finland). 72nd Annual Meeting of the Meteoritical Society, Meteoritics and Planetary Science supplement, abstract no. 5076.

Buhl D., Deutsch A. and Langenhorst F. 1990. On the significance of ages for impact melts: New Rb-Sr and Sm-Nd data for Dellen (Sweden) and Araguainha (Brazil). Meteoritics 25:352.

Bunch T. E., Cohen A. J. and Dence M. R. 1967. Natural terrestrial maskelynite. American Mineralogist 52:244-253.

Cameron A. G. W. and Ward W. R. 1976. The origin of the Moon. Lunar and Planetary Science Conference 7:120-122.

Cantlamessa G. and Di Celma C. 2005. Sedimentary features of tsunami backwash deposits in a shallow marine Miocene setting, Mejillones Peninsula, northern Chile. Sedimentary Geology 178:259-273.

Canup R. M. and Asphaug E. 2001. Origin of the Moon in a giant impact near the end of the Earth's formation. Nature 412:708-712.

Canup R. M. and Righter K. 2000 (eds.). Origin of the Earth and Moon. University of Arizona Press, Tucson, 555p.

Carporzen L. and Gilder S. A. 2006. Evidence for coeval Late Triassic terrestrial impacts from the Rochechouart (France) meteorite crater. Geophysical Research Letters 33:L19308.

Carstens H. 1975. Thermal history of impact melt rocks in the Fennoscandian shield. Contributions to Mineralogy and Petrology 50:145-155.

Chao E. T. C., Shoemaker E. M. and Madsen B. M. 1960. First natural occurrence of coesite. Science 132:220-222.

Chao E. C. T., Fahey J. J. and Littler J. 1961. Coesite from Wabar Crater, near Al Hadida, Arabia. Science 133:882-883.

Chapman C. R. 1978. Asteroid collisions, craters, regoliths, and lifetimes. In Morrison D. and Wells W. C. (eds.) Asteroids. An exploration assessment. NASA Conference Publication 2053:145–160.

Chapman C. R. 2004. The hazard of near-Earth asteroid impacts on earth. Earth and Planetary Science Letters 222:1-15.

Chapman C. R. and Morrison D. 1994. Impacts on the earth by asteroids and comets: Assessing the hazard. Nature 367:33-40.

Chèvremont P., Floc'h J. P., Ménillet F., Stussi J. M., Delbos R., Sauret B., Blès J. L., Courbe C., Vuaillat D. and Gravelat C. 1996. Note explicative, Carte Géologique de la France (1/50000), feuille Rochechouart (687). BRGM, Orléans, France, 172 p. (in French).

Ciarapica G. 2007. Regional and global changes around the Triassic–Jurassic boundary reflected in the late Norian–Hettangian history of the Apennine basins. Palaeogeography, Palaeoclimatology, Palaeoecology 244:34–51.

Cirilli S. 1985. Evidence for a climate change at the Norian-Rhaetian boundary (late Triassic): Is the Manicouagan the culprit? 4th International Workshop of the ESF Scientific Network on Impact Cratering and Evolution of Planet Earth, p. 54.

Claeys P., Casier J.-G. and Margolis S. V. 1992. Microtektites and mass extinctions: Evidence for a Late Devonian asteroid impact. Science 257:1102-1104.

Claeys P., Kyte F. T., Herbosch A. and Casier J.-G. 1996. Geochemistry of the Frasnian-Famennian boundary in Belgium: Mass extinction, anoxic oceans and microtektite layer, but not much iridium? Geological Society of America Special Paper 307:491-504.

Claeys P., Kiessling W. and Alvarez W. 2002. Distribution of Chicxulub ejecta at the Cretaceous-Tertiary boundary. Geological Society of America Special Paper 356:55-68.

Cockell C. S. and Lee P. 2002. The biology of impact craters – a review. Biological Reviews 77:279-310.

Collins G. S. and Wünnemann K. 2005. How big was the Chesapeake Bay impact? Insight from numerical modelling. Geology 33:925-928.

Collins G. S., Melosh H. J. and Marcus R. A. 2005. Earth Impact Effects Program: A web-based computer program for calculating the regional environmental consequences of a meteoroid impact on Earth. Meteoritics and Planetary Science 40:817-840.

Cook C. M., Melosh H. J. and Bottke W. F. 2003. Doublet craters on Venus. Icarus 165:90-100.

Corfu F., Hanchar J. M., Hoskin P. W. and Kinny P. 2003. Atlas of zircon textures. Reviews in Mineralogy and Geochemistry 53:469-500.

Courtinat B. Piriou S. and Rio M. 2003. Phytoclasts in palynofacies definition: the example of Rhaetian sedimentary organic matter in SE France. Revue de Micropaléontologie 46:11-21.

Crósta A. P. 1983. Geologic mapping of the Araguainha Dome using remote sensing techniques. M.S. Thesis Instituto de Pesquisas Espaciais, Sao Jose dos Campos (Brazil).

Crósta A. P. 1987. Impact structures in Brazil. In Pohl J. (ed.) Research in terrestrial impact structures. Vieweg & Sohn, Braunschweig/Wiesbaden, Germany, p. 30-38.

Crósta A. P., Kazzuo-Vieira C., Choudhuri A. and Schrank A. 2005. Vargeão Dome, State of Santa Catarina - A meteoritic impact record on volcanic rocks of the Paraná Basin. In Winge M., Schobbenhaus C., Berbert-Born M., Queiroz E T. and Campos D. A. (eds.) Sítios Geológicos e Paleontológicos do Brasil, SIGEP 114, 12 p.

Curnelle R., Dubois P. and Seguin J. C. 1982. The Mesozoic-Tertiary evolution of the Aquitaine Basin. Philosophical Transactions of the Royal Society of London A 305:63-84.

Currie K. L. 1970. New Canadian cryptoexplosion crater at Lake St. Martin, Manitoba. Nature 226:839-841.

Currie K. L. 1972. Geology and petrology of the Manicouagan resurgent caldera, Quebec. Geological Survey of Canada Bulletin, 153 p.

Davis D. W. 2008. Sub-million-year age resolution of Precambrian igneous events by thermal extraction–thermal ionization mass spectrometer Pb dating of zircon: Application to crystallization of the Sudbury impact melt sheet. Geology 36:383-386.

Dawson A. and Shi S. 2000. Tsunami deposits. Pure and Applied Geophysics 157:875-897.

Dence M. R. 1970. Shock metamorphism at the Lake St. Martin (Manitoba) structure. Geological Association of Canada, Mineralogical Association of Canada Annual Meeting, p. 19.

Deutsch A. and Koeberl C. 2006. Establishing the link between the Chesapeake Bay impact structure and the North American tektite strewn field: The Sr-Nd isotopic evidence. Meteoritics and Planetary Science 41:689-703.

Deutsch A. and Schärer U. 1994. Dating terrestrial impact events. Meteoritics 29:301-322.

Deutsch A., Buhl D. and Langenhorst F. 1992. On the significance of crater ages: New ages for Dellen (Sweden) and Araguainha (Brazil). Tectonophysics 216:205-218.

DeVor R. E., Chang T-H. and Sutherland J. W. 2007. Statistical quality design and control. Prentice Hall, New Jersey, USA, 960 p.

Dietz R. S. 1947. Meteorite impact suggested by the orientation of shatter-cones at the Kentland, Indiana, disturbance. Science 105:42-43.

Dietz R. S. 1960. Meteorite impact suggested by shatter cones in rock. Science 131:1781-1784.

Dietz R. S. and French B. M. 1973. Araguainha Dome and Serra da Cangalha, Brazil: probable astroblemes. Meteoritics 8:345-347.

Donofrio R. 1981. Impact craters: implications for basement hydrocarbon production. Journal of Petroleum Geology 3:279-302.

Donofrio R. 1998. North American impact structures hold giant field potential. Oil & Gas Journal (May 11, 1998), p. 69-83.

Dressler B. O. 1990. Shock metamorphic features and their zoning and orientation in the Precambrian rocks of the Manicouagan structure, Quebec, Canada. Tectonophysics 171:229-245.

Dressler B. O. and Reimold W. U. 2001. Terrestrial impact melt rocks and glasses. Earth-Science Reviews 56:205–284.

Dressler B. O. and Sharpton V. L. 1997. Breccia formation at a complex impact crater: Slate Islands, Lake Superior, Ontario, Canada. Tectonophysics 275:285-311.

Dressler B. O., Sharpton V. L. and Copeland P. 1999. Slate Islands, Lake Superior, Canada: A mid-size, complex impact structure. Geological Society of America Special Paper 339:109-124.

Dworak U. 1969. Stosswellenmetamorphose des Anorthosits vom Manicouagan Krater, Quebec, Canada. Contributions to Mineralogy and Petrology 24:306-347 (in German).

Dypvik H. and Jansa L. 2003. Sedimentary signatures and processes during marine bolide impacts: a review. Sedimentary Geology 161:309–337.

Dypvik H., Burchell M. and Claeys P. 2004 (eds.). Cratering in marine environments and on ice. Springer, Berlin, Heidelberg, 290 p.

Dypvik H., Plado J., Heinberg C., Håkansson E., Pesonen L., Schmitz B. and Raiskila S. 2008. Impact structures and events - A Nordic perspective. Episodes 31:107-114.

Earth Impact Database 2009. Available online at http://www.unb.ca/ passc/ImpactDatabase (accessed September 14, 2009). Maintained by the University of New Brunswick, Fredericton, New Brunswick, Canada.

Ehlers T. A. and Farley K. A. 2003. Apatite (U–Th)/He thermochronometry: methods and applications to problems in tectonic and surface processes. Earth and Planetary Science Letters 206:1-14.

El Goresy A. 1965. Baddeleyite and its significance in impact glasses. Journal of Geophysical Research 70:3453-3456.

Elo S. 1979. Paasiveden gravimetrinen minimi (Gravimetric minimum of Paasivesi). Espoo: Geological Survey of Finland, Report Q20/21/1979/3, Espoo, Finland, 14 p. (in Finnish).

Elo S., Lauerma R., Lavikainen S., and Winterhalter B. 1984. Geologisia ja geofysikaalisia havaintoja Paasivedeltä ja sen ympäristöstä Kaakkois-Suomesta—Summary: Geological and geophysical observations on Lake Paasivesi and its surroundings, southeastern Finland. Espoo: Geological Survey of Finland, Espoo, Finland, Report of Investigation 64, 24 p. (partly in Finnish).

von Engelhardt W. 1972. Shock produced rock glasses from the Ries crater. Contributions to Mineralogy and Petrology 36:265–292.

von Engelhardt W. and Graup G. 1984. Suevite of the Ries crater, Germany: Source rocks and implications for cratering mechanics. Geologische Rundschau 73:447–481.

von Engelhardt W., Arndt J., Stöffler D., Müller W. F., Jeziorkowski H., and Gubser R. A. 1967. Diaplektische Gläser in den Breccien des Ries von Nördlingen als Anzeichen für Stoßwellenmetamorphose. Contributions to Mineralogy and Petrology 15:93-102.

von Engelhardt W., Stöffler D. and Schneider W. 1969. Petrologische Untersuchungen im Ries. Geologica Bavarica 61:229–295 (in German).

von Engelhardt W., Pohl J. and Walzebuck J. 1985. Araguainha impact structure, Mato Grosso, Brazil. Meteoritics 20:640.

von Engelhardt W., Luft E., Arndt J., Schock H. and Weiskirchner W. 1987. Origin of moldavites. Geochimica et Cosmochimica Acta 51:1425-1443.

von Engelhardt W., Matthai S. K. and Walzebuck J, 1992. Araguainha impact crater, Brazil. I - The interior part of the uplift. Meteoritics 27:442-457.

Erwin D. H. 1990. The end-Permian mass extinction. Annual Review of Ecology and Systematics 21:69-91.

Evans K. R., Davis G. H., Miao X., Mickus K. L., Miller J. F. and Morrow J. R. 2008. Re-evaluating the 38th parallel serial impact hypothesis. Eos Transactions AGU 89(53), Fall Meeting, abstract P31A-1384.

Fackelman S. P., Morrow J. R., Koeberl C. and McElvain T. H. 2008. Shatter cone and microscopic shock-alteration evidence for a post-Paleoproterozoic terrestrial impact structure near Santa Fe, New Mexico, USA. Earth and Planetary Science Letters 270:290-299.

Farley K. A. 2002. (U-Th)/He dating: Techniques, calibrations, and applications. Reviews in Mineralogy and Geochemistry 47:819-844.

Farley K. A. and Stockli D. F. 2002. (U-Th)/He dating of phosphates: Apatite, monazite, and xenotime. Reviews in Mineralogy and Geochemistry 48:559-577.

Faure G. 1986. Principles of isotope geology. 2nd edition, John Wiley & Sons, New York, Brisbane, Toronto, Singapore, 589 p.

Feldman V. I. 2001. Shock-thermal decomposition of minerals as one of the main diagnostic features of shock metamorphism. Solar System Research 35:90–94.

Ferrière L., Koeberl C., Ivanov B. A. and Reimold W. U. 2008. Shock metamorphism of Bosumtwi impact crater rocks, shock attenuation, and uplift formation. Science 322:1678-1681.

Ferrière L., Koeberl C. and Reimold W. U. 2009a. Characterisation of ballen quartz and cristobalite in impact breccias: new observations and constraints on ballen formation. European Journal of Mineralogy 21:203-217.

Ferrière L., Koeberl C., Reimold W. U., Hecht L. and Bartosova K. 2009b. The origin of "toasted quartz" in impactites revisited. 40th Lunar and Planetary Science Conference, abstract no. 1751.

Firsov L. 1973. Concerning the meteoritic origin of the Puchezh-Katunki crater. Meteoritics 8:223-44.

Fleischer R. L., Viertl J. R. M. and Price P. B. 1969. Age of the Manicouagan and Clearwater Lake craters. Geochimica et Cosmochimica Acta 33:523-527.

Floran R. J. 1976. Manicouagan structure, Quebec: A terrestrial analog of Lunar multiring basins. Lunar and Planetary Science Conference 7:260-262.

Floran R. J. and Dence M. R. 1976. Morphology of the Manicouagan ring-structure, Quebec, and some comparisons with Lunar basins and craters. Proceedings of the Lunar and Planetary Science Conference 7:2845-2865.

Floran R. J., Simonds C. H., Grieve R A. F., Phinney W. C., Warner J. L., Rhodes M. J., Jahn B. M. and Dence M. R. 1976. Petrology, structure and origin of the Manicouagan melt sheet, Quebec, Canada: A preliminary report. Geophysical Research Letters 3:49-52.

Floran R. J., Grieve R. A. F., Dence M. R., Phinney W. C., Warner J. L., Blanchard D. P. and Simonds C. H. 1978. Manicouagan impact melt, Quebec. I - Stratigraphy, petrology, and chemistry. Journal of Geophysical Research 83:2737-2759.

Florensky P. V., Short N., Winzer S. R. and Fredriksson K. 1977. The Zhamanshin structure: Geology and petrography. Meteoritics 12:227-228.

Fraas E. 1919. Begleitworte zu der geognostischen Spezialkarte von Württemberg – Atlasblatt Bopfingen. Kohlhammer Stuttgart, Germany, 31 p. (in German).

Fredriksson K., Dube A., Milton D. J., and Balasundaram M. S. 1973. Lonar Lake, India: An impact crater in basalt. Science 180:862-864.

French B. M. 1998. Traces of Catastrophe. A handbook of shock metamorphic effects in terrestrial meteorite impact structures. LPI Contribution 954, Lunar and Planetary Institute, Houston, Texas, USA, 120 p.

French B. M. and Short N. M. 1968. Shock metamorphism of natural materials. Mono Book, Baltimore, Maryland, USA, 644 p.

French B. M., Hartung J. B., Short N. M. and Dietz R. S. 1970. Tenoumer crater, Mauritania: Age and petrologic evidence for origin by meteorite impact. Journal of Geophysical Research 75:4396-4406.

French B. M., Koeberl C., Gilmour I., Shirey S. B., Dons J. A., and Naterstad J. 1997. The Gardnos impact structure, Norway: Petrology and geochemistry of target rocks and impactites. Geochimica et Cosmochimica Acta 61:873–904.

von Frese R. R. B., Pitts L. V., Wells S. B., Leftwich T. E., Kim H. R., Kim J. W., Golynski A. V., Hernandez O. and Gaya-Piqué L. R. 2009. GRACE gravity evidence for an impact basin in Wilkes Land, Antarctica. Geochemistry, Geophysics, Geosystems 10:Q02014.

Gerhard L. C., Anderson S. B., LeFever J. A. and Carlson C. A. 1982. Geological development, origin, and energy mineral resources of Williston Basin, North Dakota. American Association of Petroleum Geologists Bulletin 66:989-1020.

Gersonde R., Deutsch A., Ivanov B. A. and Kyte F. T. 2002. Oceanic impacts—a growing field of fundamental geosciences. Deep Sea Research Part II: Topical Studies in Oceanography 49:951-957.

Ghosh A. and McSween H. Y. Jr. 1998. A thermal model for the differentiation of asteroid 4 Vesta, based on radiogenic heating. Icarus 134:187-206.

Gibson R. L., Armstrong R. A. and Reimold W. U. 1997. The age and thermal evolution of the Vredefort impact structure: A single-grain U-Pb zircon study. Geochimica et Cosmochimica Acta 61:1531-1540.

Glass B. P. 2002. Upper Eocene impact ejecta/spherule layers in marine sediments. Chemie der Erde - Geochemistry 62:173-196.

Glass B. P. and Burns C. A. 1988. Microkrystites - A new term for impact-produced glassy spherules containing primary crystallites. Proceedings of the Lunar and Planetary Science Conference 18:455-458.

Glass B. P., Hall C. M. and York D. 1986. ^{40}Ar–^{39}Ar laser-probe dating of North American tektite fragments from Barbados and the age of the Eocene-Oligocene boundary. Chemical Geology 59:181-186.

Glass B. P., Liu S. and Leavens P. B. 2002. Reidite: An impact-produced high-pressure polymorph of zircon found in marine sediments. American Mineralogist 87:562-565.

Glikson A. Y. 2001. The astronomical connection of terrestrial evolution: crustal effects of post-3.8 Ga mega-impact clusters and evidence for major 3.2 ± 0.1 Ga bombardment of the Earth–Moon system. Journal of Geodynamics 32:205-229.

Glimsdal S., Pedersen G. K., Langtangen H. P., Shuvalov V. and Dypvik H. 2007. Tsunami generation and propagation from the Mjølnir asteroid impact. Meteoritics and Planetary Science 42:1467-1698.

Göbel F., Reimold W. U., Baddenhausen H. and Palme H. 1980. The projectile of the Lappajärvi crater. Zeitschrift für Naturforschung 35A:197-203.

Goderis S., Kalleson E., Tagle R., Dypvik H., Schmitt R.-T., Erzinger J. and Claeys P. 2009. A non-magmatic iron projectile for the Gardnos impact event. Chemical Geology 258:145-156.

Gohn G. S., Koeberl C., Miller K. G., Reimold W. U., Browning J. V., Cockell C. S., Horton J. W. Jr., Kenkmann T., Kulpecz A. A., Powars D. S., Sanford W. E. and Voytek M. A. 2008. Deep drilling into the Chesapeake Bay impact structure. Science 320:1740-1745.

Golonka J. 2000. Cambrian–Neogene plate tectonic maps. Published Habilitation thesis, University of Kraców, Kraców, Poland, 125 pp.

Golonka J. 2007. Late Triassic and Early Jurassic palaeogeography of the world. Palaeogeography, Palaeoclimatology, Palaeoecology 244:297–307.

Goltrant O., Cordier P. and Doukhan J. C. 1991. Planar deformation features in shocked quartz: A transmission electron microscopy investigation. Earth and Planetary Science Letters 106:103-115.

Goto K. 2008. The genesis of oceanic impact craters and impact-generated tsunami deposits. In Shiki T., Tsuji Y., Yamazaki T. and Minoura K. (eds.) Tsunamiites – Features and implications. Elsevier, Amsterdam, The Netherlands, p. 277-298.

Gratz A. J., Fisler D. K. and Bohor B. F. 1996. Distinguishing shocked from tectonically deformed quartz by the use of the SEM and chemical etching. Earth and Planetary Science Letters 142:513-521.

Grieve R. A. F. 1975. Petrology and chemistry of the impact melt at Mistastin Lake crater, Labrador. Geological Society of America Bulletin 86:1617-1629.

Grieve R. A. F. 1978. The melt rocks at Brent crater, Ontario, Canada. Proceedings, 9th Lunar and Planetary Science Conference. pp. 2579–2608.

Grieve R. A. F. 1987. Terrestrial impact structures. Annual Reviews of Earth and Planetary Science 15:245–270.

Grieve R. A. F. 1991. Terrestrial impact: The record in the rocks. Meteoritics 26:175–194.

Grieve R. A. F. 1997. Target Earth: Evidence for large-scale impact events. Annals of the New York Academy of Sciences 822:319-352.

Grieve R. A. F. 2005. Economic natural resource deposits at terrestrial impact structures. Geological Society of London Special Publications 248:1–29.

Grieve R. A. F. 2006. Impact Structures in Canada. GEOText 5, Geological Association of Canada, St. John's, 210 p.

Grieve R. A. F. and Floran R. J. 1978. Manicouagan impact melt, Quebec. II - Chemical interrelations with basement and formational processes. Journal of Geophysical Research 83:2761-2771.

Grieve R. A. F. and Masaitis, V. L. 1994. The economic potential of terrestrial impact craters. International Geology Review 36:105-151.

Grieve R. A. F. and Pesonen L. J. 1992. Terrestrial impact craters: Their spatial and temporal distribution and impacting bodies. Earth, Moon, and Planets 71:357–76.

Grieve R. A. F. and Pilkington M. 1996. The signature of terrestrial impacts. Journal of Australian Geology and Geophysics 16:399-420.

Grieve R. A. F. and Therriault A. M. 2000. Vredefort, Sudbury, Chicxulub: Three of a kind? Annual Review of Earth and Planetary Sciences 28:305-338.

Grieve R. A. F., Robertson P. B. and Dence m. R. 1981. Constraints on the formation of ring impact structures, based on terrestrial data. Proceedings of Lunar and Planetary Science 12A:37-57.

Grieve R. A. F., Wood C. A., Garvin J. B., McLaughlin G. and McHone J. F. Jr. 1988. Astronaut's guide to terrestrial impact craters. LPI Technical Report 88-03, Lunar and Planetary Institute, Houston, Texas, USA, 89 p.

Grieve R. A. F., Langenhorst F., and Stöffler D. 1996. Shock metamorphism of quartz in nature and experiment: II. Significance in geosciences. Meteoritics and Planetary Science 31:6–35.

Grieve R. A. F., Cintala M. J. and Therriault M. A. 2006. Large-scale impacts and the evolution of the Earth's crust: The early years. Geological Society of America Special Paper 405:23-32.

Gurov E. P. and Gurova E. P. 1995. Impact melt composition of the Obolon crater: chlorine as a possible indicator of the submarine crater formation. Meteoritics 30, 515.

Gurov E. P. and Gurova E. P. 1998. The group of Macha craters in western Yakutia. Planetary and Space Science 46:323-328.

Gurov E. P., Valter A. A., Gurova E. P. and Serebrennikov A. I. 1978. Explosion meteorite crater El'gygytgyn in Chukotka. Akademiia Nauk SSSR, Doklady 240:1407-1410 (in Russian).

Gurov E. P., Gurova E. P., Rakitskaya R. B. and Yamnichenko A. Y. 1993. The Karakul depression in Pamirs: The first impact structure in Central Asia. Lunar and Planetary Science Conference 24:591-592.

Gurov E. P., Koeberl C., and Reimold W. U. 1998. Petrography and geochemistry of target rocks and impactites from the Ilyinets Crater, Ukraine. Meteoritics and Planetary Science 33:1317–1333.

Gurov E P., Koeberl C. and Yamnichenko A. 2007. El'gygytgyn impact crater, Russia: Structure, tectonics, and morphology. Meteoritics and Planetary Science 42:307-319.

Gurov E. P., Gurova E. P., Chernenko Y. and Yamnichenko A. 2009. The Obolon impact structure, Ukraine, and its ejecta deposits. Meteoritics and Planetary Science 44:389-404.

Haines P. W. 2005. Impact cratering and distal ejecta: the Australian record. Australian Journal of Earth Sciences 52: 481-507.

Hallam A., 1990. The end-Triassic mass extinction event. Geological Society of America Special Paper 247:577-583.

Hallam A. 2002. How catastrophic was the end-Triassic mass extinction? Lethaia 35:147-157.

Hallam A. and Wignall P. 1997. Mass extinctions and their aftermath. Oxford University Press, New York, 328 p.

Hammerschmidt K. and Engelhardt W. von 1995. $^{40}Ar/^{39}Ar$ dating of the Araguainha impact structure, Mato Grosso, Brazil. Meteoritics 30:227-233.

Hartmann W. K., Ryder G., Dones L. and Grinspoon D. 2000. The time-dependent intense bombardment of the primordial Earth/Moon system. In Canup R. M. and Righter K. (eds.) Origin of the Earth and the Moon, University of Arizona Press, Tucson, Arizona, USA, p. 805-826.

Hartung J. and Koeberl C. 1994. In search of the Australasian tektite source crater: The Tonle Sap hypothesis. Meteoritics 29:411-416.

Hassler S. W., Robey H. F. and Simonson B. M. 2000. Bedforms produced by impact-generated tsunami, ~2.6 Ga Hamersley basin, Western Australia. Sedimentary Geology 135:283–294.

Hecht L., Wittmann A., Schmitt R. T., and Stöffler D. 2004. Composition of impact melt particles and the effects of post-impact alteration in suevitic rocks at the Yaxcopoil-1 drill core, Chicxulub crater, Mexico. Meteoritics and Planetary Science 39:1169-1186.

Heizmann E. P. J. and Reiff W. 2002. Der Steinheimer Meteorkrater. Pfeil, Munich, Germany, 160 p. (in German).

Henkel H. and Aaro S. 2005. Geophysical Investigations of the Siljan Impact Structure - A Short Review. In Koeberl C. and Henkel H. (eds.) Impact Tectonics, Springer, Berlin, Heidelberg, p. 247-283.

Henkel H. and Pesonen L. J. 1992. Impact craters and craterform structures in Fennoscandia. Tectonophysics 216:31–40.

Herd C. D. K., Froese D. G., Walton E. L., Kofman R. S., Herd E. P K. and Duke M. J. M. 2008. Anatomy of a young impact event in central Alberta, Canada: Prospects for the missing Holocene impact record. Geology 36:955-958.

Hess J. C. and Lippolt H. J. 1986. Kinetics of isotopes during neutron irradiation: ^{39}Ar loss from minerals as a source of error in $^{40}Ar/^{39}Ar$ dating. Chemical Geology 59:223-236.

Hesselbo S. P., Robinson S. A., Surlyk F. and Piasecki S. 2002. Terrestrial and marine extinction at the Triassic-Jurassic boundary synchronized with major carbon-cycle perturbation: A link to initiation of massive volcanism? Geology 30:251-254.

Hesselbo S. P., McRoberts C. A. and Pálfy J. 2007. Triassic–Jurassic boundary events: Problems, progress, possibilities. Palaeogeography, Palaeoclimatology, Palaeoecology 244:1–10.

Hildebrand A. R. 1993. The Cretaceous/Tertiary Boundary impact - the Dinosaurs didn't have a chance. Journal of the Royal Astronomical Society of Canada 87:77-118.

Hildebrand A. R., Penfield G. T., Kring D. A., Pilkington M., Camargo Z. A., Jacobsen S. B. and Boynton W. V. 1991. Chicxulub Crater: A possible Cretaceous/Tertiary boundary impact crater on the Yucatán Peninsula, Mexico. Geology 19:867-871.

Hippertt J. and Lana C. 1998. Aerial crystallization of hematite in impact bombs from the Araguainha astrobleme, Mato Grosso, Central Brazil. Meteoritics and Planetary Science 33:1303-1309.

Hodych J. P. and Dunning G. R. 1992. Did the Manicouagan impact trigger end-of-Triassic mass extinction? Geology 20:51-54.

Hofmann A., Reimold W. U. and Koeberl C. 2006. Archean spherule layers in the Barberton Greenstone belt, South Africa: A discussion of problems related to the impact interpretation. Geological Society of America Special Paper 405:33-56.

Holsapple K. A. 1993. The scaling of impact processes in planetary sciences. Annual Review of Earth and Planetary Sciences 21:333-373.

Horn W. and El Goresy A. 1979. Fe-Cr-Ni-metals in rocks from the floor of the Rochechouart crater: Material of the impacting body? Meteoritics 14:424.

Horneck G., Stöffler D., Ott S., Hornemann U., Cockell C. S., Moeller R., Meyer C., de Vera J.-P., Fritz J. , Schade S. and Artemieva N. A. 2008. Microbial rock inhabitants survive hypervelocity impacts on Mars-like host planets: First phase of lithopanspermia experimentally tested. Astrobiology 8:17-44.

Hörz F. 1965. Untersuchungen an Riesgläsern. Beiträge zur Mineralogie und Petrographie 11:621-661 (in German).

Hüttner R. and Schmidt-Kaler H. 1999. Meteoritenkrater Nördlinger Ries. Pfeil, Munich, Germany. 144 p. (in German).

Ivanov B. A. 1994. Geomechanical models of impact cratering: Puchezh-Katunki structure. Geological Society of America Special Paper 293:81-91.

Ivanov B. 2008. Geologic effects of large terrestrial impact crater formation. In Adushkin V. and Nemchinov I. (eds.) Catastrophic events caused by cosmic objects, Springer, Berlin, Heidelberg, p. 163-205.

Izett G. A. and Obradovich J. D. 1992. Laser-fusion ^{40}Ar/^{39}Ar ages of Australasian tektites. Lunar and Planetary Science Conference 23:593-594.

Izett G. A., Cobban W. A., Obradovich J. D. and Dalrymple G. B. 1998. ^{40}Ar/^{39}Ar age of the Manson impact structure, Iowa, and correlative impact ejecta in the Crow Creek Member of the Pierre Shale (Upper Cretaceous), South Dakota and Nebraska. Geological Society of America Bulletin 110:361-376.

Jahn B., Floran R. J. and Simonds C. H. 1978. Rb-Sr isochron age of the Manicouagan melt sheet, Quebec, Canada. Journal of Geophysical Research 83:2799-2803.

Jansa L. F. 1993. Cometary impacts into ocean: their recognition and the threshold constraint for biological extinctions. Palaeogeography, Palaeoclimatology, Palaeoecology 104:271-286.

Janssens M.-J., Hertogen J., Talahashi H., Anders E. and Lambert P. 1977. Rochechouart meteorite crater - Identification of projectile. Journal of Geophysical Research 82:750-758.

Jones A. P., Claeys P. and Heuschkel S. 2000. Impact melting of carbonates from the Chicxulub crater. In Gilmour I. and Koeberl C. (eds.) Impacts and the Early Earth, Springer, Berlin, Heidelberg, p. 343-361.

Jourdan F. and Renne P. R. 2007. Age calibration of the Fish Canyon sanidine ^{40}Ar/^{39}Ar dating standard using primary K–Ar standards. Geochimica et Cosmochimica Acta 71:387-402.

Jourdan F., Matzel J. P. and Renne P. R. 2007a. Direct measurement of ^{39}Ar (and ^{37}Ar) recoil ejection during neutron irradiation of sanidine and plagioclase crystals. Geochimica et Cosmochimica Acta 71:2791-2808.

Jourdan F., Renne P. R. and Reimold W. U. 2007b. The problem of inherited ^{40}Ar* in dating impact glass by ^{40}Ar/^{39}Ar geochronology: Evidence from the Tswaing crater (South Africa). Geochimica et Cosmochimica Acta 71:1214-1231.

Jourdan F., Renne P. R. and Reimold W. U. 2008. High-precision ^{40}Ar/^{39}Ar age of the Jänisjärvi impact structure (Russia). Earth and Planetary Science Letters 265:438-449.

Jourdan F., Marzoli A., Bertrand H., Cirilli S., Tanner L. H., Kontak D. J., McHone G., Renne P. R. and Bellini G. 2009a. ^{40}Ar/^{39}Ar ages of CAMP in North America: Implications for the Triassic–Jurassic boundary and the ^{40}K decay constant bias. Lithos 110:167-180.

Jourdan F., Renne P. and Reimold W. U. 2009b. An appraisal of the ages of terrestrial impact structures. Earth and Planetary Science Letters 286:1-13.

Kalleson E., Corfu F. and Dypvik H. 2009. U–Pb systematics of zircon and titanite from the Gardnos impact structure, Norway: Evidence for impact at 546 Ma? Geochimica et Cosmochimica Acta 73:3077-3092.

Kamo S. L., Reimold W. U., Krogh T. E. and Collistion W. P. 1996. A 2.023 Ga age for the Vredefort impact event and a first report of shock metamorphosed zircons in pseudotachylitic breccias and Granophyre. Earth and Planetary Science Letters 144:369-387.

Keller G., Adatte T., Stinnesbeck W., Rebolledo-Vieyra M., Urrutia Fucugauchi J., Kramar U. and Stüben D. 2004. Chicxulub impact predates the K-T boundary mass extinction. Proceedings of the National Academy of Sciences 101:3753-3758.

Kelley S. P. 2002a. Excess argon in K-Ar and Ar-Ar geochronology. Chemical Geology 188:1-22.

Kelley S. P. 2002b. K-Ar and Ar-Ar dating. Reviews in Mineralogy and Geochemistry 47:785-818.

Kelley S. P. 2007. The geochronology of large igneous provinces, terrestrial impact craters, and their relationship to mass extinctions on Earth. Journal of the Geological Society 164:923-936.

Kelley S. P. and Spray J. G. 1997. A late Triassic age for the Rochechouart impact structure, France. Meteoritics and Planetary Science 32:629-636.

Kenkmann T. and Poelchau M. H. 2009. Low-angle collision with Earth: The elliptical impact crater Matt Wilson, Northern Territory, Australia. Geology 37:459-462.

Kenkmann T., Jahn A., Scherler D. and Ivanov B. A. 2005. Structure and formation of a central uplift: A case study at the Upheaval Dome impact crater, Utah. Geological Society of America Special Paper 384:85-115.

Kenkmann T., Artemieva N. A. and Poelchau M. H. 2008a. The Carancas event on September 15, 2007: Meteorite fall, impact conditions, and crater characteristics. Lunar and Planetary Institute Contribution 1391:1094-1095.

Kenkmann T., Artemieva N. A., Wünnemann K., Poelchau H., Elbeshausen D. and Núñez del Prado H. 2008b. The remarkable meteorite impact event on September 15, 2007, Carancas, Peru: What did we learn? Large Meteorite Impacts and Planetary Evolution IV, abstract no. 3063.

Kent D. V. 1998. Impacts on Earth in the Late Triassic. Nature 395:126.

Kieffer S. W. 1971. Shock metamorphism of the Coconino Sandstone at Meteor Crater, Arizona. Journal of Geophysical Research 76:5449–5473.

Kieffer S. W., Schaal R., Gibbons R., Hörz F., Milton D. and Duba A. 1976. Shocked basalt from Lonar impact crater, India, and experimental analogues. Proceedings of the Lunar Science Conference 7:1391–1412.

King Jr. D. T., Neathery T. L., Petruny L. W., Koeberl C. and Hames W. E. 2002. Shallow-marine impact origin of the Wetumpka structure (Alabama, USA). Earth and Planetary Science Letters 202:541–549.

Kirkham A. 2003. Glauconitic spherules from the Triassic of the Bristol area, SW England: probable microtektite pseudomorphs. Proceedings of the Geological Association 114:11–21.

Koeberl C. 1986. Geochemistry of tektites and impact glasses. Annual Review of Earth and Planetary Sciences 14:323-350.

Koeberl C. 1994. Tektite origin by hypervelocity asteroidal or cometary impact: Target rocks, source craters, and mechanisms. Geological Society of America Special Paper 293:133-151.

Koeberl C. 1998. Identification of meteoritic components in impactites. Special Publications of the Geological Society London 140:133–153.

Koeberl C. 1999. Craters on the Moon from Galileo to Wegener: A short history of the impact hypothesis, and implications for the study of terrestrial impact craters. Earth, Moon, and Planets 85-86:209-224.

Koeberl C. 2004. Remote sensing studies of impact craters: how to be sure? Comptes Rendus Geoscience 336:959-961.

Koeberl C. 2006a. The record of impact processes on the early Earth: A review of the first 2.5 billion years. Geological Society of America Special Paper 405:1-22.

Koeberl C. 2006b. Impact processes on the early Earth. Elements 2:211-216.

Koeberl C. 2007. Impakt und Massensterben – Ein Überblick über den aktuellen Forschungsstand. Jahrbuch der Geologischen Bundesanstalt 147, Vienna, Austria, p. 169-191 (in German).

Koeberl C. 2009. Late Eocene impact craters and impactoclastic layers – An overview. Geological Society of America Special Paper 452:17-26.

Koeberl C. and Reimold W. U. 1995a. Shock metamorphism at the Red Wing Creek structure, North Dakota: Confirmation of impact origin. Lunar and Planetary Science 26:769-770.

Koeberl C. and Reimold W. U. 1995b. The Newporte impact structure, North Dakota, USA. Geochimica et Cosmochimica Acta 59:4747-4767.

Koeberl C. and MacLeod K. G. 2002 (eds.). Catastrophic events and mass extinctions: impacts and beyond. Geological Society of America Special Paper 356, Boulder, Colorado, 746 pp.

Koeberl C., Reimold W. U. and Brandt D. 1996a. Red Wing Creek structure, North Dakota: Petrographical and geochemical studies, and confirmation of impact origin. Meteoritics and Planetary Science 31:335–342.

Koeberl C., Reimold W. U., and Gurov E. 1996b. Petrology and geochemistry of target rocks, breccias, and impact melt rocks from the Ilyinets crater, Ukraine. Lunar and Planetary Science 27:681–682.

Koeberl C., Armstrong R. A. and Reimold W. U. 1997a. Morokweng, South Africa: A large impact structure of Jurassic-Cretaceous boundary age. Geology 25:731-734.

Koeberl C., Bottomley R. D., Glass B. P. and Storzer D. 1997b. Geochemistry and age of Ivory Coast tektites and microtektites. Geochimica et Cosmochimica Acta 61:1745-1772.

Koeberl C., Masaitis V. L., Shafranovsky G. I., Gilmour I., Langenhorst F. and Schrauder M. 1997c. Diamonds from the Popigai impact structure, Russia. Geology 25:967-970.

Koeberl C., Reimold W. U., Blum J. D. and Chamberlain C. P. 1998. Petrology and geochemistry of target rocks from the Bosumtwi impact structure, Ghana, and comparison with Ivory Coast tektites. Geochimica et Cosmochimica Acta 62:2179–2196.

Koeberl C., Farley K. A.., Peucker-Ehrenbrinck B. and Sephton M. A. 2004. Geochemistry of the end-Permian extinction event in Austria and Italy: no evidence for an extraterrestrial component. Geology 32:1053-1056.

Koeberl C., Reimold W. U. and Plescia J. 2005. BP and Oasis impact structures, Libya: Remote sensing and field studies. In Koeberl C. and Henkel H. (eds.) Impact Tectonics, Springer, Berlin, Heidelberg, p. 161-190.

Koeberl C., Brigham-Grette J., Melles M. and Minyuk P. 2009. Drilling into the El'gygytgyn Impact Crater, Arctic Russia: The 2009 ICDP Project. Meteoritics and Planetary Science 44:5014 (supplement).

Kohn B. P., Osadeta K. G. and Bezys R. K. 1995. Apatite fission-tracking dating of two crater structures in the Canadian Williston Basin. Bulletin of Canadian Petroleum Geology 43:54-64.

Korochantseva E. V., Trieloff M., Lorenz C. A., Buykin A. I., Ivanova M. A., Schwarz W. H., Hopp J. and Jessberger E. K. 2007. L-chondrite asteroid breakup tied to Ordovician meteorite shower by multiple isochron ^{40}Ar-^{39}Ar dating. Meteoritics and Planetary Science 42:113-130.

Korsman K., Koistinen T., Kohonen J., Wennerström M., Ekdahl E., Honkamo M., Idman H., and Pekkala Y., eds. 1997. Suomen kallioperäkartta—Berggrundskarta över Finland - Bedrock map of Finland 1:1 000 000, Geological Survey of Finland, Espoo.

Kraus E. and Meyer R. 1928. Untersuchungen über den Krater von Sall auf Ösel. Kurlands Beiträge zur Geophysik 20:312-378 (in German).

Kraut F. 1969. A new impact occurrence in the area of Rochechouart-Chassenon (Haute Vienne et Charente, France). Geologica Bavarica 61:428-450.

Kraut F. and French B. M. 1971. The Rochechouart meteorite impact structure, France: Preliminary geological results. Journal of Geophysical Research 76:5407.

Kring D. A. 2007. Guidebook to the geology of Barringer meteorite crater, Arizona (aka Meteor Crater), Lunar and Planetary Institute Contribution no. 1355, Houston, Texas, USA, 150 p.

Kring D. A. and Cohen B. A. 2002. Cataclysmic bombardment throughout the inner solar system 3.6-4.0 Ga. Journal of Geophysical Research 107, E2:4 to 1-4-6.

Kring D. A., Melosh H. J. and Hunten D. M. 1996. Impact-induced perturbations of atmospheric sulfur. Earth Planetary Science Letters 140:201–212.

Krogh T. E., Davis D. W. and Corfu F. 1984. Precise U-Pb zircon and baddeleyite ages for the Sudbury area. In Pye E. G., Naldrett A. J. and Gilbin P. E. (eds.) The geology and ore deposits of the Sudbury structure. Ontario Geological Survey, Sudbury, Special Volume 1, p. 431-446.

Kroll H., Schmiemann I. and von Coelln G. 1986. Feldspar solid solutions. American Mineralogist 71:1-16.

Krymholts G. Y. 1972. Stratigraphy of the USSR – Vol. 10: The Jurassic System. Gosgeoltechizdat, Moscow, 524 p. (in Russian).

Kuiper Y. D. 2002. The interpretation of inverse isochron diagrams in ^{40}Ar/^{39}Ar geochronology. Earth and Planetary Science Letters 203:499-506.

Kuivasaari T., Pesonen L. J., Elo S., Plado J., and Lehtinen M. 2000. Paasselkä - The ninth meteorite impact structure in Finland. 4th European Science Foundation Workshop, Programme and Abstracts, 79.

Kulik L. 1927. On the fall of the podkamennaya tunguska meteorite in 1908. Journal of the Russian Academy of Science 1927A:399-402 (originally written in Russian).

Lambert P. 1974. La structure d'impact de météorite géante de Rochechouart. Doctoral thesis, Université Paris-Sud, 148 p. (in French).

Lambert P. 1975. Nickel enrichment of impact melt rocks from Rochechouart. Preliminary results and possibility of meteoritic contamination. Meteoritics 10:433-434.

Lambert P. 1977. The Rochechouart crater - Shock zoning study. Earth and Planetary Science Letters 35:258-268.

Lambert P., 1981a. Breccia dikes: geological constraints on the formation of complex craters. In Schultz P. H. and Merril R. B. (eds.) Multi-ring basins: formation and evolution. Pergamon, New York, p. 59-78.

Lambert P. 1981b. Rochechouart: Geochemistry. Lunar and Planetary Institute Contribution 449:26.

Lambert P. 2008. Impact deposits at Rochechouart-Chassenon. Large Meteorite Impacts and Planetary Evolution IV, abstract no. 3034.

Lambert P. 2009. Target and impact deposits at Rochechouart impact structure, France. Paper submitted to Geological Society of America Special Paper 'Large Meteorite Impact Conference IV' (in press).

Lana C. and Marangoni Y. 2009. The Araguainha impact: a South American Permo–Triassic catastrophic event. Geology Today 25:21-28.

Lana C., Tohver E., Siret D., Cawood P., Sherlock S., Marangoni Y. R., Trindade R. I. and Souza R. 2007. The Araguainha impact crater at the Permo-Triassic boundary: implications for the carbon isotope excursion and the mass extinction. American Geophysical Union Fall Meeting, EOS transactions 88, abstract no. U24 C-03.

Lana C., Souza Filho C. R., Marangoni Y. R., Yokoyama E., Trindade R. I. F., Tohver E. and Reimold W. U. 2008. Structural evolution of the 40 km wide Araguainha impact structure, central Brazil. Meteoritics and Planetary Science 43:701-716.

Lang B., Edelstein O., Steinitz G., Kovacs M. and Halga S. 1994. Ar-Ar dating of adularia; a tool in understanding genetic relations between volcanism and mineralization; Baia Mare area (Gutii Mountains), northwestern Romania. Economic Geology 89:174-180.

Lange J.-M. 1996. Tektite glasses from Lusatia (Lausitz), Germany. Chemie der Erde 56:498–510.

Langenhorst F. 2002. Shock metamorphism of some minerals: Basic introduction and microstructural observations. Bulletin of the Czech Geological Survey 77:265–282.

Langenhorst F., Kyte F. T. and Retallack G. J. 2005. Reexamination of quartz grains from the Permian-Triassic boundary section at Graphite Peak, Antarctica. 36th Lunar and Planetary Science Conference, abstract no. 2358.

Lanphere M. A. and Dalrymple G. B. 1976. Identification of excess ^{40}Ar by the ^{40}Ar/^{39}Ar age spectrum technique. Earth and Planetary Science Letters 32:141-148.

Larsson S. A. and Tullborg E.-L. 1993. Tectonic regimes in the Baltic Shield during the last 1200 Ma - A review. Svensk Kärnbränslehantering AB Technical Report 94-05, Stockholm, Sweden, 78 p.

Lavikainen S. 1986. Rääkkylän kartta-alueen kallioperä—Summary: Pre-Quarternary rocks of the Rääkkylä map-sheet area. Explanation to the geological map of Finland 1:100 000, sheet 4214, Geological Survey of Finland, Espoo, 50 p. (partly in Finnish).

Layer P. W. 2000. Argon-40/argon-39 age of the El'gygytgyn impact event, Chukotka, Russia. Meteoritics and Planetary Science 35:591-600.

Lee M.-Y. and Wei K.-Y. 2000. Australasian microtektites in the South China Sea and the West Philippine Sea: Implications for age, size and location of the impact crater. Meteoritics and Planetary Science 35:1151-1155.

Le Pichon A., Aniter K., Cansi Y., Hernandez B., Minaya E., Burgoa B., Drob D., Evers L. G. and Vaubaillon J. 2008. Evidence for a meteoritic origin of the September 15, 2007, Carancas crater. Meteoritics and Planetary Science 43:1797-1809.

Leroux H., Reimold W. U., Koeberl C., Hornemann U. and Doukhan J.-C. 1999. Experimental shock deformation in zircon: a transmission electron microscopic study. Earth and Planetary Science Letters 169:291-301.

Levy D. H. 1998. The collision of comet Shoemaker-Levy 9 with Jupiter. Space Science Reviews 85:523-545.

Lidmar-Bergström K. 1991. Phanerozoic tectonics in southern Sweden. Zeitschrift für Geomorphologie Neue Folge 82:1-16.

Lieger D., Riller U. and Gibson R. L. 2009. Generation of fragment-rich pseudotachylite bodies during central uplift formation in the Vredefort impact structure, South Africa. Earth and Planetary Science Letters 279:53-64.

Lintnerová O., Michalík J. K., Soták J. and Gaździcki A. 2004. Paleobiological and chemical record of environmental events in the Triassic/Jurassic boundary beds, Fatric Basin, western Carpathians. Proceedings of the IGCP 458 5th Field Workshop, abstract no. 253-7.

Lofgren G. 1971. Spherulitic textures in glassy and crystalline rocks. Journal of Geophysical Research 76:5635–5648.

Longo G. 2007. The Tunguska Event. In Bobrowsky P. and Rickman H. (eds.) Comet/asteroid impacts and human society, Springer, Berlin, Heidelberg, p. 303-330.

Lowe D. R., Byerly G. R., Kyte F. T., Shukolyukov A., Asaro F. and Krull A. 2003. Spherule beds 3.47–3.24 billion years old in the Barberton Greenstone Belt, South Africa: A record of large meteorite impacts and their influence on early crustal and biological evolution. Astrobiology 3:7-48.

Machado R., Lana C., Stevens G., Souza Filho C. R., Reimold W. U. and McDonald I. 2009. Generation, mobilization and crystallization of impact-induced alkali-rich melts in granitic target rocks: Evidence from the Araguainha impact structure, central Brazil. Geochimica et Cosmochimica Acta 73:7183-7201.

Mader D. 1992. Evolution of palaeoecology and palaeoenvironment of Permian and Triassic fluvial basins in Europe. Gustav Fischer Verlag, Stuttgart, New York, 738 p.

Mak E. K., York D., Grieve R. A. F. and Dence M. R. 1976. The age of the Mistastin Lake crater, Labrador, Canada. Earth and Planetary Science Letters 31:345-357.

Mänttäri I. and Koivisto M. 2001. Ion microprobe uranium-lead dating of zircons from the Lappajärvi impact crater, western Finland. Meteoritics and Planetary Science 36:1087-1095.

Mänttäri I., Kohonen J., Kujala H. and Pihlaja P. 2004. A revised age for the Sääksjärvi meteorite impact, south-western Finland: The connexion with a Caledonian foreland basin. 32nd International Geological Congress (August 20-28, 2004, Florence, Italy), abstract no. 1434.

Marcus R. A., Melosh H. J. and Collins G. S. 2004. Earth Impact Effects Program. Available online at http://www.lpl.arizona.edu/impacteffects (accessed June 23, 2009).

Martinez I., Schärer U. and Deutsch A. 1991. Determination of shock-wave peak pressure and Rb-Sr isotope systematics in a granite from the Araguainha impact crater (Brasil). Lunar and Planetary Science Conference 22:857-858.

Marzoli A., Bertrand H., Knight K. B., Cirilli S., Nomade S., Renne P. R., Verati C., Youbi N., Martini R. and Bellini G. 2008. Comment on "Synchrony between the Central Atlantic magmatic province and the Triassic–Jurassic mass-extinction event? By Whiteside et al. (2007)". Palaeogeography, Palaeoclimatology, Palaeoecology 262:189–193.

Masaitis V. L. 1999. Impact structures of northeastern Eurasia: the territories of Russia and adjacent countries. Meteoritics and Planetary Science 34, 691–711.

Masaitis V. L. and Mashchak M. S. 1990. Puchezh-Katunki astrobleme: Structure of central uplift and transformation of composing rocks. Meteoritics 25:383.

Masaitis V. L. and Pevzner L. A. 1999. Deep Drilling in the Puchezh-Katunki Impact Structure (in Russian). VSEGEI Press, Saint-Petersburg, Russia, 392 p.

Masaitis V. L., Danilin A. N., Mashchak M. S., Raikhlin A. I., Selivanovskaya T. V. and Shadenkov Y. M. 1980. The geology of astroblemes. Nedra Press, Leningrad, Russia, 232 p (in Russian).

Masaitis V. L., Mashchak M. S. and Naumov M. V. 1996. The Puchezh-Katunki astrobleme: a structural model of a giant impact crater. Astronomicheskii vestnik 30:5-13.

Matsubara K., Matsuda J.-I. and Koeberl C. 1991. Noble gases and K-Ar ages in Aouelloul, Zhamanshin, and Libyan Desert impact glasses. Geochimica et Cosmochimica Acta 55:2951-2955.

Mattmüller C. R. 1994. Ries und Steinheimer Becken. Enke, Stuttgart, Germany, 152 p. (in German).

McCabe H. R. and Bannatyne B. B. (1970) Lake St. Martin crypto-explosion crater and geology of the surrounding area. Manitoba Department of Mines and Natural Resources, Mines Branch, Geological Paper 3/70, 69 p.

McCord T. B., Adams J. B. and Johnson T. V. 1970. Asteroid Vesta. Spectral reflectivity and compositional implications. Science 168:1445-1447.

McDougall I. and Harrison T. M. 1999. Geochronology and Thermochronology by the ^{40}Ar/^{39}Ar Method. Oxford University Press, UK, 248 p.

McIntosh W. C., Sutter J. F., Chapin C. E. and Kedzie L. L. 1990. High-precision ^{40}Ar/^{39}Ar sanidine geochronology of ignimbrites in the Mogollon-Datil volcanic field, southwestern New Mexico. Bulletin of Volcanology 52:584-601.

McSween H. Y., Ghosh A., Grimm E. Wilson L. and Young E. D. 2003. Thermal Evolution Models of Asteroids. In Bottke W. F. Jr., Paolicchi P., Binzel R. P. and Cellino A. (eds.) Asteroids III. University of Arizona Press, Tucson, USA, p. 559-572.

Melosh H. J. 1980. Cratering mechanics – observational, experimental, and theoretical. Annual Review of Earth and Planetary Science 8:65-93.

Melosh H. J. 1996. Impact cratering – A geologic process. Oxford University Press, New York, 245 pp.

Melosh H. J. 1998. Craters unchained. Nature 394:222-223.

Melosh H. J. 2005. The mechanics of pseudotachylite formation in impact events. In Koeberl C. and Henkel H. (eds.) Impact Tectonics, Springer, Berlin, Heidelberg, p. 55-80.

Melosh H. J. and Stansberry J. 1991. Doublet craters and the tidal disruption of binary asteroids. Icarus 94:171-179.

Melosh H. J. and Schenk P. M. 1993. Split comets and the origin of crater chains on Ganymede and Callisto. Nature 365:731-733.

Melosh H. J. and Whitaker E. A. 1994. Lunar crater chains. Nature 369:713-714.

Melosh H. J. and Ivanov B. A. 1999. Impact crater collapse. Annual Review of Earth and Planetary Science 27:385-415.

Melosh H. J., Ingram J. and Bottke W. F. 1996. The abundance of doublet craters on Mars. Lunar and Planetary Science 27:863-864.

Merrihue C. and Turner G. 1966. Potassium-Argon dating by activation with fast neutrons. Journal of Geophysical Research 71:2852-2857.

Mertz D. F., Karpenko M. I., Ivanenko V. V. and Lippolt H. J. 1991. Evidence for jurassic tectonism in the Schwarzwald basement (SW Germany) by laser probe $^{40}Ar/^{39}Ar$ dating of authigenic K-feldspar. Naturwissenschaften 78:411-413.

Michalík J., Lintnerová O., Gaździcki A. and Soták J. 2007. Record of environmental changes in the Triassic–Jurassic boundary interval in the Zliechov Basin, Western Carpathians. Palaeogeography, Palaeoclimatology, Palaeoecology 244:71–88.

Miller S. and Tennyson J. 1995. The Jupiter-comet crash of 1994: Could it happen to the Earth? Royal Astronomical Society Quarterly Journal 36:321-335.

Milton D. J. and Sutter J. F. 1987. Revised age for the Gosses Bluff impact structure, Northern Territory, Australia, based on Ar-40/Ar-39 dating. Meteoritics 22:281-289.

Milton D. J. and Macdonald F. A. 2005. Goat Paddock, Western Australia: an impact crater near the simple – complex transition. Australian Journal of Earth Science 52:689-697.

Min K., Mundil R., Renne P. R. and Ludwig K. R. 2000. A test for systematic errors in $^{40}Ar/^{39}Ar$ geochronology through comparison with U/Pb analysis of 1.1-Ga rhyolite. Geochemica et Cosmochimica Acta 64:73-98.

Min K. Farley K. A., Renne P. R. and Marti K. 2003. Single grain (U–Th)/He ages from phosphates in Acapulco meteorite and implications for thermal history. Earth and Planetary Science Letters 209:323-336.

Mittlefehldt D. W., McCoy T. J., Goodrich C. A. and Kracher A. 1998. Non-chondritic meteorites from asteroidal bodies. Reviews in Mineralogy, Planetary Materials 36:4-1 to 4–195.

Miura Y., Gucsik A. and Thery J. 1998. Araguainha Dome crater at P/Tr boundary. Proceedings of the International Geological Correlation Programme P-384 Annual Meeting (Budapest, Hungary), p. 71-72.

Monastersky R. 1998. Geologists link a chain of craters. Science News 153:312-314.

Montanari A. and Koeberl C. 2000. Impact stratigraphy. The Italian record. Springer, Berlin, Heidelberg, New York, London, Paris, Tokyo, Hong Kong, 364 p.

Morbidelli A., Petit J.-M., Gladman B. and Chambers J. 2001. A plausible cause of the late heavy bombardment. Meteoritics and Planetary Science 36:371-380.

Mossman D. J., Grantham R. G. and Langenhorst F. 1998. A search for shocked quartz at the Triassic-Jurassic boundary in the Fundy and Newark basins of the Newark Supergroup. Canadian Journal of Earth Sciences 35:101-109.

Müller N., Hartung J. B., Jessberger E. K. and Reimold W. U. 1990. [40]Ar-[39]Ar ages of Dellen, Jänisjärvi, and Sääksjärvi impact craters. Meteoritics 25:1-10.

Mundil R., Renne P. R., Min K. K. and Ludwig K. R. 2006. Resolvable miscalibration of the [40]Ar/[39]Ar geochronometer. American Geophysical Union Fall Meeting, abstract no. V21A-0543.

Murtaugh J. G. 1972. Shock metamorphism in the Manicouagan cryptoexplosion structure, Quebec. Proceedings of the International Geological Congress 24:133-139.

Murtaugh J. C. 1976. Manicouagan impact structure. Quebec. Department of Natural Resources, Open-File Report DPV-432, 180 p.

Naumov M. V. 2005. Principal features of impact-generated hydrothermal circulation systems: Mineralogical and geochemical evidence. Geofluids 5:165–184.

Neukum G., Ivanov B. A. and Hartmann W. K. 2001. Cratering records in the inner solar system in relation to the lunar reference system. Space Science Reviews 96:55–86.

Newsom H. E. 1980. Hydrothermal alteration of impact melt sheets with implications for Mars. Icarus 44:207–216.

Nykänen O. 1975. Kerimäen ja Kiteen kartta-alueen kallioperä. Suomen geologinen kartta 1:100 000, kallioperäkartan selitykset, lehdet 4213 ja 4231—Summary: Precambrian rocks of the Kerimäki and Kitee map-sheet areas, Geological Survey of Finland, Espoo, 46 p. (partly in Finnish).

Ocampo A. C. and Pope K. O. 1996. Shuttle Imaging Radar (SIR-C) Images reveal multiple impact craters at Aorounga, northern Chad. Lunar and Planetary Science 27:977-978.

Ogg J., Ogg G. and Gradstein F. M. 2008. The concise geologic time scale. Cambridge University Press, UK, 184 p.

Öhman T., Badjukov D. D., Raitala J., Petrova T. L., and Stehlik H. 2003. Impactites of the Paasselkä and Suvasvesi South craters, Finland. 34th Lunar and Planetary Science Conference, abstract no. 1571.

O'Keefe J. D. and Ahrens T. J. 1975. Shock effects from a large impact on the Moon. Proceedings of the Lunar and Planetary Science Conference 6:2831-2844.

O'Keefe J. D. and Ahrens T. J. 1977. Impact-induced energy partitioning, melting, and vaporization on terrestrial planets. Proceedings of the Lunar and Planetary Science Conference 8:3357-3374.

O'Keefe J. D. and Ahrens T. J. 1982. The interaction of the Cretaceous-Tertiary extinction bolide with the atmosphere, ocean, and solid Earth. Geological Society of America Special Paper 190:103-120.

Okubo C. H. and Schultz R. A. 2007. Compactional deformation bands in Wingate Sandstone; additional evidence of an impact origin for Upheaval Dome, Utah. Earth and Planetary Science Letters 256:169-181.

Olsen P. E., Shubin N. H. and Anders M. H. 1987. New Early Jurassic tetrapod assemblage constrain Triassic-Jurassic tetrapod extinction event. Science 237:1025-1029.

Olsen P. E., Kent D. V., Sues H.-D., Koeberl C., Huber H., Montanari A., Rainforth E. C., Fowell S. J., Szajna M. J. and Hartline B. W. 2002. Ascent of Dinosaurs linked to an iridium anomaly at the Triassic-Jurassic boundary. Science 296:1305-1307.

Oort J. H. 1950. The structure of the cloud of comets surrounding the Solar System and a hypothesis concerning its origin. Bulletin of the Astronomical Institutes of the Netherlands 11:91-110.

Ormö J. and Lindström M. 2000. When a cosmic impact strikes the sea bed. Geological Magazine 137:67–80.

Orphal D. L. and Schulz P. H. 1978. Manicouagan, a terrestrial analog of Lunar floor-fractured craters? Meteoritics 13:591-592.

Orton, G., A'Hearn M., Baines K., Deming D., Dowling T., Goguen J., Griffith C., Hammel H., Hoffmann W., Hunten D., Jewitt D., Kostiuk T., Miller S., Noll K., Zahnle K., Achilleos N., Dayal A., Deutsch L., Espenak F., Esterle P., Friedson J., Fast K., Harrington J., Hora J., Joseph R., Kelly D., Lacy J., Lisse C., Rayner J., Sprague A., Shure M., Griep D., Kaminski C., Arden C., Chaikin A., Goldstein J., Gilmore D., Fazio G., Kanamori T., Lam H., Livengood T., MacLow M., Marley M., Momary T., Robertson D., Romani P., Sykes M., Tennyson J., Wellnitz D. and Ying S. 1995. Collision of comet Shoemaker Levy 9 with Jupiter observed by the NASA Infrared Telescope Facility. Science 267:1277-1282.

Osae S., Misra S., Koeberl C., Sengupta D. and Ghosh S. 2005. Target rocks, impact glasses, and melt rocks from the Lonar impact crater, India: Petrography and geochemistry. Meteoritics and Planetary Science 40:1473-1492.

Osinski G. R. 2003. Impact glasses in fallout suevites from the Ries impact structure, Germany: An analytical SEM study. Meteoritics and Planetary Science 38:1551–1707.

Osinski G. R. 2004. Impact melt rocks from the Ries structure, Germany: An origin as impact melt flows? Earth and Planetary Science Letters 226:529–543.

Osinski G. R. 2005. Hydrothermal activity associated with the Ries impact event, Germany. Geofluids 5:202–220.

Osinski G. R. and Grieve R. A. F. 2009. Classification of impact melt-bearing impactites: A discussion. 72nd Annual Meeting of the Meteoritical Society, Meteoritics and Planetary Science supplement, abstract no. 5335.

Osinski G. R. and Spray J. G. 2001. Impact-generated carbonate melts: evidence from the Haughton structure, Canada. Earth and Planetary Science Letters 194:17-29.

Osinski G. R., Spray J. G. and Lee P. 2001. Impact-induced hydrothermal activity within the Haughton impact structure, arctic Canada: generation of a transient, warm, wet oasis. Meteoritics and Planetary Science 36:731-745.

Osinski G. R., Spray J. G. and Grieve R. A. F. 2008a. Impact melting in sedimentary targets: An assessment. Geological Society of America Special Paper 437:1-18.

Osinski G. R., Grieve R. A. F., Collins G. S., Marion C. and Sylvester P. 2008b. The effect of target lithology on the products of impact melting. Meteoritics and Planetary Science 43:1939-1954.

Oskierski W. and Bischoff L. 1983. Petrographic, geochemical and structural studies on impact breccia dikes of the Rochechouart impact structure, SW France. Lunar and Planetary Science 14:584-585.

Pálfy J., 2004. Did the Puchezh–Katunki impact trigger an extinction? In: Dypvik H., Burchell M. and Claeys P. (eds.) Cratering in Marine Environments and on Ice. Springer, Berlin, p. 135–148.

Pálfy J., Demeny A., Haas J., Hetenyi M., Orchard M.J. and Veto I. 2001. Carbon isotope anomaly and other geochemical changes at the Triassic–Jurassic boundary from a marine section in Hungary. Geology 29:1047–1050.

Pálfy J., Friedman R. and Mundil R. 2008. Revised U-Pb ages of the Triassic-Jurassic boundary and the earliest Jurassic and their implications. Berichte der geologischen Bundesanstalt 76:66-67.

Palme H. 1980. The meteoritic contamination of terrestrial and lunar impact melts and the problem of indigenous siderophiles in the lunar highland. Proceedings of the Lunar and Planetary Science Conference 11:481-506.

Palme H., Grieve R. A. F. and Wolf R. 1981. Identification of the projectile at the Brent crater, and further considerations of projectile types at terrestrial craters. Geochimica et Cosmochimica Acta 45:2417-2424.

Passey Q. R. and Melosh H. J. 1980. Effects of atmospheric breakup on crater field formation. Icarus 42:211-233.

Pati J. K. and Reimold W. U. 2007. Impact cratering - fundamental process in geoscience and planetary science. Journal of Earth System Science 116:81-98.

Pati J. K., Reimold W. U., Koeberl C. and Pati P. 2008. The Dhala structure, Bundelkhand craton, central India – eroded remnant of a large Paleoproterozoic impact structure. Meteoritics and Planetary Science 43:1383-1398.

Pesonen L. J., Elo S., Lehtinen M., Jokinen T., Puranen R. and Kivekäs L. 1999a. Lake Karikkoselkä impact structure, central Finland: New geophysical and petrographic results. Geological Society of America Special Paper 339:131-147.

Pesonen L. J., Kuivasaari T., Lehtinen M., and Elo S. 1999b. Paasselkä: A new meteorite impact structure in eastern Finland. Meteoritics and Planetary Science 34:A90.

Pesonen L. J., Hietala S., Poutanen M., Moilanen J., Lehtinen M., and Ruotsalainen H. E. 2005. The Keurusselkä meteorite impact structure, central Finland: geophysical data. XXII Geofysiikan päivät - Proceedings of the 22nd Geophysical Days (May 19–20, 2005, Helsinki, Finland), p. 165-170.

Phillips F. M., Zreda M. G., Smith S. S., Elmore D., Kubik P. W., Dorn R. I. and Roddy D. J. 1991. Age and geomorphic history of Meteor Crater, Arizona, from cosmogenic Cl-36 and C-14 in rock varnish. Geochimica et Cosmochimica Acta 55:2695-2698.

Pike R. J. 1980a. Formation of complex impact craters - Evidence from Mars and other planets. Icarus 43:1-19.

Pike R. J. 1980b. Control of crater morphology by gravity and target type - Mars, Earth, Moon. Proceedings of the Lunar and Planetary Science Conference 11:2159-2189.

Pilkington M. and Grieve R. A. F. 1992. The geophysical signature of terrestrial impact craters. Reviews of Geophysics 30:161–181.

Plado J., Pesonen L. J., Elo S., Puura V. and Suuroja K. 1996. Geophysical research on the Kärdla impact structure, Hiiumaa Island, Estonia. Meteoritics and Planetary Science 31:289-298.

Plado J., Pesonen L. J. and Puura V. 1999. Effect of erosion on gravity and magnetic signatures of complex impact structures: Geophysical modeling and applications. Geological Society of America Special Paper 339:229-239.

Poag C. W., Koeberl C. and Reimold W. U. 2004 (eds.) The Chesapeake Bay crater – Geology and geophysics of a Late Eocene submarine impact structure. Springer, Berlin, Germany, 522 p.

Poelchau M. H. and Kenkmann T. 2009. Feather textures – A possible shock feature in quartz diagnostic of low shock pressures. 72nd Annual Meteoritical Society Meeting, Meteoritics and Planetary Science supplement, abstract no. 5127.

Pohl J. and Soffel H. 1971. Paleomagnetic age determination of the Rochechouart impact structure (France). Zeitschrift für Geophysik 37:857-866.

Pohl J., Ernstson K. and Lambert P. 1978. Gravity measurements in the Rochechouart impact structure (France). Meteoritics 13:601-604.

Prescott J. R., Robertson G. B., Shoemaker C., Shoemaker E. M. and Wynn J. 2004. Luminescence dating of the Wabar meteorite craters, Saudi Arabia. Journal of Geophysical Research, 109 (E01008), 8p.

Pufahl P. K., Hiatt E. E., Stanley C. R., Morrow J. R., Nelson G. J. and Edwards C. T. 2007. Physical and chemical evidence of the 1850 Ma Sudbury impact event in the Baraga Group, Michigan. Geology 35:827-830.

Puura V. and Plado J. 2005. Settings of meteorite impact structures in the Svecofennian crustal domain. In Koeberl C. and Henkel H. (eds.) Impact Tectonics, Springer, Berlin, Heidelberg, p. 211–246.

Ramezani J., Bowring S. A., Pringle M., Winslow III F. D. and Rasbury E. T. 2005. The Manicouagan impact melt rock: A new proposed standard for the intercalibration of U-Pb and Ar/Ar isotopic systems. Geochimica et Cosmochimica Acta 69:A321.

Rampino M. R. 1999. Impact crises, mass extinctions, and galactic dynamics: the case for a unified theory. Geological Society of America Special Paper 339:241-248.

Rampino M. R. and Haggerty B. M. 1996. Impact crises and mass extinctions: A working hypothesis. Geological Society of America Special Paper 307:11-30.

Rampino M. R. and Volk T. 1996. Multiple impact event in the Paleozoic: Collision with a string of comets or asteroids? Geophysical Research Letters 23:49–52.

Rasmussen B., Blake T. S. and Fletcher I. R. 2005. U-Pb zircon age constraints on the Hamersley spherule beds: Evidence for a single 2.63 Ga Jeerinah-Carawine impact ejecta layer. Geology 33:725-728.

Raukas A., Punning J.-M., Moora T., Kestlane Ü. and Kraut A. 2005. The structure and age of the Kaali Main Crater, Island of Saaremaa, Estonia. In Koeberl C. and Henkel H. (eds.) Impact Tectonics, Springer, Berlin, Heidelberg, p. 341-355.

Raup D. M. 1992. Large-body impact and extinction in the Phanerozoic. Paleobiology 18:80-88.

Raup D. M. and Sepkoski J. Jr. 1982. Mass extinctions in the marine fossil record. Science 215:1501-1503.

Rehfeldt-Oskierski A., Stöffler D., and Hornemann U. 1986. Deformation, transformation, and thermal annealing of experimentally shocked single crystal quartz. Lunar and Planetary Science Conference 17:697–698.

Reiff W. 1988. Zur Gleichaltrigkeit der Einschlagskrater (Meteorkrater) Steinheimer Becken und Nördlinger Ries. Jahresberichte und Mitteilungen des oberrheinischen geologischen Vereines, Neue Folge 70:383-397 (in German).

Reimold W. U. 1980. Isotopen-, Haupt- und Spurenelement-Geochemie und Petrographie der Impaktschmelzen des Lappajärvi-Kraters, Finland. Doctoral thesis, Westfälische Wilhelms-Universität, Münster, Germany (in German).

Reimold W. U. 2007a. Revolutions in the Earth sciences: Continental drift, impact and other catastrophes. South African Journal of Geology 110:1-46.

Reimold W. U. 2007b. The Impact Crater Bandwagon (some problems with the terrestrial impact cratering record). Meteoritics and Planetary Science 42:1467–1472.

Reimold W. U. and Gibson R. L. 2005. "Pseudotachylites" in large impact structures. In Koeberl C. and Henkel H. (eds.) Impact Tectonics, Springer, Berlin, Heidelberg, p. 1-53.

Reimold W. U. and Gibson R. L. 2006. The melt rocks of the Vredefort Impact Structure: Petrography, geochemistry, and implications for impact cratering and Witwatersrand evolution. Chemie der Erde 66:1-35.

Reimold W. U. and Koeberl C. 2008. Catastrophes, extinctions and evolution: 50 years of impact cratering studies. Golden Jubilee Memoir of the Geological Society of India 66:69-110.

Reimold W. U. and Oskierski W. 1987. The Rb-Sr-age of the Rochechouart impact structure, France, and geochemical constraints on impact melt-target rock-meteorite compositions. In Pohl J. (ed.) Research in terrestrial impact structures, Vieweg & Sohn, Braunschweig, Wiesbaden, Germany, p. 94–114.

Reimold W. U., Oskierski W. and Schäfer H. 1984. The Rochechouart impact melt: Geochemical implications and Rb-Sr chronology. Lunar and Planetary Science 15:685-686.

Reimold W. U., Oskierski W. and Huth J. 1987. The pseudotachylite from Champagnac in the Rochechouart meteorite crater, France. Journal of Geophysical Research 92:E737-E748.

Reimold W. U., Barr J. M., Grieve R. A. F. and Durrheim R. J. 1990. Geochemistry of the melt and country rocks of the Lake St. Martin impact structure, Manitoba, Canada. Geochemica et Cosmochimica Acta 54: 2093–2111.

Reimold W.U., Brandt D., de Jong R. and Hancox J. 1999. Tswaing meteorite crater - A natural and cultural history of the Tswaing crater region including a description of the hiking trail. Popular Geoscience Series vol. 1, Geological Survey of South Africa, Pretoria, 171 p.

Reimold W. U., Kelley S. P., Sherlock S. C., Henkel H., and Koeberl C. 2005a. Laser argon dating of melt breccias from the Siljan impact structure, Sweden: Implications for a possible relationship to Late Devonian extinction events. Meteoritics and Planetary Science 40:591–607.

Reimold W. U., Koeberl C., Gibson R. L. and Dressler B. O. 2005b. Economic mineral deposits in impact structures: a review. In Koeberl C. and Henkel H. (eds.) Impact Tectonics Springer, Berlin, Heidelberg, p. 479–552.

Reimold W. U., Horton Jr. W. and Schmitt R. T. 2008. Debate about impactite nomenclature – recent problems. Large Meteorite Impacts and Planetary Evolution IV, abstract no. 3033.

Reiners P. W. 2005. Zircon (U-Th)/He thermochronometry. Reviews in Mineralogy and Geochemistry 58:151-179.

Reiners P. W., Spell T. L., Nicolescu S. and Zanetti K. A. 2004. Zircon (U-Th)/He thermochronometry: He diffusion and comparisons with $^{40}Ar/^{39}Ar$ dating. Geochimica et Cosmochimica Acta 68:1857-1887.

Reinwaldt I. 1928. Bericht über geologische Untersuchungen am Kaalijärv (Krater von Sall) auf Ösel. Loodusuurijate Seltsi Aruanded 35:30-70.

Renne P. R., Melosh H. J., Farley K. A., Reimold W. U., Koeberl C., Rampino M. R., Kelley S. P. and Ivanov B. A. 2004. Is Bedout an impact crater? Take 2. Science 306:610-611.

Renne P. R., Jourdan F. and Reimold W. U. 2007. Status of the impact crater age database. Geochimica et Cosmochimica Acta 71:A833.

Richardson D. C., Bottke W. F. Jr. and Love S. G. 1998. Tidal distortion and disruption of Earth-crossing asteroids. Icarus 134:47-76.

Rondot J. 1993. Recognition of eroded astroblemes. Earth-Science Reviews 35:331-365.

Ryder G., Koeberl C. and Mojzis S. J. 2000. Heavy bombardment of the Earth at, 3.85 Ga: the search for petrographic and geochemical evidence. In Canup R. and Righter K. (eds.) Origin of the Earth and Moon, University of Arizona Press, Tucson, p. 475-492.

Sagy A., Reches Z. and Feinberg J. 2002. Dynamic fracture by large extraterrestrial impacts as the origin of shatter cones. Nature 418:310-313.

Salameh E., Khoury H., Reimold W. U. and Schneider W. 2008. The first large meteorite impact structure discovered in the Middle East: Jebel Waqf as Suwwan. Meteoritics and Planetary Science 43:1681-1690.

Salge T. 2007. The ejecta blanket of the Chicxulub impact crater, Yucatán, Mexico – petrographic and chemical studies of the K-P section of El Guayal and UNAM boreholes. Doctoral thesis, Humboldt-Universität zu Berlin, 190 p.

Satake K., 2007. Tsunamis. In Kanamori H. (ed.) Treatise on Geophysics vol. 4 , Elsevier, New York, p. 483–511.

Sauer A. 1901. Petrographische Studien an den Lavabomben aus dem Ries. Jahreshefte des Vereins für vaterländische Naturkunde Württemberg 57:88 (in German).

Sawatzky H. B. 1975. Astroblemes in the Williston basin. Journal of the Canadian Society of Exploration Geophysicists 10: 23-38.

Schaltegger U., Guex J., Bartolini A., Schoene B. and Ovtcharova M. 2007. Precise U–Pb age constraints for end-Triassic mass extinction, its correlation to volcanism and Hettangian post-extinction recovery. Earth and Planetary Science Letters 267:266-275.

Schenk P. M., Asphaug E., McKinnon W. B., Melosh H. J. and Weissman P. R. 1996. Cometary nuclei and tidal disruption: The geologic record of crater chains on Callisto and Ganymede. Icarus 121:249-274.

Schmidt G. and Pernicka E. 1994. The determination of platinum group elements (PGE) in target rocks and fall-back material of the Nördlinger Ries impact crater, Germany. Geochimica et Cosmochimica Acta 58:5083-5090.

Schmidt G., Palme H., and Kratz K.-L. 1997. Highly siderophile elements (Re, Os, Ir, Ru, Rh, Pd, Au) in impact melts from three European impact craters (Sääksjärvi, Mien, and Dellen): Clues to the nature of the impacting bodies. Geochimica et Cosmochimica Acta 61:2977–2987.

Schmieder M. and Buchner E. 2007. Short note: The Faya basin (N Chad, Africa) - A possible impact structure? Journal of African Earth Sciences 47:62-68.

Schmieder M. and Buchner E. 2008. Dating impact craters: palaeogeographic versus isotopic and stratigraphic methods – a brief case study. Geological Magazine 145:586-590.

Schmieder M., Buchner E. and Kröchert J. 2009a. 'Ballen silica' in impactites and magmatic rocks. 40th Lunar and Planetary Science Conference, abstract no. 1020.

Schmieder M., Buchner E. and Le Heron D. P. 2009b. The Jebel Hadid structure (Al Kufrah Basin, SE Libya)—A possible impact structure and potential hydrocarbon trap? Marine and Petroleum Geology 26:310-318.

Schmieder M., Jourdan F., Hietala S., Moilanen J., Öhman T. and Buchner E. 2009c. A high-precision late Mesoproterozoic ^{40}Ar/^{39}Ar age for the Keurusselkä impact structure (Finland). 40th Lunar and Planetary Science Conference, abstract no. 1028.

Schneider H. 1974. Shock-induced thermal transformations of Ries biotites. Contributions to Mineralogy and Petrology 43:233–243.

Schnetzler C. C. 1992. Mechanism of Muong Nong-type tektite formation and speculation on the source of Australasian tektites. Meteoritics 27:154-165.

Schwarz W. H. and Lippolt H. J. 2002. Coeval argon-40/argon-39 ages of moldavites from the Bohemian and Lusatian strewn fields. Meteoritics and Planetary Science 37:1757-1763.

Schwarz W. H. and Trieloff M. 2007a. Intercalibration of ^{40}Ar-^{39}Ar age standards NL25, HB3gr hornblende, GA-1550, SB-3, HD-B1 biotite and BMus/2 muscovite. Chemical Geology 242:218-231.

Schwarz W. H. and Trieloff M. 2007b. Revising the K decay constant. Meteoritics and Planetary Science 42:A138 (abstract).

Sekanina Z., Chodas P. W. and Yeomans D. K. 1994. Tidal disruption and the appearance of periodic comet Shoemaker-Levy 9. Astronomy and Astrophysics 289:607-636.

Sephton M. A., Amor K., Franchi I. A., Wignall P. B., Newton R. and Zonneveld J.-P. 2002. Carbon and nitrogen isotope disturbances and an end-Norian (Late Triassic) extinction event. Geology 30:1119-1122.

Simms M. J. 2003. Uniquely extensive seismite from the latest Triassic of the UK: Evidence for bolide impact? Geology 31:557-560.

Simms M. J. 2007. Uniquely extensive soft-sediment deformation in the Rhaetian of the UK: Evidence for earthquake or impact? Palaeogeography, Palaeoclimatology, Palaeoecology 244:407-423.

Shand S. J. 1916. The pseudotachylite of Parijs (Orange Free State), and its relation to 'trap-shoten gneiss' and 'flinty crush-rock'. Quarterly Journal of the Geological Society of London 72:198–221.

Sherlock S. C., Kelley S. P., Parnell J., Green P., Lee P., Osinski G. R. and Cockell C. S. 2005. Re-evaluating the age of the Haughton impact event. Meteoritics and Planetary Science 40:1777-1787.

Shoemaker E. M. 1977. Why study impact craters? In Roddy D. J., Pepin R. O. and Merrill R. B. (eds.) Impact and explosion cratering, Pergamon Press, New York, USA, p.1-10.

Shoemaker E. M. 1983. Asteroid and comet bombardment of the Earth. Annual Review of Earth and Planetary Sciences 11: 461-494.

Shoemaker E. M. and Chao E. C. T. 1961. New evidence for the impact origin of the Ries basin, Bavaria, Germany. Journal of Geophysical Research 66:3371-3378.

Short N. M. and Gold D. P. 1993. Petrographic analysis of selected core materials from the Manson (Iowa) impact structure. Meteoritics 28:436–437.

Shoval S., Champagnon B., and Panczer G. 1997. The quartz-cristobalite transformation in heated chert rock composed of micro and crypto-quartz by micro-Raman and FT-IR spectroscopy methods. Journal of Thermal Analysis 50:203–213.

Shuvalov V. V. and Artemieva N. 2002. Numerical modeling of Tunguska-like impacts. Planetary and Space Science 50:181-192.

Simonds C. H. and McGee P. E. 1979. Petrology of impactites from Lake St. Martin structure, Manitoba. Proceedings of the Lunar and Planetary Science Conference 10:2493-2518.

Simonds C. H., Warner J. L., Phinney W. C. and McGee P. E. 1976. Thermal model for impact breccia lithification - Manicouagan and the moon. Proceedings of the Lunar and Planetary Science Conference 7:2509-2528.

Simonds C. H., Floran R. J., McGee P. E., Phinney W. C. and Warner J. L. 1978. Petrogenesis of melt rocks, Manicouagan impact structure, Quebec. Journal of Geophysical Research 83:2773-2788.

Simonson B. M. 2003. Petrographic criteria for recognizing certain types of impact spherules in well-preserved Precambrian successions. Astrobiology 3:49-65.

Simonson B. M. and Glass B. P. 2004. Spherule layers - records of ancient impacts. Annual Review of Earth and Planetary Science 32:329-361.

Smit J. 1999. The global stratigraphy of the Cretaceous-Tertiary boundary impact ejecta. Annual Review of Earth and Planetary Sciences 27:75-113.

Smit J. and Hertogen J. 1980. An extraterrestrial event at the Cretaceous-Tertiary boundary. Nature 285:198-200.

Smit J., Roep Th. B., Alvarez W., Montanari A., Claeys P., Grajales-Nishimura J. M. and Bermudez J. 1996. Coarse-grained, clastic sandstone complex at the K/T boundary around the Gulf of Mexico: Deposition by tsunami waves induced by the Chicxulub impact? Geological Society of America Special Paper 307:151-182.

Smith A. G., Smith D. G. and Funnell B. M. 1994. Atlas of Mesozoic and Cenozoic coastlines. Cambridge University Press, UK, 99 p.

Spencer L. J. 1933. Meteorite craters as topographical features on the Earth's surface. The Geographical Journal 81:227-243.

Spray J. G. 2008. The Manicouagan structure as a window into Lunar impact melts. Joint Meeting of The Geological Society of America, Soil Science Society of America, American Society of Agronomy, Crop Science Society of America, Gulf Coast Association of Geological Societies with the Gulf Coast Section of SEPM, abstract no. 187-12.

Spray J. G., Kelley S. P. and Rowley D. B. 1998. Evidence for a late Triassic multiple impact event on Earth. Nature 392:171-173.

Spray J. G., Thompson L. M., Biren M. B. and O'Connell-Cooper C. 2009. The Manicouagan impact structure as a terrestrial analogue site for lunar and martian planetary science. Planetary and Space Science (in press).

Spudis P. D. 1993. The geology of multi-ring basins: The Moon and other planets. Cambridge University Press, UK, 263 p.

Stähle V., Altherr R., Koch M. and Nasdala L. 2008. Shock-induced growth and metastability of stishovite and coesite in lithic clasts from suevite of the Ries impact crater (Germany). Contributions to Mineralogy and Petrology 155:457-472.

Stearns R. G., Wilson C. W. Jr., Tiedemann H. A., Wilcox J. T. and Marsh P. S. 1968. The Wells Creek structure, Tennessee. In French B. M. and Short N. M. (eds.) Shock Metamorphism of Natural Materials, Mono Book, Baltimore, Maryland, USA, p. 323-338.

Steel D. 2008. Tunguska at 100. Nature 453:1157-1159.

Steiger R. H. and Jäger E. 1977. Subcommission on geochronology: convention on the use of decay constants in geo- and cosmochronology. Earth and Planetary Science Letters 36:359-362.

Stern A. S. 2003. The evolution of comets in the Oort cloud and Kuiper belt. Nature 424:639-642.

Stevens S. D., Hand R. J. and Sharp J. H. 1997. Polymorphism of silica. Journal of Materials Science 32:2929–2935.

Stöffler D. 1971. Progressive metamorphism and classification of shocked and brecciated crystalline rocks at impact craters. Journal of Geophysical Research 76:5541–5551.

Stöffler D. 1972. Deformation and transformation of rock-forming minerals by natural and experimental shock processes: I. Behavior of minerals under shock compression. Fortschritte der Mineralogie 49:50–113.

Stöffler D. 1974. Deformation and transformation of rock-forming minerals by natural and experimental shock processes. II. Physical properties of shocked minerals. Fortschritte der Mineralogie 51:256-289.

Stöffler D. 1984. Glasses formed by hypervelocity impact. Journal of Non-Crystalline Solids 67:465–502.

Stöffler D. and Claeys P. 1998. Earth rocked by combination punch. Nature 388:331-332.

Stöffler D. and Grieve R. A. F. 2007. Impactites. In: Towards a unified nomenclature of metamorphic petrology, Chapter 11: Impactites. A proposal on behalf of the IUGS Subcommission on the Systematics of Metamorphic Rocks. Blackwell Publishers, UK, 15 p.

Stöffler D. and Hornemann U, 1972. Quartz and feldspar glasses produced by natural and experimental shock. Meteoritics 7:371-394.

Stöffler D. and Langenhorst F. 1994. Shock metamorphism of quartz in nature and experiment: I. Basic observation and theory. Meteoritics 29:155–181.

Stöffler D. and Ryder G. 2001. Stratigraphy and isotope ages of lunar geologic units: chronological standard for the inner solar system. Space Science Reviews 96:9–54.

Stöffler D., Keil K. and Scott E. R. D. 1991. Shock metamorphism of ordinary chondrites. Geochimica et Cosmochimica Acta 55:3845-3867.

Stöffler D., Artemieva N. A. and Pierazzo E. 2002. Modeling the Ries-Steinheim impact event and the formation of the moldavite strewn field. Meteoritics and Planetary Science 37:1893-1907.

Stöffler D., Ryder G., Artemieva N. A., Cintala M. J., Grieve R. A. F. and Ivanov B. A. 2006. Cratering history and lunar chronology. Reviews in Mineralogy and Geochemistry 60:519-596.

Stöffler D., Horneck G., Ott S., Hornemann U., Cockell C. S., Moeller R., Meyer C., de Vera J.-P., Fritz J. and Artemieva N. A. 2007. Experimental evidence for the potential impact ejection of viable microorganisms from Mars and Mars-like planets. Icarus 186:585-588.

Stone D. and Therriault A. M. 2003. Cloud Creek structure, central Wyoming, USA: Impact origin confirmed. Meteoritics and Planetary Science 38:445-455.

Sturkell E. F. F. 1998. Resurge morphology of the marine Lockne impact crater, Jämtland, central Sweden. Geological Magazine 135:121–127.

Sutton, 1985. Thermoluminescence measurements on shock-metamorphosed sandstone and dolomite from Meteor crater, Arizona. 2. Thermoluminescence age of Meteor crater. Journal of Geophysical Research 90 B5:3690–3700.

Swisher III C. C., Grajales-Nishimura J. M., Montanari A., Margolis S. V., Claeys P., Alvarez W., Renne P., Cedillo-Pardoa E., Maurrasse F. J.-M. R., Curtis G. H., Smit J. and McWilliams M. O. 1992. Coeval $^{40}Ar/^{39}Ar$ ages of 65.0 million years ago from Chicxulub crater melt rock and Cretaceous-Tertiary boundary tektites. Science 257:954-958.

Tagle R. and Claeys P. 2005. An ordinary chondrite impactor for the Popigai crater, Siberia. Geochimica et Cosmochimica Acta 69:2877-2889.

Tagle R. and Hecht L. 2006. Geochemical identification of projectiles in impact rocks. Meteoritics and Planetary Science 41:1721-1735.

Tagle R., Stöffler D., Claeys P. and Erzinger J. 2003. A non-magmatic iron meteorite as impactor for the Rochechouart crater. 34th Annual Lunar and Planetary Science Conference, abstract no.1835.

Tagle R., Schmitt R. T. and Erzinger J. 2009. Identification of the projectile component in the impact structures Rochechouart, France and Sääksjärvi, Finland: Implications for the impactor population for the Earth. Geochimica et Cosmochimica Acta 73:4891-4906.

Tanner L. H. 2002. Stratigraphic record in the Fundy rift basin of the Manicouagan impact: Bolide with a bang or a whimper? Geological Society of America, Northeastern Section, 37th Annual Meeting, abstract no. 31805.

Tanner L. H. and Kyte F. 2005. Anomalous iridium enrichment at the Triassic–Jurassic boundary, Blomidon Formation, Fundy basin, Canada. Earth and Planetary Science Letters 240:634-641.

Tanner L. H., Lucas S. G. and Chapman M. G. 2004. Assessing the record and causes of Late Triassic extinctions. Earth-Science Reviews 65:103-139.

Thackrey S., Walkden G., Kelley S. Parrish R., Horstwood M., Indares A., Still J. and Spray J. G. 2008. Determining source of ejecta using heavy mineral provenance techniques; a Manicougan distal ejecta case study. 39th Lunar and Planetary Science Conference, abstract no. 1254.

Thackrey S., Walkden G., Indares A., Horstwood M., Kelley S. P. and Parrish R. 2009. The use of heavy mineral correlation for determining the source of impact ejecta: A Manicouagan distal ejecta case study. Earth and Planetary Science Letters 285:163-172.

Theilen-Willige B. 1982. The Araguainha astrobleme/central Brazil. Geologische Rundschau 71:318-327.

Théry J. M., Crósta A. P., Veto Akos E., Bilal E., Gál-Solymos K. and Dransart E. 2003. New laboratory results on field sections at the impact crater of Araguainha (MT, GO, Brazil). Area of proximal and distal impact ejecta, including microspherules dated from the end of the Permian. Large Meteorite Impacts III, abstract no. 4096.

Thomas M. D., Innes M. J. S., Dence M. R., Grieve R. A. F. and Robertson P. B. 1977. Gow Lake, Saskatchewan: Evidence for an origin by meteorite impact. Meteoritics 12:370-371.

Thomas P. C., Parker J. Wm., McFadden L. A., Russell C. T., Stern S. A., Sykes M. V. and Young E. D. 2005. Differentiation of the asteroid Ceres as revealed by its shape. Nature 378:224-226.

Trieloff M. and Jessberger E. K. 1992. ^{40}Ar-^{39}Ar ages of the large impact structures Kara and Manicouagan and their relevance to the Cretaceous-Tertiary and the Triassic-Jurassic boundary. Meteoritics 27:299-300.

Trieloff M., Reimold W. U., Kunz J., Boer R. H. and Jessberger E. K. 1994. ^{40}Ar-^{39}Ar thermochronology of pseudotachylite at the Ventersdorp Contact Reef, Witwatersrand Basin. South African Journal of Geology 97:365-384.

Trieloff M., Deutsch A. and Jessberger E. K. 1998. The age of the Kara impact structure, Russia. Meteoritics and Planetary Science 33:361-372.

167

Trieloff M., Falter M., Buikin A. I., Korochantseva E. V., Jessberger E. K. and Altherr R. 2005. Argon isotope fractionation induced by stepwise heating. Geochimica et Cosmochimica Acta 69:1253-1264.

Trnka M. and Houzar S. 2002. Moldavites: a review. Bulletin of the Czech Geological Survey 77:283–302.

Tsikalas F., Gundlaugsson S. T., Faleide J. I. and Eldholm O. 1999. Mjølnir structure, Barents Sea: A marine impact crater laboratory. Geological Society of America Special Paper 339:193-204.

Tuchscherer M. G., Reimold W. U., Gibson R. L., De Bruin D. and Späth A. 2006. Major and trace element compositions of melt particles and associated phases from the Yaxcopoil-1 drill core, Chicxulub impact structure, Mexico. Meteoritics and Planetary Science 41:1361-1379.

Turner G. and Cadogan P. H. 1974. Possible effects of ^{39}Ar recoil in ^{40}Ar-^{39}Ar dating. Proceedings of the 5th Lunar Science Conference 2:1601-1615.

Turtle E. P., Pierazzo E., Collins G. S., Osinski G. R., Melosh H. J., Morgan J. V. and Reimold W. U. 2005. Impact structures: What does crater diameter mean? Geological Society of America Special Paper 384:1-24.

Valter A. A. 2002. Obolon astrobleme in Ukraine: Probable rare type of the crater structure and formation. 8th ESF–IMPACT Workshop 'Impact Tectonism' (May 31-June 03, 2002, Mora, Sweden), p. 66.

Valter A. A. and Ryabenko V. A. 1977. Explosion craters on the Ukrainian Shield. Naukova Dumka, Kiev, Ukraine, 154 p. (in Russian).

Valter A. A., Asimov A. T., Voizizkji E. J. and Sirchenko W. W. 2000. The probably unique geological structure of the Obolon astrobleme: complicated crater form within the central hole. In Churyumova K. I. (ed.) Current problems with comets, asteroids, meteors, meteorites, astroblemes, and craters. Proceedings of the CAMMAC 99 Meeting (September 27-October 2, 1999, Vinnitsa, Ukraine), p. 343–366 (in Russian).

van den Bergh G. D., Boer W., de Haas H., van Weering Tj. C. E. and van Wijhe R. 2003. Shallow marine tsunami deposits in Teluk Banten (NW Java, Indonesia), generated by the 1883 Krakatau eruption. Marine Geology 197:13-34.

van Soest M. C., Wartho .J-A., Monteleone B. D., Hodges K., Koeberl C., Schmieder M., Buchner E., Spray J. G., Bezys R. and Reimold W. U. 2009. (U-Th)/He dating of single zircon and apatite crystals - A new tool for dating terrestrial impact structures. 40th Lunar and Planetary Science Conference, abstract no. 2041.

Verati C., Rapaille C., Féraud G., Marzoli A., Bertrand H. and Youbi N. 2007. [40]Ar/[39]Ar ages and duration of the Central Atlantic Magmatic Province volcanism in Morocco and Portugal and its relation to the Triassic–Jurassic boundary. Palaeogeography, Palaeoclimatology, Palaeoecology 244:308-325.

Versh E., Kirsimäe K., Jõeleht A., and Plado J. 2005. Cooling of the Kärdla impact crater: I. The mineral paragenetic sequence observation. Meteoritics and Planetary Science 40:3–19.

Veski S., Heinsalu A., Lang V., Kestlane Ü. and Possnert G. 2004. The age of the Kaali meteorite craters and the effect of the impact on the environment and man: evidence from inside the Kaali craters, island of Saaremaa, Estonia. Vegetation History and Archaeobotany 13:197-206.

Veski S., Heinsalu A., Poska A.,, Saarse L. and Vassiljec J. 2007. The physical and social effects of the Kaali meteorite impact — a review. In Bobrowsky P. and Rickman H. (eds.) Comet/asteroid impacts and human society. Springer, Berlin, Heidelberg, p. 265-275.

Villeneuve M., Sandeman H. A. and Davis W. J. 2000. A method for intercalibration of U-Th-Pb and [40]Ar-[39]Ar ages in the Phanerozoic. Geochimica et Cosmochimica Acta 64:4017-4030.

Vishnevsky S. A. 1986. Shock metamorphism of basic rocks as exemplified by the Logancha astrobleme. Geologiya i Geofizika 27:70-79 (in Russian).

Wagner G. A. and Storzer D. 1975. The age of the Rochechouart impact structure. Meteoritics 10:503-504.

Walkden G. A. and Parker J. 2008. The biotic effects of large bolide impacts: size versus time and place. International Journal of Astrobiology 7:209-215.

Walkden G., Parker J. and Kelley S. P. 2002. A Late Triassic impact ejecta layer in southwestern Britain. Science 298:2185-2188.

Wanless R. K., Stevens R. D., Lachance G. R. and Rimsaite R. Y. H. 1965. Age determinations and geological studies, part I. isotopic ages, report 5. Geological Survey of Canada Paper 64-17:105-106.

Ward K. T., Mauk J. L. and Hall C. 2005. New [40]Ar/[39]Ar dates of adularia from epithermal deposits in the Hauraki Goldfield, New Zealand: Proceedings of the 2005 New Zealand Minerals Conference, p. 426-433.

Ward P. D., Haggart J. W., Carter E. S., Wilbur D., Tipper H. W. and Evans T. 2001. Sudden productivity collapse associated with the Triassic-Jurassic boundary mass extinction. Science 292: 1148-1151.

Ward S. N. and Asphaug E. 1999. Asteroid impact tsunami: A probabilistic hazard assessment. Icarus 145:64-78.

Warme J. E. and Kuehner H.-C. 1998. Anatomy of an anomaly: The Devonian catastrophic Alamo impact breccia of Southern Nevada. In Ernst W. G. and Nelson C. A. (eds.) Integrated Earth and environmental evolution of the Southwestern United States, Bellwether Publishing, Columbia, Maryland, USA, p. 80-107.

Wartho J.-A., Schmieder M., van Soest M. C., Buchner E., Hodges K. V., Bezys R. K. and Reimold W. U. 2009. New (U-Th)/He zircon and apatite ages for the Lake Saint Martin impact structure (Manitoba, Canada) and implications for the Late Triassic multiple impact theory. 40th Lunar and Planetary Science Conference, abstract no. 2004.

Weihaupt J. G. 1976. The Wilkes Land anomaly: Evidence for a possible hypervelocity impact crater. Journal of Geophysical Research 81:5651-5663.

Weiss R. and Wünnemann K. 2007. Large waves caused by oceanic impacts of meteorites. In Kundu A. (ed.) Tsunami and nonlinear waves. Springer, Berlin, Heidelberg, p. 235-260.

Werner S. C., Plado J., Pesonen, L. J. and Kuulusa M. 2001. The two Suvasvesi lakes in central Finland - a possible doublet impact structure. Meteoritics and Planetary Science 36:A223.

Werner S. C., Plado J., Pesonen L. J., Janle P. and Elo S. 2002. Potential fields and subsurface models of Suvasvesi North impact structure, Finland. Physics and Chemistry of the Earth 27:1237-1245.

Whitehead J., Papanastassiou D. A., Spray J. G., Grieve R. A. F. and Wasserburg G. J. 2000. Late Eocene impact ejecta: geochemical and isotopic connections with the Popigai impact structure. Earth and Planetary Science Letters 181:473-487.

Whitehead J., Spray J. G., and Grieve R. A. F. 2002. Origin of "toasted" quartz in terrestrial impact structures. Geology 30:431–434.

Wichman P. R. and Wood C. A. 1995. The Davy crater chain: Implications for tidal disruption in the Earth-Moon system and elsewhere. Geophysical Research Letters 22:583-586.

Wittmann A., Kenkmann T., Schmitt R. T. and Stöffler D. 2006. Shock-metamorphosed zircon in terrestrial impact craters. Meteoritics and Planetary Science 41:433-454.

Wolfe S. H. 1971. Potassium-argon ages of the Manicouagan-Mushalagan Lake structure. Journal of Geophysical Research 76:5424-5436.

Wolfe S. H. 1972. Part I. Geology of the Manicouagan-Mushalagan Lakes Structure. Part II. Geochronology of the Manicouagan-Mushalagan Lakes Structure. Ph.D. thesis, Caltech, Pasadena, USA, 473 p.

Wynn J. C. and Shoemaker E. M. 1998. The day the sands caught fire. Scientific American 279:36-43.

Yeomans D. K., Barriot J.-P., Dunham D. W., Farquhar R. W., Giorgini J. D., Helfrich C. E., Konopliv A. S., McAdams J. V., Miller J. K., Owen W. M. Jr., Scheeres D. J., Synott S. P. and Williams B. G. 1997. Estimating the mass of asteroid 253 Mathilde from tracking data during the NEAR flyby. Science 278:2106-2109.

York D. 1969. Least squares fitting of a straight line with correlated errors. Earth and Planetary Science Letters 5:320-324.

Ziegler P. A. 1988. Evolution of the Arctic-North Atlantic and the western Tethys. American Association of Petroleum Geologists Memoir 43:164-196.

Ziegler P. A. 1990. Geological Atlas of Western and Central Europe. Shell, The Hague, The Netherlands, 256 p.

Ziegler P. A. and Kent P. 1982. Faulting and graben formation in Western and Central Europe. Philosophical Transactions of the royal Society of London A 305:113-143.

Ziegler A. M., Scotese C. R. and Barrett S. F. 1983. Tidal friction and the Earth's rotation II. In Brosche P. and Sundermann J. (eds.) Proceedings of a Workshop (September 28-October 3, 1981, Bielefeld, Germany), Springer, New York, p. 240-252.

Zürcher L. and Kring D. A. 2004. Hydrothermal alteration in the core of the Yaxcopoil-1 borehole, Chicxulub impact structure, Mexico. Meteoritics and Planetary Science 39:1199-1221.

Appendix

A1   Raw isotopic data

Rochechouart – sanidine

```
Argon 40 - Argon 39                                                              8. 4.2009 - 14:51

 Eingabedatei:        5541.ipf
 Ausgabedatei:        5541.opf

Derzeit verwendete Konstanten:
 Lambda(Beta):       4.962E-10
 Lambda(Epsilon):    0.581E-10
 Luftverhältnis:     277.26   ± 0.32

Korrekturfaktoren:
 (Ar36/Ar37)Ca:      4.3E-0004  ±  1.9E-0005
 (Ar39/Ar37)Ca:      9.8E-0004  ±  3.1E-0005
 (Ar40/Ar39)K:       1.5E-0002  ±  4.0E-0003
 (Ar38/Ar39)K:       1.8E-0002  ±  8.0E-0005


*********** Version vom 27.05.99 ****************************************************************************


Runnr.:    5541 RocheVidSan     Benutzter Standard:      B-Mus

Schritt   Ar36    Ar37-Ca Ar38-Ges  Ar38-Cl   Ar39-K       Ar40       Ar40*    Ar40* Ar36/Ar39  Ar37/Ar39  Ar40*/Ar39
          (fA)     (fA)    (fA)      (fA)      (fA)         (fA)       (fA)      (%)   (*100)

    1    7.8506   0.000   1.5224    0.0305    1.378     2338.542     18.687    0.80  569.7533   0.0000     13.562
         0.1291   0.000   0.0633    0.0678    0.114        0.730     38.261    1.64   48.2002   0.0000     27.791

    2    3.2793  25.867   1.1354    0.1056   23.295     1674.374    705.348   42.13   14.0773   1.1104     30.279
         0.0704   0.518   0.0410    0.0432    0.165        2.730     21.001    1.26    0.3181   0.0236      0.927

    3    2.4105  10.089   3.2909    0.0813  154.139     7037.146   6324.845   89.88    1.5638   0.0655     41.033
         0.1991   0.210   0.2159    0.2195    0.355        7.010     59.252    0.85    0.1292   0.0014      0.396

    4    1.9987  11.533   3.2108   -0.0589  161.798     7477.472   6886.871   92.10    1.2353   0.0713     42.565
         0.1494   0.232   0.1517    0.1550    0.515       25.723     51.109    0.75    0.0924   0.0015      0.344

    5    1.3393  15.618   2.0109    0.0947   93.062     4338.554   3942.790   90.88    1.4392   0.1678     42.368
         0.0558   0.312   0.1672    0.1677    0.040       13.297     21.201    0.56    0.0600   0.0034      0.229

    6    1.6222   0.000   1.9437   -0.0026   91.794     4376.901   3897.550   89.05    1.7672   0.0000     42.460
         0.0731   0.000   0.0754    0.0771    0.245       13.047     25.253    0.64    0.0798   0.0000      0.298

    7    1.9474   0.000   2.9552    0.3469  125.384     5828.382   5252.940   90.13    1.5531   0.0000     41.895
         0.0468   0.000   0.2612    0.2616    0.200       11.809     18.213    0.36    0.0374   0.0000      0.160

    8    1.6648   0.000   1.9006   -0.2275  101.505     4769.656   4277.722   89.69    1.6401   0.0000     42.143
         0.1112   0.000   0.1079    0.1104    0.323       24.892     41.227    0.98    0.1097   0.0000      0.428

    9    2.2747   0.000   1.7251    0.1592   63.731     3317.160   2644.980   79.74    3.5693   0.0000     41.502
         0.0532   0.000   0.1471    0.1475    0.118        9.095     18.170    0.59    0.0837   0.0000      0.295

   10    4.0157  18.719   1.9796    0.0471   66.029     3954.100   2767.460   69.99    6.0817   0.2835     41.913
         0.0253   0.385   0.1481    0.1483    0.212       12.781     14.879    0.44    0.0431   0.0059      0.263

   11   14.9621   0.000   3.2926   -0.0922   32.870     5824.308   1403.011   24.09   45.5185   0.0000     42.683
         0.1000   0.000   0.1343    0.1356    0.153       12.645     32.545    0.56    0.3707   0.0000      1.010

   12   52.7600   9.629  10.0932    0.0911    7.892    16022.966    432.378    2.70  668.5331   1.2202     54.788
         0.0635   0.216   0.1087    0.1093    0.092       21.056     33.449    0.21    7.8611   0.0308      4.287

Total 96.1251  91.456  35.0603    0.5751  922.877    66959.560  38554.582   57.58   10.4158   0.0991     41.777
       0.3523   1.980   0.5121    0.5289    4.893       51.713    120.830    0.19    0.0671   0.0022      0.257


J= 0.0027979 ± 0.0000015 (± 0.0000104)


          Ar39-Entgasung (%)            Alter

 1. Schritt        0.15        67.187  ± 135.147 Ma  (± 135.147 Ma)
 2. Schritt        2.52       146.705  ±   4.313 Ma  (±   4.344 Ma)
 3. Schritt       16.70       196.066  ±   1.795 Ma  (±   1.920 Ma)
 4. Schritt       17.53       202.986  ±   1.554 Ma  (±   1.706 Ma)
 5. Schritt       10.08       202.098  ±   1.037 Ma  (±   1.251 Ma)
 6. Schritt        9.95       202.514  ±   1.346 Ma  (±   1.518 Ma)
 7. Schritt       13.59       199.963  ±   0.730 Ma  (±   1.007 Ma)
 8. Schritt       11.00       201.083  ±   1.934 Ma  (±   2.056 Ma)
 9. Schritt        6.91       198.189  ±   1.339 Ma  (±   1.505 Ma)
10. Schritt        7.15       200.045  ±   1.191 Ma  (±   1.378 Ma)
11. Schritt        3.56       203.521  ±   4.555 Ma  (±   4.609 Ma)
12. Schritt        0.86       257.291  ±  18.762 Ma  (±  18.782 Ma)

   Total        100.00       199.428  ±   1.167 Ma  (±   1.357 Ma)
```

Rochechouart – adularia

```
Argon 40 - Argon 39                                                          1. 4.2009 - 17:21

 Eingabedatei:      5539.ipf
 Ausgabedatei:      5539.opf

Derzeit verwendete Konstanten:
 Lambda(Beta):      4.962E-10
 Lambda(Epsilon):   0.581E-10
 Luftverhältnis:    277.26  ± 0.32

Korrekturfaktoren:
 (Ar36/Ar37)Ca:     4.3E-0004  ±  1.9E-0005
 (Ar39/Ar37)Ca:     9.8E-0004  ±  3.1E-0005
 (Ar40/Ar39)K:      1.5E-0002  ±  4.0E-0003
 (Ar38/Ar39)K:      1.8E-0002  ±  8.0E-0005


*********** Version vom 27.05.99 *****************************************************************************


Runnr.:  5539 RocheVidAdu    Benutzter Standard:      B-Mus
```

Schritt	Ar36 (fA)	Ar37-Ca (fA)	Ar38-Ges (fA)	Ar38-Cl (fA)	Ar39-K (fA)	Ar40 (fA)	Ar40* (fA)	Ar40* (%)	Ar36/Ar39 (*100)	Ar37/Ar39	Ar40*/Ar39
1	8.2425	12.418	1.8450	0.2817	1.275	2480.600	44.952	1.81	646.4970	9.7403	35.258
	0.0986	0.250	0.2396	0.2404	0.194	2.062	29.352	1.18	98.4774	1.4921	23.636
2	3.6465	4.298	1.6653	0.0902	49.921	2712.403	1634.866	60.27	7.3045	0.0861	32.749
	0.1103	0.093	0.2306	0.2315	0.054	4.778	32.972	1.22	0.2211	0.0019	0.661
3	2.7485	10.078	3.4227	-0.0683	166.331	7403.254	6591.078	89.03	1.6524	0.0606	39.626
	0.0988	0.210	0.1781	0.1796	0.294	5.628	29.768	0.41	0.0595	0.0013	0.192
4	1.9295	16.059	3.1836	-0.1083	163.758	7367.762	6797.593	92.26	1.1783	0.0981	41.510
	0.1669	0.359	0.2590	0.2612	0.132	3.129	49.413	0.67	0.1019	0.0022	0.304
5	3.2088	13.647	4.5183	0.1554	210.236	9776.611	8828.422	90.30	1.5263	0.0649	41.993
	0.1396	0.274	0.0733	0.0798	0.263	14.788	43.832	0.47	0.0664	0.0013	0.215
6	1.3176	20.771	2.2962	0.2652	99.703	4573.512	4184.162	91.49	1.3215	0.2083	41.966
	0.1611	0.460	0.4006	0.4019	0.273	13.551	49.505	1.12	0.1616	0.0046	0.510
7	1.3192	16.557	2.0702	0.2247	89.330	4134.856	3745.037	90.57	1.4767	0.1854	41.923
	0.0705	0.332	0.1417	0.1425	0.161	7.507	22.145	0.56	0.0789	0.0037	0.259
8	1.8846	0.250	2.7945	0.2348	123.322	5761.267	5204.372	90.33	1.5282	0.0020	42.202
	0.1235	0.068	0.3135	0.3145	0.209	10.770	38.046	0.68	0.1001	0.0006	0.317
9	1.9507	3.604	3.6383	-0.0120	183.556	8301.742	7725.303	93.06	1.0627	0.0196	42.087
	0.1170	0.090	0.1610	0.1633	0.389	19.039	39.483	0.52	0.0638	0.0005	0.233
10	1.7743	5.417	3.2964	-0.0508	168.471	7607.208	7082.895	93.11	1.0532	0.0322	42.042
	0.2220	0.144	0.1905	0.1954	0.239	2.236	65.633	0.86	0.1318	0.0009	0.394
11	1.6896	4.674	2.5082	-0.1107	128.664	5900.766	5401.486	91.54	1.3132	0.0363	41.981
	0.0484	0.159	0.1683	0.1689	0.205	3.890	14.830	0.26	0.0376	0.0012	0.133
12	4.2083	5.669	3.7334	0.0416	162.307	8077.772	6834.207	84.61	2.5928	0.0349	42.107
	0.1870	0.249	0.3686	0.3705	0.275	23.216	59.970	0.78	0.1153	0.0015	0.376
13	21.2785	4.150	4.6730	0.0488	36.161	7814.247	1526.455	19.53	58.8438	0.1148	42.213
	0.1099	0.113	0.0836	0.0863	0.239	13.681	35.982	0.46	0.4935	0.0032	1.033
14	25.7155	12.039	5.0501	0.2027	2.294	7669.697	70.754	0.92	1120.8751	5.2477	30.840
	0.0732	0.250	0.1792	0.1797	0.074	10.014	25.406	0.33	36.4547	0.2020	11.119
Total	80.9141	129.633	44.6951	1.1949	1585.328	89581.696	65671.582	73.31	5.1039	0.0818	41.425
	0.4928	2.718	0.8713	0.8951	7.408	43.037	154.474	0.18	0.0392	0.0018	0.217

```
J=  0.0028005  ±  0.0000011  (±  0.0000103)
```

	Ar39-Entgasung (%)	Alter
1. Schritt	0.08	169.880 ± 108.687 Ma (± 108.688 Ma)
2. Schritt	3.15	158.306 ± 3.062 Ma (± 3.111 Ma)
3. Schritt	10.49	189.856 ± 0.877 Ma (± 1.097 Ma)
4. Schritt	10.33	198.403 ± 1.376 Ma (± 1.539 Ma)
5. Schritt	13.26	200.587 ± 0.975 Ma (± 1.197 Ma)
6. Schritt	6.29	200.467 ± 2.305 Ma (± 2.408 Ma)
7. Schritt	5.63	200.273 ± 1.174 Ma (± 1.364 Ma)
8. Schritt	7.78	201.530 ± 1.433 Ma (± 1.594 Ma)
9. Schritt	11.58	201.012 ± 1.055 Ma (± 1.264 Ma)
10. Schritt	10.63	200.809 ± 1.783 Ma (± 1.914 Ma)
11. Schritt	8.12	200.535 ± 0.607 Ma (± 0.923 Ma)
12. Schritt	10.24	201.102 ± 1.702 Ma (± 1.839 Ma)
13. Schritt	2.28	201.581 ± 4.670 Ma (± 4.722 Ma)
14. Schritt	0.14	149.450 ± 51.711 Ma (± 51.714 Ma)
Total	100.00	198.016 ± 0.984 Ma (± 1.200 Ma)

Manicouagan – impact melt rock

```
Argon 40 - Argon 39                                                    7. 5.2009 - 14:20

 Eingabedatei:        5547.ipf
 Ausgabedatei:        5547.opf

Derzeit verwendete Konstanten:
 Lambda(Beta):        4.962E-10
 Lambda(Epsilon):     0.581E-10
 Luftverhältnis:      277.26   ± 0.32

Korrekturfaktoren:
 (Ar36/Ar37)Ca:       4.3E-0004  ±  1.9E-0005
 (Ar39/Ar37)Ca:       9.8E-0004  ±  3.1E-0005
 (Ar40/Ar39)K:        1.5E-0002  ±  4.0E-0003
 (Ar38/Ar39)K:        1.8E-0002  ±  8.0E-0005


*********** Version vom 27.05.99 ***********************************************************************
```

Schritt	Ar36 (fA)	Ar37-Ca (fA)	Ar38-Ges (fA)	Ar38-Cl (fA)	Ar39-K (fA)	Ar40 (fA)	Ar40* (fA)	Ar40* (%)	Ar36/Ar39 (*100)	Ar37/Ar39	Ar40*/Ar39
1	19.9984	3.314	3.9037	0.1245	2.320	5988.960	79.422	1.33	861.9377	1.4285	34.231
	0.1084	0.070	0.1184	0.1201	0.088	9.417	34.087	0.57	32.9557	0.0619	14.749
2	46.2502	60.690	8.9914	0.1090	13.309	14397.563	730.619	5.07	347.5218	4.5602	54.898
	0.1810	1.235	0.1527	0.1565	0.315	38.345	67.685	0.47	8.3363	0.1423	5.249
3	19.0125	42.689	4.3276	-0.1363	50.862	8276.083	2657.877	32.12	37.3808	0.8393	52.257
	0.1260	0.843	0.1784	0.1800	0.174	13.531	40.138	0.49	0.2787	0.0168	0.809
4	31.3663	107.102	9.5863	0.3471	188.652	18251.437	8982.701	49.22	16.6265	0.5677	47.615
	0.0810	2.118	0.0959	0.0983	0.249	12.649	29.112	0.16	0.0482	0.0113	0.167
5	9.5418	108.264	5.8059	0.1349	217.188	13041.302	10221.702	78.38	4.3933	0.4985	47.064
	0.1166	2.139	0.2854	0.2870	0.624	24.050	42.151	0.35	0.0551	0.0100	0.237
6	2.6940	39.424	2.2654	0.2328	85.427	4708.772	3912.707	83.09	3.1535	0.4615	45.802
	0.0755	0.785	0.1864	0.1871	0.142	2.060	22.420	0.48	0.0885	0.0092	0.273
7	2.2019	56.641	2.0791	0.1460	85.002	4550.981	3900.308	85.70	2.5905	0.6664	45.885
	0.0732	1.121	0.1616	0.1625	0.294	4.902	22.193	0.50	0.0866	0.0134	0.306
8	2.1795	79.857	2.5427	0.3548	99.473	5208.403	4564.356	87.63	2.1911	0.8028	45.885
	0.1337	1.579	0.1452	0.1476	0.220	10.140	40.793	0.80	0.1345	0.0160	0.423
9	1.3684	75.559	2.6983	0.9194	85.091	4199.955	3795.592	90.37	1.6082	0.8880	44.606
	0.0359	1.493	0.0292	0.0308	0.110	13.223	16.955	0.49	0.0422	0.0176	0.207
10	1.3559	79.977	1.5432	0.3213	54.100	2774.893	2374.218	85.56	2.5063	1.4783	43.885
	0.0595	1.588	0.1210	0.1216	0.171	9.115	19.818	0.77	0.1103	0.0297	0.392
11	5.2507	499.242	4.9607	1.3133	148.943	8005.429	6453.851	80.62	3.5253	3.3519	43.331
	0.1014	9.860	0.3366	0.3374	0.302	12.839	32.657	0.43	0.0685	0.0665	0.236
12	11.7262	102.046	3.1590	0.4253	30.282	4913.431	1448.327	29.48	38.7230	3.3698	47.827
	0.1303	2.021	0.1167	0.1192	0.047	10.861	40.209	0.82	0.4346	0.0669	1.330
Total	152.9459	1254.805	51.8633	4.2920	1060.650	94317.209	49121.681	52.08	14.4200	1.1831	46.313
	0.3770	27.125	0.6198	0.6379	5.759	56.145	135.291	0.15	0.0860	0.0264	0.282

```
Runnr.:  5547 Manicou       Benutzter Standard:       B-Mus
```

J= 0.0027896 ± 0.0000067 (± 0.0000122)

	Ar39-Entgasung (%)		Alter				
1. Schritt	0.22		164.539 ±	67.757 Ma	(±	67.759 Ma)
2. Schritt	1.25		257.071 ±	22.916 Ma	(±	22.933 Ma)
3. Schritt	4.80		245.506 ±	3.596 Ma	(±	3.693 Ma)
4. Schritt	17.79		225.002 ±	0.896 Ma	(±	1.185 Ma)
5. Schritt	20.48		222.551 ±	1.165 Ma	(±	1.395 Ma)
6. Schritt	8.05		216.929 ±	1.313 Ma	(±	1.512 Ma)
7. Schritt	8.01		217.298 ±	1.448 Ma	(±	1.631 Ma)
8. Schritt	9.38		217.301 ±	1.947 Ma	(±	2.087 Ma)
9. Schritt	8.02		211.584 ±	1.044 Ma	(±	1.274 Ma)
10. Schritt	5.10		208.355 ±	1.818 Ma	(±	1.956 Ma)
11. Schritt	14.04		205.868 ±	1.158 Ma	(±	1.360 Ma)
12. Schritt	2.86		225.944 ±	5.927 Ma	(±	5.978 Ma)
Total	100.00		219.207 ±	1.350 Ma	(±	1.547 Ma)

Paasselkä – recrystallized feldspar glass

```
Argon 40 - Argon 39                                                              6. 3.2009 - 14:25

 Eingabedatei:        5535.ipf
 Ausgabedatei:        5535.opf

Derzeit verwendete Konstanten:
 Lambda(Beta):        4.962E-10
 Lambda(Epsilon):     0.581E-10
 Luftverhältnis:      277.26    ± 0.32
 Empfindlichkeit:     3.85e-11 ccm STP/fA
 K :                  4.4 %

Korrekturfaktoren:
 (Ar36/Ar37)Ca:        4.3E-0004  ±  1.9E-0005
 (Ar39/Ar37)Ca:        9.8E-0004  ±  3.1E-0005
 (Ar40/Ar39)K:         1.5E-0002  ±  4.0E-0003
 (Ar38/Ar39)K:         1.8E-0002  ±  8.0E-0005

*********** Version vom 27.05.99 ***********************************************************************

Runnr.:  5535 P1          Benutzter Standard:      B-Mus
```

Schritt	Ar36 (fA)	Ar37-Ca (fA)	Ar38-Ges (fA)	Ar38-Cl (fA)	Ar39-K (fA)	Ar40 (fA)	Ar40* (fA)	Ar40* (%)	Ar36/Ar39 (*100)	Ar37/Ar39	Ar40*/Ar39
1	9.8556	1.083	2.5637	0.2273	27.618	3916.347	1004.024	25.64	35.6848	0.0392	36.353
	0.1088	0.099	0.2243	0.2253	0.233	6.986	33.067	0.85	0.4954	0.0036	1.236
2	3.7084	2.312	2.1540	0.2792	66.014	3669.256	2573.437	70.14	5.6176	0.0350	38.983
	0.1785	0.148	0.2437	0.2461	0.216	5.688	53.076	1.45	0.2711	0.0023	0.814
3	5.7639	19.837	5.7805	0.3527	243.045	13060.444	11357.225	86.96	2.3715	0.0816	46.729
	0.0800	0.393	0.2630	0.2652	1.323	74.891	78.568	0.78	0.0354	0.0017	0.411
4	4.2960	14.534	5.6995	-0.0846	278.280	16419.961	15150.490	92.27	1.5438	0.0522	54.443
	0.1837	0.352	0.1651	0.1716	1.277	71.229	89.568	0.68	0.0664	0.0013	0.407
5	3.0531	20.913	6.3755	-0.2807	339.976	19634.787	18732.610	95.41	0.8980	0.0615	55.100
	0.0656	0.447	0.2288	0.2313	0.959	39.002	43.586	0.29	0.0195	0.0013	0.201
6	2.3066	10.627	6.9362	-0.4486	388.475	21518.871	20837.263	96.83	0.5938	0.0274	53.639
	0.1095	0.228	0.1215	0.1273	0.461	31.687	45.316	0.25	0.0282	0.0006	0.133
7	1.6348	11.915	5.6092	-0.1322	303.681	16207.494	15724.420	97.02	0.5383	0.0392	51.779
	0.0387	0.260	0.1183	0.1210	0.151	6.136	13.046	0.09	0.0127	0.0009	0.050
8	1.8866	8.772	7.5724	-0.1365	410.968	21019.979	20462.476	97.35	0.4591	0.0213	49.791
	0.1248	0.293	0.0522	0.0679	0.890	50.648	62.685	0.38	0.0304	0.0007	0.187
9	1.8345	13.920	6.4901	-0.1988	354.530	17765.129	17223.046	96.95	0.5174	0.0393	48.580
	0.1964	0.304	0.0773	0.0910	0.700	24.290	62.941	0.38	0.0554	0.0009	0.202
10	1.9675	16.377	5.1831	0.0688	265.169	13449.232	12867.846	95.68	0.7420	0.0618	48.527
	0.1603	0.375	0.3272	0.3293	0.224	5.069	47.658	0.36	0.0605	0.0014	0.184
11	2.4876	7.861	4.4959	0.0458	222.641	11452.670	10717.597	93.58	1.1173	0.0353	48.139
	0.2125	0.278	0.0405	0.0607	0.692	34.211	71.529	0.68	0.0955	0.0013	0.354
12	6.1897	8.106	8.2417	-0.0963	401.178	21126.414	19297.364	91.34	1.5429	0.0202	48.102
	0.0661	0.209	0.1417	0.1460	0.456	14.517	24.475	0.13	0.0166	0.0005	0.082
13	6.1306	1.924	5.9864	0.1297	263.178	14552.951	12741.366	87.55	2.3294	0.0073	48.413
	0.0787	0.199	0.0764	0.0826	0.999	49.593	54.829	0.48	0.0312	0.0008	0.278
14	5.8749	2.431	3.3246	-0.0433	126.813	7926.140	6190.101	78.10	4.6327	0.0192	48.813
	0.1137	0.099	0.1336	0.1361	0.579	10.788	35.340	0.46	0.0921	0.0008	0.357
15	9.6330	8.528	3.6531	0.2441	89.865	7250.013	4403.466	60.74	10.7194	0.0949	49.001
	0.1519	0.204	0.4891	0.4900	0.225	7.560	45.651	0.63	0.1712	0.0023	0.523
16	15.3676	4.435	4.7781	0.7015	67.285	7832.015	3290.876	42.02	22.8395	0.0659	48.909
	0.0496	0.115	0.1336	0.1340	0.139	12.541	19.989	0.26	0.0874	0.0017	0.314
17	10.3763	0.757	2.3350	0.1581	13.267	3690.149	623.958	16.91	78.2089	0.0571	47.029
	0.0667	0.028	0.0668	0.0680	0.121	3.223	20.288	0.55	0.8738	0.0022	1.588
Total	92.3665	154.330	87.1788	0.7861	3861.983	220491.853	193197.563	87.62	2.3917	0.0400	50.025
	0.5293	3.235	0.8426	0.9499	16.499	143.837	215.369	0.11	0.0171	0.0009	0.221

```
J=  0.0027905  ±  0.0000085 (±  0.0000133)
```

```
           Ar39-Entgasung (%)                    Alter

 1. Schritt        0.72        174.317  ±    5.671 Ma  (±    5.704 Ma)
 2. Schritt        1.71        186.298  ±    3.736 Ma  (±    3.791 Ma)
 3. Schritt        6.29        221.127  ±    1.940 Ma  (±    2.084 Ma)
 4. Schritt        7.21        255.161  ±    1.924 Ma  (±    2.112 Ma)
 5. Schritt        8.80        258.028  ±    1.146 Ma  (±    1.445 Ma)
 6. Schritt       10.06        251.641  ±    0.925 Ma  (±    1.263 Ma)
 7. Schritt        7.86        243.481  ±    0.731 Ma  (±    1.109 Ma)
 8. Schritt       10.64        234.713  ±    1.066 Ma  (±    1.336 Ma)
 9. Schritt        9.18        229.352  ±    1.111 Ma  (±    1.363 Ma)
10. Schritt        6.87        229.118  ±    1.050 Ma  (±    1.312 Ma)
11. Schritt        5.76        227.394  ±    1.703 Ma  (±    1.874 Ma)
12. Schritt       10.39        227.231  ±    0.748 Ma  (±    1.082 Ma)
13. Schritt        6.81        228.614  ±    1.396 Ma  (±    1.602 Ma)
14. Schritt        3.28        230.384  ±    1.714 Ma  (±    1.888 Ma)
15. Schritt        2.33        231.217  ±    2.408 Ma  (±    2.536 Ma)
16. Schritt        1.74        230.812  ±    1.540 Ma  (±    1.732 Ma)
17. Schritt        0.34        222.465  ±    7.098 Ma  (±    7.139 Ma)

    Total        100.00        235.749  ±    1.187 Ma  (±    1.437 Ma)
```

A2   Blank-corrected data

Rochechouart – sanidine

		Data [fA]											
Step	Temp	^{36}Ar	± 1σ	^{37}Ar$_{Ca}$	± 1σ	^{38}Ar$_{tot}$	± 1σ	^{39}Ar$_K$	± 1σ	^{40}Ar	± 1σ	^{40}Ar*	± 1σ
1	500	7.7616	0.1292	0.000	0	1.5057	0.063	1.378	0.114	2312.244	1.504	18.687	38.261
2	600	3.1235	0.0708	25.867	0.518	1.1061	0.041	23.295	0.165	1628.334	3.571	705.348	21.001
3	690	2.1526	0.1995	10.089	0.21	3.2424	0.216	154.139	0.355	6960.935	7.979	6324.845	59.252
4	740	1.6575	0.1504	11.533	0.232	3.1467	0.152	161.798	0.515	7376.635	26.212	6886.871	51.109
5	760	0.9576	0.0590	15.618	0.312	1.9392	0.167	93.062	0.04	4225.767	14.443	3942.79	21.201
6	800	1.1447	0.0769	0.000	0	1.8539	0.076	91.794	0.245	4235.796	14.832	3897.55	25.253
7	860	1.2792	0.0575	0.000	0	2.8296	0.261	125.384	0.2	5630.928	15.392	5252.94	18.213
8	930	0.6759	0.1217	0.000	0	1.7147	0.108	101.505	0.323	4477.437	28.863	4277.722	41.227
9	1000	0.8112	0.0905	0.000	0	1.4500	0.148	63.731	0.118	2884.694	23.458	2644.98	18.17
10	1100	1.4536	0.1306	18.719	0.385	1.4980	0.150	66.029	0.212	3196.994	39.955	2767.46	14.879
11	1200	10.4767	0.2456	0.000	0	2.4495	0.141	32.87	0.153	4498.863	67.468	1403.011	32.545
12	1350	42.3701	0.5234	9.629	0.216	8.1402	0.146	7.892	0.092	12952.749	154.948	432.378	33.449

Rochechouart – adularia

		Data [fA]											
Step	Temp	^{36}Ar	± 1σ	^{37}Ar$_{Ca}$	± 1σ	^{38}Ar$_{tot}$	± 1σ	^{39}Ar$_K$	± 1σ	^{40}Ar	± 1σ	^{40}Ar*	± 1σ
1	500	8,1705	0,0989	12,418	0,25	1,8315	0,2396	1,275	0,194	2459,335	2,962	44,952	29,352
2	600	3,5100	0,1111	4,298	0,093	1,6396	0,2306	49,921	0,054	2672,075	6,252	1634,866	32,972
3	665	2,5416	0,1009	10,078	0,21	3,3838	0,1781	166,331	0,294	7342,121	8,309	6591,078	29,768
4	690	1,6867	0,1687	16,059	0,359	3,1380	0,2590	163,758	0,132	7296,022	7,827	6797,593	49,413
5	700	2,9500	0,1420	13,647	0,274	4,4696	0,0735	210,236	0,263	9700,129	16,649	8828,422	43,832
6	715	1,0327	0,1636	20,771	0,46	2,2426	0,4006	99,703	0,273	4489,324	15,953	4184,162	49,505
7	740	0,9849	0,0780	16,557	0,332	2,0074	0,1418	89,33	0,161	4036,060	12,408	3745,037	22,145
8	800	1,3937	0,1329	0,250	0,068	2,7022	0,3136	123,322	0,209	5616,221	18,066	5204,372	38,046
9	880	1,1317	0,1428	3,604	0,09	3,4843	0,1617	183,556	0,389	8059,714	30,794	7725,303	39,483
10	950	0,4923	0,2564	5,417	0,144	3,0554	0,1920	168,471	0,239	7228,391	37,948	7082,895	65,633
11	1030	-0,4495	0,2193	4,674	0,159	2,1061	0,1730	128,664	0,205	5268,663	63,330	5401,486	14,83
12	1170	-1,0320	0,5564	5,669	0,249	2,7484	0,3815	162,307	0,275	6529,255	156,582	6834,207	59,97
13	1330	6,6878	1,4632	4,150	0,113	1,9304	0,2867	36,161	0,239	3502,696	431,372	1526,455	35,982
14	1450	-5,7340	3,1458	12,039	0,25	-0,8615	0,6177	2,294	0,074	-1623,640	929,388	70,754	25,406

Manicouagan – impact melt rock

Step	Temp	^{36}Ar	± 1σ	^{37}Ar$_{Ca}$	± 1σ	^{38}Ar$_{tot}$	± 1σ	^{39}Ar$_K$	± 1σ	^{40}Ar	± 1σ
1	600	19,8888	0,1090	3,8831	0,1184	2,32	0,088	5956,572	9,958	79,422	34,087
2	690	46,0783	0,1818	8,9591	0,1527	13,309	0,315	14346,769	38,680	730,619	67,685
3	760	18,7686	0,1283	4,2817	0,1785	50,862	0,174	8204,002	15,331	2657,877	40,138
4	820	31,0370	0,0874	9,5244	0,0961	188,652	0,249	18154,138	15,958	8982,701	29,112
5	840	9,1779	0,1221	5,7375	0,2855	217,188	0,624	12933,770	26,345	10221,702	42,151
6	850	2,3114	0,0846	2,1935	0,1865	85,427	0,142	4595,727	11,491	3912,707	22,42
7	870	1,7791	0,0845	1,9996	0,1618	85,002	0,294	4426,047	13,421	3900,308	22,193
8	910	1,6631	0,1433	2,4456	0,1455	99,473	0,22	5055,808	18,321	4564,356	40,793
9	980	0,6356	0,0816	2,5606	0,0323	85,091	0,11	3983,413	25,372	3795,592	16,955
10	1090	0,0858	0,1403	1,3045	0,1233	54,1	0,171	2399,570	38,623	2374,218	19,818
11	1230	2,6930	0,2751	4,4799	0,3400	148,943	0,302	7249,622	76,663	6453,851	32,657
12	1400	5,7420	0,6124	2,0342	0,1621	30,282	0,047	3145,110	177,165	1448,327	40,209

Paasselkä – recrystallized feldspar glass

Step	Temp	^{36}Ar	± 1σ	^{37}Ar$_{Ca}$	± 1σ	^{38}Ar$_{tot}$	± 1σ	^{39}Ar$_K$	± 1σ	^{40}Ar	± 1σ
1	600	9,7245	0,109	1,083	0,099	2,5391	0,2243	27,618	0,233	3877,597	7,2497
2	650	3,5314	0,17872	2,312	0,148	2,1207	0,2437	66,014	0,216	3616,949	6,26047
3	700	5,5250	0,08089	19,837	0,393	5,7356	0,263	243,045	1,323	12989,837	74,97417
4	720	4,0266	0,18419	14,534	0,352	5,6489	0,1651	278,28	1,277	16340,351	71,34013
5	740	2,7493	0,06734	20,913	0,447	6,3184	0,2288	339,976	0,959	19545,027	39,25937
6	760	1,9641	0,11083	10,627	0,228	6,8718	0,1215	388,475	0,461	21417,667	32,08849
7	780	1,2487	0,04325	11,915	0,26	5,5366	0,1183	303,681	0,151	16093,387	8,378633
8	820	1,3957	0,12719	8,772	0,293	7,4801	0,0524	410,968	0,89	20874,921	51,16468
9	860	1,2105	0,19886	13,920	0,304	6,3728	0,0775	354,53	0,7	17580,724	25,9811
10	905	1,1500	0,16543	16,377	0,375	5,0294	0,3273	265,169	0,224	13207,668	13,09879
11	970	1,2802	0,22091	7,861	0,278	4,2689	0,0417	222,641	0,692	11095,884	38,58281
12	1070	3,9897	0,12833	8,106	0,209	7,8282	0,1429	401,178	0,456	20476,308	35,59971
13	1120	3,1609	0,16805	1,924	0,199	5,4282	0,0803	263,178	0,999	13675,399	66,21714
14	1170	1,8662	0,23044	2,431	0,099	2,5711	0,1377	126,813	0,579	6741,569	60,20302
15	1250	3,1546	0,35777	8,528	0,204	2,4354	0,4921	89,865	0,225	5335,658	96,01585
16	1350	3,5633	0,5923	4,435	0,115	2,5592	0,1659	67,285	0,139	4343,832	174,8594
17	1450	-0,3782	0,54184	0,757	0,028	0,3135	0,1118	13,267	0,121	512,207	158,9298

Curriculum Vitae

Martin Schmieder

Born October 07, 1978 in Schorndorf,
Baden-Württemberg, Germany

Education:

03/2008-	Scientific employee at the Institut für Planetologie, Universität Stuttgart
03/2005-	Doctoral student at the Institut für Planetologie, Universität Stuttgart
03/2005	Diploma (Diplom-Geologe); sehr gut
	Diploma thesis: *An impact event in the Alborán Domain? – A discussion on possibly shocked quartz grains from the Betic Cordillera (Province of Murcia and Andalusia, SE Spain)*. 120 p.
1999-2005	Course in Geology/Paleontology at the Universität Stuttgart (Geology, Historical Geology, Paleontology, Mineralogy, Physical Geography)
1998	Abitur (final secondary-school examinations) at the Burg-Gymnasium, Schorndorf

Languages:	English, French (advanced skills), Russian (school basics), German (mother tongue)

Grants:	Grant by the Land Baden-Württemberg 2005-2008 (Landesgraduiertenförderung)